BINARY VAPOUR-LIQUID EQUILIBRIUM FOR SYSTEMS OF INDUSTRIAL IMPORTANCE

By

Funmilola Elizabeth Avoseh

B.Sc. Chemical and Polymer Engineering

Lagos State University, Lagos state, Nigeria.

2015

PREFACE

The work presented in this dissertation entitled “Binary Vapour-Liquid Equilibrium for Systems of Industrial Importance” was carried out in the School of Engineering at the University of KwaZulu-Natal, Howard College Campus, Durban, from April 2013 to July 2014 under the supervision of Professor D. Ramjugernath and Doctor C. Narasigadu and has been submitted in fulfillment of the academic requirements for the degree of Master of Science in Chemical Engineering at the School of Chemical Engineering, University of KwaZulu-Natal, Durban, South Africa.

DECLARATION

I, Funmilola Elizabeth Avoseh, declare that:

i. The research reported in this research proposal, except where otherwise indicated, is my original work.
ii. This research proposal has not been submitted for any degree or examination at any other university.
iii. This research proposal does not contain other persons‘ data, pictures, graphs or other information, unless specifically acknowledged as being sourced from other persons.
iv. This research proposal does not contain other persons‘ writing, unless specifically acknowledged as being sourced from other researchers. Where other written sources have been quoted, then:

(a) their words have been re-written but the general information attributed to them has been referenced;
(b) where their exact words have been used, their writing has been placed inside quotation marks, and referenced.

v This dissertation does not contain text, graphics or tables copied and pasted from the Internet, unless specifically acknowledged, and the source being detailed in the dissertation and in the References sections.

_____ _____

Avoseh F.E. Date

As the candidate’s supervisor, I, Prof. D. Ramjugernath approved this dissertation for submission.

_____

Prof. D. Ramjugernath

As the candidate’s co-supervisor, I, Dr. C. Narasigadu approved this dissertation for submission.

_____

Dr. C. Narasigadu

ACKNOWLEDGEMENT

I would like to take this opportunity to give my sincere acknowledgement to the following people who have made significant contribution to this work:

My supervisors Professor D. Ramjugernath and Doctor C. Narasigadu for their immense support and guidance in the course of this work. Thanks so much and I really appreciate

All my colleagues in the thermodynamic research unit and most especially, Kaniki, Welcome, Thokozani, Alisha, Inbanathan, Sivannah, Mark and Khalid for their assistance anytime and also to Ayanda who was never tired of giving his technical assistance at my beck and call. You guys rock.

The National Research Foundation (NRF) of South Africa for financial support.

The Deeper Life Campus Fellowship (UFH and Howard Campus) members for their prayers and encouragement

I would like to appreciate Dr Samuel Ayodele Iwarere and family, thanks a lot for the great assistance and guidance during my research work. Dr & Prof. (Mrs) O. Oyedeji for your unquantifiable counsel and support.

And lastly to my husband, my love and my life partner, Avoseh Opeyemi Nudewhenu. I appreciate your support, understanding and encouragement. Thanks for standing by me through thick and thin. I love you and will always do.

Lastly, I would like to acknowledge and thank the one who deserves all the glory in my life, the Almighty God, my Maker, my Savior, my Redeemer –Jesus Christ and the Lord of my life. Without Him this would not have been possible for me. Forever will I serve you Lord! I am grateful to You.

ABSTRACT

Most industrial chemical engineering separation processes such as distillation, extraction, absorption and adsorption rely absolutely on accurate phase equilibrium data for effective design, optimization and simulation. Carbonyls and alcohols are known to be of important use in the petrochemical industries. Ketones alongside with alcohols and carboxylic acids are found both in the product stream and waste stream of the Fischer-Tropsch process. 4-methyl-2-pentanone forms parts of these by-products and it is used in a number of industrial applications. It is generally used as solvent, as chemical intermediate in the production of paints, rubber products, chemicals, resins and drugs to mention a few, due to its low solubility in water; it is used for liquid-liquid extraction. This work focuses on measurement of new vapour-liquid equilibrium (VLE) data for binary mixtures of : 1-Propanol (1) + 4-methyl-2-pentanone (2) (at 338.15 K, 353.15 K, and 368.15 K), 2-propanol (1) + 4-methyl-2-pentanone (2) (at 323.15 K, 338.15 K, and 353.15 K) and 2-pentanone (1) + 2-methylpropan-1-ol (2) (at 343.15 K, 358.15 K, and 363.15 K). A modified (Bhownath, 2008) low pressure dynamic VLE glass recirculating still originally designed by Raal (Raal & Mühlbauer, 1998) was used for the measurements.

This work also presents the infinite dilution activity coefficients and the excess thermodynamic properties (i.e. molar excess Gibbs energy G^E, heat of mixing H^E, and excess entropy S^E). These properties were derived from the measured isothermal VLE data.

A highly non-ideal system comprised of cyclohexane + ethanol was chosen as a test system and was used to verify the reproducibility and repeatability of the apparatus. The test system had been measured in our laboratory (Joseph, 2001) and the data were found to agree excellently with those of Morachevsky and Zharov (1963) and were reported to be thermodynamically consistent according to Gmehling and Onken (1977). The results for the test system measured in this work were in excellent agreement with literature. Thus, there was confidence in the new data measured since the apparatus and the operating procedures used for the test system were able to give accurate results. The vapour pressures measured in this study were also in good agreement with literature. The temperature, pressure and composition measuring devices were well calibrated and the uncertainty acquired for each is included.

The uncertainty in the pressure measurement was estimated to be ± 0.02 kPa and controlled within 0.01 kPa. The uncertainty in the temperature measurement was estimated to be ± 0.06 K (Type B uncertainty, NIST) and was controlled within 0.04 K during manual operation. The uncertainty in the composition measurement was estimated as ± 0.002.

The 1-propanol (1) + methyl isobutyl ketone (2) system was found to exhibit a minimum boiling azeotrope at 353.15 K. The gamma-phi (γ-Φ) or combined method was used for the regression of the measured VLE data. Three activity coefficient models were investigated to account for the liquid phase deviation of the mixture from ideality: NRTL (Renon and Prausnitz, 1968), Wilson (1964) and the UNIQUAC (Abrams and Prausnitz, 1975) models. Two equation of state models were used to account for the vapour phase non- ideality: the virial EoS with the Hayden O' Connell (Hayden & Connell, 1973) correlation for the calculation of the second virial coefficient, and the Nothnagel (Nothnagel, Abrams, & Prausnitz, 1973) formulation. The maximum likelihood regression technique was used to determine the regressed parameters of the activity coefficient models. These models were found to fit the measured data well. The measured VLE data passed the point test of Van Ness(et al., 1973) and the direct test (Van Ness, 1995).

TABLE OF CONTENTS

Contents

LIST OF FIGURES

APPENDIX A

APPENDIX B

APPENDIX C

LIST OF TABLES

NOMENCLATURE

English Letter		Units
a_i	Activity of a liquid	(-)
A_i	Constant in the Antoine equation	(-)
a_{ij}	Constants for temperature dependency of model parameters	(-)
B_i	Constant in the Antoine equation	(-)
B_{ii}	Second virial coefficient of pure component *i*	[cm^3/mol]
b_{ij}	Constants for temperature dependency of model parameters	(-)
B_{ij}	Second virial coefficient for species i – species j interaction	[cm^3/mol]
C_i	Constant in the Antoine equation	(-)
c_{ij}	Constants for temperature dependency of model parameters	(-)
d_{ij}	Constants for temperature dependency of model parameters	(-)
e_{ij}	Constants for temperature dependency of model parameters	(-)
f	Fugacity	[kPa]
$f_i^{\,0}$	Fugacity of the pure component *i* in a standard (or reference) state	(-)
$\hat{f}_i$	Fugacity in solution of component *i*	[kPa]
F	Degrees of freedom of the system (Gibbs phase rule)	(-)
f_{ij}	Constants for temperature dependency for model parameters	(-)
g_{ij}-g_{ii}	Parameter in NRTL (1968) model representing interactions between species	(-)
G	Molar or specific Gibbs energy	[J/mol]
$\bar{G}_i$	Partial molar Gibbs free energy	(-)
H	Molar or specific Enthalpy	[J/mol]
K_i	Chemical equilibrium constant for association equilibria	(-)

l_i	Parameter in the UNIQUAC (1975) model	(-)
n_i	Number of moles of component *i*	(-)
N	Number of chemical species or components present in a system	(-)
P	System pressure	[kPa]
q_i	Pure component area parameter in the UNIQUAC (1975) model	(-)
Q	Energy transferred as heat energy	(-)
r_i	Pure component volume parameter in the UNIQUAC (1975) model	(-)
R	Universal gas constant	[J/mol.K]
S	Molar or specific entropy	[J/mol.K]
T	System temperature	[^{0}C or K]
U	Molar or specific internal energy	(J)
V	Molar or specific volume	[cm^3/mol]
V_m	Molar volume	[cm^3/mol]
w	Normalizing factor	(-)
W	Work done on a system	(J)
x_i	Mole fraction of component *i* in the liquid phase	(-)
y_i	Mole fraction of component *i* in the vapour phase	(-)
z	Co-ordination number in the UNIQUAC (1975) model	(-)
Z	Compressibility factor	(-)

Greek Letters

α_{12}	Non-randomness parameter in NRTL (1968) model
γ_i	Activity coefficient of component *i*
δ	Denotes a residual (e.g. δT)
Δ	Denotes the residual for the point test
η	Solvation (unlike species) and association (pure species) parameters (HOC)
θi and θ_i'	Area fractions in UNIQUAC (1975) equation
λ_{ii}	Parameter representing interactions between species in the Wilson (1964) model
Λ_{ij}	Parameter in Wilson (1964) model
μ_i	Chemical potential of component *i*
π	Number of phases present in a system (Gibbs phase rule)
τ_{ij}	Parameter in the NRTL (1968) model and UNIQUAC (1975) model
ϕ	Fugacity coefficient
$\hat{\phi}$	Fugacity coefficient in solution
Φ	Ratio of fugacity coefficients, with the pointing correction factor
φ_i	True species fugacity coefficient

Superscripts

exp	Denotes values calculated from experimental data
E	Denotes an excess property
id	Denotes an ideal solution
L	Denotes the liquid phase
Lit	Refers to literature data

Sat	Denotes a saturated value
V	Denotes the vapour phase

Subscripts

1	Denotes component 1 (the more volatile component in a binary mixture)
2	Denotes component 2 (the less volatile component in a binary mixture)
avg	Denotes an average value
c	Denotes a critical property
rev	Denotes reversible processes

CHAPTER 1

INTRODUCTION

In chemical industries, it has been shown that the total cost of separation is up to 40-70% of the total operating cost of a plant. Therefore, adequate knowledge of separation is highly important for the practicing engineer. Distillation is considered as the oldest and most widely used separation process in the chemical and petrochemical industries. Phase equilibrium analysis forms the basis of distillation process design.

Accurate and reliable phase equilibrium data (which includes VLE) is essential for the design and optimum operation of distillation columns and other separation processes. Experimental data for several systems are scarce and rarely available in the literature thereby causing difficulties in designing separation processes for some specific systems in the industries. Most process designers have been left with the choice of using different thermodynamic models for predicting phase behavior of components for systems of interest. Predictive methods are easy and fast to access but may be unreliable for complex and highly non-ideal systems. Measurement of VLE data though quite expensive and time consuming has been found to be more reliable and accurate than the so-called predictive method. In addition, experimental data have always been used in the understanding of phase change phenomena. Nowadays, experimental data together with useful thermodynamic models are used to account for the various aspects of intermolecular interactions of mixtures (Prausnitz , 1999). The applications of some of these models in phase equilibria have been quite successful. Though experimental data measurements could be time and cost consuming, they still offer best results due to their reproducibility and its consistency.

Phase equilibrium data also provides the thermodynamic knowledge of highly non-ideal systems. information on azeotropic or near azeotropic behavior which is an example of non-ideality helps in the design of distillation process as ordinary distillation process is not suitable for separating systems that exhibit azeotropes (Narasigadu et al., 2013). There are various methods available for separating systems that are azeotropic in nature (Seader and Henley, 1998). This work was undertaken as a result for need of new VLE data for some ketone + alcohol systems. These chemicals form part of the constituent components in the industrial waste streams of petrochemical plants. In order to design and optimize these

process plants, and also to recover useful by-products, accurate and reliable VLE data as well as the relationship between varying temperatures, pressures and compositions of these components is required. Some previous isothermal VLE measurements comprising ketone and alcohols binary systems have been done in our Thermodynamic Research Unit at the School of Chemical Engineering. Jeremy Pillay (Pillay, 2009) measured 2-propanone (1) + 2-butanol (2) at 333.15, 353.15 and 373.15 K. Prashant Reddy (Reddy, 2006) measured 1-propanol (1) + 2-butanol (2) at 373.15, 393.15 and 423.15 K. As a result of lack of experimental data in open literature, this study focused on experimental measurement and modelling for these systems:

- 1-propanol (1) + 4-methyl-2-pentanone (2) at 338.15 K, 353.15 K and 368.15 K
- 2-propanol (1) + 4-methyl-2-pentanone (2) at 323.15 K, 338.15 K and 353.15 K
- 2-pentanone (1) + 2-methylpropan-1-ol (2) at 343.15K, 358.15 K and 363.15K

In process simulation, it is necessary to properly select thermodynamic models as this serves as a starting point for an accurate simulation. In the course of this work, NRTL, , UNIQUAC, and the Wilson liquid phase activity coefficient models were used to account for the nonideality in the liquid phase while the vapour phase nonideality was accounted for with the virial equation of state using the Hayden−O'Connell and the Nothnagel second virial coefficient correlations. These equations were found to fit the experimental data well. The new measured VLE data were subjected to rigorous thermodynamic testing to check for the consistency of the measured data. These measurements were undertaken using a low pressure dynamic recirculating still designed by Raal (Raal and Mühlbauer, 1998) and modified by Bhownath (Bhownath, 2008). The measured data were regressed using different thermodynamic models in ASPEN (ASPEN PLUS, 2014) in order to obtain the model parameters.

In separation technology, infinite dilution activity coefficients are of great importance in the production of high purity reagents therefore; for each isothermal VLE system measured in this work the activity coefficients at infinite dilution were calculated by using the method of Ellis and Jonah (1962) as modified by Maher and Smith (1979).

CHAPTER 2

REVIEW OF SOME EXPERIMENTAL METHODS FOR VLE MAESUREMENT

A reliable and acceptable process design requires accurate VLE data measurements and an appropriate theory and equations to describe and predict the VLE behavior of components. There are different equipment for VLE measurements because a number of variables and several ranges of conditions are considered. In other words, the equipment employed will depend largely on the temperature, pressure and the mixture to be studied. These data are determined experimentally with equipment that ensures equilibrium between the vapour and liquid phases. there are many reviews of experimental procedures and equipment in open literature such as those of Hala et al.(1967), Abbott (1986) , Malanowski (1982), Raal and Mühlbauer (1994) Dvoskin Nataliya (2004). This chapter however focuses on some experimental techniques for VLE measurements and extends to the proper description of the equipment employed for this study.

2.1 Classes of experimental VLE equipment.

Experimental VLE equipment can be grouped into two main types based on the type of operation namely; static equipment and dynamic (circulation) equipment. The static method can also be subdivided into analytical (direct sampling method) and synthetic (indirect sampling) methods depending on how the compositions of the two coexisting phases are determined. In the static analytical method, the phase equilibrium compositions are determined by sampling and analyzing each of the phases. While the static synthetic method involves synthetically preparing the mixture composition.

Several methods for experimental data measurement of VLE have been developed and modified for different systems.

Hala et al. (1967), classified several available VLE methods into the following categories:

1. Dynamic methods
2. Static methods
3. Distillation methods
4. Flow methods
5. Dew and Bubble Point methods

A skeletal review of these methods will be made in this chapter with the main focus on the dynamic method for low pressure VLE, in particular the recirculating stills. Raal & Mühlbauer, (1998), classified stills according to the phase circulation through the equilibrium chamber. In other words, continual circulation is generally known as the dynamic method or flow method, otherwise it is a static method. A systematic breakdown of some methods is shown in Figure 2-1 below.

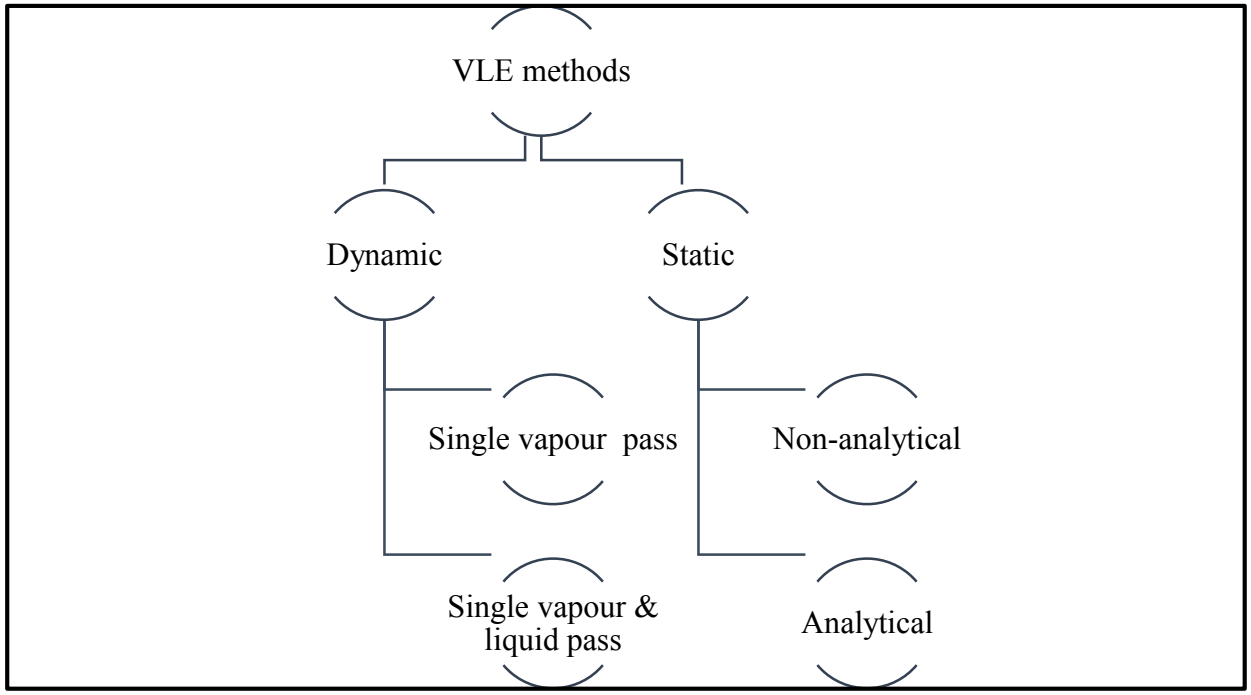

Figure 2-1: Schematic description of some VLE methods (Raal & Mühlbauer, 1994)

2.1.1 Static Method

The static method can be subdivided into static analytical method, in which the compositions of both are sampled and analysed, and the static synthetic method in which sampling of the phases is not required. In the static synthetic method, the system pressure is the principal measurement. The static-synthetic (non-analytic) method entails preparing a mixture of a particular known concentration, and allowing the equilibrium of phases to occur within a cell, usually at isothermal conditions. The exact liquid composition is calculated after making allowances for vapour holdup (Raal and Ramjugernath, 2001). The vapour phase composition can then be calculated from P-x data. Calculation of vapour phase composition from P-x data saves time and effort and also eliminates the chances of thermodynamic consistency testing of the data. Since only the measurement of the system pressure is required in the static synthetic or static nonanalytical method, the major disadvantage of this method is the problem of complete degassing of the system. The system has to be completely degassed which is a time consuming process and its avoidance leads to measurement of inaccurate pressures.

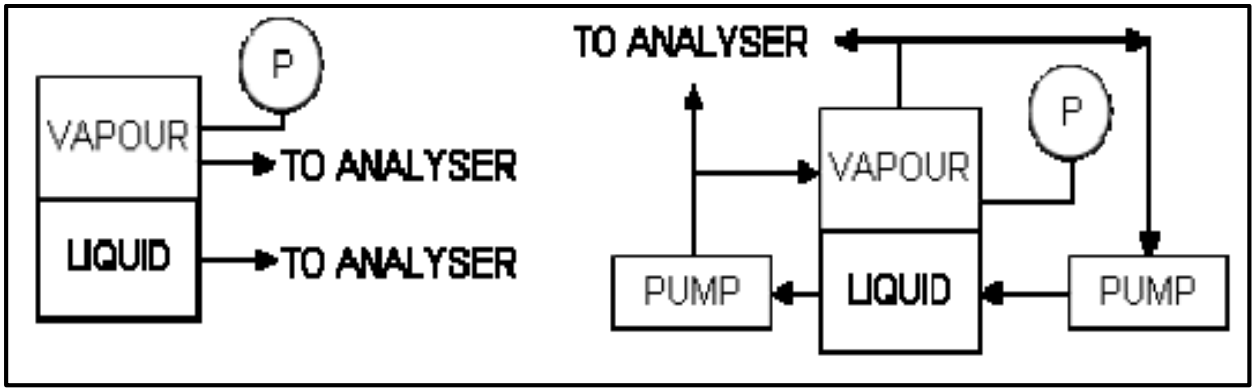

Figure 2-2: The general principles of a static VLE equipment (Uusi-kyyny, 2004)

2.1.2 Dew and Bubble Point Method

In this method, the cell used is considered to be of a variable volume placed in a constant temperature bath. The sample is placed in the cell and the volume of the cell is adjusted until vaporization occurs. The point and volume at which vaporization starts to occur is found by observation if the cell is of glass or by deducing it on the pressure volume plot. However since the composition of the sample is predetermined, analysis of the phases is not required. When a liquid mixture begins to boil, the composition of the vapour differs from that of the liquid. The more volatile component will preferentially boil off. Thus, as boiling continues, there is a drop in the concentration of the least volatile component. Consequently a rise in the boiling point occurs. The temperatures over which boiling occurs set the bubble and dew points of the mixture. Readers are referred to the work of Uusi-Kyyny (2004) for more details on the dew and bubble point method.

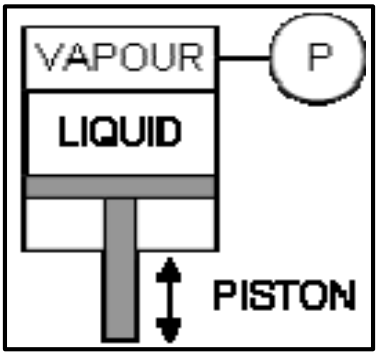

Figure 2-3:The principle of the dew and bubble point method (Uusi-kyyny, 2004)

2.1.3 Dynamic Method

VLE data measurement that employs circulation of one or both vapour or liquid phase/s through the equilibrium chamber is known as the dynamic method or simply circulation method (Hala et al., 1967). Developed by Carveth in 1899 (Carveth, 1899), the principle of its operation involves discharge of a liquid mixture into a distilling flask, boiled to bring about separation of the vapour phase. The vapour rises and condenses at the cooling arm of the still into a receiver. The advantage of this method is that it is flexible for both isothermal and isobaric operations.

The amount of test sample per run is also small (Joseph, 2001). more details on the dynamic method are presented in Phase Equilibria: measurement and computation (Raal and Mühlbauer, 1998)

Classification of this method based on the type of phase under circulation has been done under two categories (Hala et al. 1967):

1. Circulation of the vapour phase only
2. Circulation of both the liquid and vapour phases

2.2 Features of Recirculating Still

Certain features must be satisfied for a recirculating still as outlined by Malanowski (1982):

- The design should ensure accurate measurement of vapour and liquid composition at a fixed temperature or pressure.
- Small sample volumes should be used for analysis of vapour and liquid phases.
- Attainment of a true dynamic equilibrium rapidly.
- Condensation of vapour on the temperature sensor should not be allowed.
- Constant stirring of the components in the reboiler and in the condensate receiver should be ensured at all time. This allows the circulated phases to be well mixed with the boiling liquid to maintain uniform composition.
- Upon sample introduction and taking of samples to and from the still, great care should be taken to avoid equilibrium disturbance.

Recirculation of Vapour Phase Only

The Othmer (1928) apparatus was among the earliest types of equipment designed for the recirculation of the vapor phase only. Figure 2.4 gives the schematic description of the apparatus. Other typical examples were the apparatus of Carveth (1899), Sameshima (1918) and Jamaguchi (1913). In the originally designed experimental apparatus of Othmer (1928), the vapour is generated by boiling; the vapour is condensed in the condenser arm. Re-introduction of the condensate back to the boiling flask is done via the condensate trap.

However, there are several sources of error in the original design which led to numerous modifications to the design. For example, the condensate receiver is large and there is no stirring of the condensate (preferably mechanically), the equilibrium temperature measurement is insupportable, whether the thermometer is placed in the vapour phase or in the liquid. There is also no stirring in the boiling chamber and it is advisable to have thorough stirring by mechanical means because of flashing of a vapour rich in the more volatile component(s) upon entering the boiling chamber. There is also the problem of partial condensation of the vapour on the wall of the boiling flask, which produces non-equilibrium vapour (Raal and Mühlbauer , 1998).

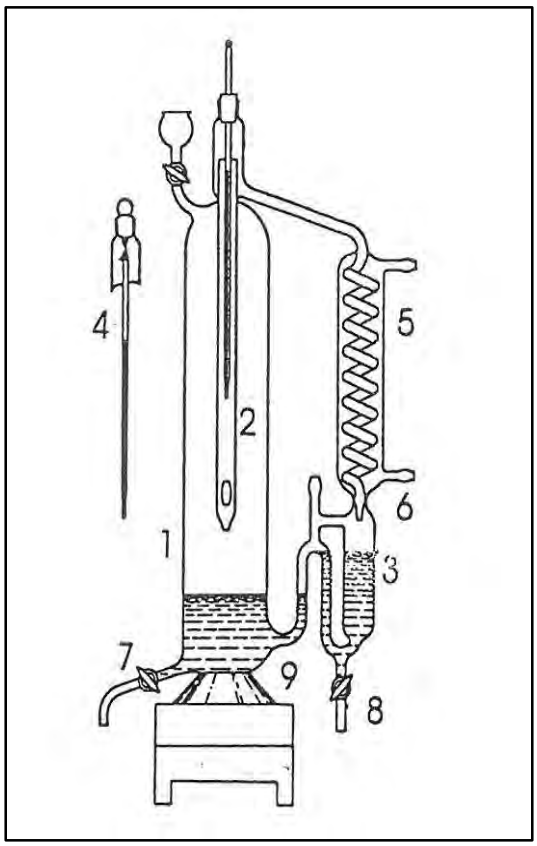

Figure 2-4: Original Othmer dynamic VLE still taken from Raal and Mühlbauer (1998)
1, boiling chamber; 2, vapour tube; 3, condensate receiver; 4, thermometer; 5, condenser; 6, drop counter; 7, liquid sampling point; 8, vapor sampling point; 9, heater.

An improvement on the Othmer apparatus was made in the area of measurement of partially miscible systems by Stockhardt and Hull, (1931) giving rise to a simple set up and easy to operate apparatus. Its limitation is that it produces vapours that are rich in the more volatile components; and thus suffers from the same problem as the Othmer still. Fractionation is caused by the scrubbing action of reflux which passes down the neck of the apparatus prior to sampling. Also, it can only be used for systems that are homogenous at their boiling points Hala (et al., 1958). The modification of Baker et al. (1982) was able to prevent condensed vapour returning to the boiling pot; however, it was not possible to determine true equilibrium temperature because of the contact of the thermometer with both phases and the large volume of chemicals required. Other modifications of the recirculation of vapour phase type stills were developed, but according to Raal and Mühlbauer (1998), their measurements are not advisable because of inaccurate measurements.

Recirculation of both Liquid and Vapour Phases

The limitations and drawbacks of single phase circulation of VLE measurements, led to a more elaborate design by Lee (et al., 2005) which incorporated the circulation of both liquid and vapour phases.

2.3 The Gillepsie Design

The modification by Gillespie (1946) thereafter led to a more acceptable form of the still with the incorporation of the Cottrell pump into the boiling chamber. The Cottrell pump is a narrow tube where the force of the boiling liquid pumps the two-phase vapour-liquid mixture upwards into the equilibrium chamber. The Gillepsie set-up is shown in Figure 2-5. The boiling of the mixture is carried out in the boiling chamber. After boiling, the Cottrell pump introduces the mixture of both phases (liquid and vapour) into the disengagement chamber where the temperature is measured. The sample trap thereafter returns the condensed vapour into the boiling chamber, mixing it with the liquid from the equilibrium chamber in the boiling flask Gillepsie (1946).

According to Raal and Mühlbauer (1998), withdrawn liquid samples from the boiling chamber is not in equilibrium with the recirculating vapour. There is also the possibility of partial condensation at the walls of the chamber. In addition, withdrawal of samples had an effect on the operation and finally the mass transfer in the Cottrell pump was not optimal as a result of the short contact time.

2.3.1 Modifications to the Gillespie Still

Several modifications to the still have been done with the aim to minimize some of the errors and limitations of the earlier designs. The still developed by Thornton (1951) incorporates the Cottrell pump as developed by Gillespie (1946). The still is used for systems with low miscibility, having a special feature of an insulated receiver located in the vapour phase for condensate collection. Although equilibrium is reached based on the functionality of the Cottrell pump, Raal and Mühlbauer (1998) observed that this cannot serve as the right apparatus for equilibrium attainment. The sampling process may also disturb the still operation. Other modifications to the Gillespie still were made by Ellis and Garbett (1960). They incorporated vibratory stirrers for the liquid and the condensate which is the principle employed for attainment of equilibrium. Complexity of the equipment and its long hours for equilibrium attainment are some of its limitations.

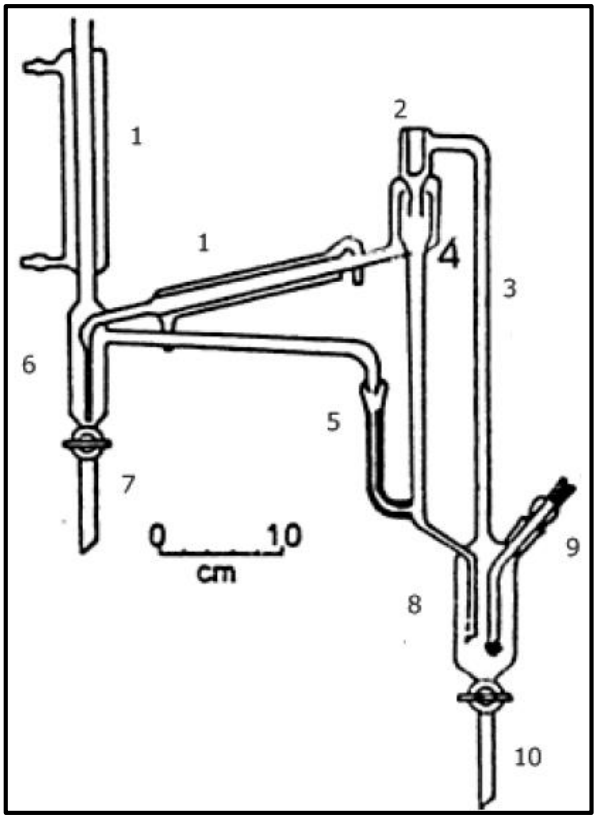

Figure 2-5: Schematic of the Original Gillespie still (Gillepse, 1946)

(1)Vapour condensers; (2) thermometer; (3) Cottrell tube; (4) disengagement chamber; (5) droplet counter; (6) condensate receiver; (7) condensate sample cock; (8) boiling chamber; (9) internal heater; (10) liquid sample cock.

2.4 The Yerazunis (1964) Still Design

Yerazunis et al. (1964) designed equipment that allows for the circulation of both the vapour and liquid phase. The novel feature of his design was that the vapour-liquid mixture in the packed equilibrium chamber (constructed with ¼ in Fenske helices) flows downwards concurrently. The packed column design was earlier used by Heertjes (1960), and use of the vapour phase as a thermal barrier by Rose and Williams (1955). Specialised flow through sampling valves was provided for the vapour and liquid flow to allow sampling without equilibrium disturbance (Raal and Mühlbauer, 1998).

The setback however of this apparatus is its sampling valves which are awkward, inconvenient and could be replaced by a simple yet effective sampling point with built-in septa.

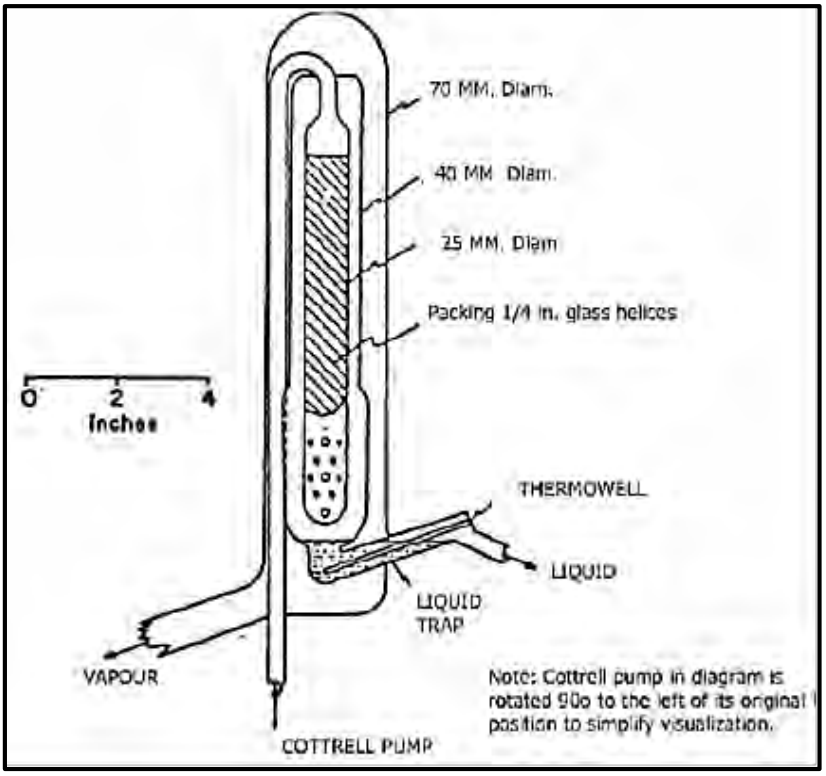

Figure 2-6: A typical Yerazunis apparatus (Yerazunis et al., 1964)

2.5 The Malanowski Still Design (1982)

Swietoslawski's (1945) ebulliometer principle of bubble formation via the activation of the walls of the boiling chamber with sintered glass, forms the basis for Malanowski's (1982) design. Equilibrium was established in the thermo-well and the equilibrium chamber is embedded in a vacuum jacket to reduce heat losses. In addition to other features, this design contains a mixing chamber which collects and mixes the overflow from the liquid and vapour phases as shown in Figure 2-7.

The main advantage of the chamber is to ensure a uniform concentration and composition of fluid returning to the reboiler. Consequently, equilibrium was achieved via the Cottrell pump, which Joseph et al. (2002) observed as not too acceptable a medium to reach perfect equilibrium.

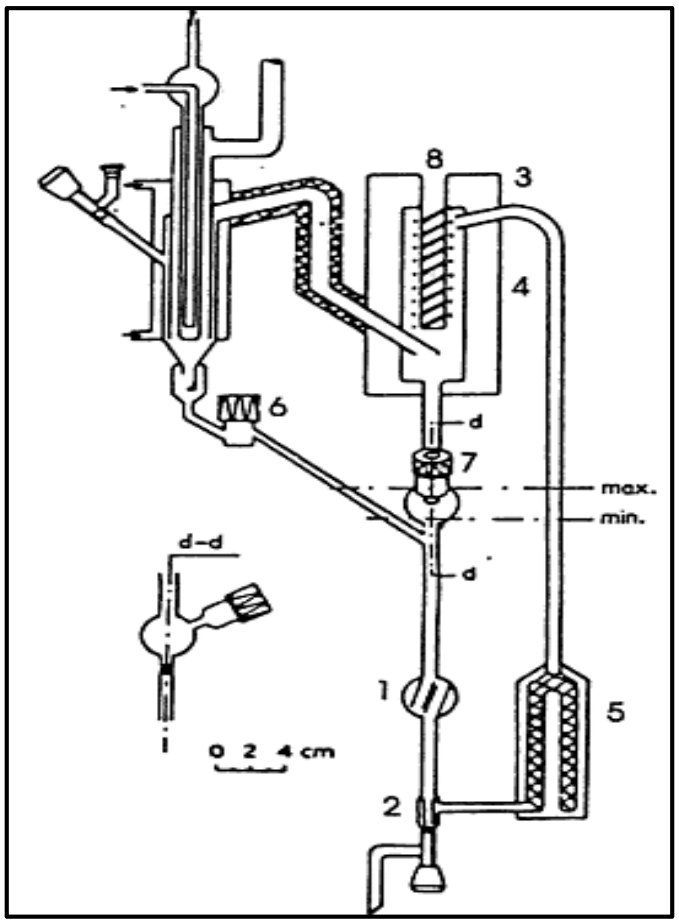

Figure 2-7: The Malanowski (Malanowski, 1982) still design

1&2: mixing chamber; 3&4: equilibrium chamber; 5: boiling chamber; 6: vapour sampling point; 7: liquid sampling point; 8: thermowell.

2.6 Low Pressure VLE still of Raal (Raal and Mühlbauer, 1998)

A modification to this still was adopted in this experimental work and a detailed description is made in Chapter 4. Based on the design of Yerazunis (1964), (Raal and Mühlbauer, 1998) designed a robust equilibrium still to minimize some of the limitations on earlier designs. For an excellent review on this glass recirculating still, readers are referred to (Raal and Mühlbauer, 1998).

Distinctive characteristics of this design are:

- Attainment of equilibrium is brought about by the maximum contact between the liquid and vapour phase in the packed column which promotes quick equilibrium attainment.

- The compact dynamic VLE still attains a true dynamic equilibrium rapidly and can be constructed at moderate cost (Joseph et al., 2002).
- The equilibrium chamber is packed and concentric around a vacuum-insulated cottrell tube.
- The problem of partial condensation of the vapour and heat loss were removed by vacuum jacketing the Cottrell tube and the equilibrium chamber.
- The centrally located vacuum-insulated Cottrell pump also insulates the equilibrium chamber.
- The concentric design around the packed section of the equilibrium chamber minimizes liquid drop entrainment in the vapour phase and forces the vapour to surround the equilibrium chamber, serving as a thermal lagging.
- Magnetic stirrers were employed for constant stirring in both the boiling chamber and the condensate receiver.
- Incorporation of internal and external heaters into the boiling chamber allows for rapid and even boiling (internal heater) and external heater to balance heat losses to the environment.

A modified version of Raal and Mühlbauer (1998) VLE glass still was used in this experimental work and detailed description is made in Chapter 4.

2.7 The VLE still of Joseph (Joseph, 2001)

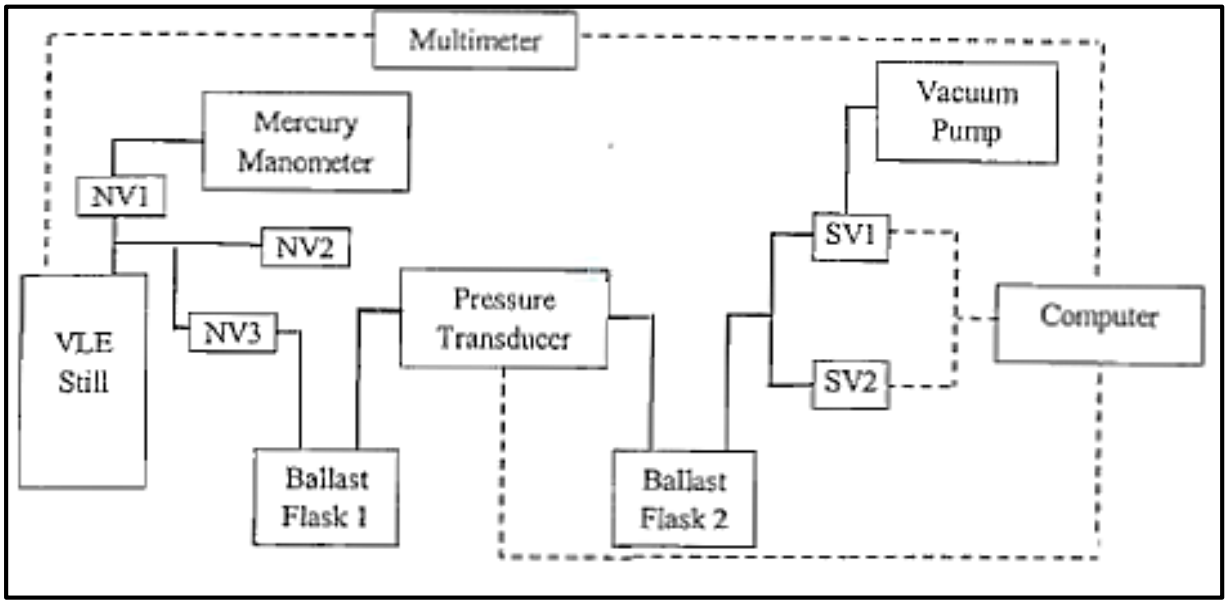

Figure 2-8: Block diagram of the apparatus of Joseph taken from (Bhownath, 2008)

The dynamic VLE glass recirculating still designed by Raal (Raal and Mühlbauer, 1998) went through modification by Joseph (2001). The VLE still originally designed by Raal is capable of measuring isothermal and isobaric data, Joseph (et al., 2001) improved on the isothermal operation of the VLE still by manually adjusting the pressure set point on the pressure controller to achieve the desired temperature. This new design which made possible both the isobaric and isothermal operation of the VLE still was based on pulse-width modulation control strategy with the aid of computer. The modified version of the VLE still was used by Joseph (2001), Sewnarain (et al, 2002), Clifford (2004), Samuel (Iwarere, 2009) to mention a few. This still was described in detail by Joseph (2001) and Joseph et al. (2002). Figure 2-8 represents the block diagram of the apparatus of Joseph (et al., 2002). The only disadvantage of this still is that it is unsuitable for VLE measurement of highly volatile systems. For additional information on this type of modified VLE still, readers are referred to the listed references.

2.8 The modified VLE still of Ndlovu (Ndlovu, 2005)

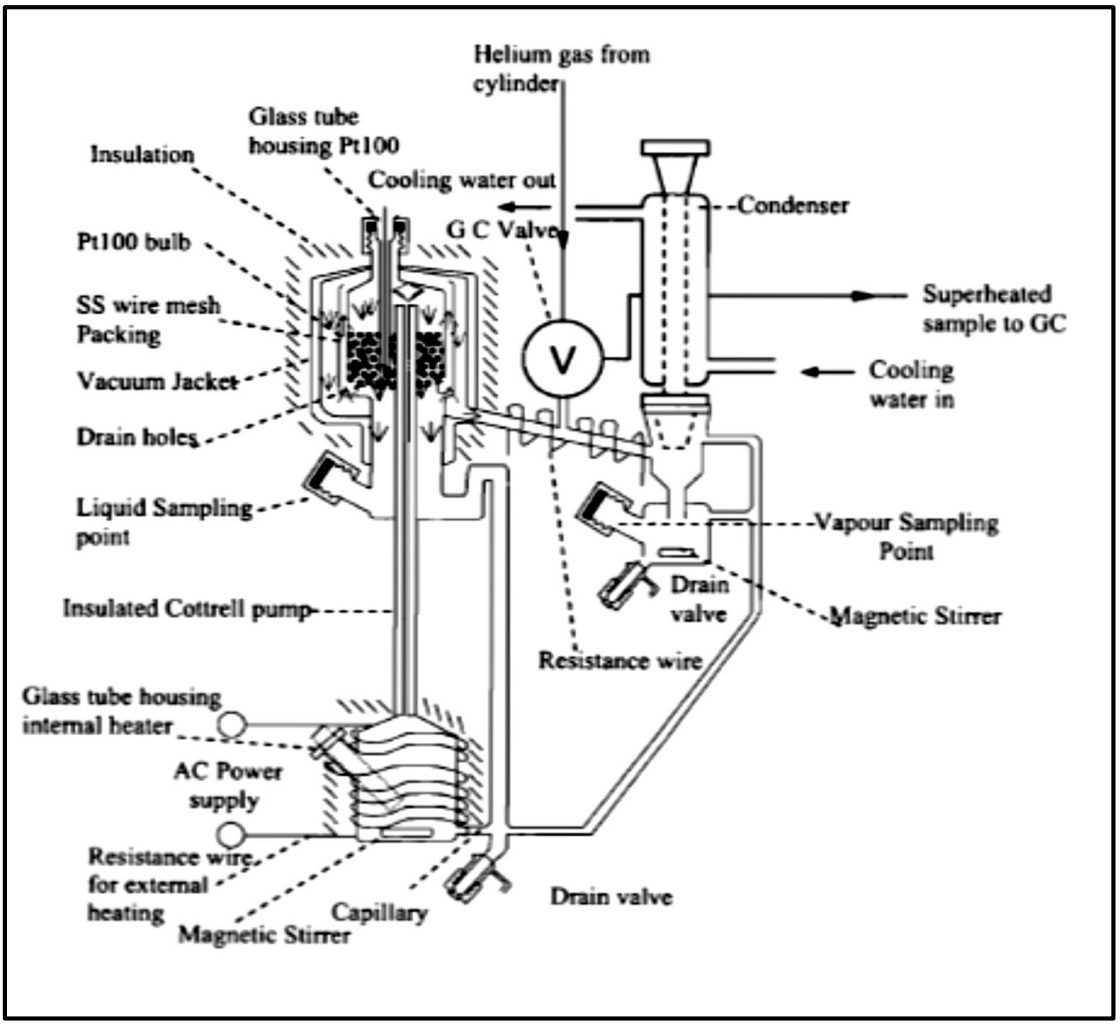

Figure 2-9: The VLE still of Ndlovu (2005) taken from (Bhownath, 2008)

The most notable features of the modified still of Ndlovu (2005) are:

- A packed equilibrium chamber which allows mass transfer between the phases and enhances increase in contact time.
- The packed equilibrium chamber also allows equilibrium to be reached rapidly
- The equilibrium chamber serves as a medium for the separation of the vapour and liquid phases

- The equilibrium chamber is designed on the still in an angular symmetric way to allow the direct upward flow of the phases into it and hence prevents the occurrence of concentration gradients
- Incorporation of efficient magnetic stirring in the reboiler and the vapour condensate trap. This prevents both temperature and concentration gradients in the condensate receiver, in the reboiler, it prevents flashing and promotes homogeneity
- The siphon break was incorporated to prevent backflow of the returning phases.
- Smooth and rapid boiling was also achieved through the incorporation of the internal and external heaters. The latter compensates for heat loss around the reboiler.

Ndlovu (Ndlovu, 2005) implemented some modifications to the VLE still of Joseph (et al. 2002) based on the design of Raal (Raal and Mühlbauer, 1998). The still presented in Joseph (2001) was found non ideal for the measurements of both VLE and VLLE of partially miscible liquids. During the operation of the still, it was found out that there was partial vapour condensation throughout the downward pass of vapour in the equilibrium chamber due to contact with the outside walls. However, for homogeneous systems, partial condensation of the vapour before sampling does not affect the overall composition of the vapour, but for partially miscible liquids, condensation of vapour before sampling affects the true composition of the components and thus should be avoided. Ndlovu (2005) made improvement to the vapour sampling by providing a means of sending the vapour samples directly to the gas chromatograph. The problem of partial condensation was prevented by slightly superheating the vapour exiting the equilibrium chamber and then sending the vapour through a six-port gas chromatograph valve.

2.9 The modified VLE still of Rinay Bhownath (Bhownath, 2008)

Rinay Bhownath (2008) made some modifications to the VLE still of Ndlovu (2005) to handle systems of high relative volatility. This still was used for the measurements in this work. The VLE still of Ndlovu (2005) was incapable of accurately measuring binary LPVLE data for systems with high relative volatility. These systems are found to exhibit large concentration differences between the returning vapour and liquid phases in the return lines. These differences in concentration result in significant difference in the densities of the vapour and liquid exiting the equilibrium chamber. As a result of this, there is need for more agitation to create a homogenous mixture returning into the boiling chamber as short contact times and inadequate mixing in the boiling chamber may lead to flashing. In order to correct this problem, the modified LPVLE still of Rinay Bhownath(2008) that was utilized for this work contains a tee formation where the returning vapour and liquid streams are combined. The mixing tee has a glass spiral which enhances the mixing and contact between the vapour and liquid streams without interfering with the liquid hold up.

For further vigorous agitation of the liquid mixture, and to ensure complete homogenous mixing of the liquid entering into the reboiler, a circular mixing chamber was also incorporated. The returning liquid mixture from the 'mixing tee' enters into the mixing chamber tangentially creating a vortex. This is similar to the principle of a liquid entering a hydrocyclone. The schematic diagram of this still is shown in Figure 4-1.

CHAPTER 3

THEORETICAL ASPECTS OF VAPOUR-LIQUID EQUILIBRIUM

3.1 INTRODUCTION

Since the design and optimization of separation processes depends mainly on VLE data, theoretical knowledge of phase equilibrium is therefore important in modern industrial separation processes. The data needed for a specific separation process may not be within the available conditions of temperature and pressure in which the data were measured and therefore there will be need for interpolation or extrapolation of the measured VLE data. The main goal of this chapter is to present a review of some theoretical aspects of thermodynamic treatment of VLE data which include the concept of fugacity and fugacity coefficient, fugacities from the second virial equation of state, activity and activity coefficient and activity coefficient models. This chapter also reviews the data regression approach and the thermodynamic consistency tests used in this work.

Furthermore, this chapter does not provide detailed principles of thermodynamics, only the important principles that are applicable to vapour liquid equilibrium and most especially those that are related to this work are detailed in this chapter. More theoretical treatment of solution thermodynamics for vapour liquid equilibrium can be found elsewhere (Smith et al., 2005).

Liquid and vapour phase properties from experimental VLE data

In a multicomponent system, the fugacity of species i in a mixture is the same in all the phases:

$$\hat{f}_i^{\alpha} = \hat{f}_i^{\beta} = \cdots = \hat{f}_i^{\gamma} \tag{3-1}$$

Therefore for component i in vapour-liquid equilibrium, the vapour phase fugacity equals the liquid phase fugacity:

$$\hat{f}_i^{V} = \hat{f}_i^{L} \quad (i=1,2,\ldots..,N) \tag{3-2}$$

This expression is termed as the criterion for equilibrium and can therefore be related to:

$$\hat{f}_i^{\,v} = y_i \hat{\phi}_i^{\,v} P \tag{3-3}$$

The dimensionless function $\hat{\phi}_i^{\,v}$ is known as the fugacity coefficient of species i in solution. It is used to account for the non-ideality in the vapour phase. This equation is used to calculate the vapour phase fugacity of species i in a mixture and also relates Equation (3-2) to measurable variables such as pressure, temperature and composition.

Also the fugacity coefficient of either saturated liquid or saturated vapour in equilibrium is given as:

$$\phi_i^{\,sat} = \frac{f_i^{\,sat}}{p_i^{\,sat}} \tag{3-4}$$

where $\phi_i^{\,sat}$ is the fugacity coefficient of pure species i in saturated state.

For vapour-liquid equilibrium of a pure component, the following expression is applicable:

$$\phi_i^{\,v} = \phi_i^{\,l} = \phi_i^{\,sat} \tag{3-5}$$

For the liquid phase, the right hand side of Equation (3-2) is related to measurable quantities by bringing in a dimensionless quantity γ. This quantity accounts for the liquid phase non-ideality.

$$\hat{f}_i^{\,l} = x_i \gamma_i f_i \tag{3-6}$$

From the expression that relates the fugacity of component i to its chemical potential:

$$\mu_i = \Gamma_i(T) + RT\ln f_i \tag{3-7}$$

$$\lim_{P\to 0}\frac{f}{P} = 1$$

Since $\mu_i = G_i$, the Gibb's free energy for an ideal gas in solution can also be written as:

$$G_i = \Gamma_i(\mathrm{T}) + RT\ln f_i \tag{3-8}$$

where $\Gamma_i(\mathrm{T})$ is an integration constant and temperature dependent only. In a multicomponent system, the fugacity of species *i* in a mixture is the same in all the phases:

Differentiating Equation (3-8) above, we get:

$$dG_i = RTd\ln f_i \tag{3-9}$$

From the fundamental property relation of Gibb's free energy for a homogeneous fluid of constant composition:

$$dG = VdP - SdT \tag{3-10}$$

By changing the state of pure species i from a saturated liquid to a compressed liquid at constant temperature and composition, Equation (3-10) can therefore be integrated to give:

$$G_i - G_i^{sat} = \int_{P_i^{sat}}^{P} V_i dP \tag{3-11}$$

Equation (3-8) can be substituted twice for the left hand side of Equation (3-11), and subtracting yields:

$$G_i - G_i^{sat} = R\mathrm{T} \ln \frac{f_i}{f_i^{sat}} \tag{3-12}$$

Setting Equations (3-11) and (3-12) equal we obtain:

$$\ln \frac{f_i}{f_i^{sat}} = \frac{1}{R\mathrm{T}} \int_{P_i^{sat}}^{P} V_i dP \tag{3-13}$$

where V_i is the liquid phase molar volume and it is also a very weak function of P at temperatures well below the critical temperature T_c. Integrating Equation (3-10) at a condition where Vi is approximately assumed constant at the value for saturated liquid volume V_i^l. Then,

$$\ln \frac{f_i}{f_i^{sat}} = \frac{V_i^l \left(P - P_i^{sat}\right)}{R\mathrm{T}} \tag{3-14}$$

Substituting Equation (3-4) into Equation (3-11) and solving for fi gives:

$$f_i = \phi_i^{sat} P_i^{sat} \exp\left[\frac{V_i^l \left(P - P_i^{sat}\right)}{R\mathrm{T}}\right] \tag{3-15}$$

The exponential term is known as the poynting correction factor and it allows for the correction of the liquid phase fugacity from vapour pressure to the system pressure. Combing Equations (3-3) and (3-6), we obtain:

$$y_i \hat{\phi}_i P = x_i \gamma_i f_i \tag{3-16}$$

Substituting fi from Equation (3-15) into Equation (3-16):

$$y_i \hat{\phi}_i P = x_i \gamma_i \ \phi_i^{sat} P_i^{sat} \exp\left[\frac{V_i^l \left(P - P_i^{sat}\right)}{R\mathrm{T}}\right] \tag{3-17}$$

where:

$$\Phi_i = \frac{\hat{\phi}_i}{\phi_i^{sat}} \exp\left[\frac{-V_i^l \left(P - P_i^{sat}\right)}{R\mathrm{T}}\right] \tag{3-18}$$

the saturated liquid molar volume v_i^L is determined using the Rackett (1970) equation:

$$V_i^L = V_c Z_c^{(1-T_r)^{2/7}} \tag{3-19}$$

where subscript c represents the critical point, Z is the compressibility factor and T_r ($T_r = T/T_c$) is the reduced temperature. Figure 3-1 shows the common types of VLE curves and the detailed explanations on it is described by Raal and Mühlbauer (1998).

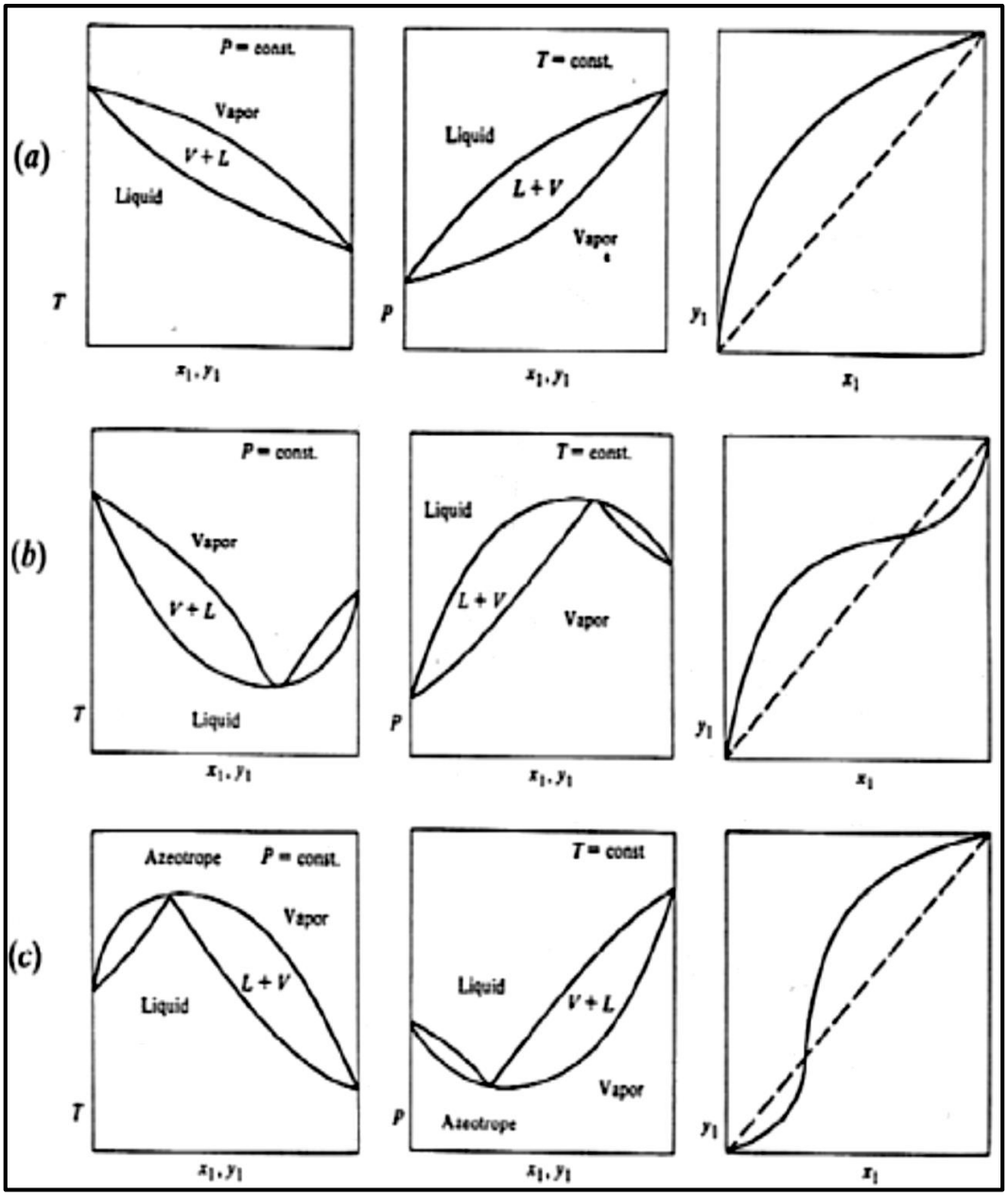

Figure 3-1: Types of binary T-x-y, P-x-y and x-y phase equilibrium curves: (a) intermediate-boiling systems; (b) systems displaying a minimum boiling azeotrope; (c) systems displaying a maximum boiling azeotrope (Raal and Mühlbauer, 1998).

3.2 Fugacity coefficients from the virial equation of state

Fugacity coefficients of a component in the vapour phase can be calculated from different types of equations of state. The virial equation of state is one of the types. Its applicability to gases at low to moderate pressures makes it distinct among the other types. The second virial coefficient which depends only on the interactions between binary pairs is obtained from rigorous statistical mechanics calculations and can be used to correlate accurately the behavior of gases and the non-idealities in the vapour phase. It is a function of temperature and composition.

The truncated virial equation of states in pressure explicit form is simplified as:

$$Z = 1 + \frac{BP}{RT} \tag{3-20}$$

Where Z is a dimensionless quantity and is known as the compressibility factor. Z equates to unity for an ideal gas. B is termed the second virial coefficient of a mixture and is a function of temperature and composition. The equation giving its composition dependence based on statistical mechanics is:

$$B_{mix} = \sum_i \sum_j y_i y_j B_{ij} \tag{3-21}$$

Where indices *i* and *j* identify two species and the bimolecular interaction between two species *i* and *j* are characterized by the virial coefficient B_{ij}, hence, $B_{ij} = B_{ji}$. *y* is the mole fraction in the vapour phase. When the second virial equation of state is used to describe the vapour phase, the fugacity coefficient expressed in Equation (3-18) is modified to:

$$\Phi_i = \exp\left[\frac{\left(B_{ij} - V_i^L\right)\left(P - P_i^{sat}\right) + P y_j^{\,2} \delta_{ij}}{RT}\right] \tag{3-22}$$

where

$$\delta_{ij} = 2B_{ij} - B_{ii} - B_{jj} \tag{3-23}$$

B_{ii} and B_{ij} can be determined experimentally by various methods. One of the methods involves the calculation of volume in a high pressure VLE cell presented by Ramjugernath (2000). Several methods have also been developed for the calculation of the second virial coefficient values such as the correlations of Hayden-O'Connell(1975), Nothnagel et.al. (1973) and the correlation of Tsonopoulos (1974). The correlations of Hayden and O'Connell (1975) and Nothnagel et.al (1973) were employed in this work. Each of these correlations is discussed in the following sections.

3.2.1 Hayden-O'Connell second virial equation of state

Hayden and O'Connell (1975) developed a well-accepted method for determining the second virial coefficient for simple and complex systems. Their method is made acceptable for systems containing polar, non-polar and associating compounds and incorporates the chemical theory of dimerization. The model also account for the strong association and solvation effects found in systems containing organic acids. From Equation (3-20), the second virial coefficient Bij is given by:

$$B_{ij} = \left(B_{free-nonpolar}\right)_{ij} + \left(B_{free-polar}\right)_{ij} + \left(B_{metastable}\right)_{ij} + \left(B_{bound}\right)_{ij} + \left(B_{chem}\right)_{ij} \tag{3-24}$$

Values of *Bij* are depended only on interaction between two molecules. The terms $(B_{free}$ - $nonpolar)_{ij}$ and $(B_{free}$ - $polar)_{ij}$ refer to contribution by free pairs of molecules (non-polar, non-associating molecules) and $(B_{measurable})_{ij}$, $(B_{bound})_{ij}$ and $(B_{chem})_{ij}$ account for the chemically bonding molecules. The calculation for this correlation requires parameters for the pure component properties which include: the dipole moment μd, critical temperature T_c, critical pressure Pc, mean radius of gyration Rd and the solvation and association parameters η.

These basic parameters can be found in literature sources such as Prausnitz et al. (1980), Reid et al. (1988), Fredunslund et al. (1977) and the Dortmund Data Bank (DDB) (2013). While the dipole moments for pure compounds are available from McClellan (1963-1974), the solvation and association values can be found in the ASPEN Physical property system. The limitation of this correlation is that it is only applicable for low to moderate pressures because the truncated second virial equation does not likely hold for systems of high pressures.

3.2.2 The second virial correlation of Nothnagel et al. (1973)

The correlation of Nothnagel et al. (1973) is applicable to systems that display strong vapour phase dimerization. The model uses the chemical theory of dimerization for determining vapour phase fugacity coefficients.

The equation is expressed as:

$$P = \frac{RT}{V_m - b} \tag{3-25}$$

where V_m is the molar volume calculated as the total volume divided by the true number of species i.e. $\frac{V}{n^t}$ and b is the molar excluded volume of a mixture of monomers and dimers:

$$b = \sum_{i=1}^{nc} y_i b_i + \sum_{i=1}^{nc} \sum_{j=1}^{i} y_{ij} b_{ij} \tag{3-26}$$

$$b_{ij} = \left(b_i^{1/3} + b_j^{1/3} \right)^3 \Big/ 8 \tag{3-27}$$

n_c is the number of components in the mixture. The following reversible association reactions in chemical theory are assumed to take place at low to moderate pressures in the vapour phase.

$$2A_1 \xleftrightarrow{K_A} A_2 \tag{3-28}$$

$$2B_1 \xleftrightarrow{K_B} B_2 \tag{3-29}$$

Where A_1, B_1 and A_2, B_2 represent the monomers and dimers that are included in the individual species of the mixture respectively. K_A and K_B are the chemical equilibrium constant for the dimerization reaction on pressure basis and are related to the true mole fractions and fugacity coefficients by:

$$K_A = \frac{z_{A_2}}{z^2{}_{A_1} P} \frac{\varphi_{A_2}}{\varphi_{A_1{}^2}} \tag{3-30}$$

$$K_B = \frac{z_{B_2}}{z^2{}_{B_1} P} \frac{\varphi_{B_2}}{\varphi_{B_1{}^2}} \tag{3-31}$$

Where φ_i is the true fugacity coefficient of specie i; P is the total pressure of the system; z_i (i represents A_1, A_2, B_1, B_2) is the true specie mole fraction; A_1 and B_1 represent the true mole fractions of monomers and A_2 and B_2 are the true mole fractions of dimers.

Values for ϕ_i and φi can be determined from the following equations respectively:

$$\phi_i = \frac{z_i \varphi_i}{y_i} \tag{3-32}$$

$$\varphi_i = \exp \frac{b_i P}{RT} \tag{3-33}$$

Where y_i is the vapour phase mole fraction of specie i.

Another form Equation (3-24) can be rewritten is:

$$z = \frac{PV_m}{RT} = 1 + \frac{Pb}{RT} \tag{3-34}$$

This expression is in agreement with the virial equation of state

3.2.3 The Pitzer-Curl correlation for the second virial coefficient

Pitzer and Curl (1957)developed a generalized correlation for the second virial coefficient. The basis for their correlation is Equation (3-19):

$$Z = 1 + \frac{BP}{RT} = 1 + \left(\frac{BP_c}{RT_c}\right)\frac{P_r}{T_r} \tag{3-35}$$

Their correlation provided an expression for $\left(\frac{BP_c}{RT_c}\right)$as:

$$\frac{B_{virial}P_c}{RT_c} = B^{\circ} + \omega B' \tag{3-36}$$

The acentric factor ω was introduced by Pitzer et al. (1955) for characterizing the phases of pure components. It is defined as a measure of the non sphericity of molecules. The constants B^o and B' are functions of the reduced temperature only ($T_r = T/T_c$) and are represented respectively as:

$$B^{\circ} = 0.083 - \frac{0.422}{T_r^{1.6}} \tag{3-37}$$

$$B' = 0.139 - \frac{0.172}{T_r^{4.2}} \tag{3-38}$$

Equation (3-36) gives the expression for the pure component virial coefficient. A generalized equation that includes cross coefficient was later proposed by Prausnitz (1999):

$$B_{ij} = \frac{R(T_c)_{ij}}{(P_c)_{ij}}\left(B^{\circ} + \omega_{ij}B'\right) \tag{3-39}$$

Prausnitz et al.(1999) also introduced empirical mixing rules for calculating the cross coefficient constants $(Tc)_{ij}$, $(Pc)_{ij}$, and ω_{ij} :

$$(T_c)_{ij} = \sqrt{((T_c)_i - (T_c)_j)}(1 - k_{ij}) \tag{3-40}$$

$$(P_c)_{ij} = \frac{(Z_c)_{ij} R(T_c)_{ij}}{(V_c)_{ij}} \tag{3-41}$$

and

$$\omega_{ij} = \frac{\omega_i + \omega_j}{2} \tag{3-42}$$

where

$$(V_c)_{ij} = \left[\frac{(V_c)_i^{1/3} + (V_c)_j^{1/3}}{2} \right]^3 \tag{3-43}$$

and

$$(Z_c)_{ij} = \frac{(Z_c)_i + (Z_c)_j}{2} \tag{3-44}$$

where k_{ij} in Equation (3-40) is an empirical binary interaction parameter.

3.3 Activity and activity coefficient

Activity (a) can be explained as the ratio of the fugacity of a substance in solution to its fugacity in some defined standard state. It is determined with reference to an ideal state and on a mole fraction basis (i.e. $a_i = x_i$). Activity (a) of a species in solution can be expressed as:

$$a_i = \frac{\hat{f}_i}{f_i^\circ} \tag{3-45}$$

Activity coefficient (γ) is used to account for the deviation of a solution from ideality. It is defined as the ratio of the activity of species in solution to its mole fraction or the ratio of species' actual fugacity in solution to the product of the mole fraction and the standard state fugacity:

$$\gamma_i = \frac{a_i}{x_i} \tag{3-46}$$

or

$$\gamma_i = \frac{\hat{f}_i}{x_i f_i^{\circ}} \tag{3-47}$$

In order to have accurate models for the activity coefficient, the activity coefficient must be related to partial derivatives of the excess Gibbs energy.

The relations are given by:

$$\ln \gamma_i = \frac{\partial}{\partial n_i}\left(\frac{n_T G^E}{RT}\right)_{P,T,n_j} \tag{3-48}$$

$$\frac{G^E}{RT} = \sum_i x_i \ln \gamma_i \tag{3-49}$$

For the experimental VLE data in this work, three local composition based activity coefficient models were used to account for the non-ideality in the liquid phase and will be discussed in the following sections. These are the Wilson model (1964), the NRTL (Non-Random Two Liquid) model (Renon, and Prausnitz, 1968) and the UNIQUAC (Universal Quasi-Chemical Theory) model (Abrams and Prausnitz, 1975).

3.3.1 The Wilson's equation

The concept of local composition (contrary to the overall liquid composition) within a liquid solution was introduced by Wilson (1964). He proposed that local compositions are presumed to account for the short range order and nonrandom molecular orientation within a solution which result from differences in intermolecular forces and sizes. Wilson's (1964) equation for the Gibbs free energy of a binary system consisting of m components is:

$$\frac{G^E}{RT} = -\sum_{i=1}^{m} x_i \ln\left(\sum_{j=1}^{m} x_i \Lambda_{ij}\right) \tag{3-50}$$

where Λ_{ij} and Λ_{ji} are the two adjustable parameters of the Wilson equation and are related to the pure component molar volumes and to characteristic energy differences by:

$$\Lambda_{ij} = \frac{v_j}{v_i} \exp\left(-\frac{\lambda_{ij} - \lambda_{ii}}{RT} \right) \tag{3-51}$$

$$\Lambda_{ji} = \frac{v_i}{v_j} \exp\left(-\frac{\lambda_{ji} - \lambda_{jj}}{RT} \right) \tag{3-52}$$

In ASPEN Plus (the process simulator utilized for regressing experimental data in this work), the version of the Wilson model used for the regression of experimental data does not employ the liquid molar volumes, rather Λ_{ij} is set as a function of temperature only:

$$\Lambda_{ij} = \exp\left(a_{ij} + \frac{b_{ij}}{T} + c_{ij} \ln T + d_{ij} T \right) \tag{3-53}$$

The expression for the activity coefficient for any component k is:

$$\ln \gamma_k = -\ln\left(\sum_{j=1}^{m} x_j \Lambda_{ki} \right) + 1 - \sum_{i=1}^{m} \frac{x_i \Lambda_{ik}}{\sum_{j=1}^{m} x_j \Lambda_{ij}} \tag{3-54}$$

The two important advantages of the Wilson model are; it can be readily generalized to multi-component systems without introducing parameters other than those for the constituent binaries and it can predict multicomponent properties from binary data. The application of this model is limited to systems that are completely miscible. Hence, a modified Wilson equation was developed by Tsuboka and Katayama (1975) which allows accurate modelling of partially miscible systems. Furthermore, this model is not useful for systems where the logarithms of the activity coefficient, when plotted against x_1, show maximum or minimum.

3.3.2 The NRTL (Non-Random-Two-Liquid) model

An improved local composition local composition model was proposed by Renon and Prausnitz (1968). The derivation of the Non Random Two Liquid (NRTL) model was based on the assumption of non-randomness like the one used by Wilson and the two-liquid model of Smith. Contrary to the Wilson's equation, the NRTL model is applicable to miscible and

partially miscible systems. This equation is also applicable for highly non-ideal systems and can be generalized for multi-component systems.

The NRTL equation for the Gibbs energy of a system consisting of e components is:

$$\frac{G^E}{RT} = \sum_{i=1}^{e} x_i \frac{\sum_{j=1}^{e} \tau_{ji} G_{ji} x_j}{\sum_{l=1}^{e} G_{li} x_l} \tag{3-55}$$

where

$$\tau_{ij} = \frac{g_{ij} - g_{jj}}{RT} \tag{3-56}$$

and

$$G_{ij} = \exp\left(-\alpha_{ij} \tau_{ij}\right) \tag{3-57}$$

The τ_{ij} parameter in temperature dependent form in ASPEN is given as:

$$\tau_{ij} = a_{ij} + \frac{b_{ij}}{T} + e_{ij} \ln T + f_{ij} T \tag{3-58}$$

During regression in ASPEN only the first two terms of Equation (3-58) are used while for isothermal data regression, a_{ij} and a_{ji} can be set to zero, thus Equation (3-58) is reduced to Equation (3-56) based on the DECHEMA data set. When the parameter αij is zero it indicates complete randomness in the mixture. It has been shown from the regression of large sets of experimental data of binary systems that values of α_{ij} lie within 0.20 to 0.47. ASPEN suggests a value of 0.2 for saturated hydrocarbons consisting of polar non-associated liquids and for immiscible systems, and 0.47 for systems of strongly non-associated and non-polar components. Walas (1985) proposed that values of the non-randomness parameter should be set to roughly 0.3 for non-aqueous systems and 0.4 for aqueous organic mixtures. Raal and Mühlbauer (1998) however suggest that values for αij should be obtained from the regression of sufficient experimental data.

Another advantage of the NRTL equation is that it can be used sufficiently for aqueous systems compared to other models. This model has some disadvantages which are: the multiplicity in the interdependence of the parameters, the concept of choosing a value for the non-randomness parameter which may affect the accuracy of the regression.

3.3.3 The UNIQUAC (Abrams and Prausnitz, 1975) model

Due to the fact that experimental data for binary systems are insufficient to yield three significant binary parameters and the derivation of the NRTL equation agrees more with h^E than G^E, a more suitable model was developed by Abrams and Prausnitz (1975) known as the UNIQUAC equation. This model was proposed to obtain a two-parameter equation for G^E that could retain at least some of the advantages of the Wilson's equation and not be restricted to completely miscible liquids. The equation consists of two parts: the combinatorial part that takes into account the differences in molecules shapes and sizes and the residual part that depends on the intermolecular forces between the molecules.

The UNIQUAC equation is expressed as:

$$\frac{G^E}{RT} = \left(\frac{G^E}{RT}\right)_{combinational} + \left(\frac{G^E}{RT}\right)_{residual} \tag{3-59}$$

For a binary system consisting of e components, the Gibbs excess energy for the two parts of the equation can be written as:

$$\left(\frac{G^E}{RT}\right)_{combinational} = \sum_{i=1}^{e} x_i \ln\frac{\Phi_i^*}{x_i} + \frac{z}{2}\sum_{i=1}^{e} q_i x_i \ln\frac{\theta_i}{\Phi_i^*} \tag{3-60}$$

$$\left(\frac{G^E}{RT}\right)_{residual} = -\sum_{i=1}^{e} q_i' x_i \ln\left(\sum_{j=1}^{e} \theta_j' \tau_{ji}\right) \tag{3-61}$$

where z is the coordination number usually set to 10, Φ^* is the segment fraction, θ and θ' are the area fractions. Φ^*, θ and θ' are represented by the following equations respectively:

$$\Phi_i^* = \frac{r_i x_i}{\sum_{j=1}^{e} r_j x_j} \tag{3-62}$$

$$\theta_i = \frac{q_j x_j}{\sum_{j=1}^{e} q_j x_j} \tag{3-63}$$

$$\theta_i' = \frac{q_i' x_i}{\sum_{j=1}^{e} q_j' x_j} \tag{3-64}$$

The parameters r, q and q′ are pure component molecular structure constants. r accounts for molecular sizes while q and q′ account for the external surface areas of the molecules.

The two adjustable binary interaction parameters τ_{ij} and τ_{ji} (isothermal operations) are related to the characteristic energies u_{ij} and u_{ji} by:

$$\tau_{ij} = \exp\left(-\left[\frac{u_{ij} - u_{jj}}{RT}\right]\right) \tag{3-65}$$

The characteristic energies (u_{ij} and u_{ji}) are at most times weakly dependent on temperature (Prausnitz et al. 1986).

The ASPEN version of Equation (3-66) for the UNIQUAC adjustable parameter is expressed as:

$$\tau_{ij} = \exp\left(a_{ij} + \frac{b_{ij}}{T} + c_{ij}\ln(T) + d_{ij}T + \frac{e_{ij}}{T^2}\right) \tag{3-66}$$

The activity coefficient γ for the UNIQUAC equation is given by:

$$\ln\gamma_i = (\ln\gamma_i)_{combitorial} + (\ln\gamma_i)_{residual} \tag{3-67}$$

$$(\ln\gamma_i)_{combitorial} = \ln\frac{\Phi_i}{x_i} + \frac{z}{2} q_i \ln\frac{\theta_i}{\Phi_i} + l_i - \frac{\Phi_i}{x_i}\sum_{j=1}^{e} x_j l_j \tag{3-68}$$

$$\left(\ln \gamma_i\right)_{residual} = -q_i' \ln\left(\sum_{j=1}^{e} \theta_j' \tau_{ji}\right) + q_i' - q_i' \sum_{j=1}^{e} \frac{\theta_j' \tau_{ij}}{\sum_{k=1}^{e} \theta_k' \tau_{kj}} \tag{3-69}$$

where

$$l_i = \frac{z}{2}\left(r_i - q_i\right) - \left(r_i - 1\right) \tag{3-70}$$

The UNIQUAC model (Abrams and Prausnitz, 1975) is applicable to binary and multicomponent systems containing polar and non-polar liquids such as systems containing ketones, alcohols, amines, esters, nitriles, water and hydrocarbons. This model has shortcomings of the need for pure component parameters and entails algebraic complexity.

3.4 Low pressure VLE data reduction

The importance of experimental VLE data in chemical processes cannot be overemphasized. These data are essential in: providing conclusive basis to estimate competing processes, optimizing design processes and assuring the performance of process plants. However most times these data are not always available or the required data are not within the condition range (temperature and pressure) of the available ones and this gave rise to the development of thermodynamic models to solve this problem. Experimental data are correlated to these models in order to provide a set of parameters that allow accurate extrapolation of experimental data at the desired conditions. Furthermore, these models also allow the prediction of multi-component VLE from pairs of binary VLE data and they give the possibility of thermodynamic consistency testing of experimental data.

Different methods have been proposed in literature for the correlation of phase equilibrium data, due to their reliability and ease of application, the two common ones are the combined method or often referred to as the γ-Φ formulation of VLE data and the second one is known as the direct method or the Φ-Φ method (i.e. equation of state method). But for the regression of data in this work, only the combined method (γ-Φ) was used which is discussed in detail below.

3.4.1 The combined method (γ-Φ) for VLE data regression

The combined method employs an activity coefficient model (Gibbs excess model) to determine the activity coefficient that accounts for the liquid phase non-idealities and an equation of state to determine the fugacity coefficient which accounts for the non-idealities in the vapour phase. This method relies on the liquid phase activity coefficient model like; the Wilson (1964) model, the NRTL (Renon and Prausnitz, 1968) model and the UNIQUAC (Abrams and Prausnitz, 1975) model to represent VLE data. More than one model is normally used for regressing experimental data owing to the fact that a particular system is represented better with specific models. Equation (3-16) represents the γ-Φ equation and it is used in the regression of VLE data. Figures (3-2) and (3-3) illustrates the algorithm employed in the γ-Φ method for the regression of isothermal (bubble point pressure) and isobaric (bubble point temperature) VLE data respectively.

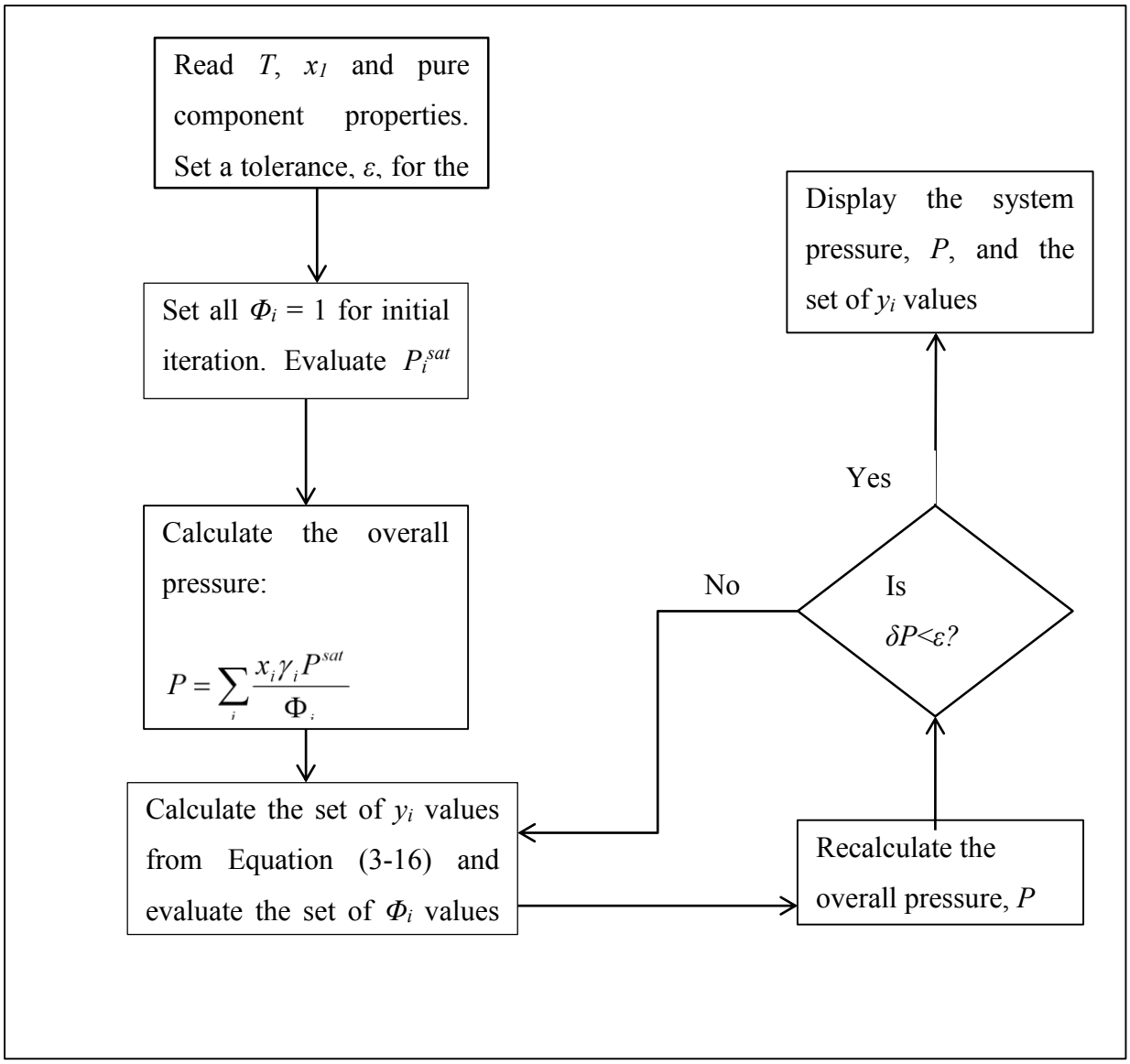

Figure 3-2: Block diagram for the bubble point pressure calculation. (Smith et al., 2004)

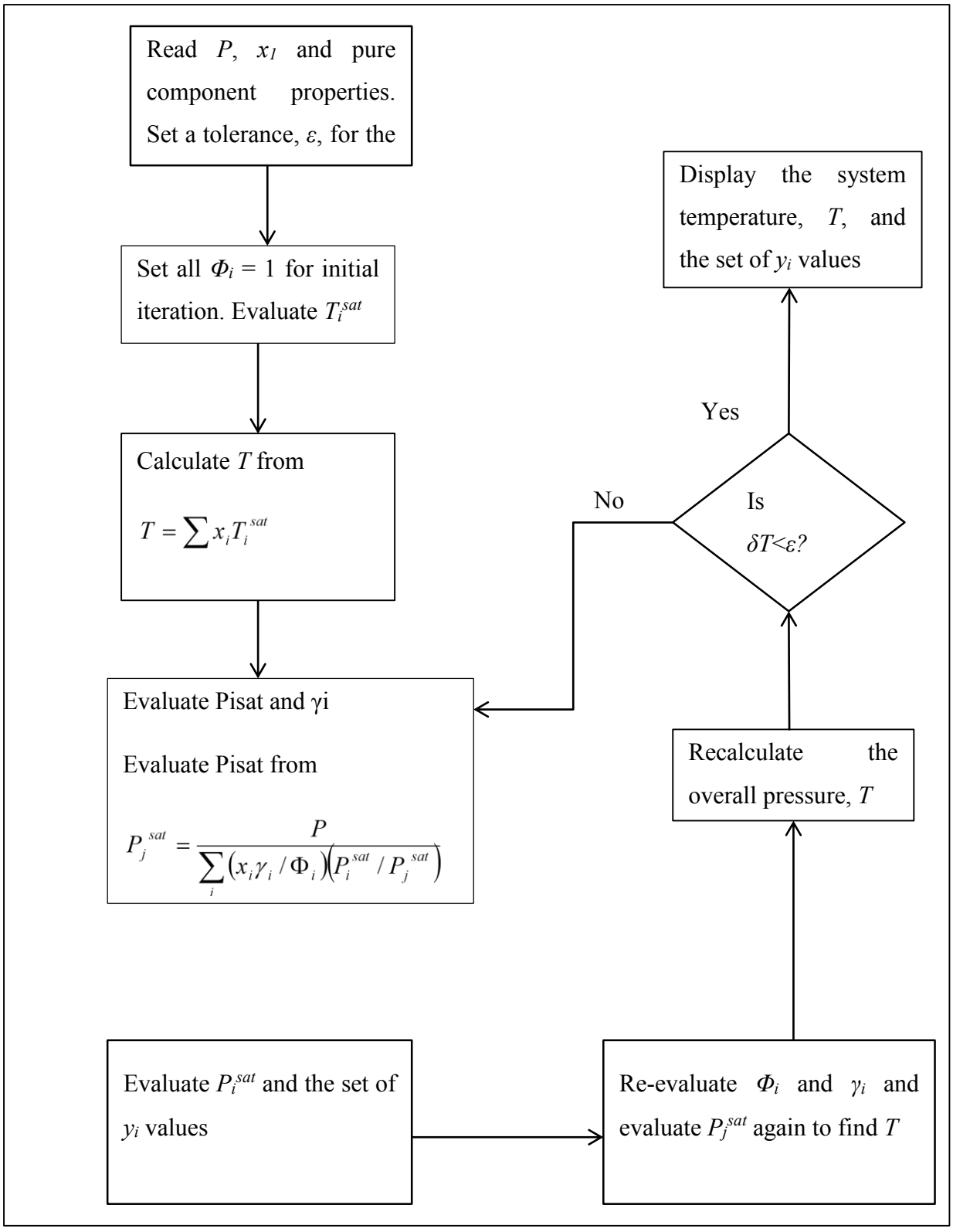

Figure 3-3: Block diagram for the bubble point temperature calculation. (Smith et al., 2004)

3.5 Thermodynamic consistency testing

Graphical representation of experimental data may be misleading regarding the quality of the experimental data. These data are liable to systematic errors and the errors are mainly from the vapour phase. . The Gibbs Duhem equation is the basis for thermodynamic consistency testing and is given as:

$$\sum x_i d\ln\gamma_i = \frac{\overline{V}^E}{RT}dP - \frac{\overline{H}^E}{RT^2}dT \tag{3-71}$$

Experimental VLE data must agree with the equation above to be thermodynamically consistent. Two types of thermodynamic consistency tests were used in this work to evaluate the consistency of the measured VLE data, these are: the point test and direct test. Each of these is discussed below.

3.5.1 Point Test

The point test for thermodynamic consistency testing was introduced by Van Ness (Van Ness et al., 1973). Measuring all the four variables (*P, T, x_1 and y_1*) for a binary system results in an over specification of the system as the fourth variable can be determined from the other three experimentally obtained variables by using solution thermodynamics. However, measuring the four variables helps in employing the point test. As mentioned earlier, in most cases the vapour phase compositions introduce the most error (Smith et al., 2004), thus the measured vapour compositions are used to test for the consistency of the data. The point test involves finding the differences between the experimental vapour composition values *(y_{exp})* and the calculated values *(y_{calc})*. The calculated values are obtained from the other three variables through the data regression either by using the combined method or direct method. The absolute average deviation of the vapour compositions should be obtained and according to Gess et al. (Gess et al., 1991), this value should be less than or equal to 0.01 in order for the data to pass the thermodynamic consistency testing:

$$\Delta y_{AAD} = \frac{1}{n}\left(\left|y_{\exp} - y_{calc}\right|\right) \tag{3-72}$$

where n is the total number of experimental points. This test was employed for the data measured in this study.

3.5.2 The Direct Test

Van Ness (1995) proposed the direct test. He developed a simple and direct way of testing for the thermodynamic consistency of each measured VLE data point with respect to the Gibbs-Duhem formulation. The direct test formulation is given by the following definitions:

$$\varepsilon^*_P = \frac{V^E}{RT}\frac{dP}{dx_1} \tag{3-73}$$

$$\varepsilon^*_T = \frac{-H^E}{RT^2}\frac{dT}{dx_1} \tag{3-74}$$

For isothermal data consistency, Equation (3-73) is used while for isobaric data Equation (3-74) is used, where ε_P* is set to zero for isobaric data and ε_T* is zero for isothermal data. Only one of the equations is required for the direct test consistency testing. For binary VLE data, the direct test formulation is expressed as:

$$\delta \ln\frac{\gamma_1}{\gamma_2} = x_1\frac{d\ln\gamma_1^{ex}}{dx_1} + x_2\frac{d\ln\gamma_2^{ex}}{dx_1} - \varepsilon * \tag{3-75}$$

where the residual term $\delta \ln\frac{\gamma_1}{\gamma_2}$ is defined as the difference between the calculated activity coefficient values and the corresponding experimental values, γ_1^{ex} and γ_2^{ex} represent experimental gamma one and gamma two respectively, ε depends on the type of experimental VLE data (i.e. whether isothermal or isobaric). Setting $\sum(\delta g)^2$ as the objective function, the isothermal or isobaric VLE data is reduced by minimizing $\sum(\delta g)^2$, where:

$$g^E = \frac{G^E}{RT} = x_1\ln\gamma_1 + x_2\ln\gamma_2 \tag{3-76}$$

According to the Gibbs-Duhem equation, experimental data is said to be consistent when the right hand side of Equation (3-75) is zero. The deviations of the experimental data from the Gibbs-Duhem equation is measured by the residual on the left hand side (i.e. the difference between the calculated activity coefficient values and the experimental values) and the measure of the deviation from consistency is given by the extent to which this residual fails to

scatter about zero (1995). Table (3-1) represents the consistency index that quantifies the degree of departure of the experimental data for the direct test of Van Ness (1995).

Table 3-1: The direct test (Van Ness, 1995) consistency table

Index	RMS $\delta \ln(\gamma_1/\gamma_2)$	
1	> 0	≤ 0.025
2	> 0.025	≤ 0.050
3	> 0.050	≤ 0.075
4	> 0.075	≤ 0.100
5	> 0.100	≤ 0.125
6	> 0.125	≤ 0.150
7	> 0.150	≤ 0.175
8	> 0.175	≤ 0.200
9	> 0.200	≤ 0.225
10	> 0.225	

Table (3-1) represents the quantitative criterion developed by Van Ness (1995). For the direct test, an index of one indicates data of high accuracy while an index of ten signifies data of poor quality.

3.6 Infinite dilution activity coefficient

The infinite dilution activity coefficient γ^{∞} also referred to as the limiting activity coefficient; plays important roles in separation processes particularly in the production of high purity chemicals. however, it has been shown by Hartwick and Howart (1995) that extrapolating binary activity coefficient curves to the end points most times gives inaccurate values of limiting activity coefficients These values can be accurately determined from experimental isothermal VLE data by employing the method of Ellis and Jonah (1962) as modified by Maher and Smith (1979b). The γ^{∞} values are calculated from total pressure measurements using the concept of pressure deviation P_D and liquid composition x_i to calculate the limiting change in pressure with respect to composition, $\left(\frac{\partial P}{\partial x_1}\right)^{\infty}_{x_1=0}$.

The deviation pressure, P_D, is expressed as:

$$P_D = P - \left[P_2^{sat} + \left(P_1^{sat} - P_2^{sat}\right)x_1\right] \tag{3-77}$$

Where P is the total pressure and P_1^{sat} are the saturation pressures of component 1 and 2

Differentiating equation (3-78) and taking the limit as $x_1 \rightarrow 0$ gives the following:

$$\left(P_D \big/ x_1 x_2\right)_{x_1=0} = \left(\partial P \big/ \partial x_1\right)_{x_1=0} - P_1^{sat} + P_2^{sat} \tag{3-78}$$

The term on the left hand side of equation (3-79) is determined by extrapolating a plot of P_D/x_1x_2 vs. x_1 to $x_1 = 0$. If the slope of P_D/x_1x_2 is not linear, then Maher and Smith suggest that x_1x_2/P_D be plotted against x_1. Thus, as shown by Raal et al. (2006), the partial derivative of pressure with respect to liquid composition is related to the infinite dilution activity coefficient by:

$$\gamma_1^{\infty} = \varepsilon_1^{\infty}\left(P_2^{sat} \big/ P_1^{sat}\right)\left(1 + \beta_2\left(1 \big/ P_2^{sat}\right)\left(\partial P \big/ \partial x_1\right)_T^{x_1=0}\right) \tag{3-79}$$

$$\varepsilon_1^{\infty} = \exp\left(\frac{\left(B_{11} - V_1\right)\left(P_2^{sat} - P_1^{sat}\right) + \delta_{12}P_2^{sat}}{RT}\right) \tag{3-80}$$

$$\beta_2 = 1 + P_2^{sat}\left(B_{22} - V_2/RT\right) \tag{3-81}$$

$$\delta_{12} = 2B_{12} - B_{11} - B_{22} \tag{3-82}$$

where, B_{11} and B_{22} are the second virial coefficients of the pure components one and two respectively, and B_{12} is the second virial cross coefficient. V_1 and V_2 represent the liquid molar volumes of components one and two respectively. The accuracy of the infinite dilution activity Coefficient depends on the accuracy of the calculated partial derivative in Equation (3-80). This method was employed in this work to calculate the infinite dilution activity coefficient values from the experimental VLE data measured.

3.6.1 Excess Thermodynamic Properties

The fundamental excess property relation is given as:

$$d\left(\frac{nG^E}{RT}\right) = \left(\frac{nV^E}{RT}\right)dP - \left(\frac{nH^E}{RT^2}\right)dT + \sum \ln \gamma_i dn_i \tag{3-83}$$

For the restrictive case of constants P, T and x, equation (3-84) reduces to:

$$\left(\frac{V^E}{RT}\right) = \left(\frac{\partial\left(G^E/RT\right)}{\partial P}\right)_{T,x} \tag{3-84}$$

$$\left(\frac{H^E}{RT}\right) = -T\left(\frac{\partial\left(G^E/RT\right)}{\partial T}\right)_{P,x} \tag{3-85}$$

The molar Gibbs energy (G^E) as a function of composition can be calculated from experimental VLE data by using the parameters of the appropriate correlating equations. It is important that three isotherms are examined in order to calculate $\left(\frac{\partial\left(G^E/RT\right)}{\partial T}\right)_{P,x_1}$. It is also necessary that the plot of $\left(\frac{\left(G^E/RT\right)}{RT}\right)$ vs T is linear in order to estimate $\left(\frac{\Delta\left(G^E/RT\right)}{\Delta T}\right)$.

The excess enthalpy, H^E (heat of mixing) can therefore be calculated. If G^E and H^E are known, then excess entropy S^E can be determined from the excess property relation:

$$G^E = H^E - TS^E \tag{3-86}$$

This method of evaluating excess properties from experimental isothermal VLE data is limited by the accuracy of the measured data, the linearity of the $\left(\frac{\left(G^E/RT\right)}{RT}\right)$ vs T plot, and the accuracy of the excess Gibbs free energy model used to correlate the measured data (Moodley, 2012).

CHAPTER 4

EQUIPMENT AND EXPERIMENTAL PROCEDURE

4.1 Equipment description

Many factors are to be considered when designing equipment for experimental purposes. Since the experimental data are expected to be of benefit for industrial applications, the equipment should be able to produce as accurate results as possible. It is also necessary that the design and mode of operation of the equipment should be made as simple as possible. Based on the conditions chosen for this work (at temperatures below 100^0C and sub atmospheric pressures), the dynamic glass recirculating VLE still designed by Raal (Raal &Mühlbauer, 1998) and which was later modified by Bhownath (2008) was used to carry out the measurements in this work. However, there are limitations to the usage of this still because the still was not designed to operate above atmospheric pressure and also the septa used on the still cannot withstand temperatures beyond 180^0C.

4.1.1 The dynamic VLE recirculating still

The VLE recirculating still utilized in this work had been previously used by Rinay Bhownath (2008) and a similar type of still had been used and greatly described by Ndlovu (2005). The schematic diagram of the VLE apparatus is presented in Figure 4-1. For more details on the mode of operation of the still, readers are referred to the work of Rinay Bhownath (2008).

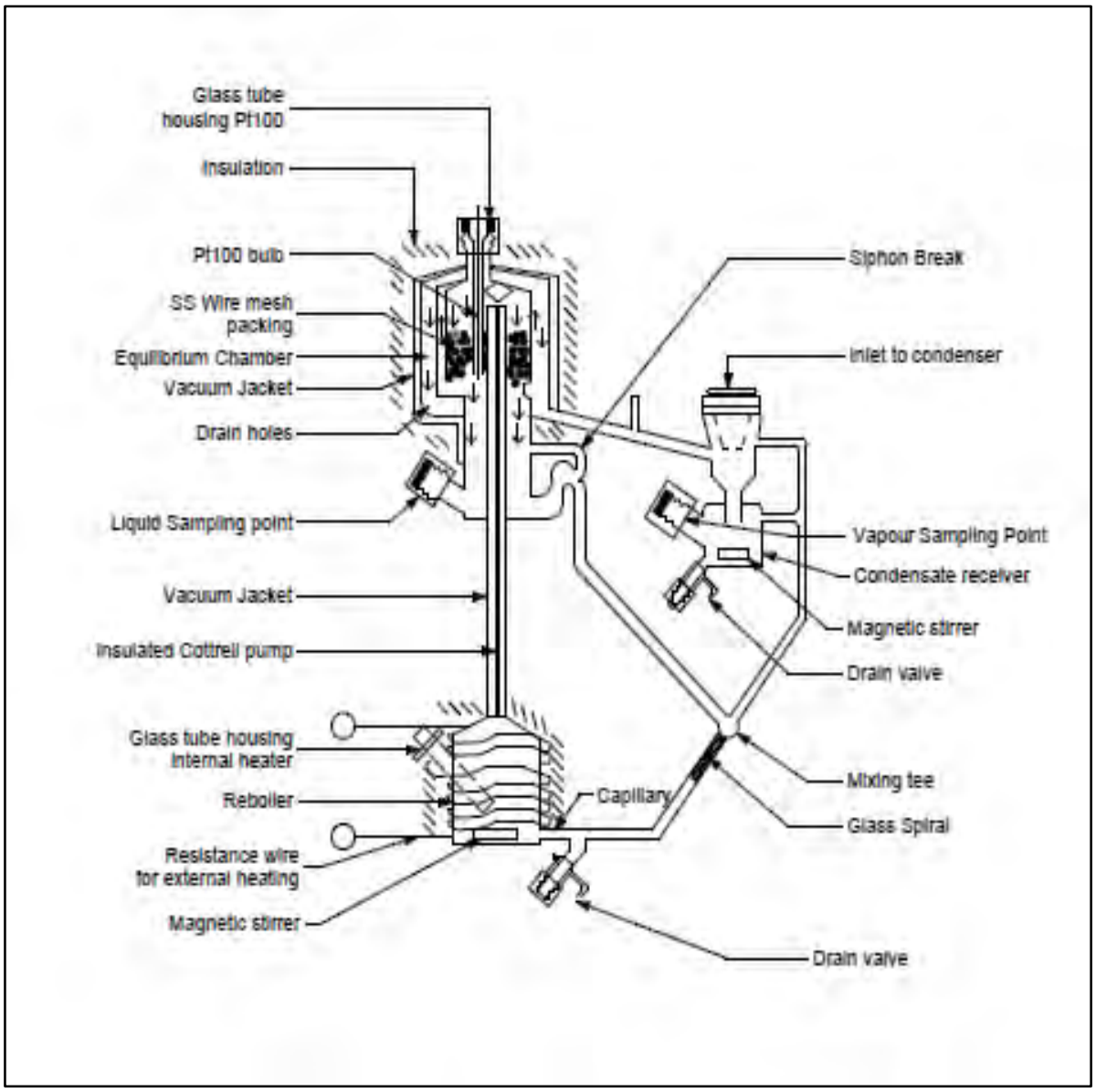

Figure 4-1: Modified VLE apparatus of Bhownath (2008)

The VLE apparatus used for this work consists of the following equipment:

- The VLE dynamic recirculating still
- A labotech water bath with a pump filled with ethylene glycol as the cooling medium
- A 25L ballast tank
- Two solenoid valves for controlling the pressure
- A WIKA P10 pressure transmitter
- Pt-100 temperature sensors

- An HP (model 34401) multi-meter for setting the voltage needed to bring about boiling and for reading the equilibrium temperature in ohms
- A labotech chilling unit
- A vacuum pump controller unit
- A shinko ACS pressure controller
- A computer
- DC power supply unit
- A helium gas cylinder
- A Schimadzu 2014 gas chromatograph

The reboiler is loaded with the mixture through the liquid or vapour sampling point and brought to boiling with the aid of the internal and external heaters. The internal heater (principle heating) is made up of heater cartridge placed in a glass tube in the reboiler which brings about smooth boiling, precise control of circulation rate and established nucleation sites for smooth boiling while the external heater consists of a nichrome wire that is wrapped around the reboiler and this is used to compensate for the heat loss to the environment. As the mixture boils, the mixture flows upward in the Cottrell pump into the equilibrium chamber. The central vacuum insulated cottrell tube consists of a thermal lift pump which helps the upward movement of the mixture into the equilibrium chamber. The movement of the vapour around the equilibrium chamber provides an important role of thermal lagging of the chamber. The equilibrium chamber is confined in a vacuum jacket in order to ensure adiabatic operation within it. It is packed with packed 3mm rolled wire mesh cylinders which allow for sufficient mass transfer between the phases through interfacial surface area expansion and contact between the vapour and liquid phases. A Pt-100 temperature sensor is housed in a glass tube placed within the equilibrium chamber and extends to the base of the chamber to measure the equilibrium temperature of the mixture.

Both phases are separated in the equilibrium chamber, the equilibrium vapour is condensed and collected into the condensate receiver and the equilibrium liquid flows downwards through the holes into the liquid sampling point. The vapour and liquid are both combined in the mixing chamber (mixing tee) and extensively mixed by the use of a glass spiral mixer thereafter, the stream enters into the reboiler. Back flow is prevented with the help of a

siphon break which was introduced to the still by Joseph (2001). There is also a capillary section at the base of the reboiler which prevents backflow of the returning phases.

4.1.2 Pressure measurement and control

A WIKA model P10 pressure transmitter which can measure from 0 to 1 bar of pressure was used to measure the system pressure in this work. Working pressure was set through the use of a SWS ACS01M software installed on the PC connected to a Shinko ACS pressure controller. Pressure was controlled and stabilized through the use of a vacuum pump that was connected to a 25 L ballast tank. Two solenoid valves were connected to the apparatus which also controlled the system pressure. The uncertainty in the pressure measurement was estimated to be $\pm$ 0.02 kPa and controlled within 0.01 kPa during operation; this will be discussed in the next chapter.

4.1.3 Temperature measurement and control

The temperature in the equilibrium chamber was measured with a Pt-100 temperature sensor confined in a glass tube and extends to the base of the chamber to provide contact with the liquid and vapour phases. This sensor was connected to a HP digit multi-meter which enabled the equilibrium temperature to be read in resistance. However, for isothermal operation, the equilibrium temperature can be equally controlled from a SWS ACS01M software programme installed on the PC by regulating the set pressure of the system. Increase in pressure brings about increase in temperature and vice versa. The uncertainty in the temperature measurement was estimated to be ± 0.06 K and controlled within 0.04 K.

4.1.4 Sampling and composition analysis

1ml each of equilibrium samples were carefully withdrawn from both vapour and liquid sample traps through a chemically resistance septum with a gas-tight liquid syringe. This was done with care in such a way that the operation of the system was not interfered with. The withdrawn samples were injected separately into two separate vials and analysed. The test system analysis was done with a refractometer while the new binary VLE measurements were carried out with the gas chromatograph.

An ATAGO 7000α refractometer with a reported uncertainty of 0.0001 was used for the phase composition measurements of the test system. Gas chromatography was chosen for phase composition analysis for the new systems measured in this work due to its simple mode of operation, accuracy, reproducibility, convenience, and it also requires small amounts of samples for detection.

A Schimadzu 2014 GC with a thermal conductivity detector was employed to carry out the composition analyses in this study. A flame ionization detector (FID) was not used since water being one of the impurities in alcohols (part of the systems measured) cannot be detected with an FID. Helium was used as the carrier gas. Several columns were tested for accurate separation of the components but none gave better separation than the CRS Porapak Q column. This packed column has a length of 4meters and 2mm inner diameter with a maximum allowable operating temperature of 250 ºC.

4.2 Experimental procedure

For accurate VLE measurements, it is necessary for researchers to apply a thorough procedure in performing experiments in the laboratory as this would affect the experimental data. An inconsistent experimental procedure would compromise data quality. Good knowledge of the chemicals and the auxiliary equipment on the apparatus cannot be overemphasized.

This chapter deals with the detailed discussion of the experimental procedures undertaken in this work in order to achieve accurate VLE data. It focuses on the preparation of the VLE apparatus and the chemicals used, operation of the still and the calibrations of the equipment utilized.

4.2.1 Preparation of the VLE still

4.2.1.1 Leak Detection

The presence of leaks in the still or on the joints can lead to inaccurate data measurement. Leaks cause fluctuation in the system pressure which leads to difficulty in controlling and stabilizing the pressure or temperature. Therefore, it is necessary to detect and eliminate all form of leaks from the still before starting any experimental run as all the experimental works were undertaken below atmospheric pressure.

Detection of leaks was done by subjecting the still under vacuum at a pressure set point below atmospheric pressure. It was then isolated for a period of time by switching off the vacuum pump and all the valves. The rate of pressure increase was observed carefully and recorded. Liquid acetone was added to the joints on the still and a minute spike in the set pressure which is usually caused by flashing of the liquid acetone indicated a leak. Vacuum grease was therefore applied to all the joints in order to eliminate the leaks.

4.2.1.2 Cleaning of the VLE equipment

The VLE still must be void of impurities as these may contaminate the chemicals and affect the accuracy of the data. Therefore cleaning of the still is important in order to eliminate all impurities. This was achieved by operating the still with pure acetone in it at atmospheric pressure for 30 minutes after which the still was drained and the process was repeated until the still was completely cleaned. All valves and caps were then opened and the still was left to air-dry for a few. The remaining acetone in the still was vapourised by operating the still under vacuum at very low pressure of about 5 kPa.

4.2.1.3 Preparation of the chemical system

Not only must the still be free from impurities, but the chemicals to be used also must be checked by various means to make sure that no impurity was present. Three major purity checks were performed for each chemical used in this work to ensure that the purity was in accordance with that stated by the supplier. The results were found to be satisfactory before further usage. A gas chromatograph (GC) was used to obtain the area fraction of each chemical which was compared with the stated purity by the supplier. The refractive index

was also checked for each chemical using the ATAGO 7000α refractometer and finally an Anton Paar DMA 5000 density meter was used to check the density of the chemicals. The results of these purity checks are presented in Chapter 5.

4.2.2 Temperature, pressure and GC calibration

4.2.2.1 Temperature calibration

The Pt-100 (Type A) temperature sensor was calibrated against a WIKA CTH 6500 standard temperature sensor. The Pt-100 sensor was closely tied to the standard sensor and both were inserted into a WIKA CTB 9100 oil bath. The temperature controller of the oil bath was used to set a specific temperature reading within the bath. At each set point, the temperature was allowed to stabilize for about 30 minutes after which the readings of the two sensors were taken consistently. This procedure was repeated for various temperature readings within the desired temperature range. The readings of the Pt-100 sensor were displayed in resistance on the HP 34401A multimeter while the actual temperature readings from the standard sensor were displayed in degree Celsius and these readings were plotted against the displayed resistance readings of the Pt-100 sensor.

The plot gave a linear relationship as shown in Figure 4-2. The standard uncertainty estimated for the temperature calibration according to the NIST standards (NIST Technical Note 1994) was ±0.1 K (Type B evaluation according to NIST) and controlled within 0.04 K.

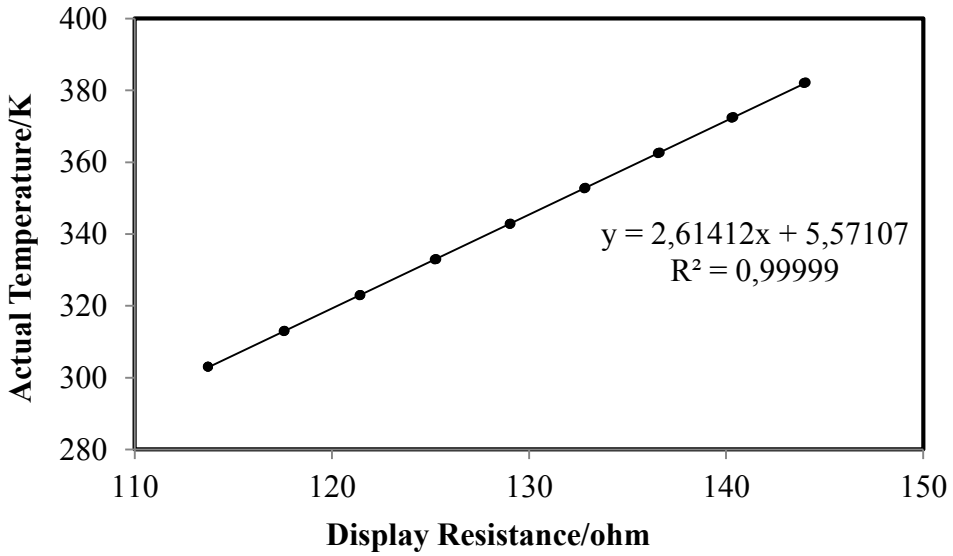

Figure 4-2: Temperature calibration plot for the Pt-100 temperature sensor used in the VLE still.

4.2.2.2 Pressure calibration

The pressure calibration was done by an in-situ calibration method where the WIKA P- 10 pressure transmitter and a standard pressure transmitter were used to measure the system pressure. The two transmitters were connected in series to the still and a Shinko ACS pressure controller was used to control the pressure within the still with the aid of a vacuum pump. At each set point, the pressure was allowed to stabilize and the readings were taken. The readings from the standard transmitter were recorded from the WIKA CPH 6000 standard display unit. Similar to the temperature calibration, this process was also done for various pressure readings. The actual pressure readings from the standard transmitter were plotted against the display pressure readings from the P-10 pressure transmitter to obtain the equation relating the two. Figure 4-3 represents the calibration plot for the pressure transmitter. The standard uncertainty estimated for the pressure calibration was ± 0.04 kPa.

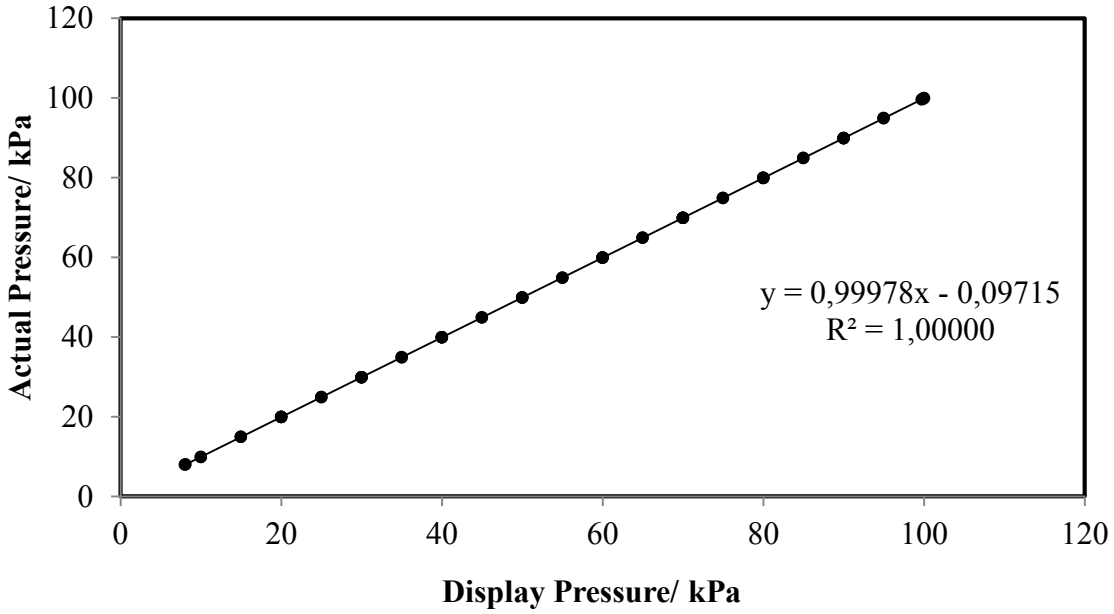

Figure 4-3: Pressure transmitter calibration plot for the VLE still

4.2.2.3 Gas chromatograph detector calibration

A Shimadzu 2014 GC with a thermal conductivity detector (TCD) was used for the analyses of the phase compositions in this work. A 4 m × 1/8 inch stainless steel CRS Porapak Q packed column was used for the separation of the components. The choice of this column was based on its ability to give good separation of the components, produce sharp and reproducible peaks. The column was conditioned before usage in order to eliminate any impurity or material that may produce ghost peaks in the chromatogram and adversely affect the performance of the column.

The column conditioning was done by heating the column at a temperature 25ºC lower than the maximum operating temperature of the column for 17 hours with helium gas flowing through. The operating condition for the GC for each binary system measured in this work is shown in Section 5-4.

The calibration method used was the area ratio method proposed by Raal and Mühlbauer (1998). This method employs the use of area ratios to determine the response factors of the GC TCD. Liquid samples for binary mixtures were prepared by gravimetrically weighing mole fractions ratios (x_1/x_2) evenly over the composition range. The number of moles (n) of a component passing through the detector of the GC is proportional to the peak area (A) obtained from an electronic integrator software via a computer.

$$n_i = \mathrm{A}_i F_i \tag{4-1}$$

Where F_i is the proportionality constant also known as the response factor. Raal and Mühlbauer (1998) proposed the use of area ratios since absolute areas cannot be used because the amount of sample injected is not generally reproducible. The response factor for a binary mixture is represented as:

$$\frac{n_1}{n_2} = \left[\frac{F_1}{F_2}\right]\left[\frac{A_1}{A_2}\right] = \frac{x_1}{x_2} \tag{4-2}$$

Where F_1/F_2 is the response factor ratio and is also the slope obtained when A_1/A_2 is plotted against x_1/x_2 over the full composition range. F_1/F_2 is the proportionality constant for the plot passing through the origin. The inverse of the slope obtained for the plot (provided the plot is linear) of A_2/A_1 against x_2/x_1 should be equal to F_1/F_2 (i.e. F_2/F_1 equals the inverse of F_1/F_2 and vice versa). These plots should however pass through the origin. The detector type and

system under investigation determine the shape of the calibration curves, therefore for thermal conductivity detectors, nonlinear plots are not uncommon.

4.3 Refractometer operation

The analysis for the test system (cyclohexane + ethanol) measured in this work was done with the ATAGO ® 7000α refractometer. The measuring surface of the refractometer was cleaned with pure liquid acetone before commencing the measurements. It was then switched on and set to zero adjust by using distilled water as indicated by the supplier. Calibration of the refractometer and measurements for the test system were carried out at 20 ºC. For the calibration, liquid samples for binary mixture were also prepared by gravimetrically weighing mole fractions of x_1/x_2 evenly over the composition range as similar for the GC detector calibration. Samples were analysed five times and an average deviation for the refractive indexes within a tolerance of 0.0001 was obtained. At equilibrium, vapour and liquid samples were analysed on the refractometer for the test system after each of the operations described above (isothermal and isobaric) had been carried out. It was ensured that the surface of the refractometer was cleaned with liquid acetone after each sampling. Second order polynomial curves were obtained when mole fractions x_1 and x_2 were plotted against the refractive indexes. The uncertainty for the refractometer was reported as 0.0001. Plots for the calibration and measurements of the test system are shown in Section 5-5.

4.4 Operating procedures

4.4.1 Isobaric operation

The following outlined steps were taken in order to achieve successful isobaric operation.

Step 1: The Labotech chilling unit and the cold finger were switched on to allow the temperature of the ethylene glycol solution in the water bath to sufficiently cool to about -5ºC. Once this set point is reached, the DC power supply to the HP multi-meter, pressure controller and display, computer and vacuum pump were switched on.

Step 2: After switching on all these devices, the clean still was then charged with one of the pure components up to a visible level of about ±4 cm above the boiling chamber. This is to ensure that when boiling begins, the liquid will be forced up the Cottrell pump.

Step 3: The vacuum pump was then switched on. This maintains and control the pressure set in the still with the help of the two solenoid valves at sub-atmospheric pressure.

Step 4: The desired operating pressure was set on the Shinko ACS pressure controller. The pressure then decreased to the set-point pressure.

Step 5: Boiling of the liquid in the reboiler was then brought about by switching on the internal and external heaters. The internal heater provided the actual boiling while heat losses to the environment were compensated for by the external heater.

Step 6: After step 4, the stirrers motors for the reboiler and the vapour sampling point were switched on. This was to provide sufficient stirring of the component in order to prevent temperature gradients.

Step 7: The voltage of the internal heater was carefully increased until the plateau region (i.e. the slope) was established. This is the point at which there is no increase or decrease in the temperature of a boiling mixture regardless of any slight change in the input voltage as stated by Kneisl et al. (Kneisl et al., 1989).

Step 8: Once the plateau region had been achieved, the system was observed carefully to attain equilibrium i.e. at the time when the system temperature remains constant. This was also accompanied by large drop rates and good circulation rates. Adequate heat is important to be applied in order to have good circulation rate and vigorous upward movement of the liquid in the Cottrell tube, where the drop rate from the condenser was observed to determine the circulation rate. For most systems, it takes about 30-45 minutes to attain equilibrium. However, for all the systems measured in this work 50 minutes was found sufficient to attain equilibrium.

Step 9: At the equilibrium point, the temperature was recorded and the liquid and vapour samples were withdrawn with a gas tight liquid syringe for GC analysis. A 0.5µl gas tight liquid GC syringe was used to inject into the samples into the GC. Three to four samples of each phase were analyzed in order to ensure reproducibility and to have an average deviation within 0.001 tolerances for the area ratios.

Step 10: After analyzing the vapour and liquid samples, the vapour and liquid sample traps were drained such that the total volume of the liquid removed was 4 ml. Approximately 4 ml

of the second component was injected into the still through the liquid sample trap and the system was left to attain a new equilibrium point after which the vapour and liquid samples were withdrawn for GC analysis.

Step 11: Thereafter, the procedure was repeated until half of the entire composition range had been completed.

Step 12: The operation of the still was then stopped and the still was left to cool. The VLE still was cleaned and dried and then charged with the second component.

Measurements for the second half of the composition range were then done repeating the same procedures of the first half. This procedure helps to obtain many points in dilute regions and also verifies the accuracy of the measurement since the two halves of the phase diagram must meet without discontinuity (Nala, 2012). Figure 4-4 gives the summary of the procedures described above.

4.4.2 Isothermal operation

The successful isobaric operation of the VLE still is really important because the isothermal operation of the still is dependent on the isobaric conditions and manual control of the system temperature. The operating procedures for both operations are therefore the same. Figure 4-5 gives the summary of the procedures used for isothermal operation in this work as outlined below:

Step 1: A particular pressure was set for the system to attain equilibrium, the equilibrium temperature at this point was found to be close to the desired operating temperature.

Step 2: The temperature of the system was then controlled manually to the desired value by adjusting the system pressure. Increasing or decreasing the pressure set point would increase or decrease the system temperature respectively. The pressure at that time was then noted.

Step 3: Once this was done, the plateau region (was found and the system was left to reach equilibrium.

Step 4: The vapour and liquid samples were then taken and analysed in the same manner as in the isobaric operation.

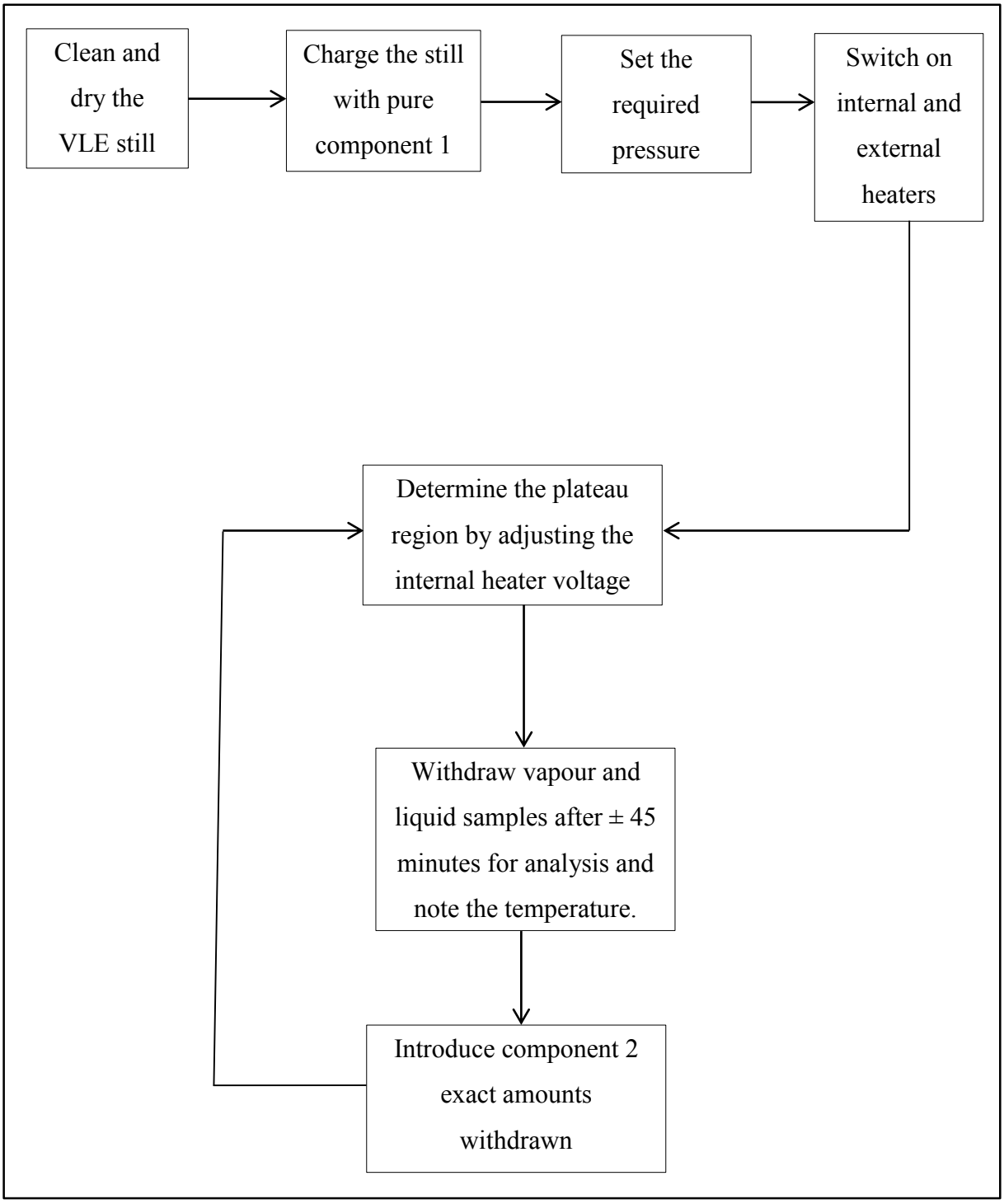

Figure 4-4: Flow diagram to show the steps taken to measure isobaric VLE data using a low pressure dynamic VLE recirculating still.

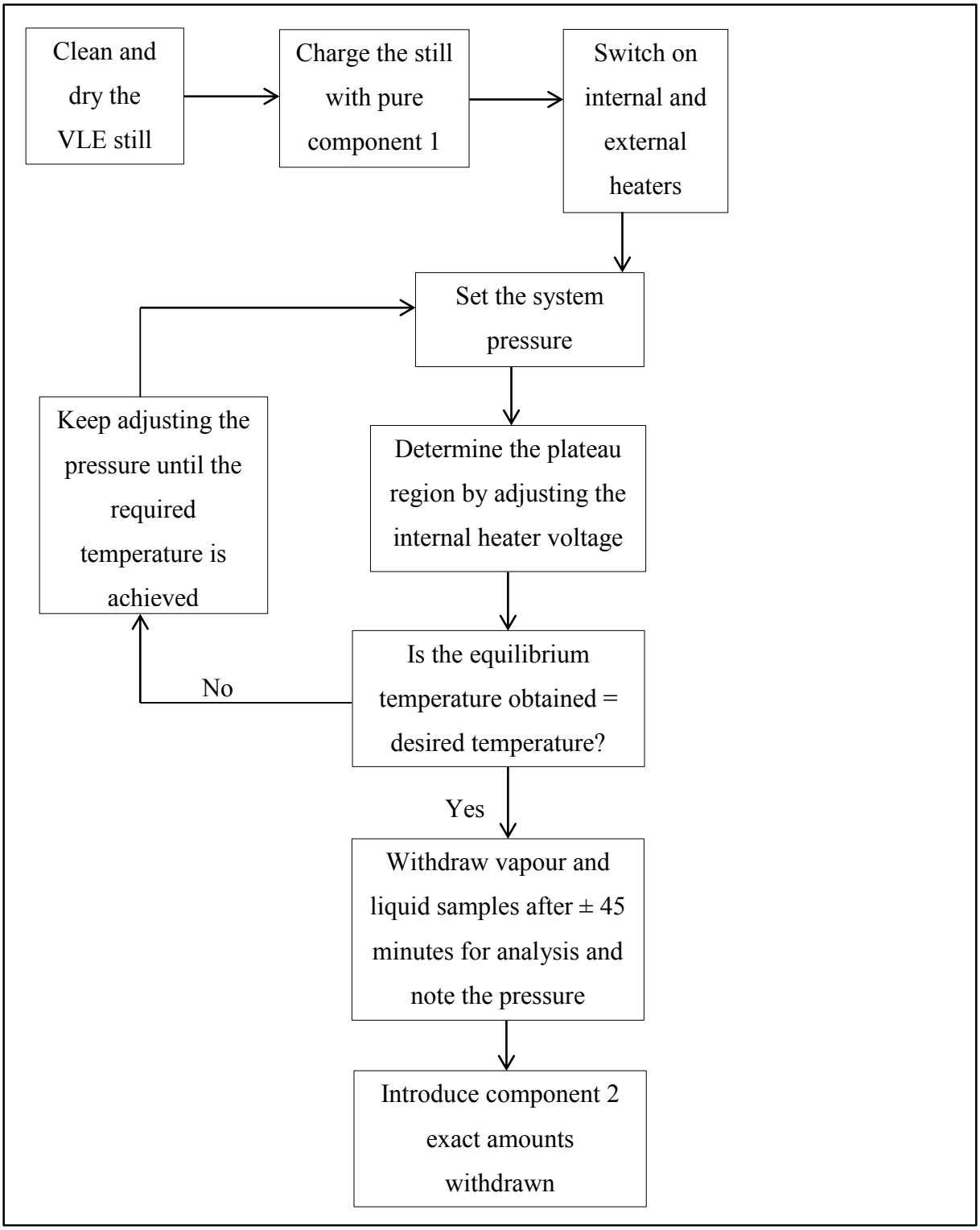

Figure 4-5: Flow diagram to show the steps taken to measure isothermal VLE data using a low pressure dynamic VLE recirculating still.

4.5 Plateau region

In phase equilibrium measurement, the plateau region is important to operate in order to achieve accurate boiling point measurement. The concept of the plateau region is that as the mixture boils, increasing the energy input of the internal heater results in increase in the temperature of the boiling mixture. This continues until a certain point is reached where further slight increase or decrease in the input energy does not cause any change in the temperature of the boiling mixture. This point is referred to as the plateau region. Further heating beyond the plateau region results in superheating and increasing the input energy results in increase in the temperature of the boiling mixture. It is therefore important to supply adequate energy input to the reboiler for the system to operate in the plateau region. More details on the plateau region are presented by Kneisl et al., 1989. Figure 4-6 illustrates the concept of the plateau region for a well behaved system.

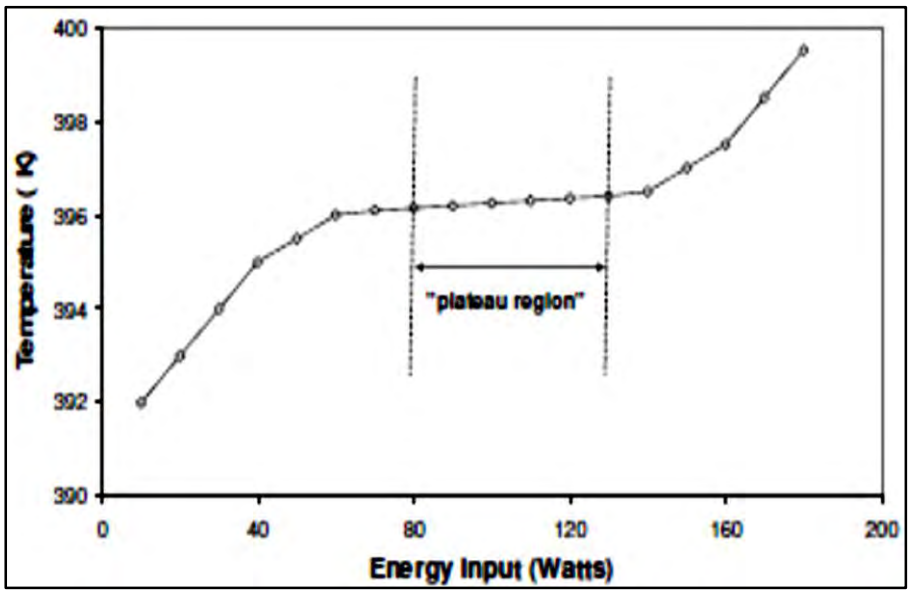

Figure 4-6: Temperature vs energy input curve showing the "plateau region" for a well behaved system (Pillay, 2009)

CHAPTER 5

EXPERIMENTAL RESULTS

The results of all the measurements carried out in this work are detailed in this chapter. The accuracy of the temperature, pressure and composition measurement as well as the purity of the chemicals used has great influence on the accuracy of the measured experimental data. In order to ensure proper operation of the still, a test system consisting of cyclohexane (1) + ethanol (2) was therefore measured at 40 kPa and 313 K using the operating procedures described in Chapter 4. This non ideal system was chosen because there are reliable literature data available that could be used as comparison.

The purities of the chemicals used are discussed and presented in Section 5-1. The measured vapour pressure data are compared with literature and presented in Section 5.3. This chapter also includes the results obtained for the test system, the new isothermal VLE data for the systems; 1-propanol + 4-methyl-2-pentanone (at 338.15, 353.15 and 368.15 K), 2-propanol + 4-methyl-2-pentanone (at 323.15, 338.15 and 353.15 K) and 2-pentanone + 2-methylpropan-1-ol (at 343.15, 358.15 and 363.15K). The analysis and discussion of these experimental measurements are detailed in Chapter 6.

5.1 Chemical Purity

Purity checks were performed on each chemical before commencing the measurements. 2-propanol, 4-methyl-2-pentanone, ethanol, 2-pentanone, and 2-methylpropan-1-ol were purchased from Merck, while 1-propanol was purchased from Sigma-aldrich and cyclohexane was purchased from Fluka. The purity of these chemicals was verified with; the GC (area fraction), the refractometer and the density meter. The refractive index of each chemical was measured at 293 K using the ATAGO ® 7000α with a reported uncertainty of 0.0001 and the results were compared with literature. The density of each chemical was measured using the Anton Paar DMA 5000 density meter with a reported uncertainty of ± 0.0001 g/cm3 in density and ± 0.01 K in temperature. The values obtained were compared with literature. There was no further purification of these reagents as all indicated no significant impurities.

Table 5-1: Chemical purities and refractive indices.

Reagents	Refractive index (293.15 K)		GC analysis (Peak Area %)	Min. purity (Mass %)[b]
	Exp	Lit[a]		
Ethanol	1.3613	1.3611	99.8	≥99.5
1-propanol	1.3851	1.3850	99.3	≥99.0
Cyclohexane	1.4264	1.4266	99.7	≥99.5
4-methyl-2-pentanone	1.3959	1.3962	99.8	≥99.0
2-methylpropan-1-ol	1.3959	1.3955	99.1	≥99.0
2-pentanone	1.3906	1.3895	99.3	≥99.0
2-propanol	1.3772	1.3776	99.4	≥99.5

[a]CRS Handbook of Chemistry and Physics 76th Edition (David R. Lide, 1995-1996)

[b]as stated by the supplier

5.2 Uncertainty measurement

Uncertainty and error are often used interchangeably but there are significant differences between the two. Error or deviation can be defined as the difference between a measured value and the true value while uncertainty is defined as the range within which the true value of a measured variable has the possibility of residing. For each data point there is always a value of error and which could be corrected if the sources were known. All non-negligible possibilities of uncertainty must be identified when estimating the uncertainty of an experimental result. These possibilities are mostly attributed to the instruments used for the experiment. Table 5-2 below summarizes the estimated uncertainty of the temperature, pressure and composition for this work. The combined standard uncertainty *(u_c)* of a measured variable (θ) is given by:

$$u_c = \pm\sqrt{\sum_i u_i(\theta)^2} \tag{5-1}$$

$u_i(\theta)$ is the standard uncertainty from any possible source like, the errors induced from the temperature and pressure calibration standards, calibration polynomials, reproducibility etc. Considering all possible sources of uncertainty in the temperature and pressure measurement, the combined standard uncertainty is written for each respectively as:

$$u_c(T) = \pm\sqrt{u_{rep}(T)^2 + u_{calib}(T)^2 + u_{prec}(T)^2} \quad (5\text{-}2)$$

$$u_c(P) = \pm\sqrt{u_{rep}(P)^2 + u_{calib}(P)^2 + u_{prec}(P)^2} \quad (5\text{-}3)$$

where $u_{rep}(x)$ is the standard uncertainty due to repeatability of measurement (Type B, NIST) (temperature, pressure or composition), $u_{calib}(x)$ is the standard uncertainty due to calibration correlation (Type B, NIST) and $u_{prec}(x)$ is the standard uncertainty due to precision error from instrument as specified by supplier.

The uncertainty in phase composition measurement through the method of Raal and Mühlbauer is linked to three sources: the uncertainty from the mass balance, uncertainty in converting TCD areas to composition and uncertainty due to repeatability. The combined uncertainty for composition measurement is given as:

$$u_c(x_i) = \pm\sqrt{u_{rep}(x_i)^2 + u_{calib}(x_i)^2} \quad (5\text{-}4)$$

Where:

$$u_{calib}(x_i) = \pm\sqrt{u_{corr}(x_i)^2 + u_{bal}(x_i)^2} \quad (5\text{-}5)$$

Table 5-2: Experimental uncertainties for temperature, pressure and composition of the measured VLE binary systems.

System	$u_c(P)$/kPa	$u_c(T)$/K	$u_c(x)$
Cyclohexane (1) + ethanol (2)	± 0.02	± 0.06	0.002
1-propanol (1) +4-methyl-2-pentanone (2)	± 0.02	± 0.06	0.005
2-propanol (1) + 4-methyl-2-pentanone (2)	± 0.02	± 0.06	0.003
2-pentanone (1) + 2-methylpropan-1-ol (2)	± 0.02	± 0.06	0.005

5.3 Vapour pressures

Vapour pressure measurement for each of the chemicals is necessary as this also serves as a measure for testing the operation of the equipment and the experimental procedures. The vapour pressures of each of the pure chemicals used in this work namely; ethanol, cyclohexane, 4-methyl-2-pentanone, 2-methylpropan-1-ol, 2-pentanone, 1-propanol and 2-propanol were measured and compared with values from two literature sources. Deviations between experimental data and literature data were calculated for the comparison The data as well as the deviations are presented in Table 5-3 to 5-9 The experimental vapour pressure data were compared to the literature values in NIST and Poling et.al. (2001). Experimental vapour pressure data for 2-propanol were compared to only the literature sources of Poling et.al.(2001) as there were no sources available in NIST at the temperature range for this work. The plots also show the comparisons between the measured values and the two literature values. These data were regressed to obtain the parameters for the Antoine equations.

The absolute difference between the experimental and literature data is given by:

$$|\Delta X| = X^{\text{experimental}} - X^{\text{calculated}} \qquad (6\text{-}1)$$

Table 5-3: Experimental Vapour pressure data for 1-propanol.[a]

P (kPa)	*T (K)*	ΔP *(kPa)*[b]	ΔP *(kPa)*[c]	ΔT *(K)*[b]	ΔT *(K)*[c]
14.90	326.98	0.2827	0.2083	0.0212	0.1139
25.89	338.09	0.1520	0.2085	0.0613	0.1056
29.90	341.12	0.2930	0.3426	0.0943	0.1289
39.89	347.45	0.5780	0.6132	0.1237	0.1432
51.21	353.14	0.7753	0.8009	0.1698	0.1814
59.89	356.86	0.8359	0.8595	0.1803	0.1898
69.89	360.59	0.8117	0.8388	0.2096	0.2193
79.88	363.91	0.6914	0.7282	0.2326	0.2445
93.89	368.02	0.3710	0.4311	0.2708	0.2879
99.88	369.61	0.1828	0.2563	0.2923	0.3123

a standard uncertainties u are u(P) = ± 0.02 kPa and u(T) = ± 0.06

b Poling et al.,2001

c NIST Chemistry Web Book

$\Delta X = Xexp - Xlit$

Table 5-4: vapour pressure data for 2-methylpropan-1-ol[a]

P (kPa)	*T (K)*	*ΔP (kPa)[b]*	*ΔP (kPa)[c]*	*ΔT (K)[b]*	*ΔT (K)[c]*
9.90	329.02	0.3599	0.3065	0.0087	0.0847
20.45	343.05	0.0908	0.2679	0.1234	0.0460
29.90	351.10	0.4093	0.6926	0.1647	0.0357
41.04	358.19	0.6165	1.0137	0.1385	0.0818
50.94	363.16	0.6451	1.1328	0.0161	0.2141
59.89	367.21	0.5515	1.1127	0.1190	0.1163
69.89	371.08	0.3212	0.9563	0.1055	0.1326
79.88	374.47	0.0328	0.6680	0.0468	0.1921
89.88	377.56	0.5018	0.2570	0.0067	0.2314
99.88	380.36	1.0784	0.2685	0.0534	0.2896

a standard uncertainties u are u(P) = ± 0.02 kPa and u(T) = ± 0.06

b Poling et al.,2001

c NIST Chemistry Web Book

ΔX = Xexp - Xlit

Table 5-5: vapour pressure data for 2-pentanone [a]

P (kPa)	***T (K)***	***ΔP (kPa)[b]***	***ΔP (kPa)[c]***	***ΔT (K)[b]***	***ΔT (K)[c]***
19.90	329.59	0.7477	0.5940	0.4744	0.2920
34.33	343.47	0.4146	0.2328	0.4350	0.2958
39.89	347.55	0.3260	0.1402	0.4198	0.2931
49.89	353.77	0.2425	0.0556	0.3309	0.2234
58.58	358.45	0.2527	0.0699	0.3077	0.2144
69.30	363.50	0.3711	0.1983	0.2684	0.1904
79.88	367.91	0.5997	0.4407	0.2471	0.1824
89.88	371.68	0.9129	0.7700	0.2308	0.1773
98.88	374.74	1.2720	1.1457	0.1621	0.1179

[a] standard uncertainties u are *u(P) = ± 0.02 kPa and u(T) = ± 0.06*

[b] Poling et al.,2001

[c] NIST Chemistry Web Book

$\Delta X = X^{exp} - X^{lit}$

Table 5-6: vapour pressure data for 4-methyl-2-pentanone [a]

P (kPa)	*T (K)*	*ΔP (kPa)[b]*	*ΔP (kPa)[c]*	*ΔT (K)[b]*	*ΔT (K)[c]*
9.22	322.82	0.1544	0.1014	0.0056	0.1268
9.90	324.41	0.1290	0.0739	0.0195	0.0995
17.52	337.85	0.1429	0.2007	0.0994	0.0207
18.41	339.11	0.1706	0.2264	0.1262	0.0531
31.36	352.88	0.4354	0.4202	0.0693	0.0561
32.13	353.54	0.4426	0.4212	0.0877	0.0693
39.89	359.60	0.4540	0.3578	0.1642	0.0939
53.99	368.46	0.2650	0.0099	0.3679	0.2065
69.89	376.36	0.2639	0.7921	0.6779	0.4190

[a] standard uncertainties u are *u(P) = ± 0.02 kPa and u(T) = ± 0.06*

[b] Poling et al.,2001

[c] NIST Chemistry Web Book

$\Delta X = X^{exp} - X^{lit}$

Table 5-7: vapour pressure data for 2-propanol[a]

P (kPa)	*T (K)*	*ΔP (kPa)[b]*	*ΔT (K)[b]*
14.90	314.43	0.5747	0.4222
23.43	323.03	0.3839	0.3026
29.90	327.97	0.2469	0.3009
39.89	333.98	0.0854	0.2255
48.34	338.14	0.0084	0.1765
59.89	342.90	0.0031	0.0931
69.89	346.45	0.0739	0.0556
79.88	349.64	0.2289	0.0604
92.40	353.14	0.5282	0.0168
98.88	354.82	0.7270	0.0097

[a] standard uncertainties u are u(P) = ± 0.02 kPa and u(T) = ± 0.06

[b] Poling et al.,2001

$\Delta X = X^{exp} - X^{lit}$

Table 5-8: vapour pressure data for cyclohexane[a]

P (kPa)	*T (K)*	*ΔP (kPa)[b]*	*ΔP (kPa)[c]*	*ΔT (K)[b]*	*ΔT (K)[c]*
19.90	308.09	0.2112	0.2998	0.0391	0.1429
29.90	318.15	0.0195	0.0660	0.0009	0.0715
39.89	325.80	0.1888	0.0993	0.0186	0.0421
49.89	332.05	0.2806	0.1804	0.0303	0.0269
59.89	337.38	0.2920	0.1753	0.0288	0.0293
69.89	342.06	0.2245	0.0861	0.0183	0.0432
79.88	346.24	0.0811	0.0837	0.0055	0.0610
89.88	349.98	0.1348	0.3303	0.0463	0.0262
99.88	353.46	0.4197	0.6499	0.0333	0.0459

[a] standard uncertainties u are *u(P) = ± 0.02 kPa and u(T) = ± 0.06*

[b] Poling et al.,2001

c NIST Chemistry Web Book

$\Delta X = X^{exp} - X^{lit}$

Table 5-9: vapour pressure data for ethanol[a]

P (kPa)	*T (K)*	ΔP *(kPa)*[b]	ΔP *(kPa)*[c]	ΔT *(K)*[b]	ΔT *(K)*[c]
19.90	315.29	0.2626	0.2715	0.0857	0.0904
29.90	323.45	0.0360	0.0489	0.0158	0.0125
39.89	329.64	0.1156	0.1080	0.0717	0.0607
49.89	334.58	0.1787	0.1846	0.0618	0.0451
59.89	338.79	0.1522	0.1793	0.0955	0.0754
69.89	342.35	0.0390	0.0938	0.0246	0.0030
79.88	345.56	0.1570	0.0682	0.0244	0.0031
89.88	348.46	0.4314	0.3033	0.0301	0.0106
99.88	351.10	0.7802	0.6077	0.0309	0.0144

[a] standard uncertainties u are $u(P) = \pm 0.02$ *kPa* and $u(T) = \pm 0.06$

b Poling et al.,2001

c NIST Chemistry Web Book

$\Delta X = X^{exp} - X^{lit}$

5.4 Operating conditions for the Shimadzu 2014 gas chromatograph

Tables 5-10 to 5-12 represent the GC operating conditions used for the quantitative analysis of the new systems measured in this work. These conditions were found to be the most appropriate for generating good and sharp peaks for the GC detector calibrations and measurements of the new systems. A Shimadzu 2014 GC with a thermal conductivity detector and a Porapak Q column was used for the phase composition analysis of the three new systems measured in this study. These settings were also used for the GC purity check.

Table 5-10: GC operating conditions for the 1-propanol (1) + 4-methyl-2-pentanone (2) system.

Operating conditions	1-propanol (1) + 4-methyl-2-pentanone (2) system
Carrier gas	Helium
Detector type	TCD
Column used	Porapak Q
Injector temperature (K)	503.15
Injector mode	split less
Carrier gas flow rate (mL/min)	30
Pressure (kPa)	351.4
Temperature control mode	Isothermal
Column temperature (K)	493.15
Detector temperature (K)	503.15

Table 5-11: GC operating conditions for the 2-propanol (1) + 4-methyl-2-pentanone (2) system.

Operating conditions	2-propanol (1) + 4-methyl-2-pentanone (2) system
Carrier gas	Helium
Detector type	TCD
Column used	Porapak Q
Injector temperature (K)	503.15
Injector mode	split less
Carrier gas flow rate (mL/min)	30
Pressure (kPa)	351.4
Temperature control mode	Isothermal
Column temperature (K)	493.15
Detector temperature (K)	503.15

Table 5-12: GC operating conditions for the methyl propyl ketone (1) + 2-methylpropan-1-ol (2) system.

Operating conditions	2-pentanone (1) + 2-methylpropan-1-ol (2) system
Carrier gas	Helium
Detector type	TCD
Column used	Porapak Q
Injector temperature (K)	523.15
Injector mode	split less
Carrier gas flow rate (mL/min)	30
Pressure (kPa)	339.4
Temperature control mode	Isothermal
Column temperature (K)	473.15
Detector temperature (K)	523.15

5.5 Binary vapour-liquid equilibrium measurements

5.5.1 Cyclohexane (1) + ethanol system (2)

A test system of cyclohexane + ethanol was measured at 40 kPa and 313.15 K before commencing the measurement of the new systems. This helps to check the correct operation (isobaric and isothermal operations respectively) of the VLE apparatus. This system was chosen as a test system because it is highly non ideal and there available literature values for comparisons. The vapour and liquid equilibrium sample analysis was done with the ATAGO® 7000α refractometer. The calibration and operation of this refractometer for the test system had been previously discussed in Section 4-3 of Chapter 4. The phase equilibrium data were compared with the literature data of Joseph (2001). The experimental data agree fairly well with the literature source. The discussion is presented in Chapter 6.The refractometer calibration plots, P-x-y, T-x-y and x-y plots are shown below.

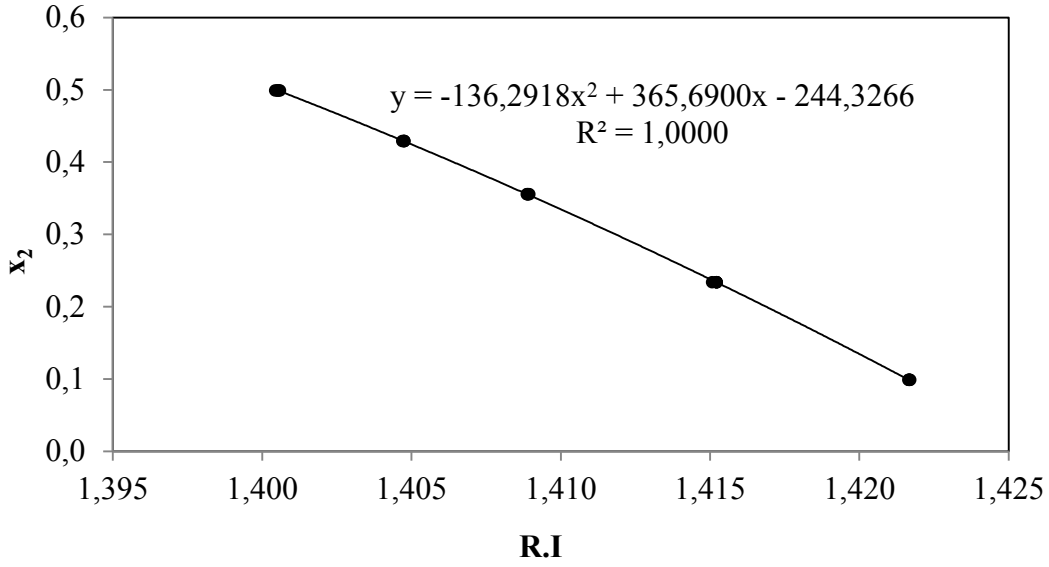

Figure 5-1: Refractometer calibration plot for the cyclohexane (1) + ethanol (2) system (ethanol dilute region) at 293.15 K

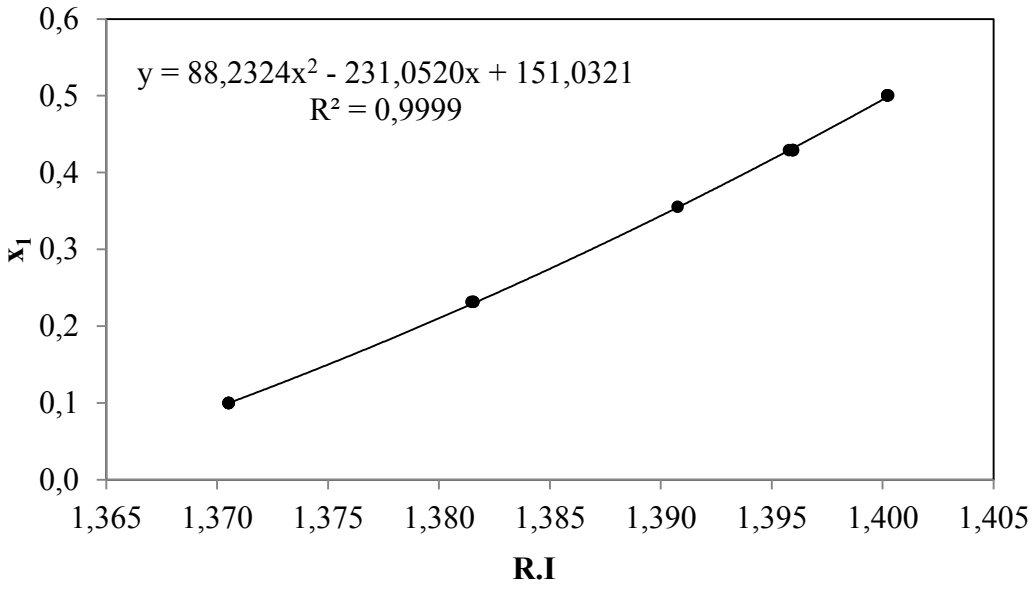

Figure 5-2: Refractometer calibration plot for the cyclohexane (1) + ethanol (2) system (cyclohexane dilute region) at 293.15 K

5.5.1.1 Cyclohexane (1) + ethanol (2) system at 40 kPa

Table 5-13: Vapour-liquid equilibrium data for the cyclohexane (1) + ethanol (2) at 40 kPa[a].

T (K)	x_1	y_1	γ_1	γ_2
329.64	0.000	0.000		0.997
327.03	0.021	0.125	5.803	1.003
324.68	0.036	0.226	6.636	1.005
322.53	0.053	0.312	6.713	1.007
321.07	0.076	0.376	5.943	1.005
319.13	0.096	0.423	5.684	1.044
318.87	0.117	0.449	4.996	1.034
314.59	0.383	0.603	2.406	1.323
314.53	0.621	0.618	1.524	2.079
314.61	0.695	0.627	1.377	2.514
314.69	0.774	0.633	1.244	3.325
314.98	0.866	0.649	1.127	5.289
316.59	0.965	0.705	1.032	15.732
325.83	1.000	1.000	1.002	

[a]Standard uncertainties u are $u(P) = \pm 0.02$ kPa, $u(T) = \pm 0.06$ K and $u(x_1) = u(y_1) = 0.002$

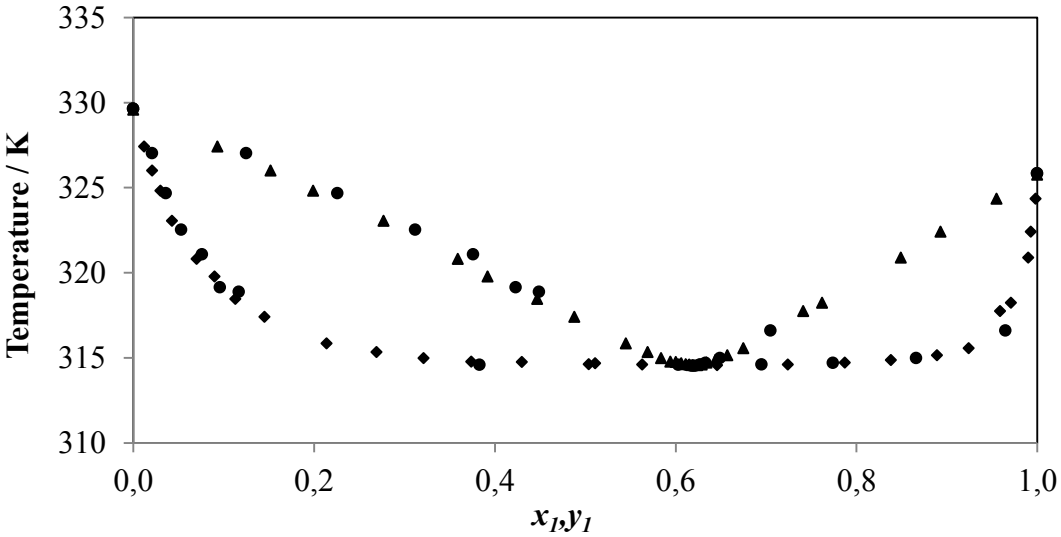

Figure 5-3: T-x_1-y_1 plot for cyclohexane (1) + ethanol (2) system at 40 kPa; (▲) (♦), Joseph (2001); (•), this work

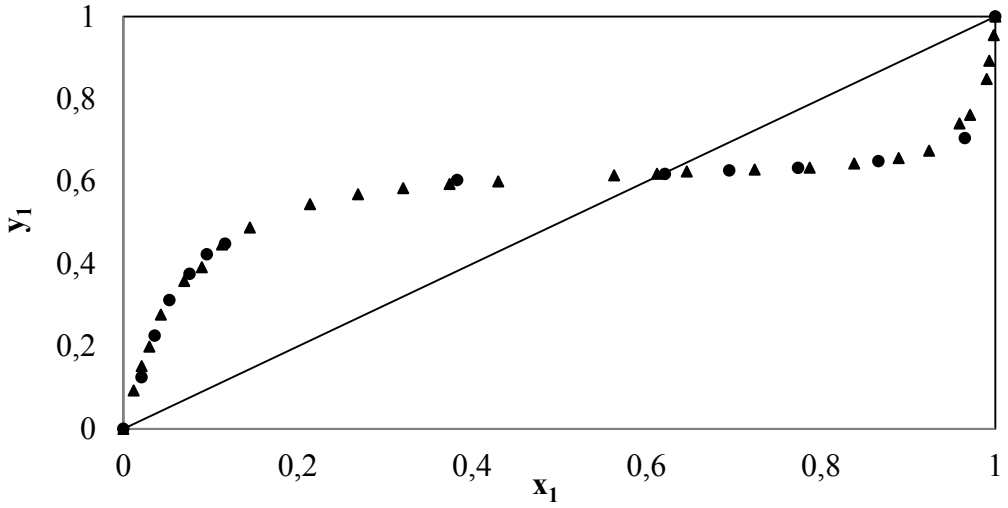

Figure 5-4: x_1-y_1 plot for cyclohexane (1) + ethanol (2) system at 40 kPa; (▲) Joseph (2001); (•), this work.

5.5.1.2 Cyclohexane (1) + ethanol (2) system at 313.15 K

Table 5-14: Vapour-liquid equilibrium data for cyclohexane (1) + ethanol (2) at 313.15 K.[a]

P(kPa)	x_1	y_1	γ_1	γ_2
18.88	0.000	0.000		1.049
22.04	0.015	0.092	5.570	1.126
24.03	0.023	0.157	6.746	1.148
24.95	0.030	0.21	7.171	1.125
26.35	0.039	0.265	7.339	1.115
27.14	0.046	0.297	7.175	1.106
30.79	0.105	0.459	5.482	1.030
32.35	0.117	0.475	5.344	1.064
34.81	0.187	0.541	4.087	1.087
36.24	0.217	0.562	3.804	1.121
37.61	0.255	0.579	3.458	1.175
37.65	0.272	0.586	3.284	1.184
38.1	0.339	0.588	2.675	1.313
37.74	0.642	0.629	1.496	2.166
37.67	0.696	0.633	1.386	2.519
37.45	0.792	0.639	1.222	3.601
37.28	0.882	0.651	1.113	6.112
24.61	1.000	1.000	1.000	

[a]Standard uncertainties u are $u(P) = \pm 0.02$ kPa, $u(T) = \pm 0.06$ K and $u(x_1) = u(y_1) = 0.002$

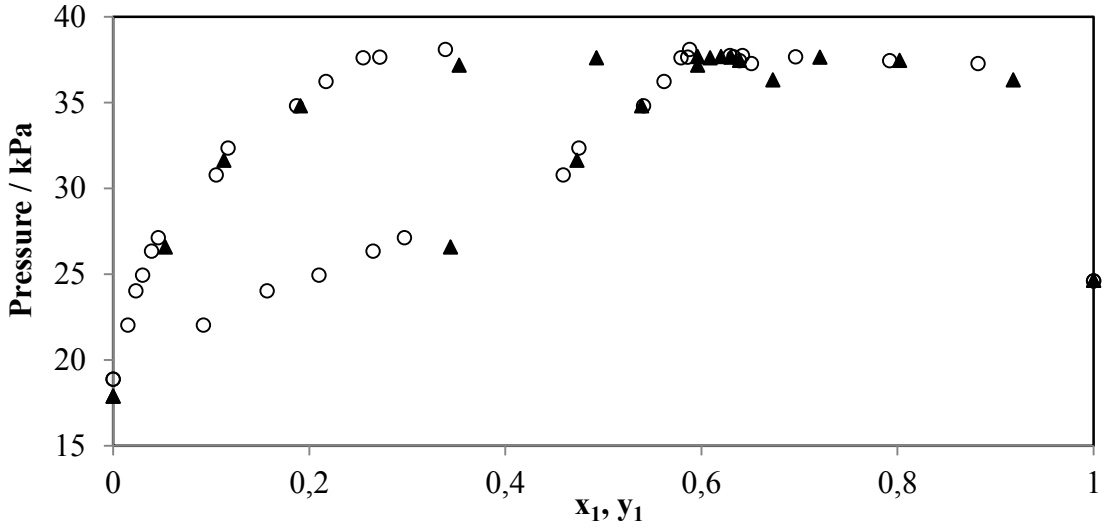

Figure 5-5: P-x_1-y_1 plot for cyclohexane (1) + ethanol (2) system at 313.15 K; (▲), Joseph (2001); (○), this work

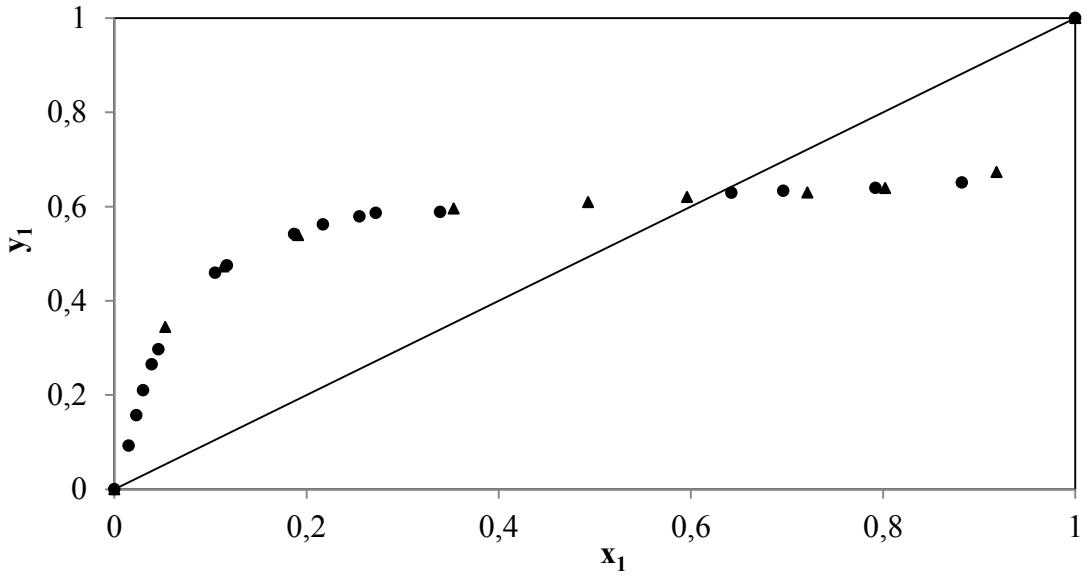

Figure 5-6: x_1-y_1 plot for cyclohexane (1) + ethanol (2) system at 313.15 K; (▲) Joseph (2001); (•), this work

5.5.2 1-propanol (1) + 4-methyl-2-pentanone (2) system.

Isothermal VLE measurements were measured for the 1-propanol (1) + 4-methyl-2-pentanone (2) system at 338.15, 353.15 and 368.15 K. Data for this system at these three isotherms are also new VLE data as this system has not been previously measured. The equilibrium phases were analyzed with the Shimadzu 2014 GC. The operating conditions of the GC are given in Table 5-10. At isotherm 353.15 K, there was a minimum boiling azeotrope displayed at approximately $x_1 = y_1 = 0.89$. The GC detector calibration plot, experimental data including the gamma values, P-x_1-y_1 and x_1-y_1 plot for each isotherm are presented below.

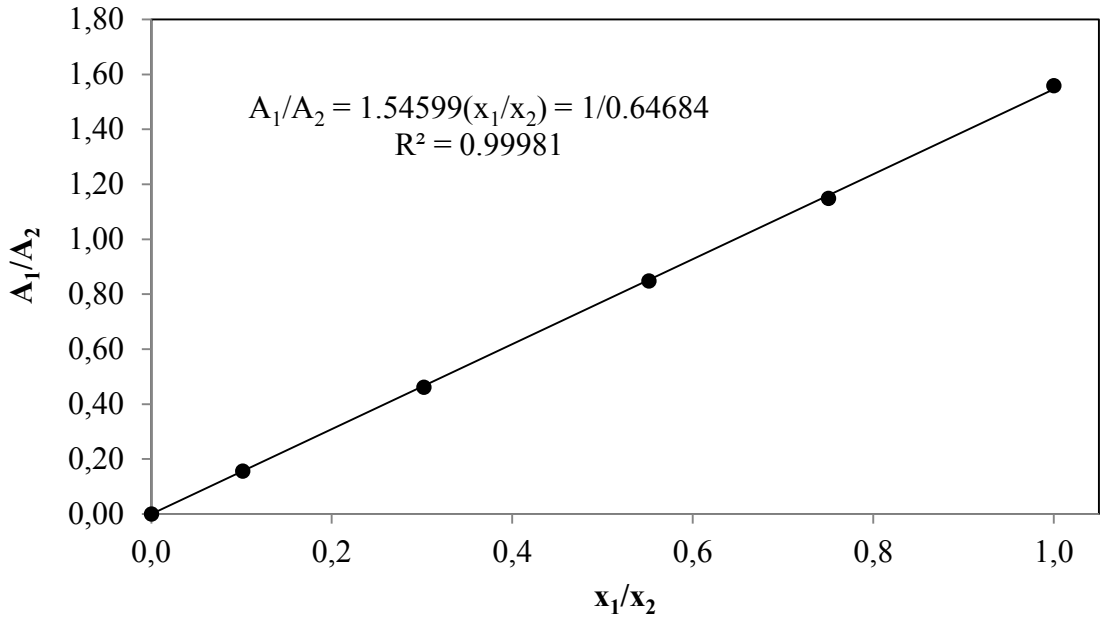

Figure 5-7: GC calibration plot for the 1-propanol (1) + 4-methyl-2-pentanone (2) system (1-propanol dilute region).

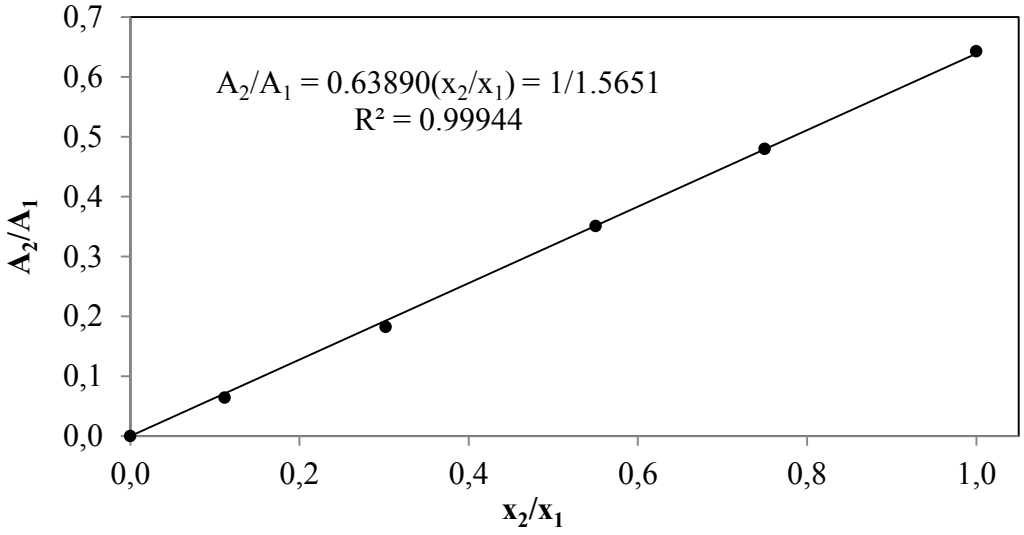

Figure 5-8: GC calibration plot for 1-propanol (1) + 4-methyl-2-pentanone (2) system (4-Methyl-2-pentanone dilute region).

Table 5-15: Vapour –liquid equilibrium data for the 1-propanol (1) + 4-methyl-2-pentanone (2) system at 338.15 K.[a]

P (kPa)	x_1	y_1	γ_1	γ_2
17.57	0.000	0.000	2.203	1.000
21.32	0.100	0.212	1.846	1.009
23.11	0.211	0.371	1.569	1.040
24.53	0.315	0.458	1.386	1.087
25.16	0.388	0.513	1.289	1.130
25.81	0.459	0.569	1.214	1.181
26.09	0.513	0.600	1.167	1.226
26.61	0.645	0.687	1.082	1.360
26.95	0.717	0.735	1.050	1.449
26.98	0.799	0.795	1.025	1.566
26.94	0.845	0.833	1.014	1.640
26.84	0.892	0.876	1.007	1.722
26.46	0.955	0.945	1.001	1.845
25.92	1.000	1.000	1.000	1.941

[a]Standard uncertainties u are $u(P) = \pm 0.02$ kPa, $u(T) = \pm 0.06$ K and $u(x_1) = u(y_1) = 0.005$

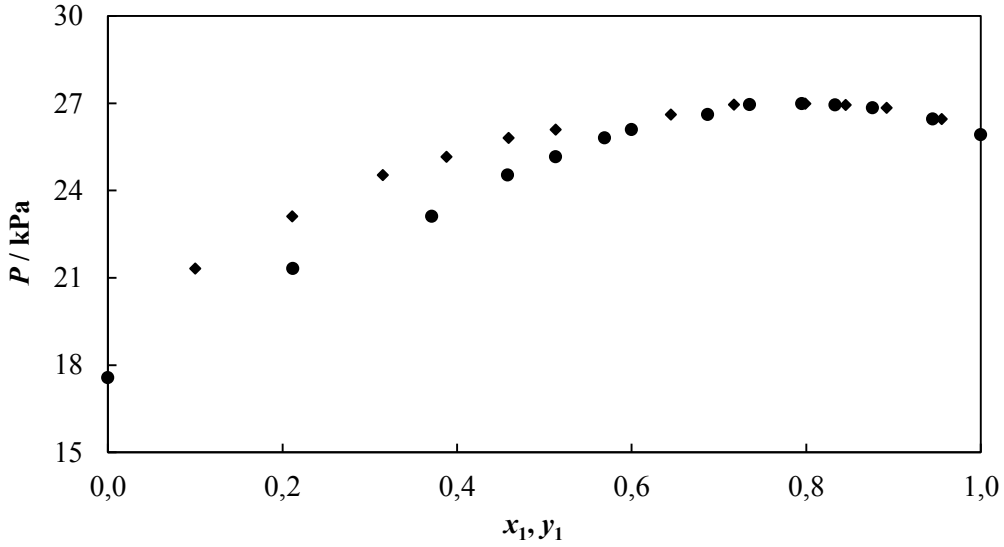

Figure 5-9: P-x_1-y_1 plot for the 1-propanol (1) + 4-methyl-2-pentanone (2) system at 338.15 K.; (♦), P-x_1; (•), P-y_1

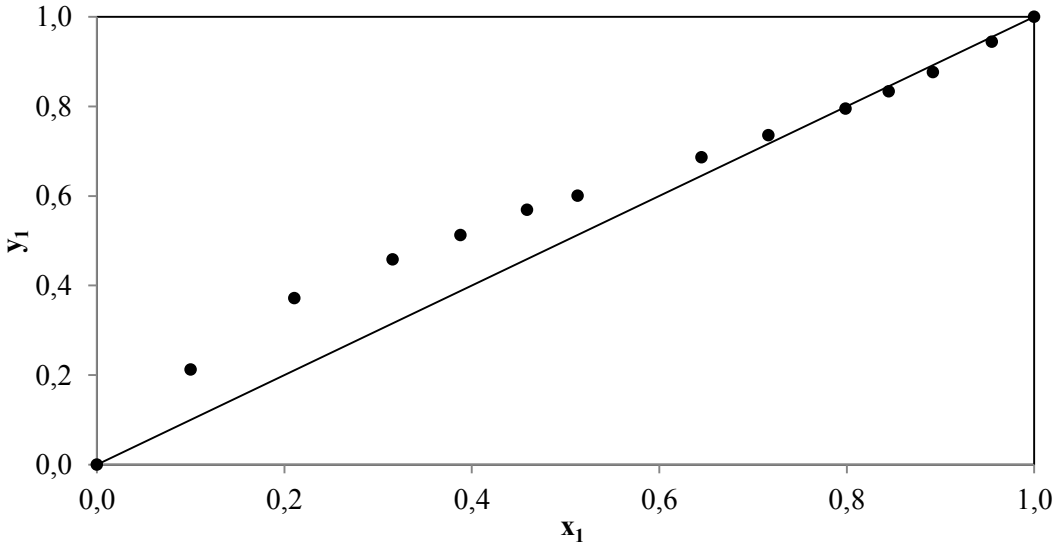

Figure 5-10: x_1-y_1 plot for the 1-propanol (1) + 4-methyl-2-pentanone (2) system at 338.15 K.

Table 5-16: Vapour-liquid equilibrium data for the 1-propanol (1) + 4-methyl-2-pentanone (2) system at 353.15 K.[a]

P/kPa	x_1	y_1	γ_1	γ_2
31.41	0.000	0.000	1.851	1.000
37.91	0.116	0.240	1.602	1.009
41.61	0.218	0.375	1.438	1.031
44.45	0.312	0.469	1.319	1.063
46.03	0.390	0.536	1.241	1.099
47.29	0.455	0.581	1.186	1.136
48.18	0.509	0.620	1.148	1.171
49.76	0.655	0.705	1.069	1.292
50.66	0.738	0.756	1.039	1.380
51.26	0.803	0.815	1.022	1.460
51.66	0.849	0.850	1.013	1.523
51.64	0.890	0.889	1.007	1.585
51.54	0.939	0.934	1.002	1.665
51.00	1.000	1.000	1.000	1.778

[a]Standard uncertainties u are $u(P) = \pm 0.02$ kPa, $u(T) = \pm 0.06$ K and $u(x_1) = u(y_1) = 0.005$

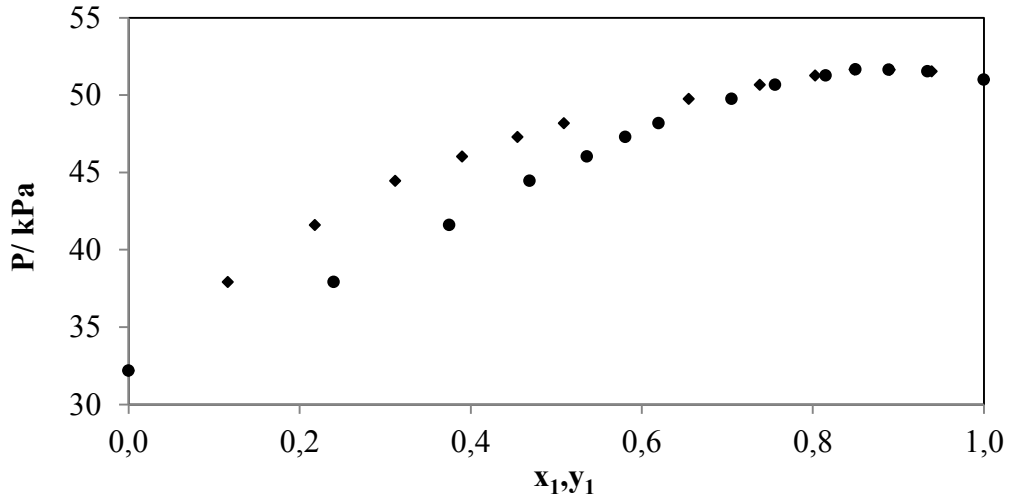

Figure 5-11: P-x_1-y_1 plot for the 1-propanol (1) + 4-methyl-2-pentanone (2) system at 353.15 K.; (♦), P-x_1; (•), P-y_1

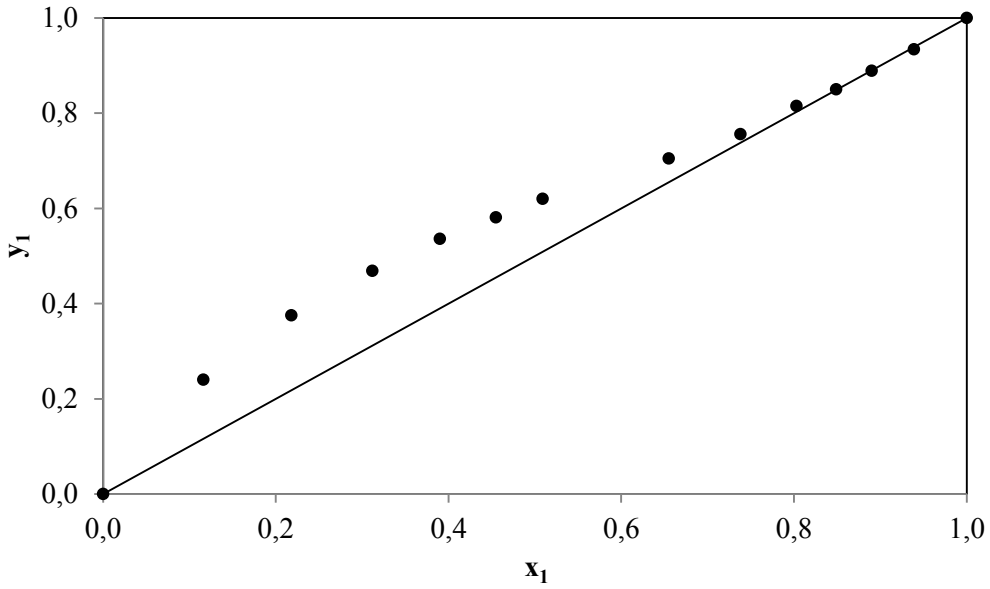

Figure 5-12: x_1-y_1 plot for the 1-propanol (1) + 4-methyl-2-pentanone (2) system at 353.15 K.

Table 5-17: Vapour-liquid equilibrium data for the 1-propanol (1) + 4-methyl-2-pentanone (2) system at 368.15 K.[a]

P/kPa	x_1	y_1	γ_1	γ_2
54.04	0.000	0.000	1.656	1.000
63.68	0.116	0.229	1.473	1.007
70.25	0.215	0.378	1.352	1.025
76.25	0.311	0.478	1.258	1.051
79.52	0.388	0.541	1.196	1.080
82.17	0.457	0.590	1.150	1.111
84.15	0.510	0.630	1.120	1.139
89.97	0.747	0.777	1.030	1.312
92.57	0.856	0.864	1.010	1.423
93.43	0.896	0.901	1.005	1.470
93.90	0.939	0.942	1.002	1.524
93.92	1.000	1.000	1.000	1.608

[a]Standard uncertainties u are $u(P) = \pm 0.02$ kPa, $u(T) = \pm 0.06$ K and $u(x_1) = u(y_1) = 0.005$

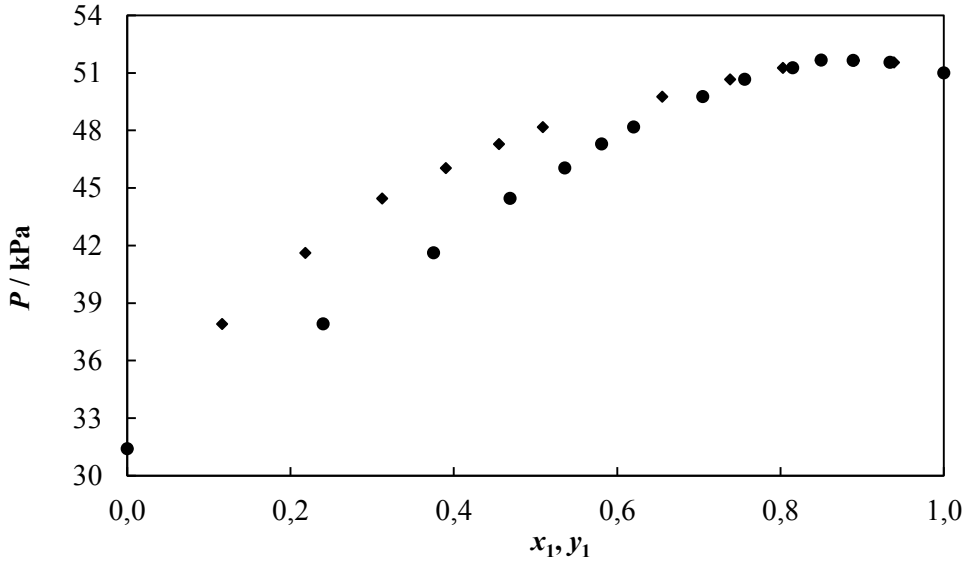

Figure 5-13: P-x_1-y_1 plot for the 1-propanol (1) + 4-methyl-2-pentanone (2) system at 368.15 K.; (♦), P-x_1; (•), P-y_1

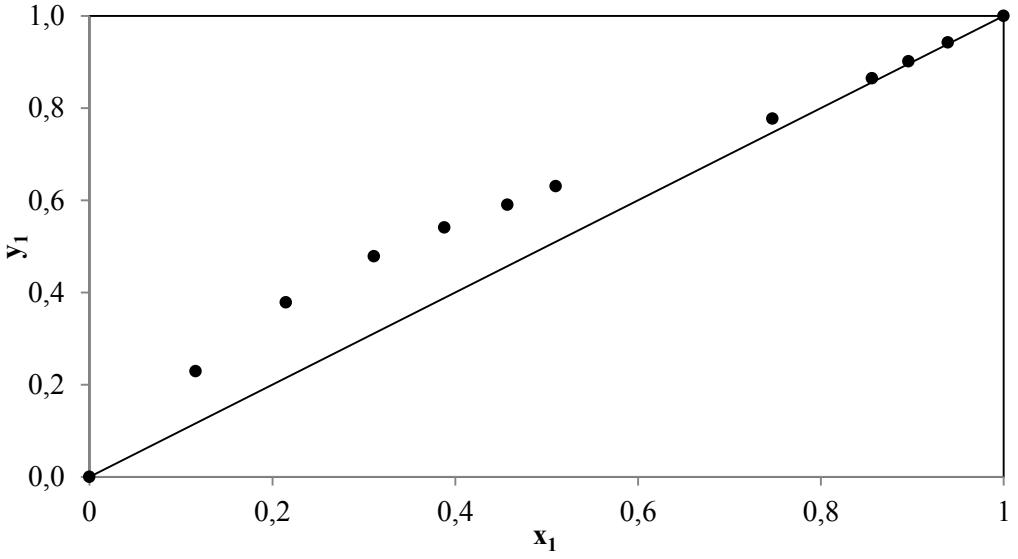

Figure 5-14: x_1-y_1 plot for the 1-propanol (1) + 4-methyl-2-pentanone (2) system at 368.15 K.

5.5.3 2-Propanol (1) + 4-methyl-2-pentanone (2) system

New isothermal vapour-liquid equilibrium measurements for this system were carried out at 323.15, 338.15 and 353.15 K. Data for this system at these three isotherms have not been previously measured. The phase composition analysis was done using the Shimadzu 2014 GC with a Porapak Q column as previously described in Table 5-11. The GC detector calibration plots, measured experimental data, plots of P-x_1-y_1 and x_1-y_1 for each isotherm are presented below.

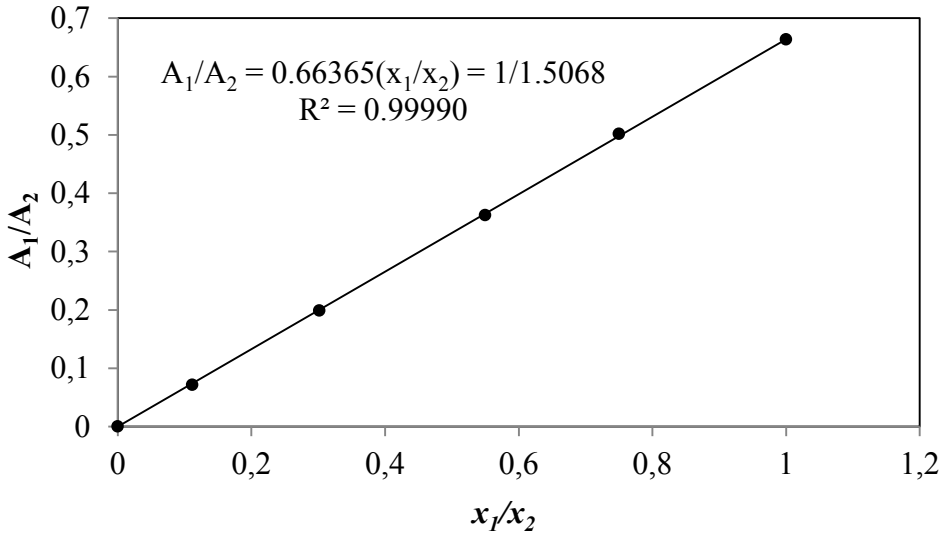

Figure 5-15: GC detector calibration plot for the 2-propanol (1) + 4-methyl-2-pentanone (2) system (2-propanol dilute region).

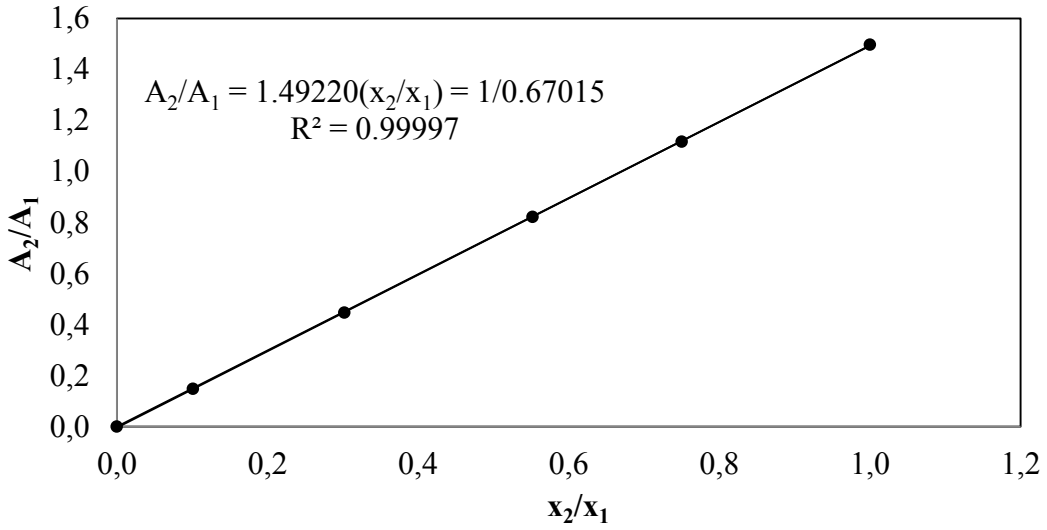

Figure 5-16: GC detector calibration plot for the 2-propanol (1) + 4-methyl-2-pentanone (2) system (4-methyl-2-pentanone dilute region).

Table 5-18: Vapour –liquid equilibrium data for the 2-propanol (1) + 4-methyl-2-pentanone (2) system at 323.15 K.[a]

P/kPa	x_1	y_1	γ_1	γ_2
9.22	0.000	0.000	2.081	1.000
12.76	0.097	0.323	1.833	1.007
15.07	0.194	0.490	1.633	1.027
16.76	0.268	0.579	1.506	1.052
17.95	0.342	0.625	1.399	1.086
19.52	0.459	0.681	1.262	1.164
20.99	0.601	0.752	1.140	1.305
21.67	0.677	0.798	1.092	1.410
22.3	0.760	0.838	1.051	1.554
22.91	0.843	0.887	1.022	1.740
23.14	0.899	0.920	1.009	1.895
23.39	0.953	0.958	1.002	2.074
23.48	1.000	1.000	1.000	2.258

[a]Standard uncertainties u are $u(P) = \pm 0.02$ kPa, $u(T) = \pm 0.06$ K and $u(x_1) = u(y_1) = 0.003$

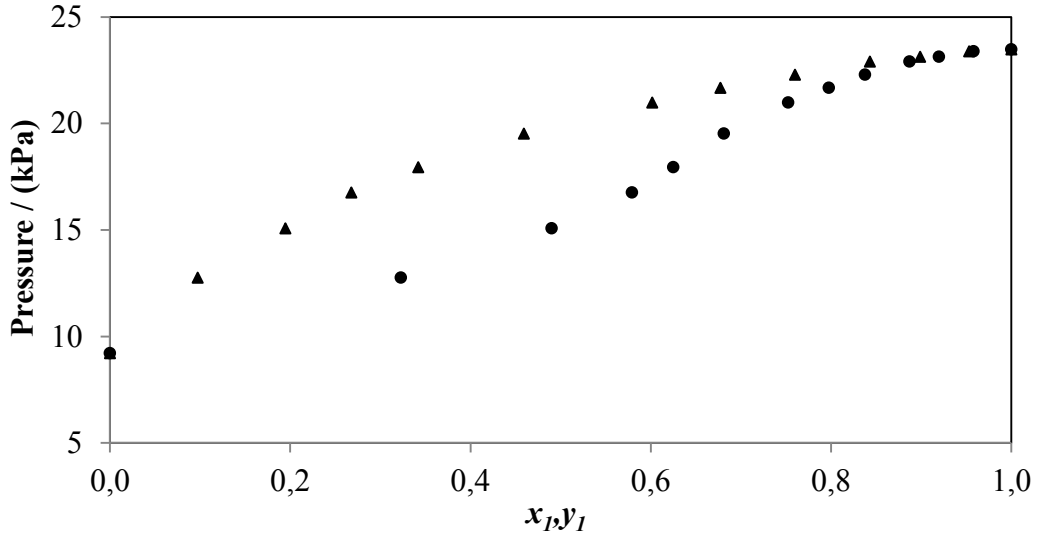

Figure 5-17: P-x_1-y_1 plot for the 2-propanol (1) + 4-methyl-2-pentanone (2) system at 323.15 K; (▲), P-x_1; (•), P-y_1

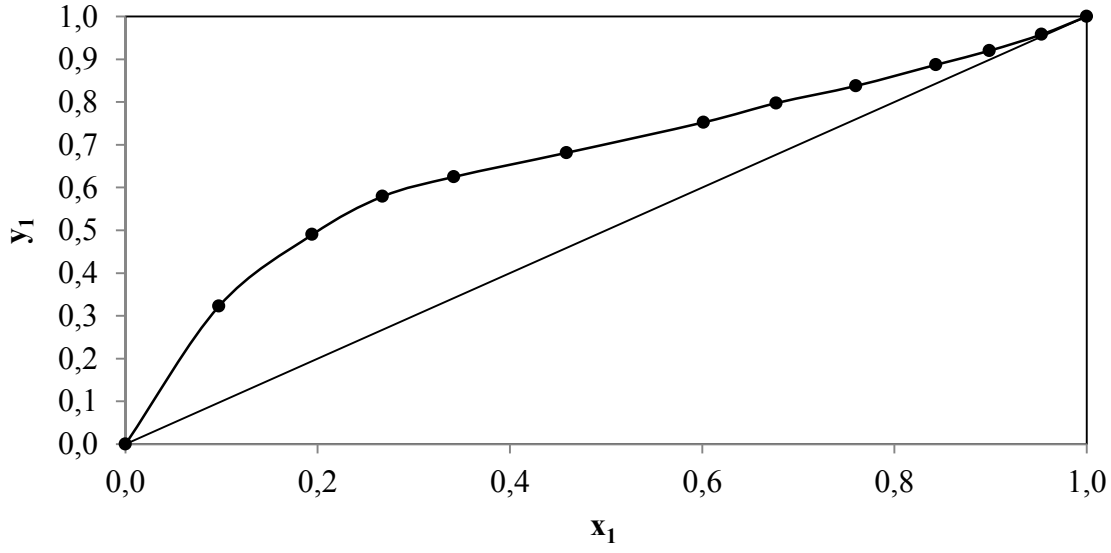

Figure 5-18: x_1-y_1 plot for the 2-propanol (1) + 4-methyl-2-pentanone (2) system at 323.15 K.

Table 5-19: Vapour –liquid equilibrium data for the 2-propanol (1) + 4-methyl-2-pentanone (2) system at 338.15 K.[a]

P/kPa	x_1	y_1	γ_1	γ_2
17.57	0.000	0.000	1.885	1.000
28.92	0.190	0.486	1.535	1.022
32.18	0.275	0.561	1.417	1.047
38.07	0.460	0.688	1.223	1.141
41.39	0.594	0.771	1.124	1.253
43.03	0.675	0.814	1.080	1.345
44.68	0.756	0.854	1.045	1.459
46.13	0.841	0.898	1.019	1.611
46.91	0.895	0.927	1.009	1.728
47.71	0.950	0.963	1.002	1.869
48.45	1.000	1.000	1.000	2.018

[a]Standard uncertainties u are $u(P) = \pm 0.02$ kPa, $u(T) = \pm 0.06$ K and $u(x_1) = u(y_1) = 0.003$

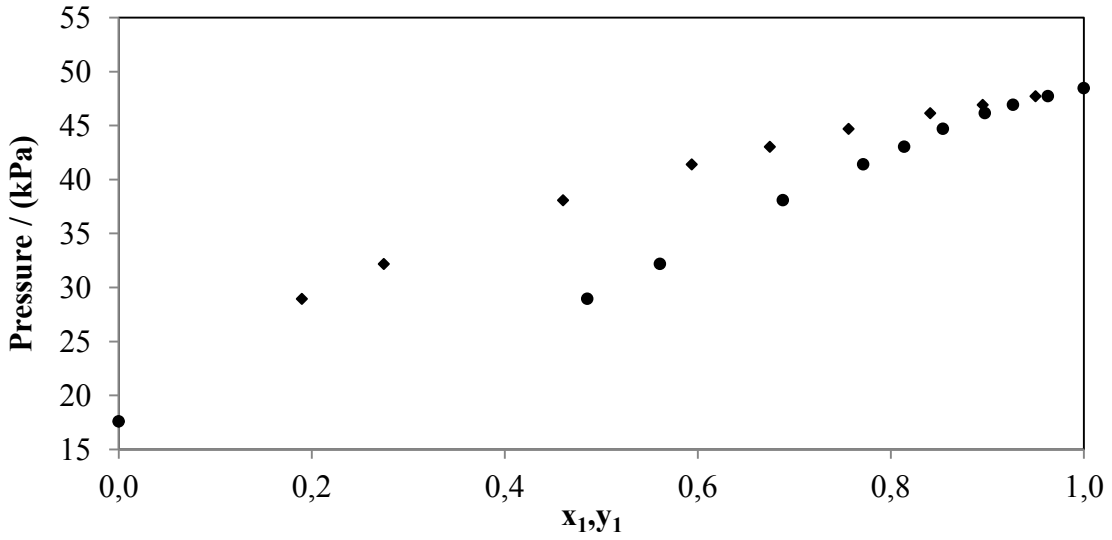

Figure 5-19: P-x_1-y_1 plot for the 2-propanol (1) + 4-methyl-2-pentanone (2) system at 338.15 K; (♦), P-x_1; (•), P-y_1.

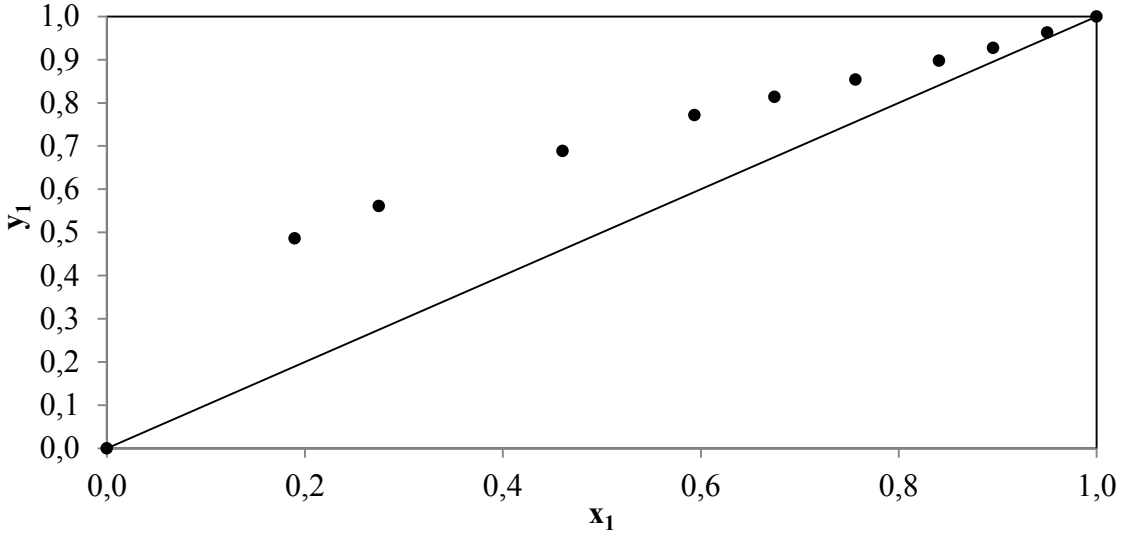

Figure 5-20: x_1-y_1 plot for the 2-propanol (1) + 4-methyl-2-pentanone (2) system at 338.15 K.

Table 5-20: Vapour –liquid equilibrium data for the 2-propanol (1) + 4-methyl-2-pentanone (2) system at 353.15 K.[a]

P/kPa	x_1	y_1	γ_1	γ_2
31.41	0.000	0.000	1.623	1.000
42.51	0.099	0.301	1.507	1.004
61.56	0.336	0.618	1.281	1.051
65.66	0.399	0.671	1.232	1.075
69.08	0.455	0.710	1.193	1.102
76.20	0.590	0.789	1.112	1.189
79.66	0.670	0.827	1.074	1.262
83.35	0.756	0.866	1.042	1.362
86.70	0.839	0.907	1.019	1.488
88.57	0.895	0.936	1.008	1.593
90.61	0.948	0.969	1.002	1.712
92.48	1.000	1.000	1.000	1.851

[a]Standard uncertainties u are $u(P) = \pm 0.02$ kPa, $u(T) = \pm 0.06$ K and $u(x_1) = u(y_1) = 0.003$

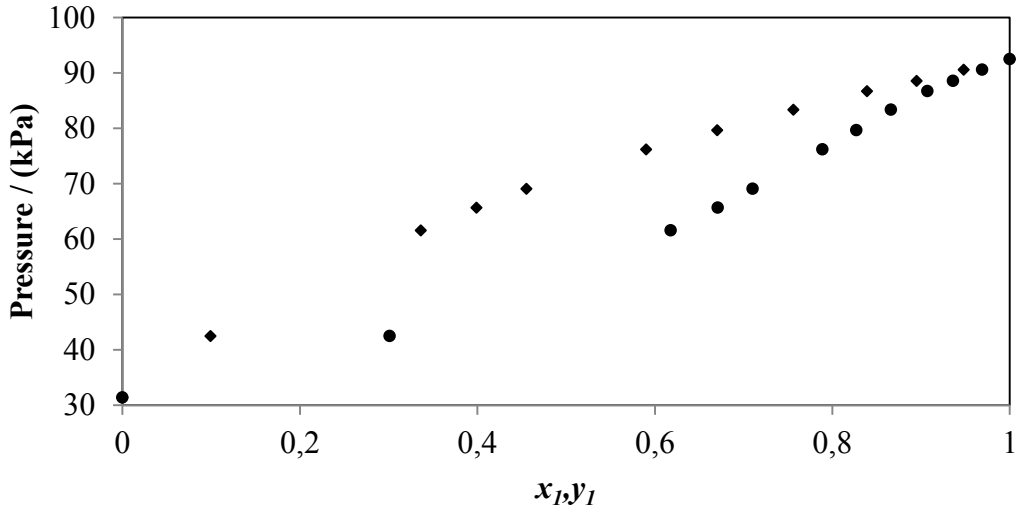

Figure 5-21: P-x_1-y_1 plot for the 2-propanol (1) + 4-methyl-2-pentanone (2) system at 353.15 K; (♦), P-x_1; (•), P-y_1

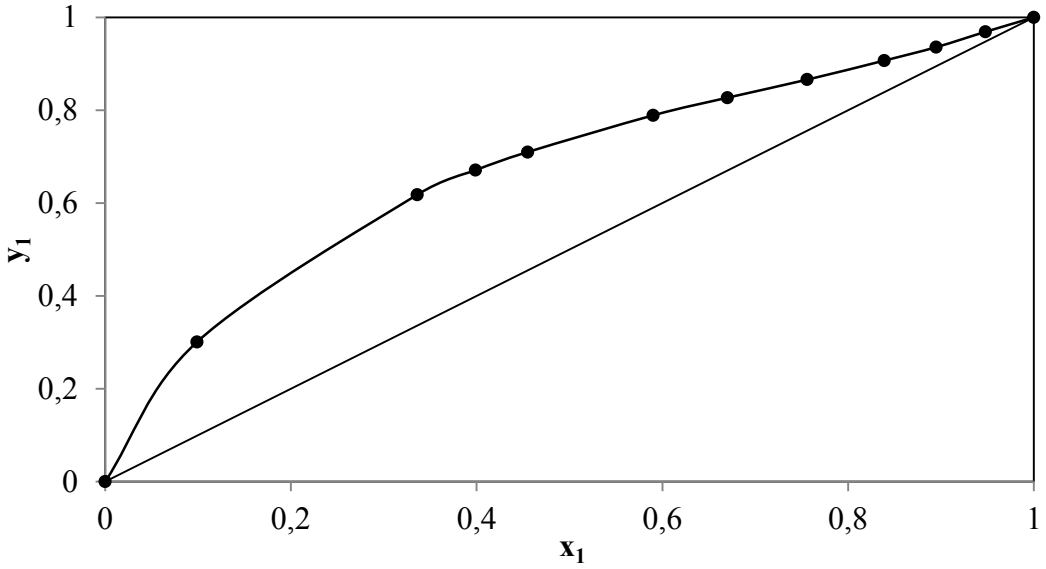

Figure 5-22: x_1-y_1 plot for the 2-propanol (1) + 4-methyl-2-pentanone (2) system at 353.15 K.

5.5.4 2-pentanone (1) + 2-methylpropan-1-ol (2) system.

New isothermal VLE data were measured for this system at: 343.15, 358.15 and 363.15 K. There is no data previously available for this system at the three isotherms. The phase equilibrium analyses were performed with the Shimadzu 2014 GC. The GC detector calibration plots did not fit well with a linear plot therefore quadratic equations (2nd order polynomial) were used for the phase composition determination. The GC detector calibration plots as well as the experimental data, P-x_1-y_1 and x_1-y_1 plots for each isotherm are presented below.

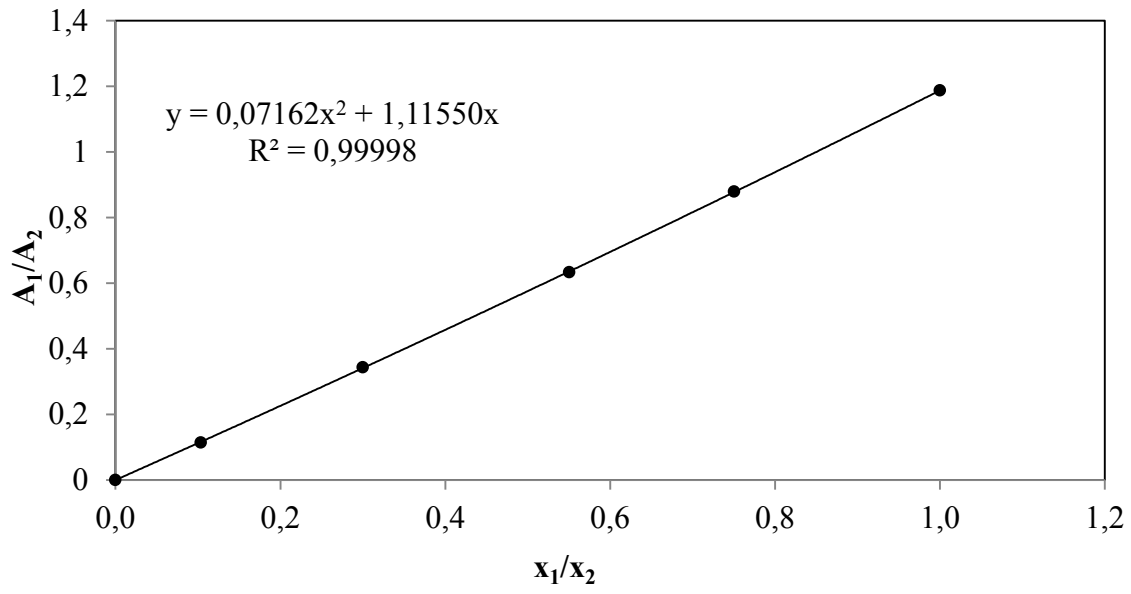

Figure 5-23: GC detector calibration plot for the methyl propyl ketone (1) + 2-methylpropan-1-ol (2) system (2-pentanone dilute region).

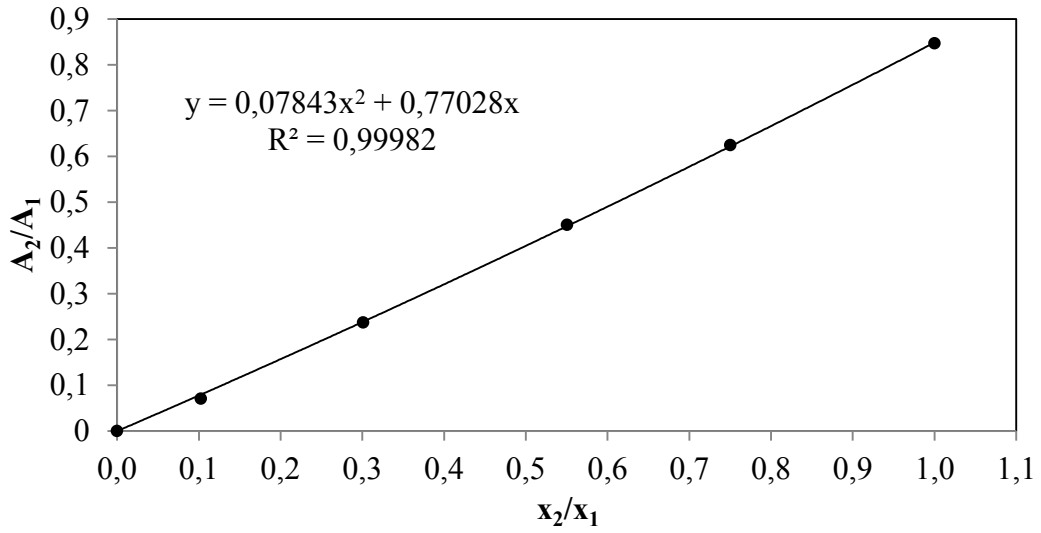

Figure 5-24: GC detector calibration plot for the 2-pentanone (1) + 2-methylpropan-1-ol (2) system (2-methylpropan-1-ol dilute region).

Table 5-21: Vapour–liquid equilibrium data for the methyl propyl ketone (1) + 2-methylpropan-1-ol (2) system at 343.15 K.[a]

P/kPa	x_1	y_1	γ_1	γ_2
20.50	0.000	0.000	1.625	1.000
22.75	0.069	0.147	1.515	1.003
24.33	0.127	0.244	1.435	1.008
25.6	0.183	0.328	1.368	1.017
26.65	0.239	0.382	1.309	1.029
27.85	0.301	0.454	1.252	1.046
28.78	0.366	0.513	1.201	1.068
30.84	0.531	0.635	1.103	1.145
31.52	0.598	0.686	1.074	1.185
32.08	0.652	0.726	1.055	1.222
32.63	0.721	0.777	1.034	1.274
33.20	0.801	0.842	1.017	1.344
33.80	0.887	0.905	1.006	1.431
34.40	1.000	1.000	1.000	1.567

[a]Standard uncertainties u are $u(P) = \pm 0.02$ kPa, $u(T) = \pm 0.06$ K and $u(x_1) = u(y_1) = 0.005$

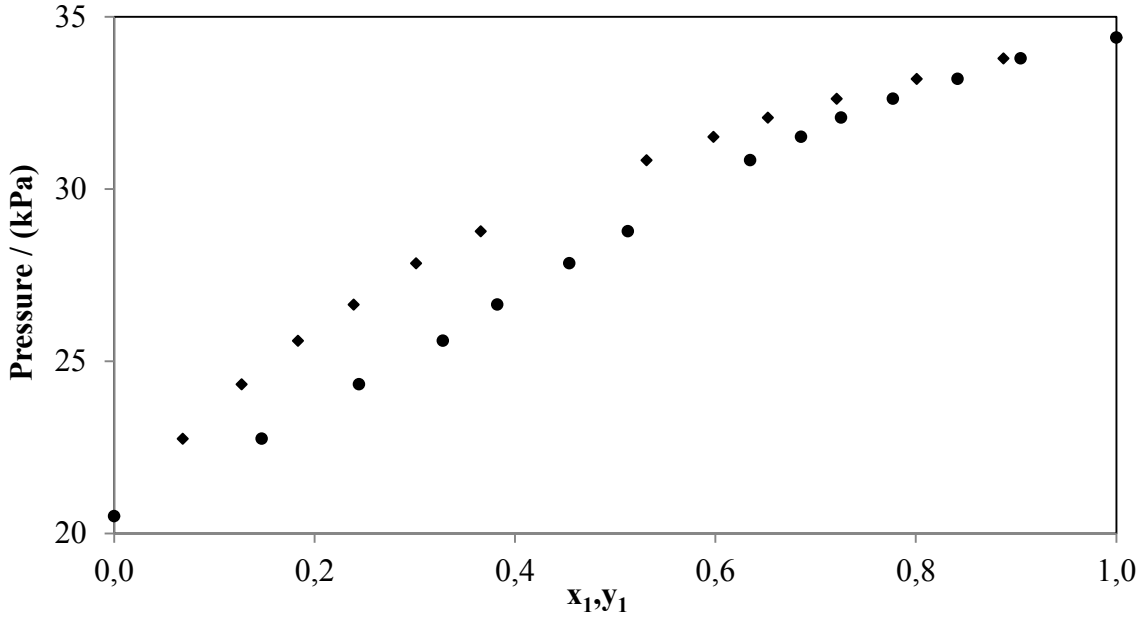

Figure 5-25: P-x_1-y_1 plot for the 2-pentanone (1) + 2-methylproan-1-ol (2) system at 343.15 K.; (♦), P-x_1; (•), P-y_1

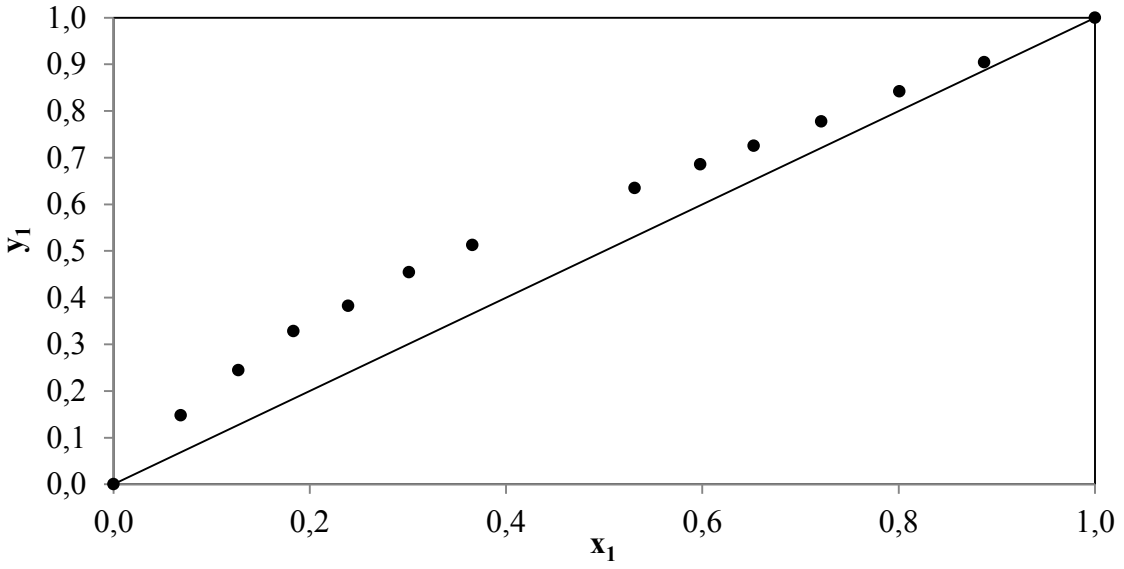

Figure 5-26: x_1-y_1 plot for the 2-pentanone (1) + 2-methylpropan-1-ol (2) system at 343.15 K.

Table 5-22: Vapour–liquid equilibrium data for the 2-pentanone (1) + 2-methylpropan-1-ol (2) system at 358.15 K.

P/kPa	x_1	y_1	γ_1	γ_2
41.07	0.000	0.000	1.351	1.000
43.88	0.077	0.139	1.303	1.002
45.93	0.144	0.238	1.264	1.005
47.63	0.208	0.321	1.229	1.011
49.00	0.266	0.378	1.199	1.019
50.66	0.334	0.453	1.166	1.031
51.83	0.401	0.512	1.137	1.047
54.48	0.531	0.603	1.087	1.089
55.39	0.599	0.655	1.065	1.118
55.90	0.652	0.701	1.050	1.145
56.79	0.723	0.758	1.032	1.188
57.39	0.799	0.827	1.017	1.244
58.06	0.893	0.900	1.005	1.330
58.64	1.000	1.000	1.000	1.458

aStandard uncertainties u are u(P) = ± 0.02 kPa, u(T) = ± 0.06 K and u(x_1) = u(y_1) = 0.005

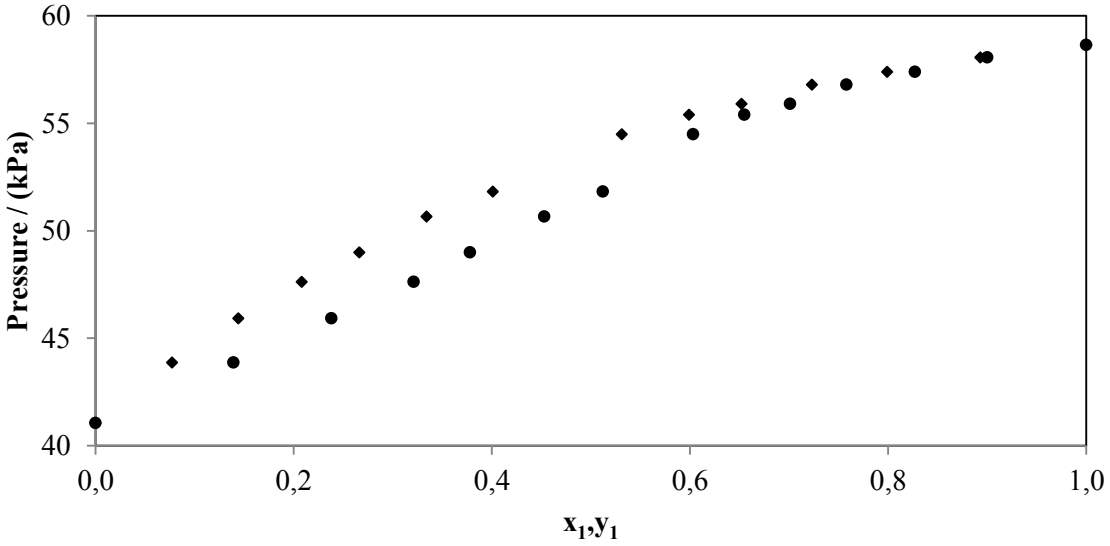

Figure 5-27: P-x_1-y_1 plot for the 2-pentanone (1) + 2-methylpropan-1-ol (2) system at 358.15 K.; (♦), P-x_1; (•), P-y_1

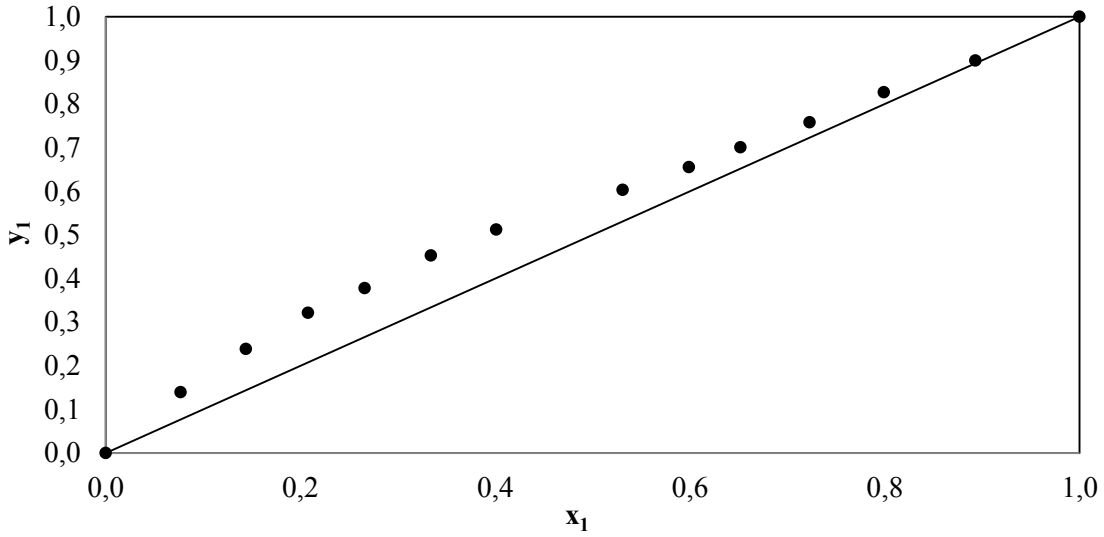

Figure 5-28: x_1-y_1 plot for the 2-pentanone (1) + 2-methylpropan-1-ol (2) system at 358.15 K.

Table 5-23: Vapour –liquid equilibrium data for the 2-pentanone (1) + 2-methylpropan-1-ol (2) system at 363.15 K.[a]

P±0.02/kPa	x_1	y_1	γ_1	γ_2
50.99	0.000	0.000	1.335	1.000
53.94	0.075	0.134	1.286	1.002
55.97	0.143	0.226	1.246	1.005
57.80	0.210	0.308	1.209	1.012
59.20	0.266	0.367	1.181	1.019
61.11	0.334	0.446	1.149	1.031
62.33	0.402	0.499	1.121	1.046
65.04	0.532	0.593	1.075	1.086
65.96	0.598	0.646	1.056	1.111
66.65	0.651	0.696	1.042	1.135
67.38	0.721	0.751	1.027	1.172
68.01	0.802	0.820	1.014	1.222
68.29	0.891	0.895	1.004	1.288
69.36	1.000	1.000	1.000	1.390

[a]Standard uncertainties u are $u(P) = \pm 0.02$ kPa, $u(T) = \pm 0.06$ K and $u(x_1) = u(y_1) = 0.005$

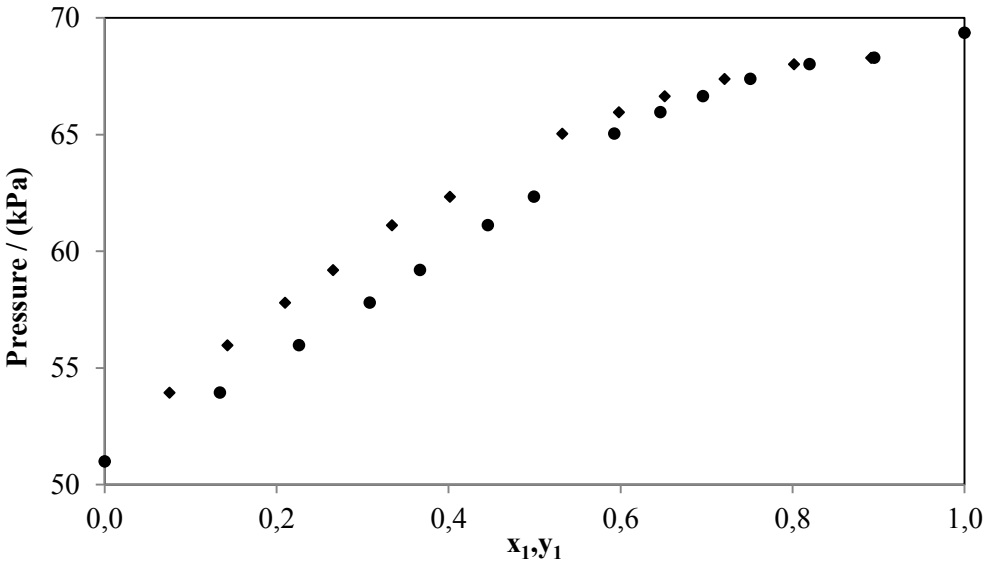

Figure 5-29: P-x_1-y_1 plot for the 2-pentanone (1) + 2-methylpropan-1-ol (2) system at 363.15 K.; (♦), P-x_1; (•), P-y_1

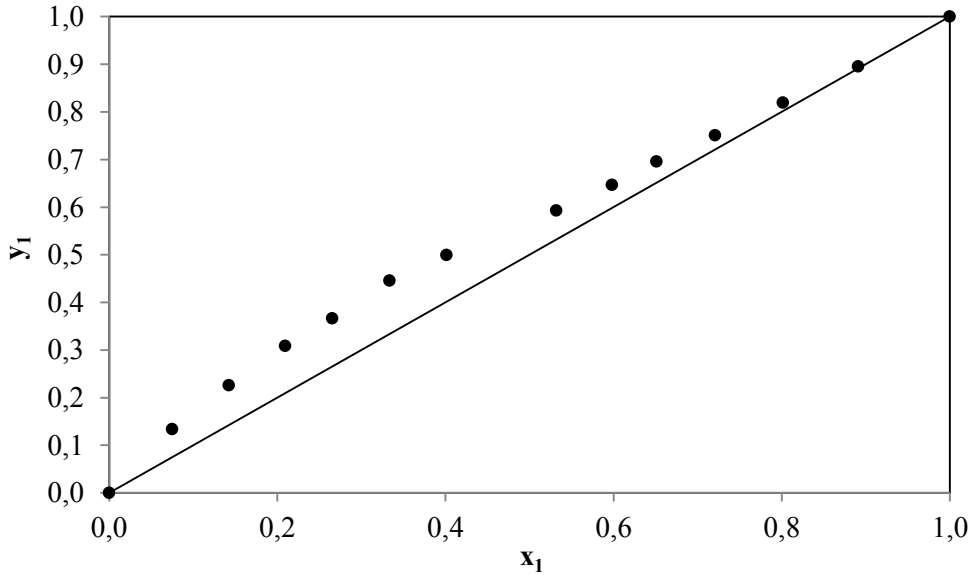

Figure 5-30: x_1-y_1 plot for the 2-pentanone (1) + 2-methylpropan-1-ol (2) system at 363.15 K.

CHAPTER 6

DATA ANALYSIS AND DISCUSSION

This chapter focuses on the discussion and analysis of the experimental data measured in this work which had been presented in Chapter 5. This entails analysis on the measured vapour pressure data which includes regression of the data to get the fitting Antoine parameters, data regression of the newly measured VLE systems comprising the combined method approach with suitable models available in ASPEN PLUS (ASPEN PLUS, 2013) for each system and the thermodynamic consistency testing applied for the measured VLE data to verify the consistency of the isothermal VLE data sets. The theoretical concepts applied in this chapter were discussed in Chapter 3. This Chapter also reports the plots showing the comparison between the experimentally determined liquid-phase activity coefficients and those calculated from the NRTL model, results obtained for the infinite dilution activity coefficients from the newly measured isothermal VLE data as well as the G^E, H^E and S^E data are presented in the latter part of this Chapter

6.1 Vapour pressure data regression

Vapour pressure measurement can provide a check on the; purity of a chemical, experimental procedure of the apparatus, and operation of the temperature and pressure sensors. It was then necessary to measure the vapour pressure of all the chemicals used in this work and compare with literature sources. The data as earlier presented in Chapter 5 (Tables 5-3 to 5-9) were compared with the literature values of NIST (NIST Technical Note 1994) and Poling et al. (Poling et al., 2001). The vapour pressure data of 1-propanol, 2-methylpropan-1-ol, 2-pentanone, 4-methyl-2-pentanone, cyclohexane and ethanol were compared with two literature sources. The experimental vapour pressure data for all the pure chemicals were regressed to get the parameters for the Antoine equation:

$$\ln(P)/(kPa) = A - \frac{B}{T^{\circ}/C + C} \tag{6-1}$$

The Antoine parameters from the vapour pressure data regression for all the components studied are presented in Table 6-1 below. The $\sum(\Delta T^2)$ values for each data set are also included, where $\sum(\Delta T^2)$ is given by:

$$\sum(\Delta T^2) = \sum_{i}^{n} \left(T_i^{\exp} - T_i^{calc} \right)^2 \qquad (6\text{-}2)$$

Table 6-1: Parameters obtained for the Antoine equation

Component	A	B	C	$\sum(\Delta T^2)$ /K
1-propanol	13.29	2052.52	139.74	0.34
2-methylpropan-1-ol	12.04	1601.10	107.83	1.30
2-pentanone	11.84	1799.62	146.58	0.39
4-methyl-2-pentanone	11.54	1810.66	144.32	1.31
2-propanol	13.87	2206.43	155.97	0.21
cyclohexane	12.03	1885.23	173.48	0.13
ethanol	14.05	2315.65	167.14	0.11

The Antoine equation was chosen for the regression of the vapour pressure data because of its simplicity when compared to the Wagner equation. The Antoine equation in its simplicity has only three adjustable parameters while Wagner equation has four. This reduces chances of error in the reduction as the more the parameters the more the chances of error. From Table 6-1, it can be seen that the $\sum(\Delta T^2)$ values are between 0.11 to 1.31 kPa which shows that the Antoine equation correlated the measured vapour pressure data well.

6.2 Refractometer calibration for the test system

A test system of cyclohexane (1) + ethanol (2) was measured at 40 kPa (T-x-y) and also at 313 K (P-x-y) in order to test for reproducibility of data and the correct operation of the VLE still. This system was chosen because of its highly non-ideal and complex nature and there are thermodynamically consistent literature data (Joseph, 2001) to compare the experimental data with. An ATAGO 7000α refractometer was used for the analysis of the phase compositions for the test system. The refractometer has a reported uncertainty of 0.0001 as stated by the supplier. Calibration of the refractometer for the phase equilibrium measurements was done at 20 ºC. All phase composition measurements of the test system were also done at this temperature. The plots for the calibration as presented in Figures 5-1

and 5-2 where it was found that a second order polynomial trend provided a better fit to the data. Calibration was done for each dilute region and the appropriate calibration relationship was used to determine the phase composition. The VLE data measured for the test system was compared with the literature data of Joseph (Joseph, 2001), (Narasigadu, 2006) and (Pillay, 2009) and as graphically represented in Figures 5-3 to 5-6, it is can be seen that the data measured for the test system gave satisfactory agreement with literature data of Joseph (2001). This shows that the operating procedure was appropriate and the apparatus was working correctly.

6.2.1 Modelling results for the cyclohexane (1) + ethanol (2) system at 313.15 K.

The cyclohexane (1) + ethanol (2) system measured at 313.15 K was used as a test system to ensure correct operation of the VLE apparatus and to confirm that the experimental procedure used was accurate. The NRTL-HOC model combination was used for the regression of the measured isothermal VLE data. For the NRTL-HOC model combination, the non randomness parameter α_{12} was fixed to 0.47 for the operation. The P-x-y data with the gamma values have been presented in Chapter 5 (Table 5-14). Tables 6-2 reports the regressed temperature dependent model binary interaction parameters, the Δyavg, ΔPavg (the deviation between measured values and modelled values) and the RMSD $\delta \ln (\gamma_1/\gamma_2)$ values obtained from the regression of the measured data at 313.15 K. figures 6-1 to 6-3 presents the plots for the x_1-y_1, P-x-y and ln γ values. As shown in Figure 6-1, the NRTL-HOC model combination gave a good fit to the data set for the test system at 313.15 K.

Table 6-2: modelling results obtained for the cyclohexane (1) + ethanol (2) system at 313.15 K

model	T/K	a_{ij}	a_{ji}	b_{ij}	b_{ji}	AAD ΔP/kPa	AAD Δy	RMSD δln(γ_1/γ_2)
NRTL-HOC	313.15	8.99	-3.89	-1991.6	1665.1	0.059	0.015	0.160

u(T) = 0.06 K.

b_{ij} and a_{ij} are the binary interaction parameters for the activity coefficient models in ASPEN, ($\tau ij = aij + bij/T$), α_{ij} (non-randomness parameter) set to 0.47 for the NRTL-HOC model combination, RMSD δln(γ_1/γ_2) (the Root Mean Square deviation for the direct test)

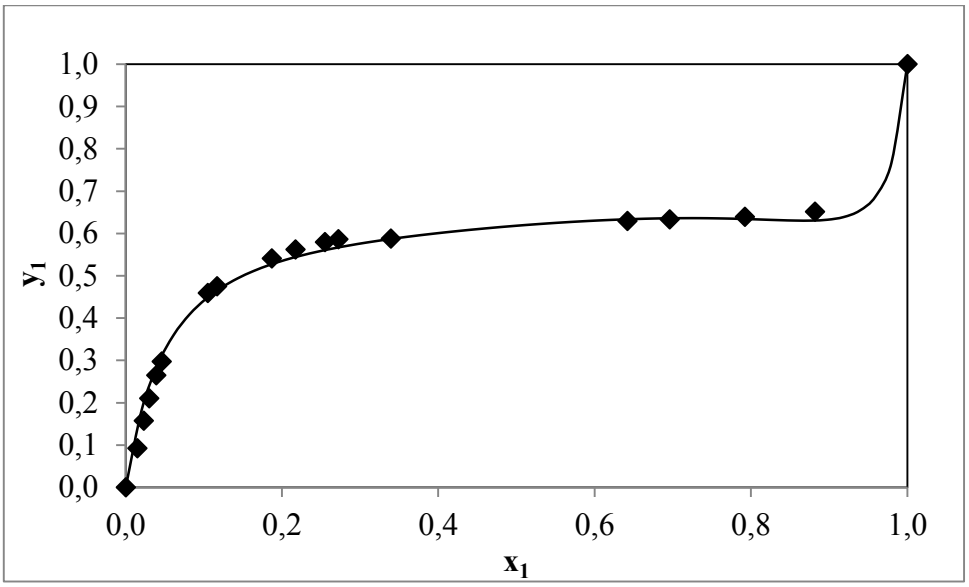

Figure 6-1: Fit of the NRTL-HOC model combination to the x-y plot of the cyclohexane (1) + ethanol (2) system at 313.15 K

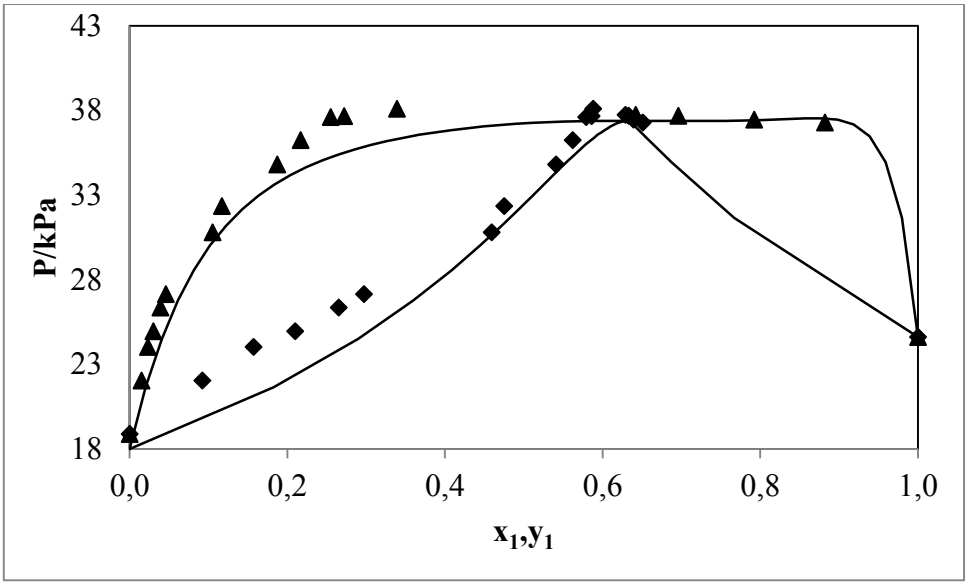

Figure 6-2: Fit of the NRTL-HOC model combination to the P-x-y plot of the cyclohexane (1) + ethanol (2) system at 313.15 K

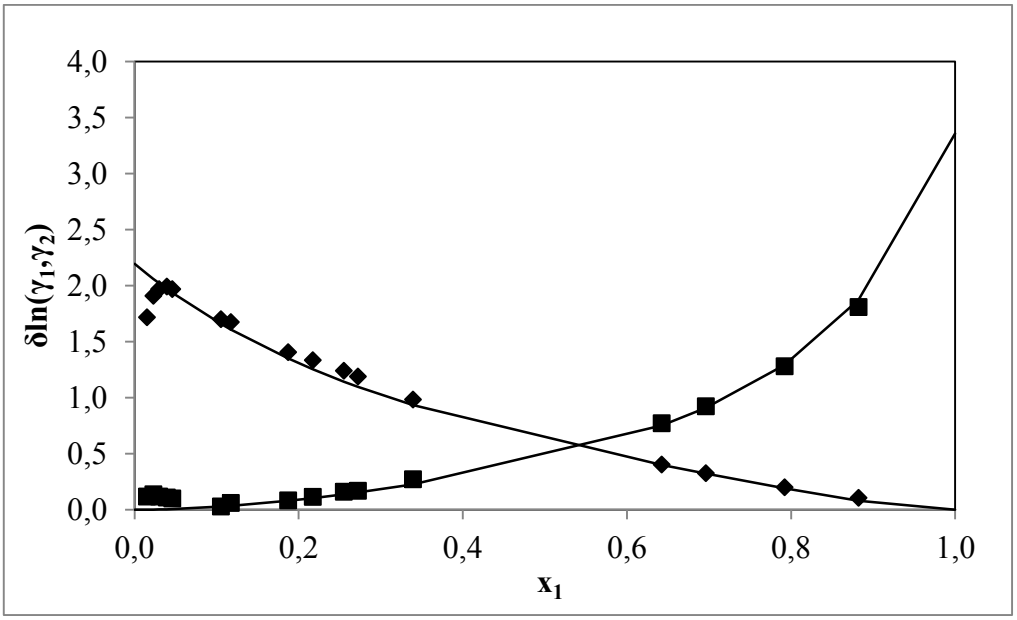

Figure 6-3: Comparison of the experimental activity coefficients and those calculated from the NRTL-HOC model combination for the cyclohexane (1) + ethanol (2) system at 313.15 K. (♦) experimental ln γ_1, (■) experimental ln γ_2, (−) NRTL-HOC model combination.

6.2.2 Modelling results for the cyclohexane (1) + ethanol (2) system at 40 kPa.

The cyclohexane (1) + ethanol (2) system measured at 40 kPa was also used as a test system to ensure correct operation of the VLE apparatus and to confirm that the experimental procedure used was accurate. The NRTL-HOC and WILSON-HOC model combinations were used for the regression of the measured isobaric VLE data. For the NRTL-HOC model combination, the non randomness parameter α_{12} was also fixed to 0.47 for the operation. The T-x-y data with the gamma values have been presented in Chapter 5 (Table 5-13). Tables 6-3 reports the regressed temperature dependent model binary interaction parameters, the Δyavg, ΔTavg (the deviation between measured values and modelled values) and the RMSD $\delta\ln(\gamma_1/\gamma_2)$ values obtained from the regression of the measured data at 40kPa. Figures 6-4 to 6-6 presents the plots for the x_1-y_1, T-x-y and ln γ values.

Table 6-3: modelling results obtained for the cyclohexane (1) + ethanol (2) system at 40 kPa

model	P/kPa	a_{ij}	a_{ji}	b_{ij}	b_{ji}	AAD ΔP/kPa	AAD Δy	RMSD $\delta\ln(\gamma_1/\gamma_2)$
NRTL-HOC	40	1.58	-0.35	327.29	545.1	0.074	0.010	0.078
WILSON-HOC	40	0.35	0.97	-480.29	-1290.1	0.244	0.008	0.069

u(P) = 0.02 kPa

b_{ij} and a_{ij} are the binary interaction parameters for the activity coefficient models in ASPEN, (τij = aij + bij/T), α_{ij} (non-randomness parameter) set to 0.47 for the NRTL-HOC model combination, RMSD $\delta\ln(\gamma_1/\gamma_2)$ (the Root Mean Square deviation for the direct test)

Both model combinations provided good fits to the isobaric data sets as shown in Figures 6-4 and 6-5. Two thermodynamic consistency testing were performed for the measured data sets (direct and point test). On Table 6-3, it can be seen that the WILSON-HOC model combination gave the lowest values for the Δy (point test) and RMSD $\delta\ln(\gamma_1/\gamma_2)$ (direct test). The measured data for the test system passed the two consistencies testing with the WILSON-HOC model combination.

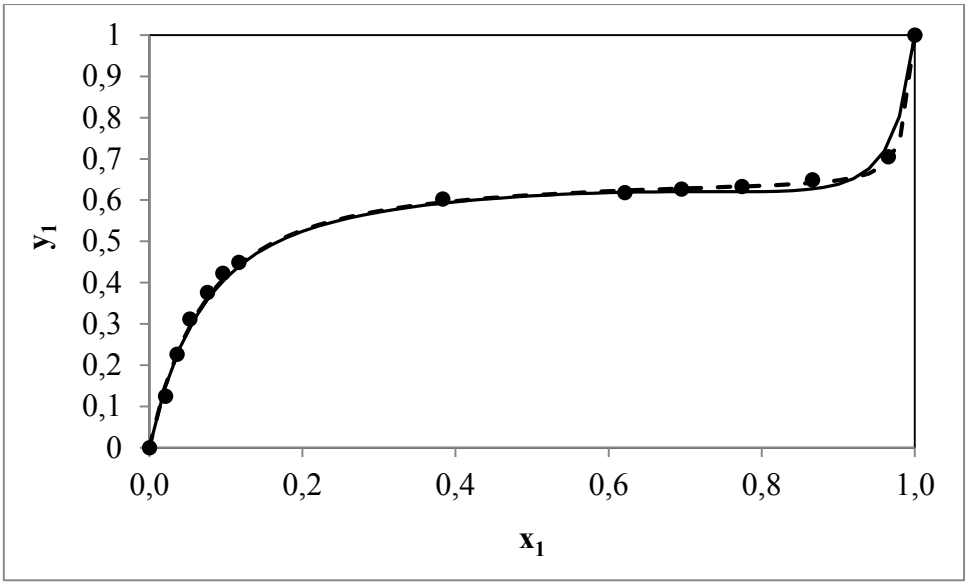

Figure 6-4: Fit of the NRTL-HOC and WILSON-HOC model combinations to the x-y plot of the cyclohexane (1) + ethanol (2) system at 40 kPa. (●) this work, (−) NRTL-HOC, (- - -) WILSON-HOC

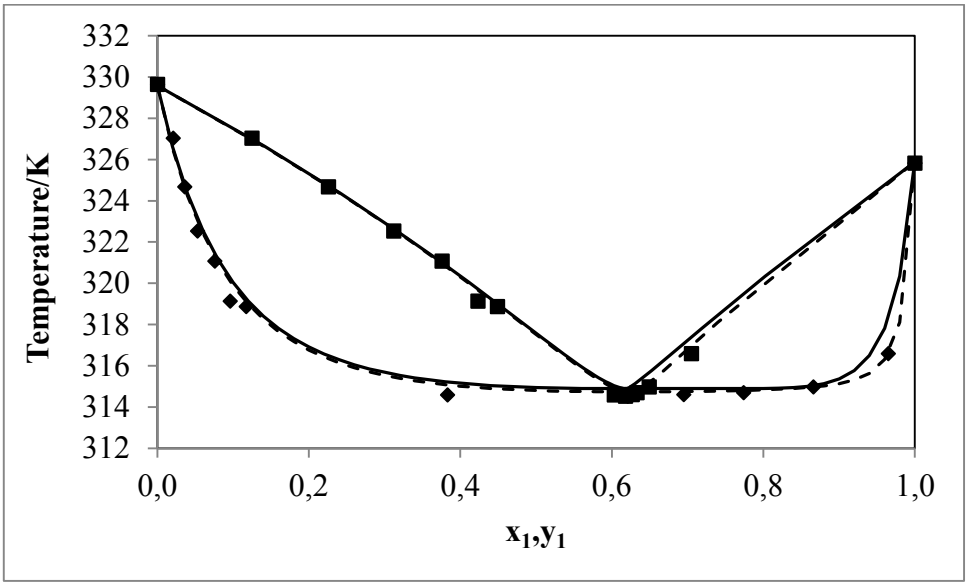

Figure 6-5: Fit of the NRTL-HOC and WILSON-HOC model combinations to the T-x-y plot of the cyclohexane (1) + ethanol (2) system at 40 kPa. (♦) P-x_1, (■) P-y_1, (−) NRTL-HOC, (- - -) WILSON-HOC

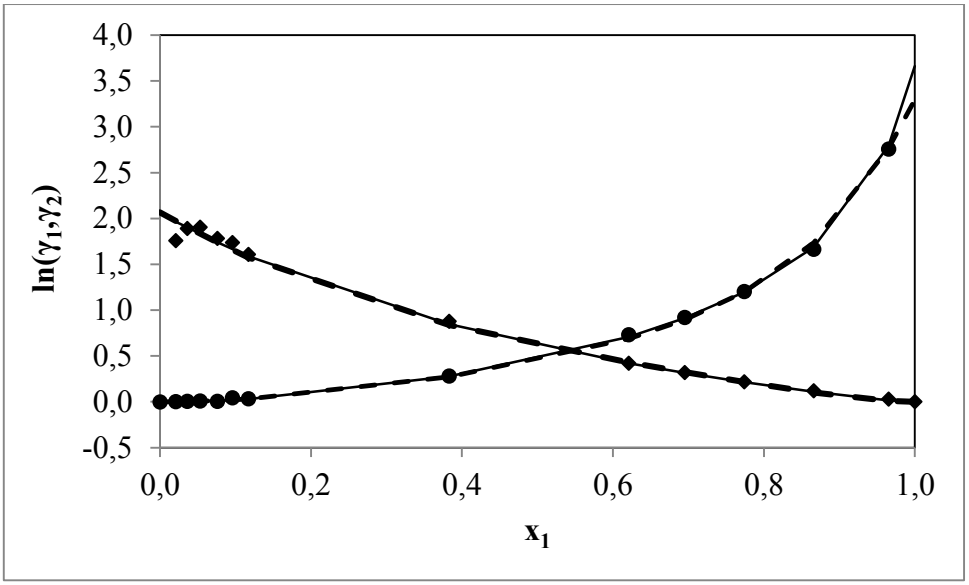

Figure 6-6: Comparison of the experimental activity coefficients and those calculated from the NRTL-HOC and WILSON-HOC model combinations for the cyclohexane (1) + ethanol (2) system at 40 kPa. (♦) experimental ln γ_1, (●) experimental ln γ_2, (−) NRTL-HOC, (- - -) WILSON-HOC.

6.3 Gas chromatograph calibration for the new systems

The Shimadzu 2014 GC was used for phase composition analysis for the new systems measured in this work. The GC detector calibrations plots for the new systems were linear and they passed through the origin except for the system of methyl propyl ketone (1) + 2-methylpropan-1-ol as shown in Figures 5-23 and 5-24 of Chapter 5 where all the points did not fit well with a linear curve. A second order polynomial regression type was therefore used for the calibration plots of this system. For this reason, since the slope of one dilute region cannot be equal to the inverse of the slope of the other region, a single calibration plot could not represent the entire composition range. The area ratio method proposed by Raal and Mühlbauer (1998) as earlier discussed in Chapter 4 was used for the second order polynomial to calculate the phase compositions. The appropriate calibration relationship was used to determine the phase compositions. For the calibration plots of the other two systems: 1-propanol (1) + 4-methyl-2-pentanone (2) and 2-propanol (1) + 4-methyl-2-pentanone (2) as presented in Chapter 5 (Figures 5-7 to 5-8 and 5-15 to 5-16 respectively), the inverse of their response factors were not exactly the same. A similar procedure to that of 2-pentanone (1) + 2-methylpropan-1-ol system for the phase composition determination was therefore used i.e. the calibration plots were used for the correct dilute regions.

6.4 VLE data regression

The process simulator tool used for the regression of experimental data in this work was ASPEN PLUS as it is a well-used process design simulator and provides a convenient means for modelling and predicting the performance of industrial plants. All the experimental data in this work were performed at isothermal conditions ranging from low to moderate pressures. From the two common methods for regression of phase equilibrium data, the γ-Φ approach was chosen as this utilizes an activity coefficient model to account for the non-ideality in the liquid phase and an equation of state model to account for the vapour phase non-ideality. The three most widely used activity coefficient models namely: the Wilson (1964) model, the NRTL (Non Random Two Liquid) (Renon and Prausnitz, 1968) model and the UNIQUAC (Abrams and Prausnitz, 1975) model were employed. The vapour phase non-ideality was accounted for with two different correlations for determining the fugacity coefficients which are: the HOC (Hayden-O'Connell, 1975) correlation and the Nothnagel et al., 1973 correlation abbreviated by NTH. The Tsonopoulos (1974) equation of state model was not used since it was not available in ASPEN PLUS, the process simulator used in the regression of the measured VLE data. All these models and their combinations were chosen due to their capabilities and their past successful applications to systems of alcohols + ketones at isothermal conditions (Pillay, 2009).

For the objective function, the modified Baker method, ordinary least square method and the maximum likelihood method are all available in ASPEN and are applicable to the nature of the systems measured in this work. After rigorous application of each method to the regression, the maximum likelihood method gave the best convergence minimizing P and y data. Therefore, it was chosen for the regression of all the data measured in this work. The algorithm chosen was the Britt-Luecke as opposed to the Deming method which is also available although there was not much difference in their convergences. The initialization method of Deming was used but the weighted least squares is also available in ASPEN. All the parameters were regressed except the NRTL non-randomness parameter (α) which was set to a value of 0.3 for all the systems as earlier discussed in Chapter 3.

In order to verify the quality of the measured data, the regressed data were subjected to thermodynamic consistency testing of both the point test (Van Ness et al., 1973) and the direct test (Van Ness et al., 1975).For the point test, the calculated y_i values were compared with the experimental values to get the yi residuals (δy_i) for each data set. The absolute

average deviation between the experimental vapour phase composition and the calculated vapour phase composition must be less than 0.01 and a plot of Δy vs x_1 must show random scattering about the zero axis in order for the data to be thermodynamic consistent. While for the direct test, the RMSD for $\delta\ln(\gamma_1/\gamma_2)$ must be calculated and compared with the consistency index table of Van Ness (1995). The RMSD $\delta\ln(\gamma_1/\gamma_2)$ was calculated for each data set at a specific isotherm for each model used and compared with the consistency index table of Van Ness (1995) (as shown in Table 3-1).

6.4.1 Modelling results for the 1-propanol (1) + 4-methyl-2-pentanone (2) system

Isothermal VLE data were measured for this system at low to moderate pressures. The regression was done with the combined method (γ-Φ approach). Table 6-4 presents the regressed temperature dependent model binary interaction parameters, the Δy_{avg}, ΔP_{avg} (the deviation between measured values and modelled values) and the RMSD $\delta\ln(\gamma_1/\gamma_2)$ values obtained from the regression of each isotherm. All the regression procedures used for this system were explained earlier in Section 6-4. The models and their combinations were carefully chosen in order to obtain the best fit to the experimental VLE data set. The data measured for the three isotherms of this system were regressed with four different types of thermodynamic model combinations namely: the NRTL-HOC, the WILSON-HOC, the UNIQUAC-HOC and the NRTL-NTH model combinations. This system exhibits an azeotrope at isotherm 353.15 K at $x_1 = y_1 = 0.11$. For the regression of each isotherm, two correlations for determining the fugacity coefficients (the HOC and the NTH) were each combined with an activity coefficient model (the NRTL) in order to determine the combination that best describes the experimental VLE data sets (i.e. the NRTL-HOC and the NRTL-NTH model combinations). The three activity coefficient models (the NRTL, WILSON and the UNIQUAC models) were varied with an equation of state model (HOC) for this same reason.

When the HOC equation of state model was combined with each of the three activity coefficient models, the three model combinations gave the same values for the Δy_{1avg} and ΔP_{avg} at 338.15K, but based on the RMSD $\delta\ln(\gamma_1/\gamma_2)$ the NRTL-HOC model combination gave the best fit though not with much significant difference. When the NRTL activity coefficient model was combined with the HOC and NTH correlations for this isotherm

(338.15 K) both model combinations gave the same values for the Δy_{1avg} and ΔP_{avg} but based on the RMSD $\delta\ln(\gamma_1/\gamma_2)$ the NRTL-HOC combination fit the data well.

Following the same process explained above for the second isotherm (353.15 K), the same values of Δy_{1avg} and RMSD $\delta\ln(\gamma_1/\gamma_2)$ were obtained when the HOC equation of state model was combined with each of the three activity coefficient models but based on the ΔP_{avg} the NRTL-HOC gave the best fit. When the NRTL activity coefficient model was combined with the HOC and the NTH correlations, the NRTL-HOC model combination gave the best fit based on the Δy_{1avg}. The RMSD $\delta\ln(\gamma_1/\gamma_2)$ and ΔPavg are the same.

For the third isotherm (368.15 K), the NRTL-HOC gave the best fit when equation of state model (HOC) was combined with each of the three activity coefficient models and when the activity coefficient model was combined with the two equations of state models. In order to verify the quality and consistency of the measured data, thermodynamic consistency testing was performed for the data set employing the point test (Van Ness, 1973) and direct test (Van Ness, 1975). The Δy_{avg} obtained for each VLE data set were compared with the value provided by Danner and Gess (1990) that for a data to be thermodynamically consistent the Δyavg must be less than 0.01 (point test of Van Ness, 1973). All the data set measured for this system passed this quantitative criterion and as shown on the Δy and ΔP plots for each isotherm, there is random scattering about the x-axis. The only exception is the data set of the third isotherm (368.15 K) that has the highest value of 0.012 for the NRTL-NTH model combination. Plots for the point test (y and P residuals) for each isotherm with the different model combinations are shown in Appendix A. The RMSD $\delta\ln(\gamma_1/\gamma_2)$ values calculated for each data set were compared with the consistency index table of Van Ness (1995) in Chapter 3. All the data sets measured in this work (with no exception) passed this test with the highest value being 0.082 for the NRTL-NTH model combination at 368.15 K. the P-x-y plots showing the comparison of the three activity coefficient models for each isotherm are presented in Appendix A while the plots for the consistency tests performed for each isotherm are presented in Appendix A. The graphical representation of the comparison of the model fits to experimental VLE data for the three isotherms are presented below. All other P-x-y plots are presented in Appendix A. These plots show that the model combinations chosen for this work are able to describe the 1-propanol (1) + 4-methyl-2-pentanone well at the three isotherms.

In conclusion, the NRTL-HOC model combination was found to fit all the data set measured for this system at the three isotherms well more than the other model combinations and the newly isothermal VLE data measured in this work are thermodynamically consistent.

Table 6-4: modelling results obtained for the 1-propanol (1) + 4-methyl-2-pentanone (2) system

model	T/ K	a_{ij}	a_{ji}	b_{ij}	b_{ji}	AAD ΔP/kPa	AAD Δy	RMSD δln(γ_1/γ_2)
NRTL-HOC	338.15	15.44	-10.7	-5055	3716	0.008	0.003	0.023
	353.15	5.13	7.79	-1691	-2644	0.011	0.004	0.034
	368.15	1.49	13.3	-519	-4706	0.031	0.010	0.074
NRTL-NTH	338.15	6.05	-5.82	-1876	2049	0.008	0.003	0.024
	353.15	5.32	7.93	-1754	-2692	0.011	0.005	0.034
	368.15	1.28	13.55	-438	-4798	0.030	0.012	0.082
WILSON-HOC	338.15	0.00	0.00	-97.9	-162	0.008	0.003	0.025
	353.15	0.00	0.00	-120	-116	0.013	0.004	0.034
	368.15	0.00	0.00	-179	-42.19	0.032	0.011	0.075
UNIQUAC-HOC	338.15	-0.63	0.266	0.00	0.00	0.008	0.003	0.024
	353.15	0.00	0.00	-187	79.39	0.013	0.004	0.034
	368.15	0.00	0.00	-137	47.68	0.033	0.011	0.075

u(T) = 0.06 K

b_{ij} and a_{ij} are the binary interaction parameters for the activity coefficient models in ASPEN, ($\tau ij = aij + bij/T$), α_{ij} (non-randomness parameter) set to 0.3 for the NRTL-HOC and NRTL-NTH model combinations, RMSD δln(γ_1/γ_2) (the Root Mean Square deviation for the direct test)

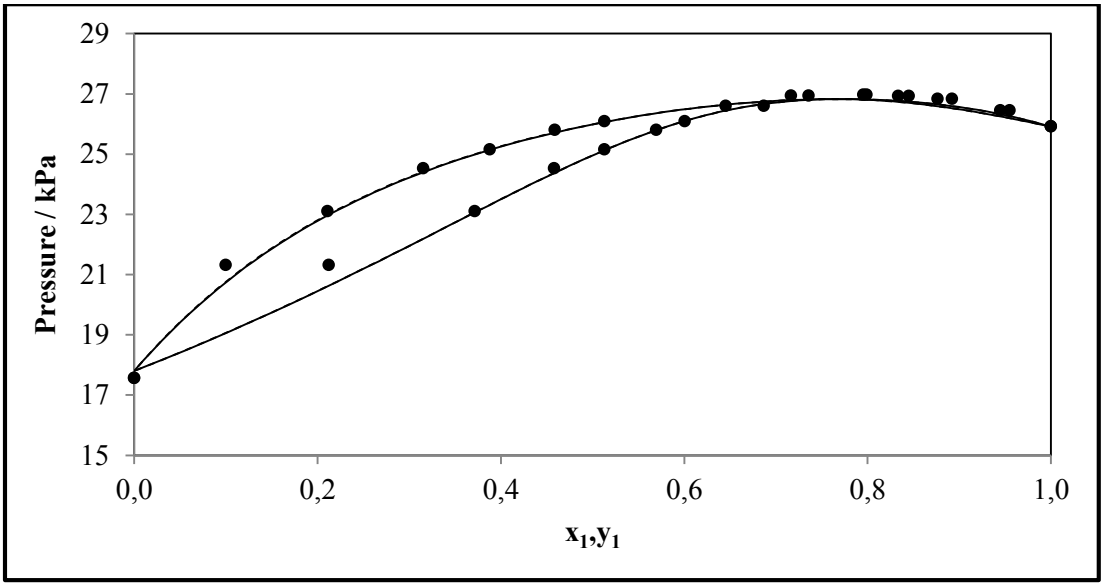

Figure 6-7: Fit of the NRTL-HOC and NRTL-NTH model combinations to the p-x-y plot of the 1-propanol (1) + 4-methyl-2-pentanone (2) system at 338.15 K for the combined method: (•) this work, (—) NRTL-HOC, (- - - -) NRTL-NTH

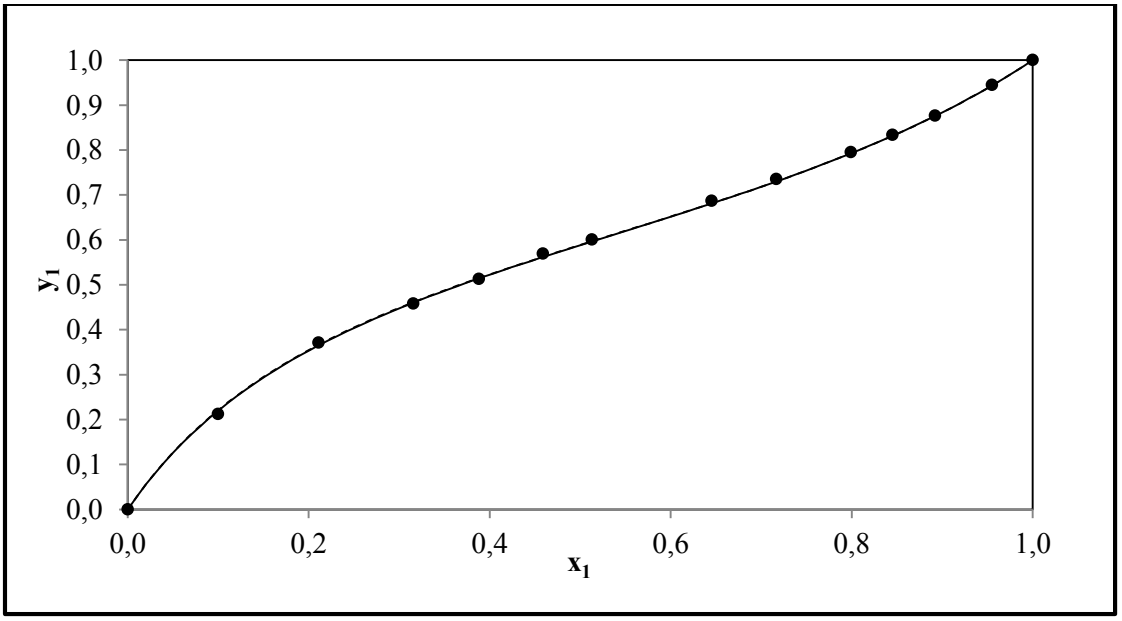

Figure 6-8: Fit of the NRTL-HOC and NRTL-NTH model combinations to the x-y plot of the 1-propanol (1) + 4-methyl-2-pentanone (2) system at 338.15 K for the combined method: (•) this work, (—) NRTL-HOC, (- - - -) NRTL-NTH

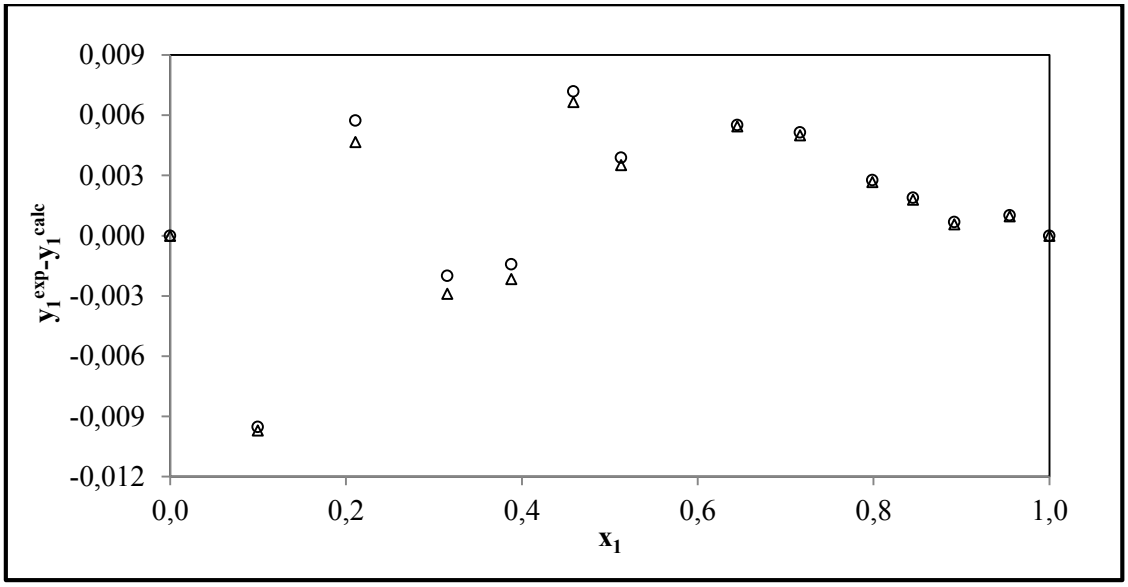

Figure 6-9: Point test (varying EOS) Δy_1 for the 1-propanol (1) + 4-methyl-2-pentanone (2) system at 338.15 K: (◦) NRTL-HOC, (Δ) NRTL-NTH

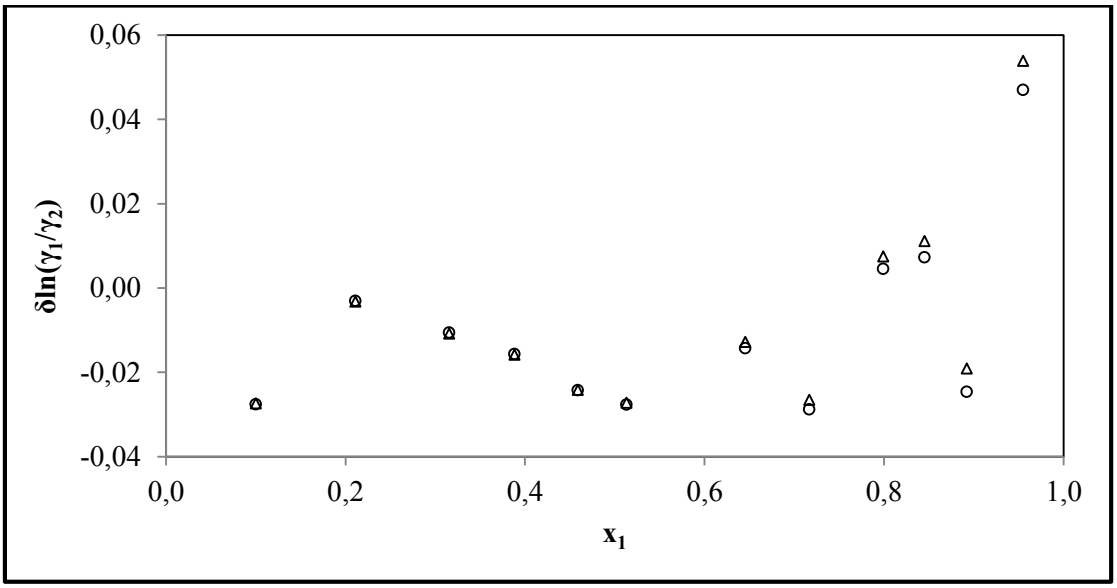

Figure 6-10: Direct test (varying EOS): $\delta\ln(\gamma_1/\gamma_2)$ for the 1-propanol (1) + 4-methyl-2-pentanone (2) system at 338.15 K : (◦) NRTL-HOC, (Δ) NRTL-NTH

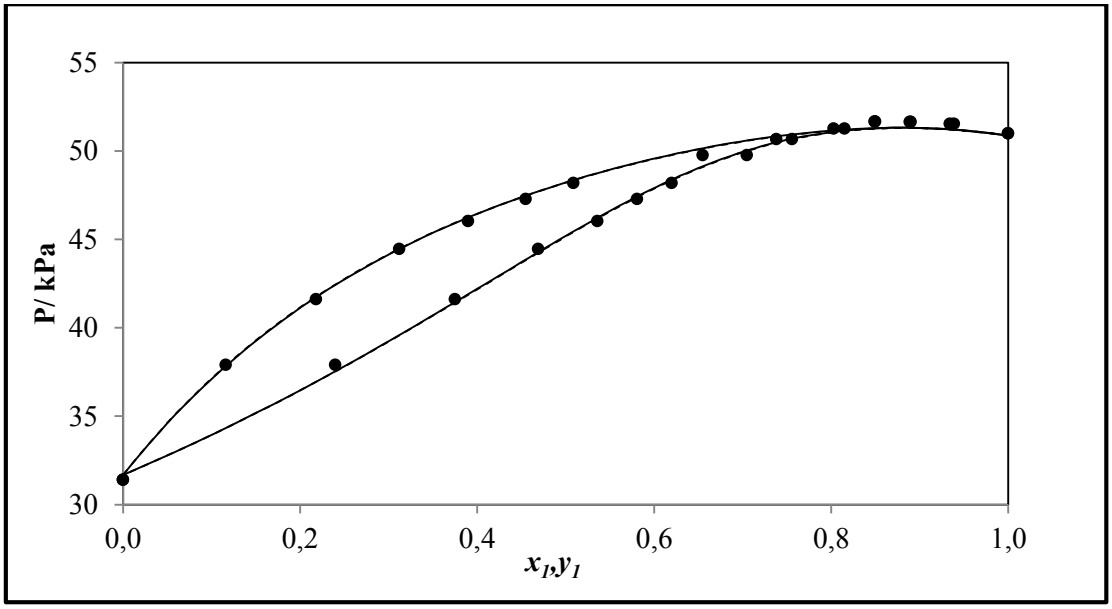

Figure 6-11: Fit of the NRTL-HOC and NRTL-NTH model combinations to the P-x-y plot of the 1-propanol (1) + 4-methyl-2-pentanone (2) system at 353.15 K for the combined method: (•) this work, (—) NRTL-HOC, (- - - -) NRTL-NTH

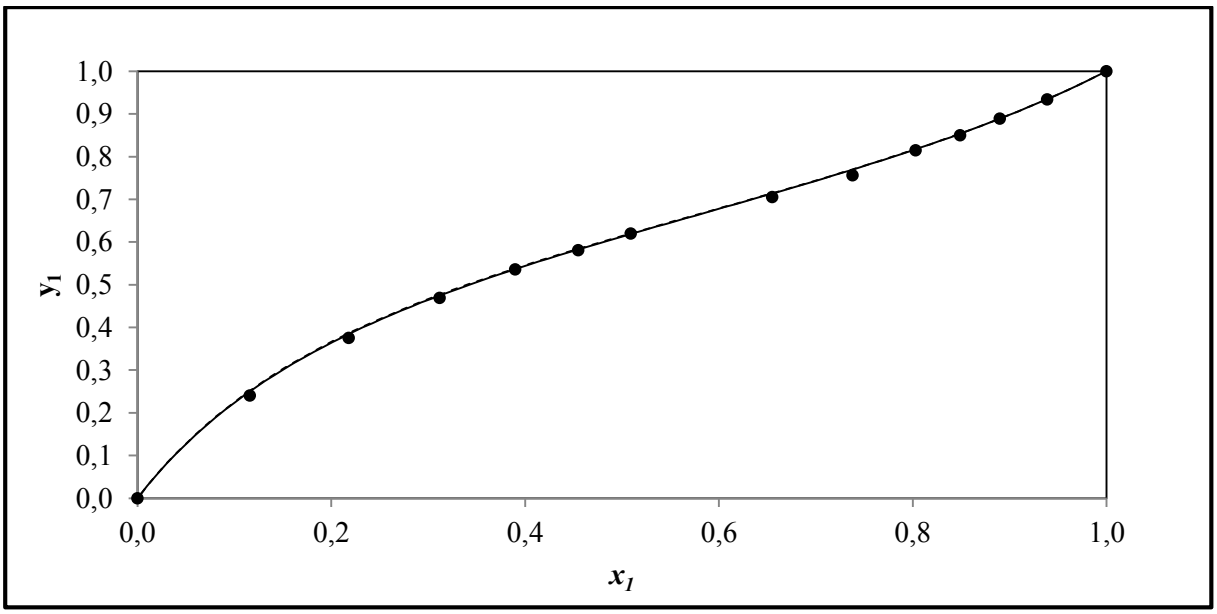

Figure 6-12: Fit of the NRTL-HOC and NRTL-NTH model combinations to the x-y plot of the 1-propanol (1) + 4-methyl-2-pentanone (2) system at 353.15 K for the combined method: (•) this work, (—) NRTL-HOC, (- - - -) NRTL-NTH

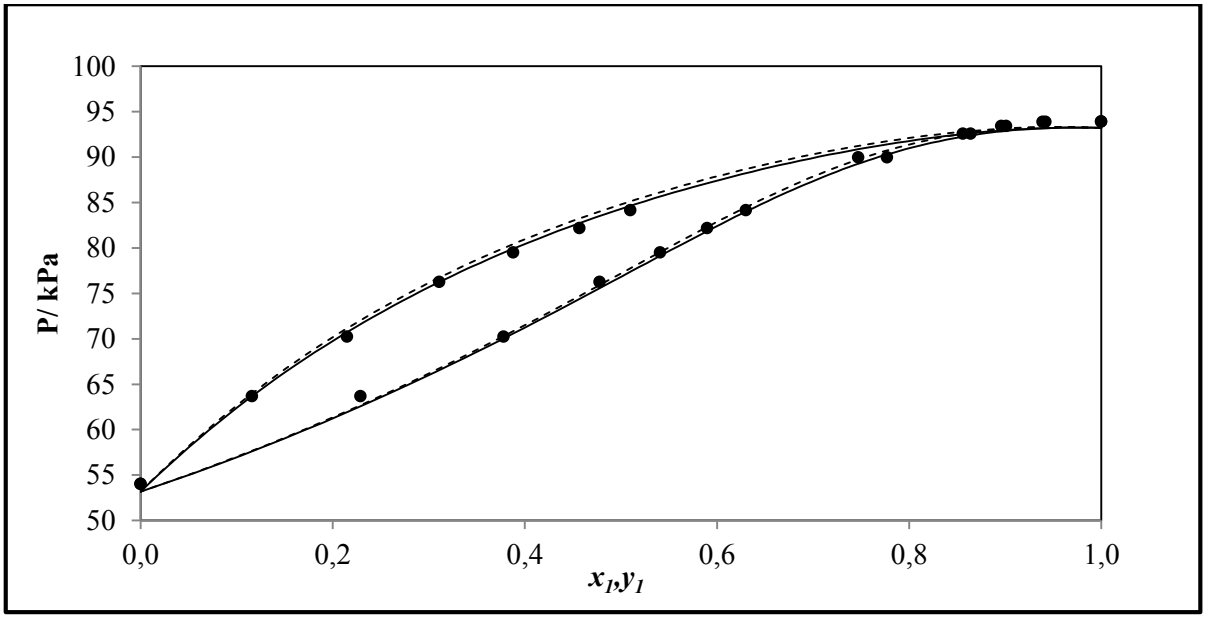

Figure 6-13: Fit of the NRTL-HOC and NRTL-NTH model combinations to the P-x-y plot of the 1-propanol (1) + 4-methyl-2-pentanone (2) system at 368.15 K for the combined method: (•) this work, (—) NRTL-HOC, (- - - -) NRTL-NTH

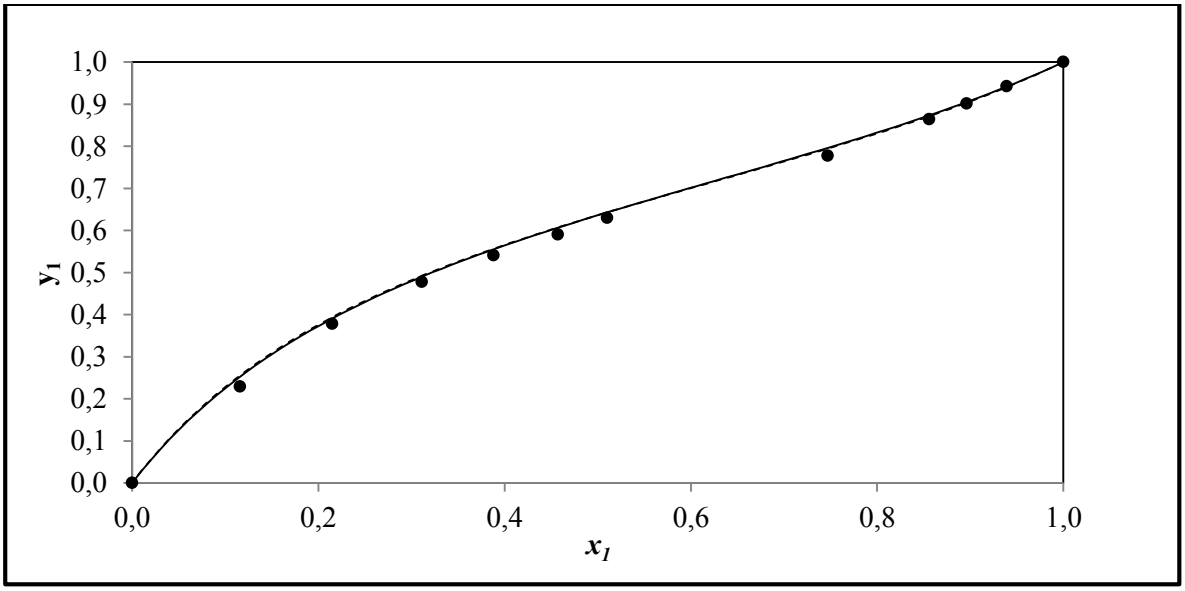

Figure 6-14: Fit of the NRTL-HOC and NRTL-NTH model combinations to the x-y plot of the 1-propanol (1) + 4-methyl-2-pentanone (2) system at 368.15 K for the combined method: (•) this work, (—) NRTL-HOC, (- - - -) NRTL-NTH

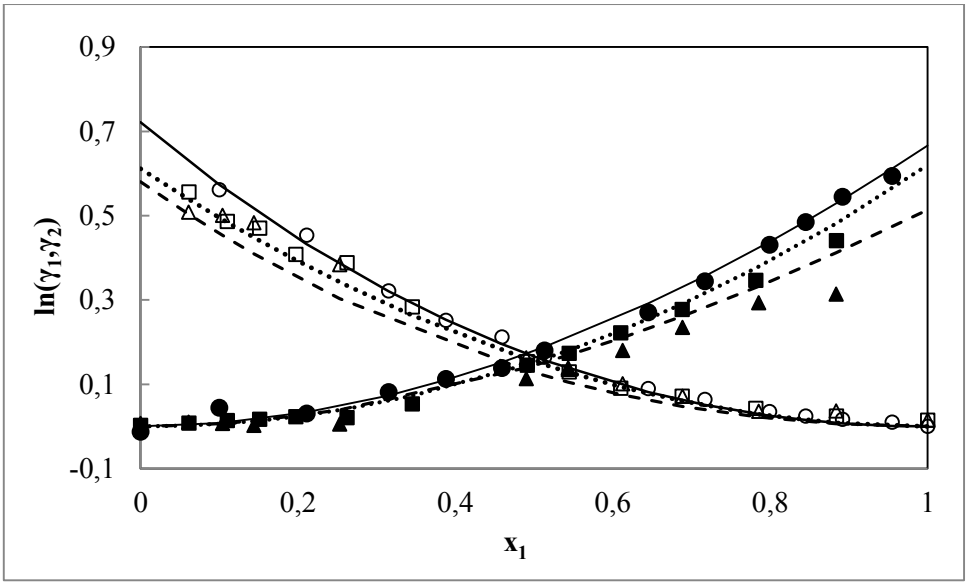

Figure 6-15: Comparison between the experimentally determined liquid-phase activity coefficients and those calculated from the NRTL model for 1-propanol (1) + 4-methyl-2-pentanone (2) system at 338.15 K, 353.15 K and 368.15 K. 338.15 K (—), 353.15 K (…) and 368.15 K (- - -) for NRTL-HOC model combination; 338.15 K (○), 353.15 K (□) and 368.15 K (Δ), for experimental γ_1; 338.15 K (●), 353.15 K (■) and 368.15 K (▲), for experimental γ_2

Figure 6-15 is the illustrative plot of the liquid phase activity coefficient for the 1-propanol (1) + 4-methyl-2-pentanone system at 338.15 K, 353.15 K and 368.15 K. As shown on the plot, the NRTL-HOC model combination provided a good fit to the isothermal VLE data set.

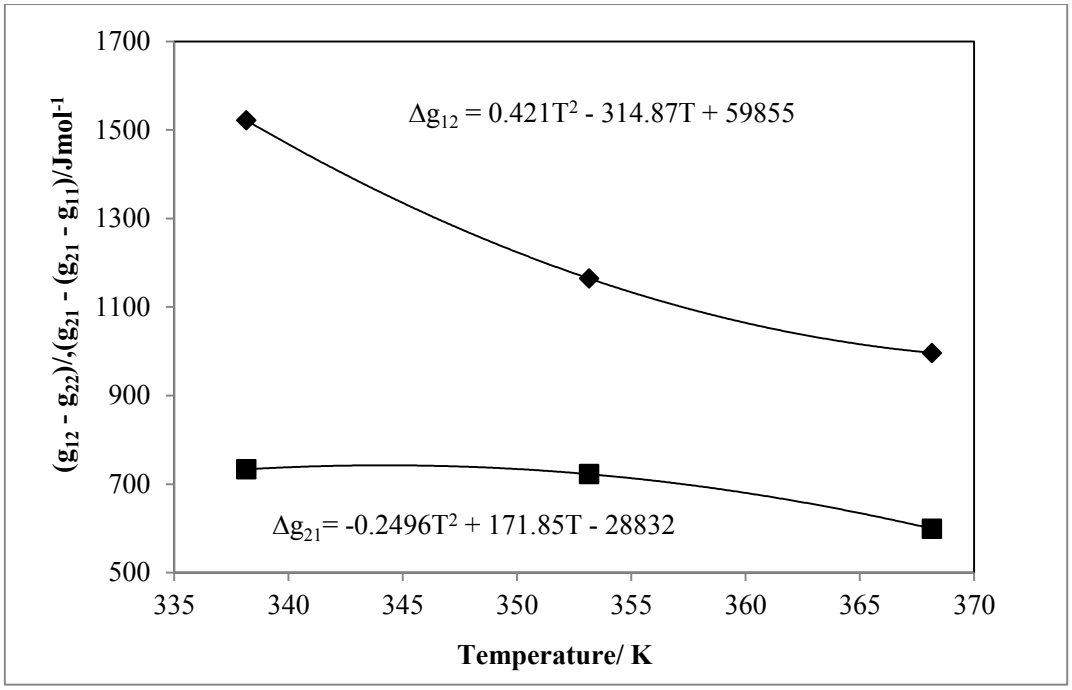

Figure 6-16: Temperature dependence of the NRTL-HOC model combination parameters for 1-propanol (1) + 4-methyl-2-pentanone (2) system. (■), g_{21}-g_{12}; (♦) g_{12}-g_{21}

6.4.2 Modelling results for the 2-propanol (1) + 4-methyl-2-pentanone (2) system

This system was measured at three different isotherms (323.15, 338.15 and 353.15) K. The temperature dependent binary interaction parameters obtained for the model combinations, the average absolute deviation for the vapour phase compositions (Δy_1), the absolute deviation for the pressure *(ΔP)* and the RMSD $\delta\ln(\gamma_1/\gamma_2)$ values obtained from the regression of each isotherm are presented in Table 6-3. Four different model combinations were employed in the regression of the isothermal VLE data measured namely: NRTL-HOC, NRTL-NTH, WILSON-HOC and UNIQUAC-HOC. The NRTL activity coefficient model was combined with the HOC and NTH models in order to obtain the model combination that best fit the experimental VLE data sets. As shown in Table 6-5, at 353.15 K the NRTL-HOC model combination gave the best fit as compared with the NRTL-NTH model combination although with not much significant difference. Based on the ΔPavg the NRTL-HOC model combination gave the highest ΔPavg value of 0.024 kPa at 338.15 K. It can also be seen that the WILSON-HOC and the UNIQUAC-HOC have the same Δy_{1avg}, ΔP_{avg} and RMSD $\delta(\ln\gamma_1/\gamma_2)$ values of 0.006, 0.01 and 0.051 at 323.15 K respectively. At 353.15 K the WILSON-HOC and UNIQUAC-HOC also have the same Δy_{1avg}, ΔP_{avg} and RMSD $\delta\ln(\gamma_1/\gamma_2)$

values of 0.006, 0.022 and 0.053 respectively.

In summary, it can be seen that the $\Delta y_1 avg$ values obtained for each data set are lower than 0.01 indicating that at each isotherm the VLE data measured pass the first criterion of the point test (Van Ness, 1973). As observed in Figures (6-19) the y residuals plot for isotherm 323.15K with the NRTL-HOC and NRTL-NTH model combinations show important negative bias and failed in the random scattering about the x-axis this was due to the systematic error in the calibration of the temperature probe and the pressure transducer. Also comparing the RMSD $\delta \ln(\gamma_1/\gamma_2)$ values (the highest value being 0.066) obtained for the data sets with the consistency index table of Van Ness (Van Ness, 1995) as discussed earlier shows that the measured data passed the direct test.

Generally, all the model combinations fit the data set at the three different isotherms well as shown in the Figures below and the P-x-y plots presented in Appendix A. For the 323.15 K isotherm, Figures (6-17) and (6-18) give the comparison of the model fits to the experimental data. The graphical representation of the point test and direct test is shown in Figures (6-19 and 6-20). The P-x-y plots showing the comparison of the activity coefficient models for the three isotherms are shown in Appendix A. The point test and direct test plots for this system are presented in Appendix A.

Table 6-5: Model results obtained for the 2-propanol (1) + 4-methyl-2-pentanone (2) system

model	*T/ K*	a_{ij}	a_{ji}	b_{ij}	b_{ji}	AAD ΔP/kPa	AAD (Δy)	RMSD $\delta \ln(\gamma_1/\gamma_2)$
NRTL-HOC	323.15	11.6	-3.98	-3564.3	1360.34	0.011	0.006	0.050
	338.15	8.41	6.21	-2688.7	-1986.5	0.024	0.006	0.053
	353.15	-12.4	-0.40	4555.28	152.99	0.019	0.006	0.053
NRTL-NTH	323.15	13.11	-0.11	-4040.3	112.47	0.010	0.006	0.053
	338.15	8.34	6.71	-2690.1	-2142.7	0.025	0.007	0.059
	353.15	12.25	0.22	-4137.8	-49.82	0.024	0.008	0.066
WILSON-HOC	323.15	-0.07	-0.2	-81.24	-113.96	0.010	0.006	0.051
	338.15	-2.51	-3.44	731.15	1025.66	0.023	0.006	0.055
	353.15	1.77	3.11	-676.05	-1253.6	0.022	0.006	0.053
UNIQUAC-HOC	323.15	46.44	-155	0.00	0.00	0.01	0.006	0.051
	338.15	0.00	0.00	65.59	-172.11	0.023	0.006	0.056
	353.15	-0.07	0.09	79.59	-173.69	0.022	0.006	0.053

u(T) = 0.06 K b_{ij} and a_{ij} are the binary interaction parameters for the activity coefficient models in ASPEN, ($\tau_{ij} = a_{ij} + b_{ij}/T$), α_{ij} (non-randomness parameter) set to 0.3 for the NRTL-HOC and NRTL-NTH model combinations, RMSD $\delta \ln(\gamma_1/\gamma_2)$ (the Root Mean Square deviation for the direct test)

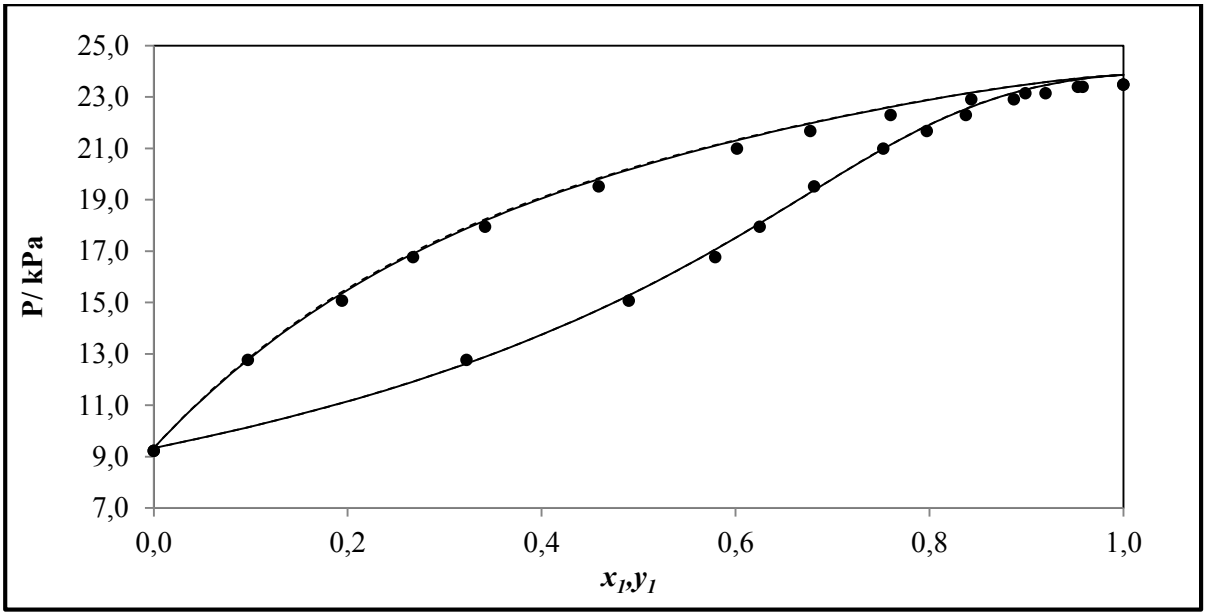

Figure 6-17: Fit of the NRTL-HOC and the NRTL-NTH models to the P-x-y plot of the 2-propanol (1) + methyl isobutyl (2) system at 323.15 K for the combined method: (•) this work, (—) NRTL-HOC, (- - - -) NRTL-NTH

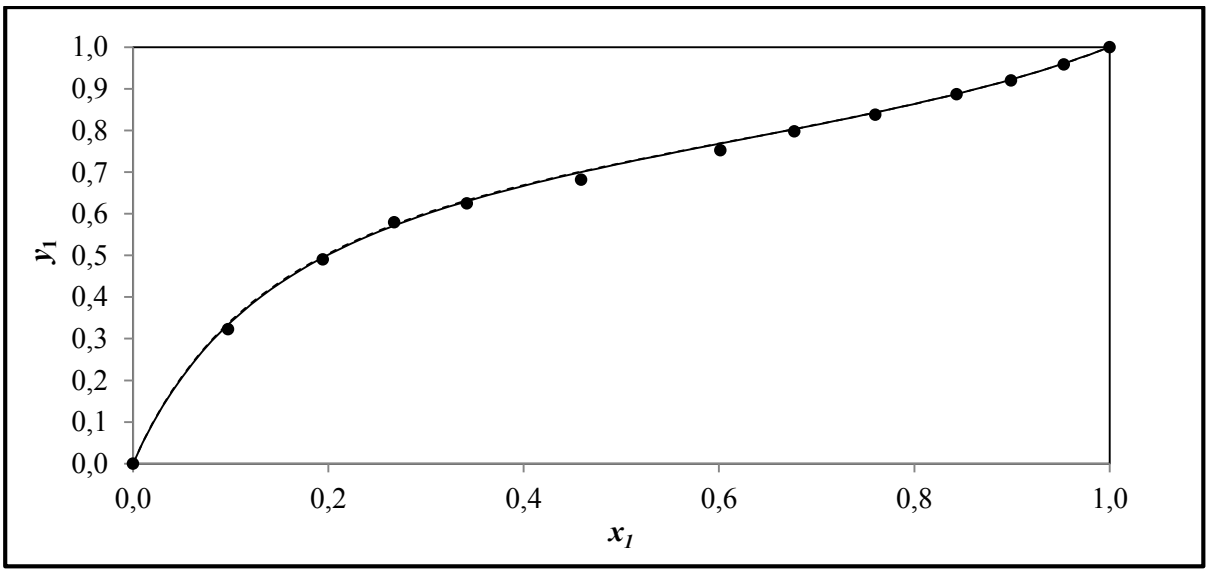

Figure 6-18: Fit of the NRTL-HOC and NRTL-NTH model combinations to the x-y plot of the 2-propanol (1) + methyl isobutyl ketone (2) system at 323.15 K for the combined method: (•) this work, (—) NRTL-HOC, (- - - -) NRTL-NTH

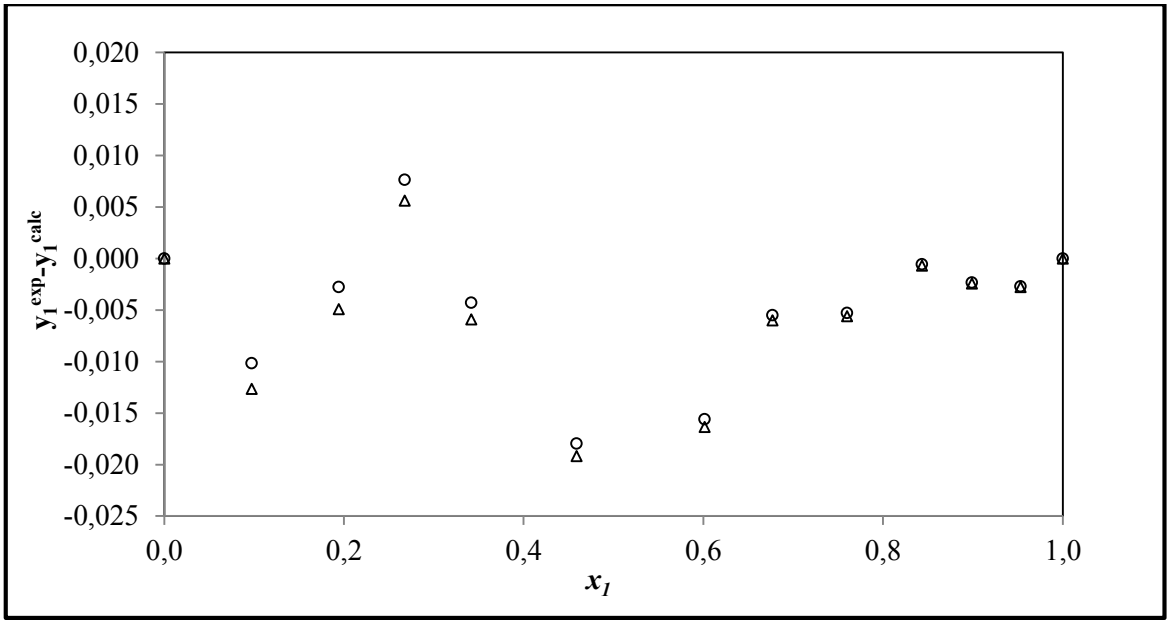

Figure 6-19: Point test (varying EOS): Δy_1 for the 2-propanol (1) + methyl isobutyl ketone (2) system at 323.15K: (○) NRTL-HOC, (Δ) NRTL-NTH

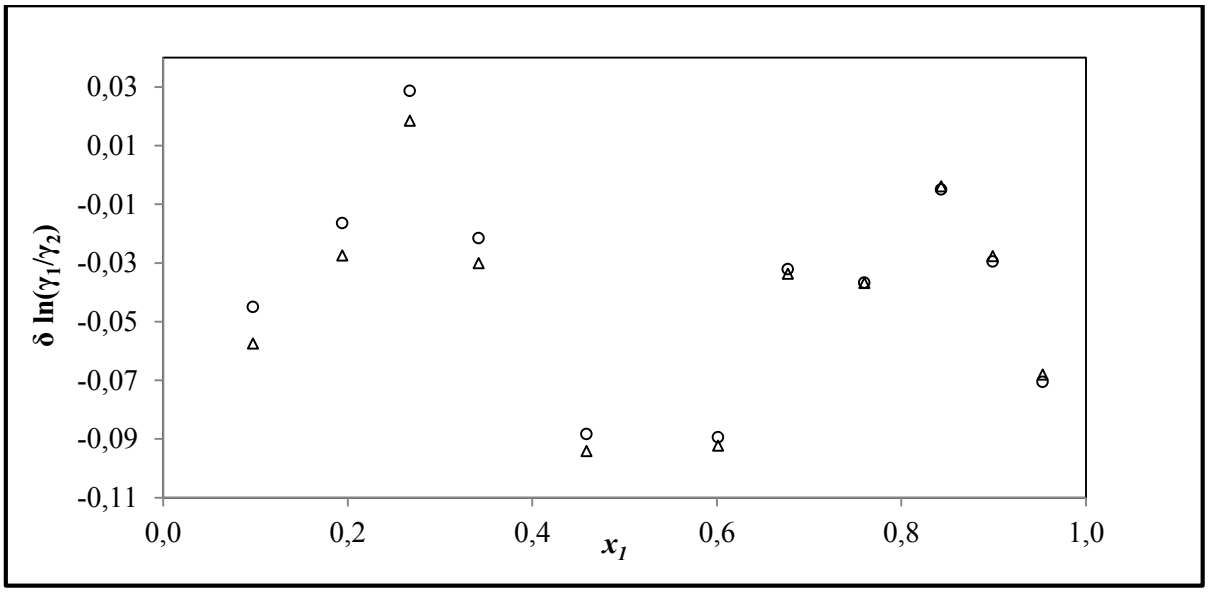

Figure 6-20: Direct test (varying EOS): $\delta\ln(\gamma_1/\gamma_2)$ for the 2-propanol (1) + 4-methyl-2-pentanone (2) system at 323.15K: (○) NRTL-HOC, (Δ) NRTL-NTH

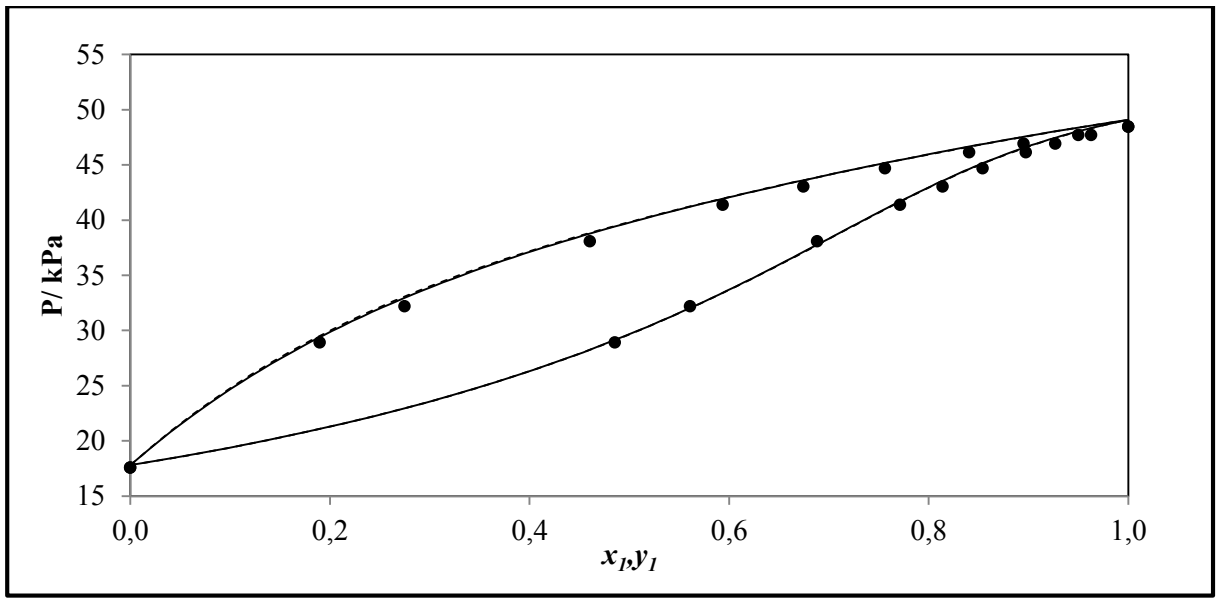

Figure 6-21: Fit of the NRTL-HOC and NRTL-NTH model combinations to the p-x-y plot of the 2-propanol (1) + 4-methyl-2-pentanone (2) system at 338.15 K for the combined method: (•) this work, (—) NRTL-HOC, (- - - -) NRTL-NTH

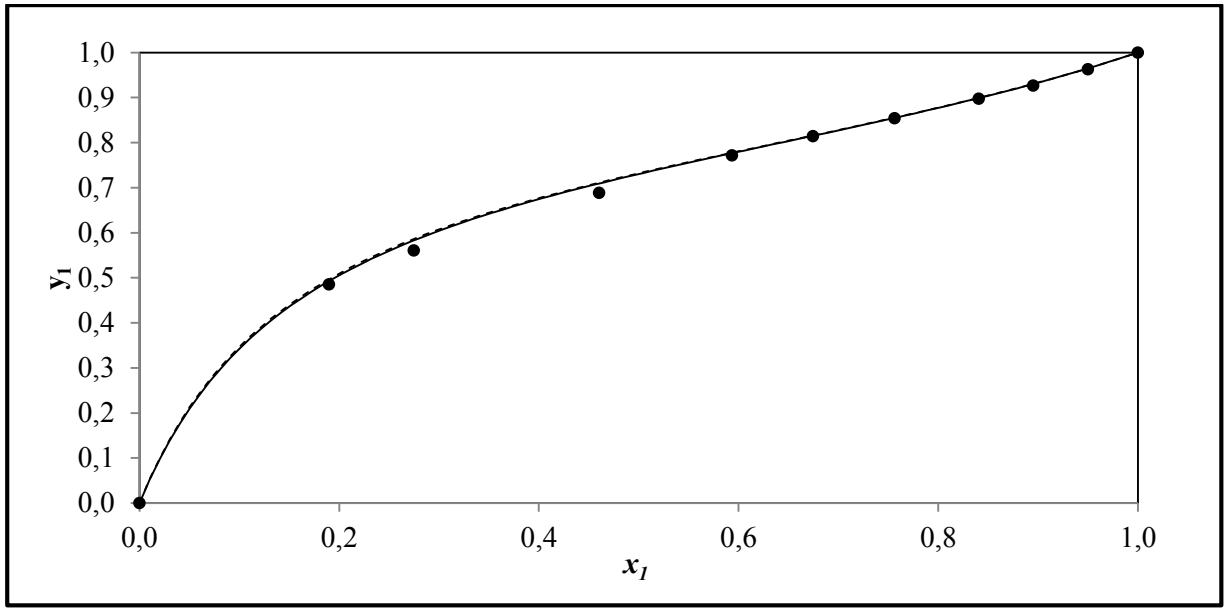

Figure 6-22: Fit of the NRTL-HOC and NRTL-NTH model combinations to the x-y plot of the 2-propanol (1) + 4-methyl-2-pentanone (2) system at 338.15 K for the combined method: (•) this work, (—) NRTL-HOC, (- - - -) NRTL-NTH

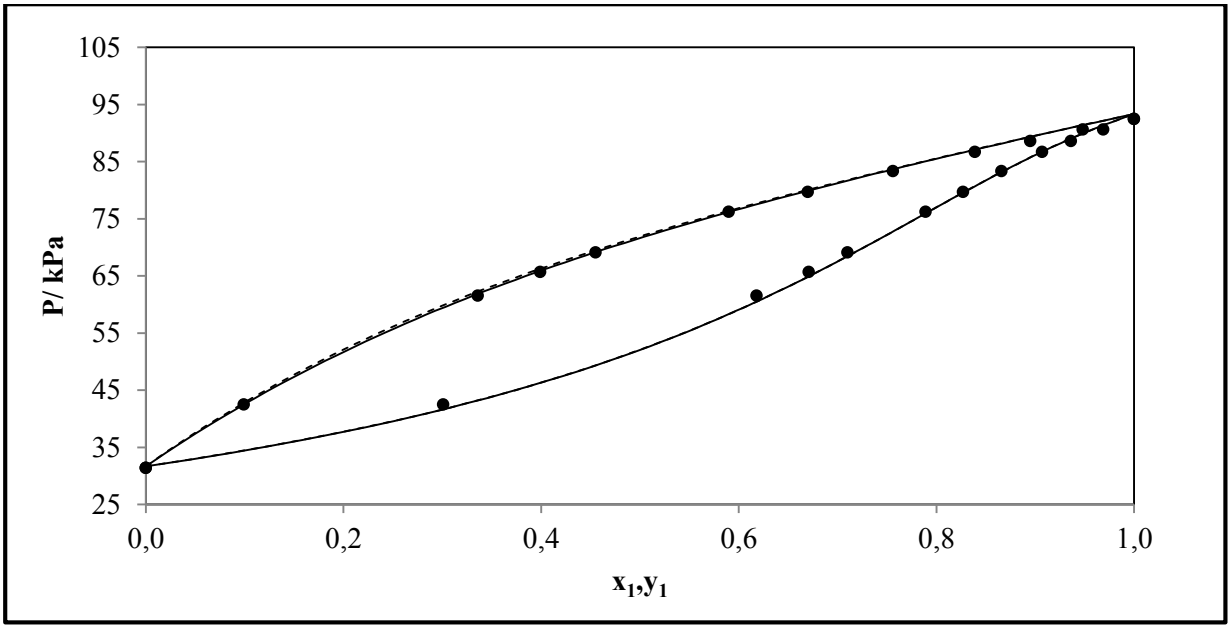

Figure 6-23: Fit of the NRTL-HOC and NRTL-NTH model combinations to the p-x-y plot of the 2-propanol (1) + 4-methyl-2-pentanone (2) system at 353.15 K for the combined method: (•) this work, (—) NRTL-HOC, (- - - -) NRTL-NTH

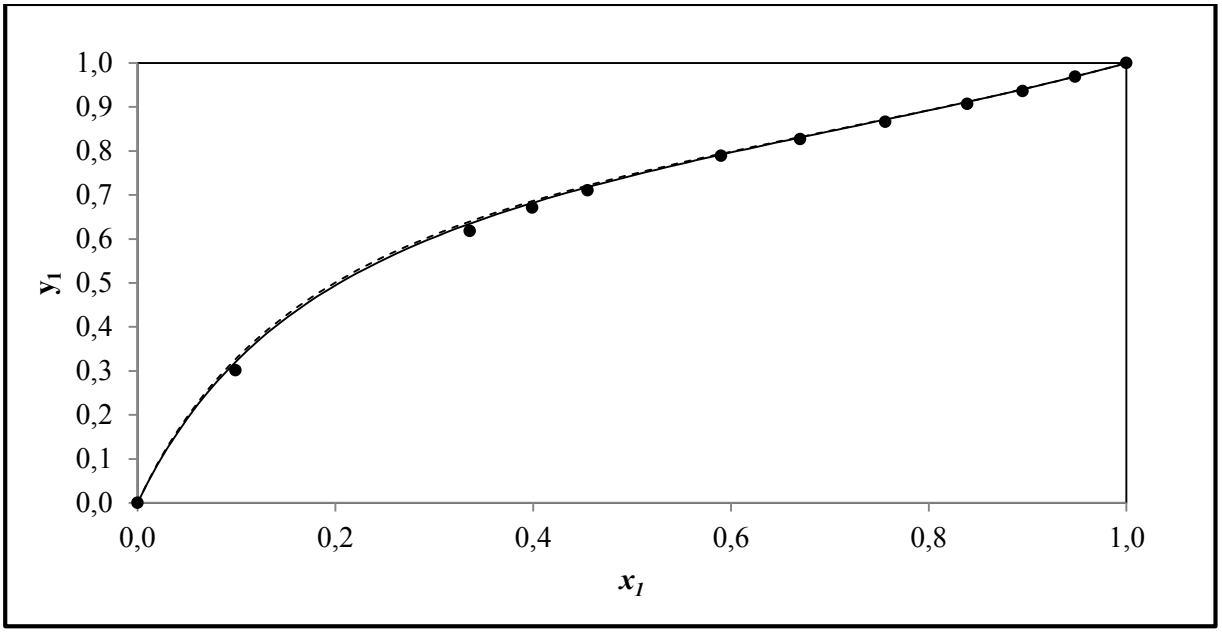

Figure 6-24: Fit of the NRTL-HOC and NRTL-NTH model combinations to the x-y plot of the 2-propanol (1) + 4-methyl-2-pentanone (2) system at 353.15 K for the combined method: (•) this work, (—) NRTL-HOC, (- - - -) NRTL-NTH

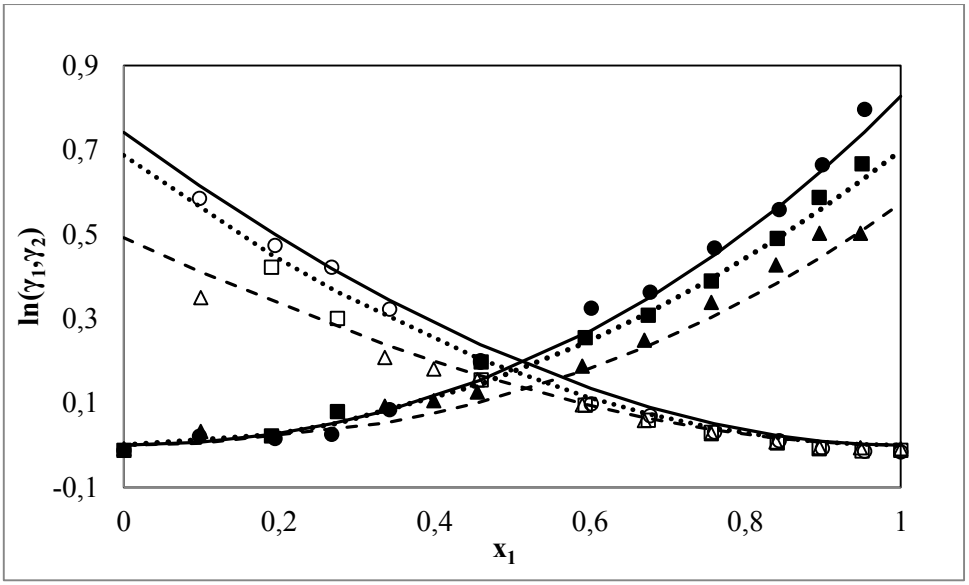

Figure 6-25: Comparison between the experimentally determined liquid-phase activity coefficients and those calculated from the NRTL-HOC model combination for 2-propanol (1) + 4-methyl-2-pentanone (2) system at 323.15 K, 338.15 K and 353.15 K. 323.15 K (—), 338.15 K (…) and 353.15 K (- - -) for NRTL-HOC model combination; 323.15 K (○), 338.15 K (□) and 353.15 K (Δ), for experimental γ_1; 323.15 K (●), 338.15 K (■) and 353.15 K (▲), for experimental γ_2

A representative plot of the comparison between the calculated liquid phase activity coefficients and the values obtained from the NRTL-HOC model combination is shown in Figure 6-25. From the figure, it shows that the NRTL-HOC model combination fitted the data set well.

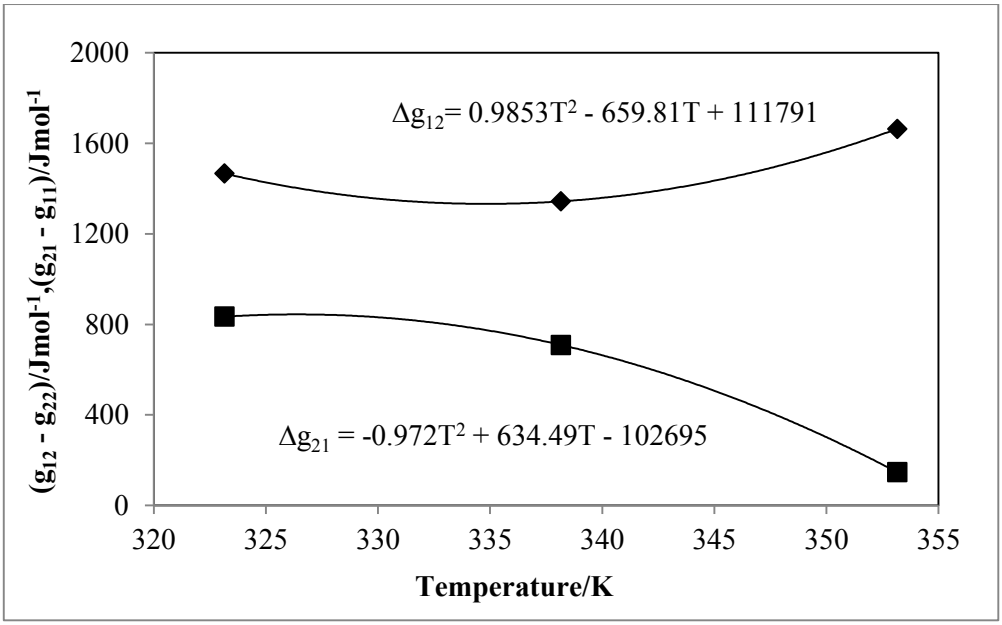

Figure 6-26: Temperature dependence of the NRTL-HOC model combination parameters for 2-propanol (1) + 4-methyl-2-pentanone (2) system. (■) g_{21}-g_{12}; (♦) g_{12}-g_{21}

6.4.3 Modelling results obtained for the 2-pentanone (1) + methylpropan-1-ol system

Three isothermal VLE data sets were measured for this system and the data sets were regressed with the combined method approach following the procedure explained in section 6-4. Table 6-6 summarizes the results obtained for the temperature dependent binary interaction parameters, the Δy_{avg}, ΔP_{avg} and the RMSD $\delta \ln (\gamma_1/\gamma_2)$ for the three isotherms. Similarly to the previously discussed systems, four model combinations were used for the regression of the data sets in order to obtain the best fit as a model combination may fit a data set well than the others. The model combinations are: the NRTL-HOC, the NRTL-NTH, the WILSON-HOC and the UNIQUAC-HOC model combinations. The model variations were done to determine of the best fit model combinations.

Varying the equation of state for the first isotherm (343.15 K) i.e. using the NRTL-HOC and NRTL-NTH model combination, the NRTL-NTH combination gave the best fit for the VLE data set based on the Δy_{avg} values, although both gave the same value for the ΔP_{avg}. The WILSON-HOC and UNIQUAC-HOC gave the best fit when the activity coefficient models were varied for this isotherm; both have the same values for Δy_{avg} and ΔP_{avg}.

For the 358.15 K, the NRTL-NTH model combination gave the best fit based on ΔP_{avg} when the equations of state models were varied. The NRTL-HOC and the WILSON-HOC gave the same values for Δy_{avg} and ΔP_{avg} but the UNIQUAC-HOC has the best fit based on ΔP_{avg} when activity coefficient models were varied.

The NRTL-HOC model combination fitted the data set for the 363.15 K both when the equations of state models were varied and when the activity coefficient models were varied. The experimental VLE data sets were subjected to thermodynamic consistency testing with the point test (Van Ness, 1973) and direct test (Van Ness, 1975) in order to verify the quality of the measured VLE data. For the point test, the Δy_{avg} values calculated for each data set were compared with the value of 0.01 (suggested by Danner and Gess, 1995) and for the direct test, the RMSD $\delta \ln (\gamma_1/\gamma_2)$ values calculated also for each data set were compared with the consistency index table of Van Ness (Van Ness, 1995). The y and P residuals for the three isotherms scatter well about the x-axis. The measured VLE data for the three isotherms pass the two thermodynamic consistency tests indicating that the newly measured VLE data are thermodynamically consistent. The P-x-y plots showing the comparison of the model fit to experimental data are shown in Appendix A. Plots for the point and direct test are shown in Appendix A. The graphical representations of the comparison of the model fit to the experimental VLE data are shown in Figures 6-28 to 6-35.

Table 6-6: modelling results obtained for the 2-pentanone (1) + 2-methylpropan-1-ol system

model	*T/ K*	a_{ij}	a_{ji}	b_{ij}	b_{ji}	*AAD* ΔP*/kPa*	*AAD* (Δy)	*RMSD* $\delta ln(\gamma_1/\gamma_2)$
NRTL-HOC	343.15	-1.97	-11.3	631.67	4072.9	0.006	0.005	0.036
	358.15	0.73	8.48	-299.5	-2863	0.015	0.005	0.031
	363.15	2.53	10.34	-990.6	-3546	0.026	0.005	0.035
NRTL-NTH	343.15	-2.49	-11.7	803.3	4245.3	0.006	0.004	0.033
	358.15	1.27	8.86	-504.4	-2991	0.014	0.005	0.032
	363.15	3.10	10.76	-1211	-3687	0.026	0.005	0.036
WILSON-HOC	343.15	0.00	0.00	-163.4	-2.186	0.006	0.005	0.035
	358.15	0.00	0.00	-132.0	-0.87	0.015	0.005	0.033
	363.15	0.00	0.00	-160.6	26.29	0.026	0.005	0.037
UNIQUAC-HOC	343.15	0.00	0.00	12.75	-61.95	0.006	0.005	0.035
	358.15	0.00	0.00	2.509	-42.07	0.014	0.005	0.033
	363.15	0.00	0.00	28.27	-69.09	0.026	0.005	0.037

u(T) = 0.06 K b_{ij} and a_{ij} are the binary interaction parameters for the activity coefficient models in ASPEN, ($\tau_{ij} = a_{ij} + b_{ij}/T$), αij (non-randomness parameter) set to 0.3 for the NRTL-HOC and NRTL-NTH model combinations, RMSD $\delta ln(\gamma_1/\gamma_2)$ (the Root Mean Square deviation for the direct test)

Table 6-7: Best model for the new isotherms measured in this work

Systems	Temperature (K)	Best model
1-propanol (1) + 4-methyl-2-pentanone	338.15	NRTL-HOC
	353.15	WILSON-HOC
	368.15	NRTL-HOC
2-propanol (1) + 4-methyl-2-pentanone	323.15	NRTL-HOC
	338.15	WILSON-HOC
	353.15	WILSON-HOC
2-pentanone (1) + 2-methylpropan-1-ol	343.15	NRTL-HOC
	358.15	NRTL-HOC
	363.15	NRTL-HOC

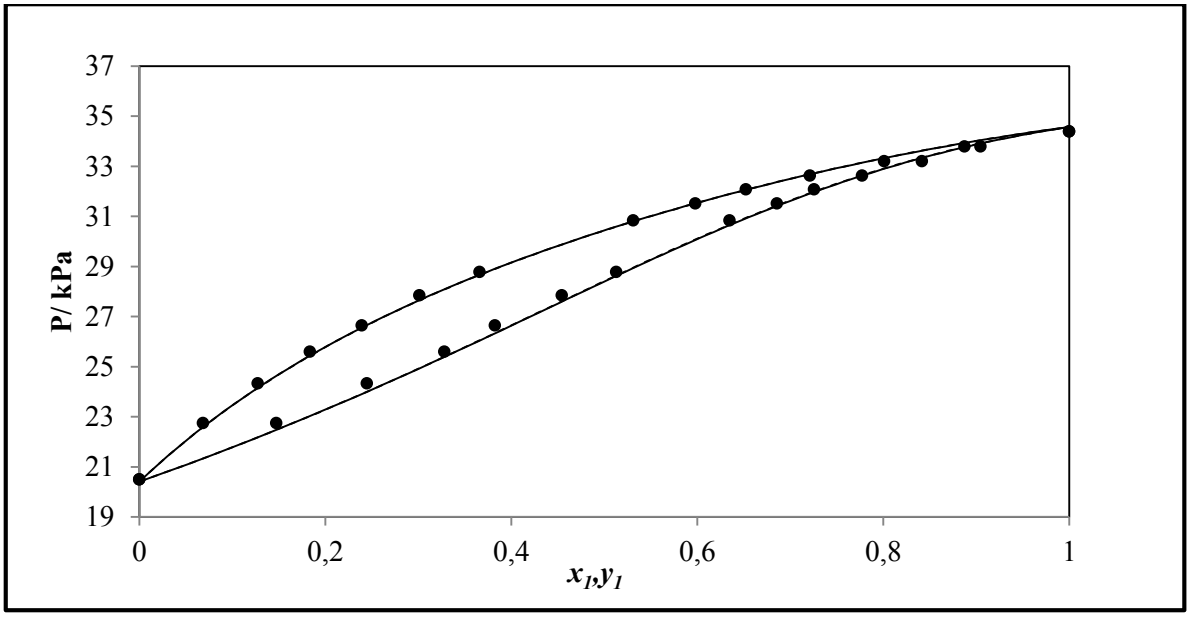

Figure 6-27: Fit of the NRTL-HOC and NRTL-NTH model combinations to the P-x-y plot of the 2-pentanone (1) + 2-methylpropan-1-ol (2) system at 343.15 K for the combined method: (•) this work, (—) NRTL-HOC, (- - - -) NRTL-NTH

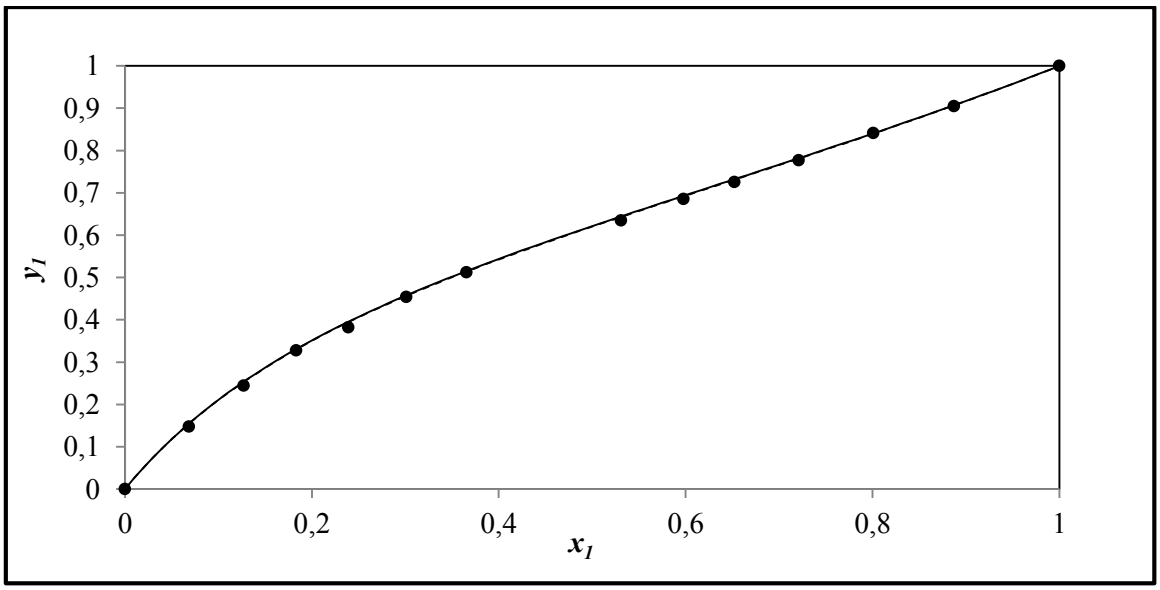

Figure 6-28: Fit of the NRTL-HOC and NRTL-NTH model combinations to the x-y plot of the 2-pentanone (1) + 2-methylpropan-1-ol (2) system at 343.15 K for the combined method: (•) this work, (—) NRTL-HOC, (- - - -) NRTL-NTH

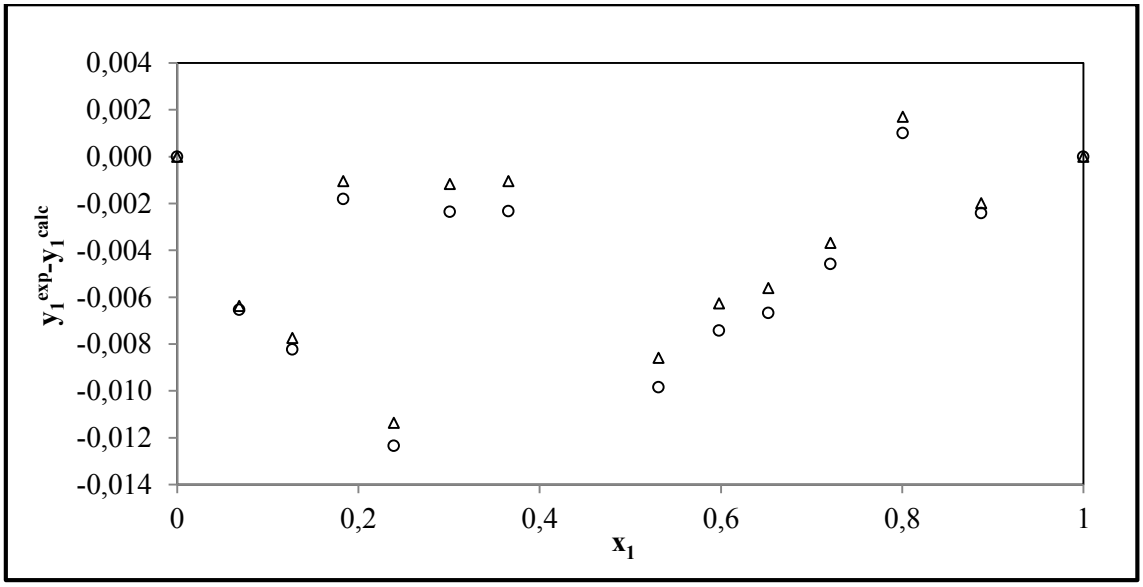

Figure 6-29: Point test (varying EOS): Δy_1 for the 2-pentanone (1) + 2-methylpropan-1-ol (2) system at 343.15 K: (◦) NRTL-HOC, (Δ) NRTL-NTH

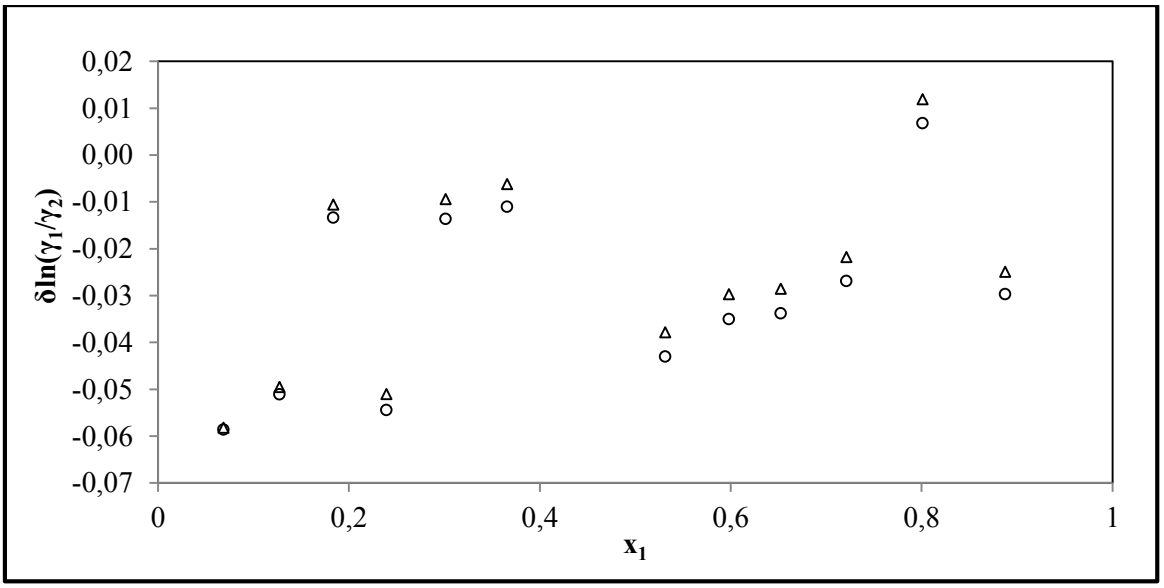

Figure 6-30: Direct test (varying EOS): δln(γ1/γ2) for the 2-pentanone (1) + 2-methylpropan-1-ol (2) system at 343.15 K: (◦) NRTL-HOC, (Δ) NRTL-NTH

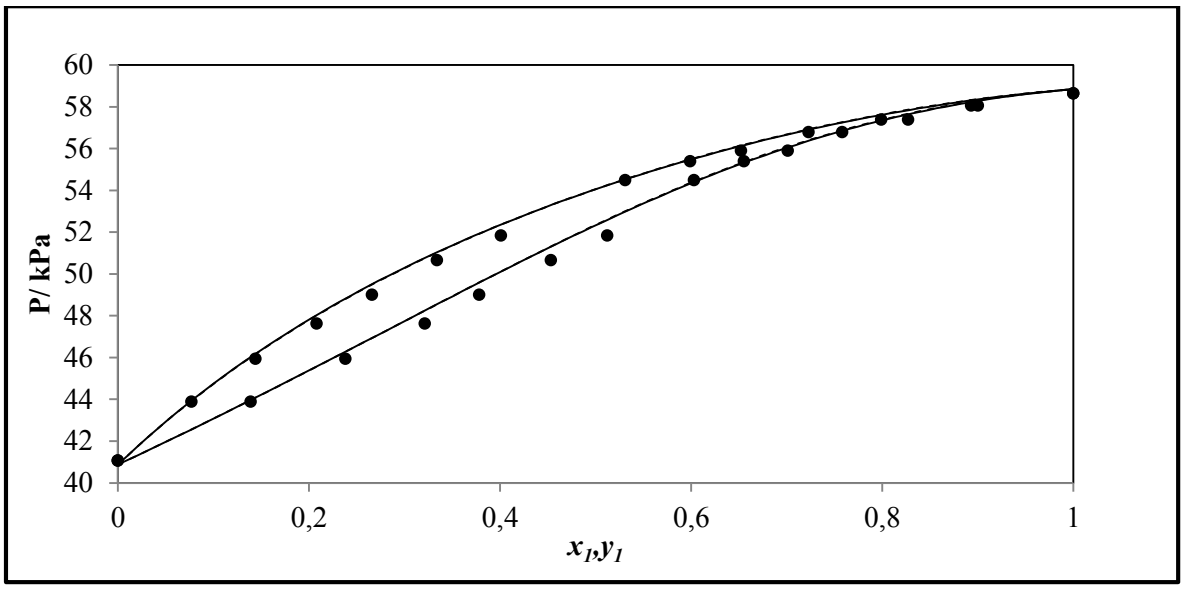

Figure 6-31: Fit of the NRTL-HOC and NRTL-NTH model combinations to the P-x-y plot of the 2-pentanone (1) + 2-methylpropan-1-ol (2) system at 358.15 K for the combined method: (•) this work, (—) NRTL-HOC, (- - - -) NRTL-NTH

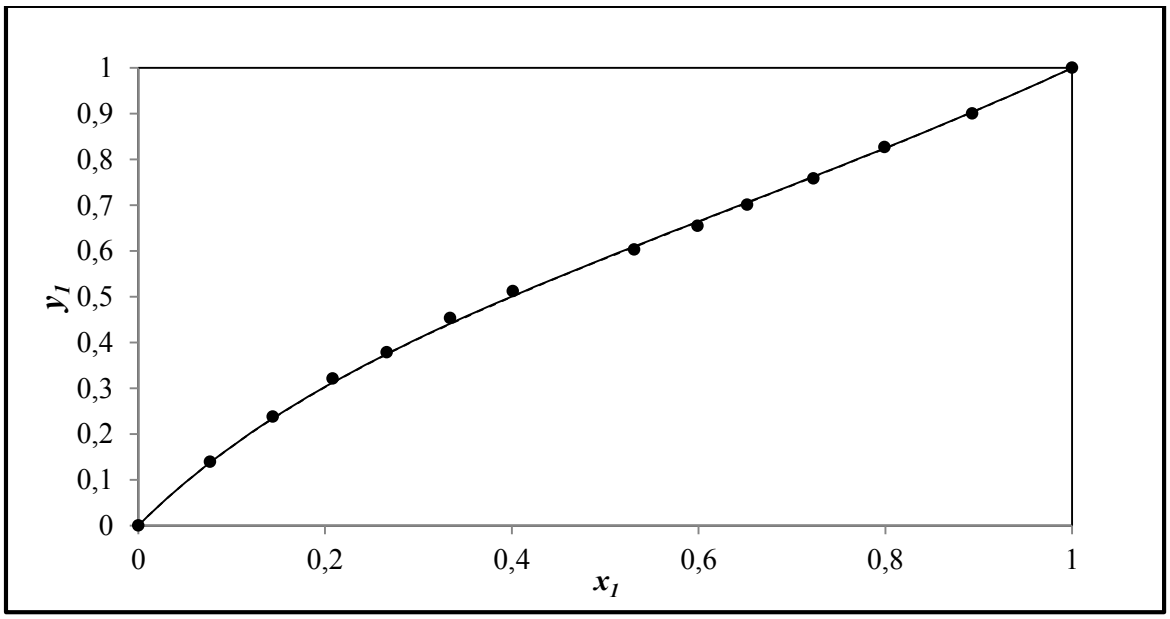

Figure 6-32: Fit of the NRTL-HOC and NRTL-NTH model combinations to the x-y plot of the 2-pentanone (1) + 2-methylpropan-1-ol (2) system at 358.15 K for the combined method: (•) this work, (—) NRTL-HOC, (- - - -) NRTL-NTH

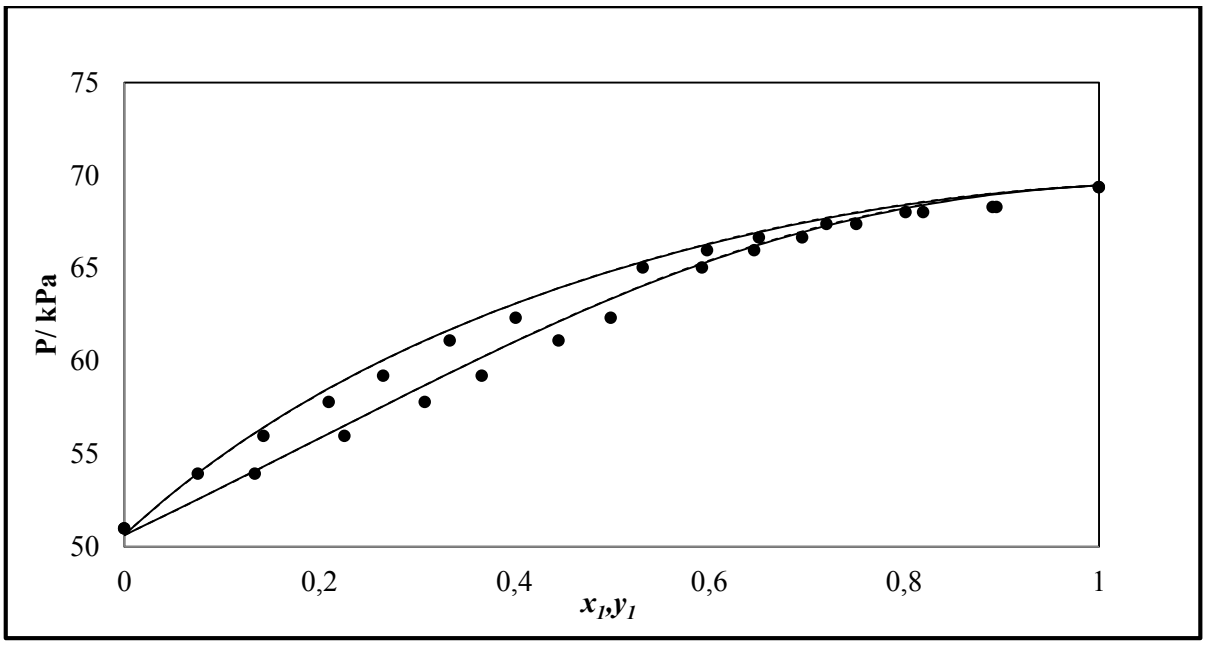

Figure 6-33: Fit of the NRTL-HOC and NRTL-NTH model combinations to the P-x-y plot of the 2-pentanone (1) + 2-methylpropan-1-ol (2) system at 363.15 K for the combined method: (•) this work, (—) NRTL-HOC, (- - - -) NRTL-NTH

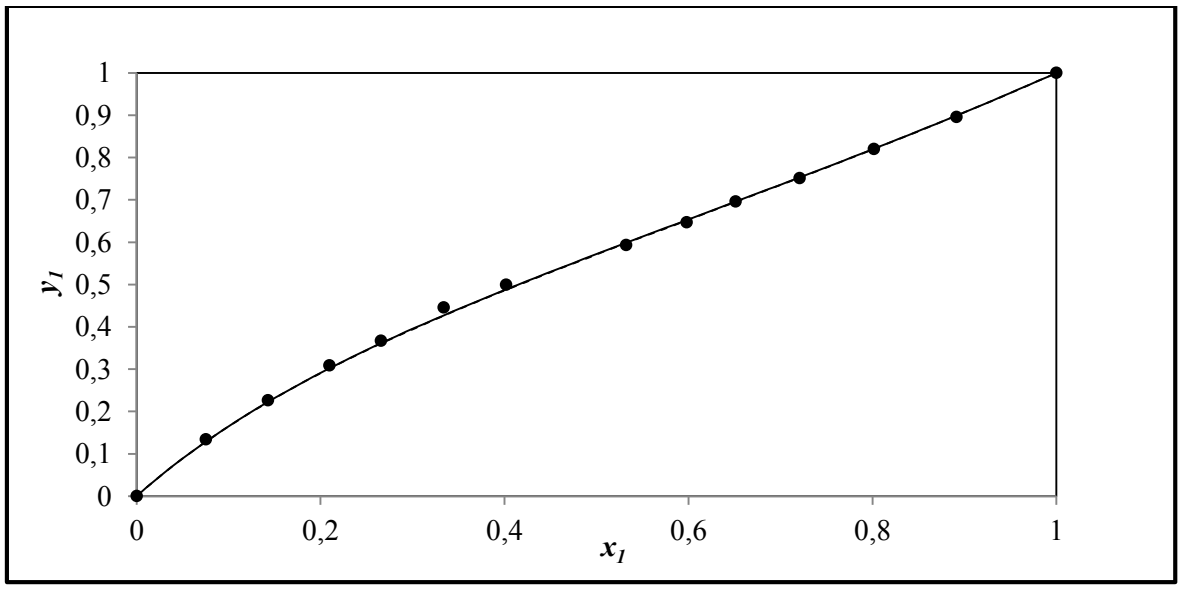

Figure 6-34: Fit of the NRTL-HOC and NRTL-NTH model combinations to the x-y plot of the 2-pentanone (1) + 2-methylpropan-1-ol (2) system at 363.15 K for the combined method: (•) this work, (—) NRTL-HOC, (- - - -) NRTL-NTH

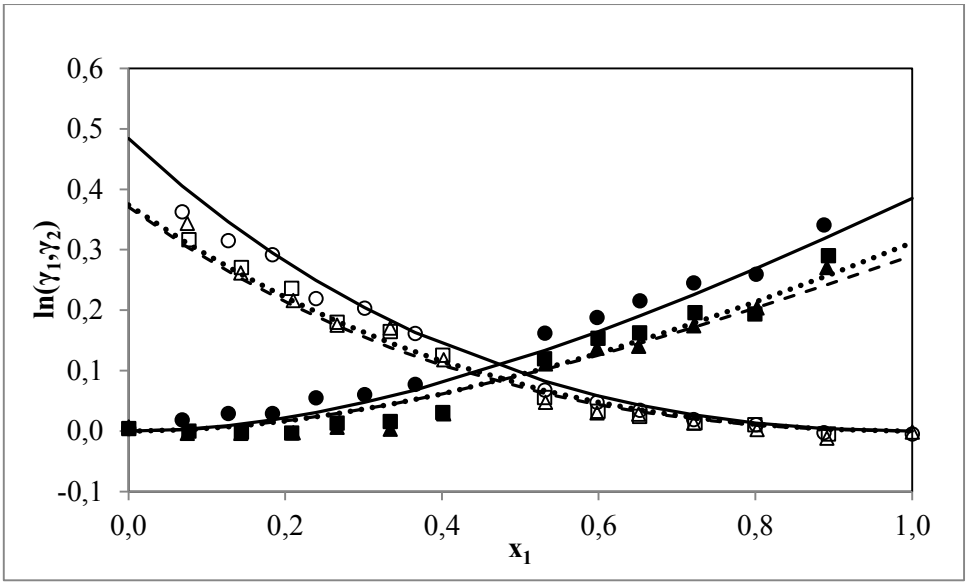

Figure 6-35: Comparison between the experimentally determined liquid-phase activity coefficients and those calculated from the NRTL-HOC model combination for 2-pentanone (1) + 2-methylpropan-1-ol (2) system at 343.15 K, 358.15 K and 363.15 K. (—) 343.15 K, (…) 358.15 K and (- - -) 363.15 K for NRTL-HOC model combination; (○) 343.15 K, (□) 358.15 K and (Δ) 363.15 K for experimental γ_1; (●) 343.15 K, (■) and (▲) 363.15 K for experimental γ_2

Figure 6-36 shows the illustrative plot of the comparison between the experimentally calculated activity coefficients and those derived from the NRTL-HOC model combination for the three isotherms. It can also be seen from the plot that the NRTL-HOC model combination used for the regression of the isothermal VLE data sets provided good fit.

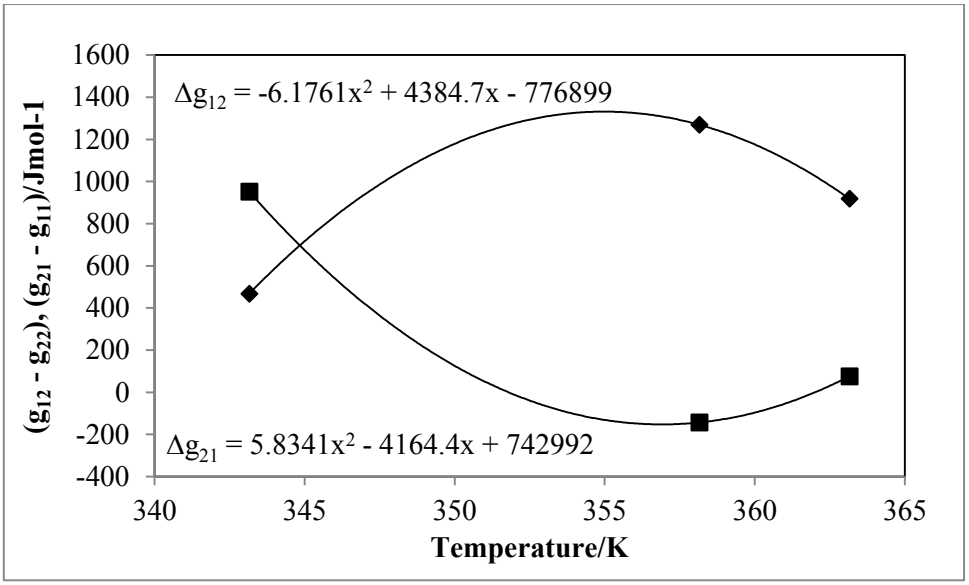

Figure 6-36: Temperature dependence of the NRTL-HOC model combination parameters for 2-pentanone (1) + 2-methylpropan-1-ol (2) system. ($g_{12} - g_{22}$) (♦), ($g_{21} - g_{11}$) (■)

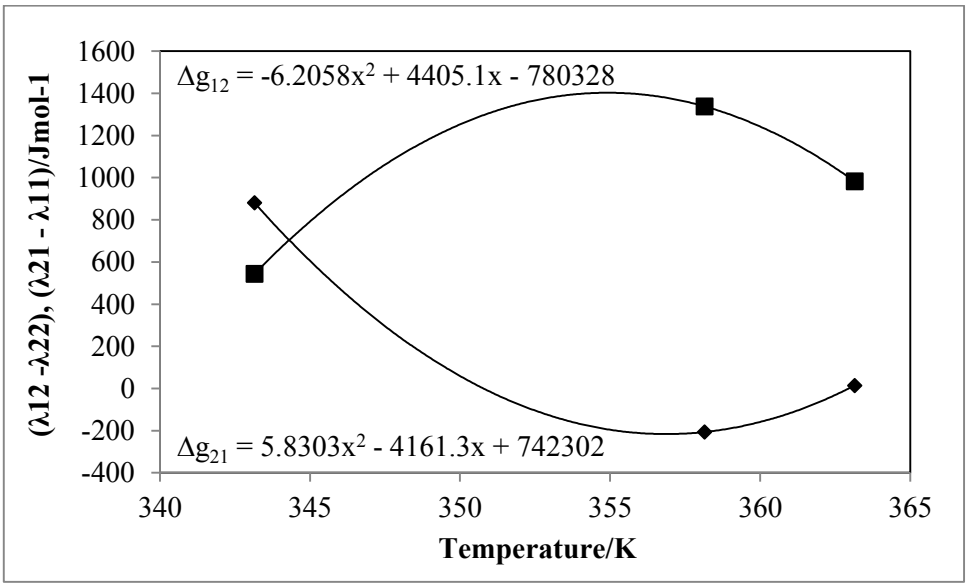

Figure 6-37: Temperature dependence of the WILSON-HOC model combination parameters for 2-pentanone (1) + 2-methylpropan-1-ol (2) system. ($\lambda_{12} - \lambda_{22}$) (♦), ($\lambda_{21} - \lambda_{11}$) (■)

6.5 Thermodynamic consistency testing results obtained for the systems measured.

6.5.1 Consistency results for the 1-propanol (1) + methyl isobutyl ketone (2) system.

The model combinations used were found well fit for the VLE data set measured for this system at the three different isotherms of 338.15 K, 353.15 K and 368.15 K. The data set measured passed the point test at these isotherms except for the 368.15 K where the four model combinations: NRTL-NTH, NRTL-HOC, WILSON-HOC and UNIQUAC-HOC provided Δy_{1avg} values of 0.012, 0.010, 0.011 and 0.011 respectively slightly more than the point test margin of 0.01. But when the direct test was performed for the data set at this isotherm, the root mean square deviation using the four model combinations fall on index four. The measured VLE data sets for the 338.15K and 353.15 K passed both the point test and direct test. Table (6-7) gives the summary of the analysis of the two consistency testing employed for this system. The graphical representation of the Δy and ΔP are shown in Appendix A.

Table 6-8: Results for the point and direct test performed for the data set measured for the 1-propanol (1) + 4-methyl-2-pentanone (2) at 338.15 K, 353.15 K and 368.15 K

	NRTL-HOC	NRTL-NTH	WILSON-HOC	UNIQUAC-HOC
		338.15 K		
Δ Pavg/ kPa	0.008	0.008	0.008	0.008
Δy_1	0.003	0.003	0.003	0.003
RMSD $\delta \ln(\gamma_1/\gamma_2)$	0.023	0.024	0.025	0.024
		353.15 K		
Δ Pavg/ kPa	0.011	0.011	0.013	0.013
Δy_1	0.004	0.005	0.004	0.004
RMSD $\delta \ln(\gamma_1/\gamma_2)$	0.034	0.034	0.034	0.034
		368.15 K		
Δ Pavg/ kPa	0.031	0.030	0.032	0.033
Δy_1	0.010	0.012	0.011	0.011
RMSD $\delta \ln(\gamma_1/\gamma_2)$	0.074	0.082	0.075	0.075

6.5.2 Consistency results for the 2-propanol (1) + 4-methyl-2-pentanone (2) system.

All the model combinations employed in the regression of the VLE data sets measured for this system at the three isotherms (323.15K, 338.15 K and 353.15 K) fitted the data well. The quantitative criterion of the point test (Δy_{avg} must be less than 0.01) was passed for the three isotherms. The highest value for Δy_{avg} (0.008) was obtained for the 353.15 K when the NRTL-NTH model combination was used for the regression. For the direct test, the root mean square deviation values obtained for the data set at the three isotherms from the different model combinations used fall on index 3 on Table (3-1) (an index of one indicates an excellent data and an index of ten very poor data). The NRTL-HOC model combination also provided the highest value for the root mean square deviation at 353.15 K which is 0.066. The models used were found to fit the data set measured for this system well and the data sets are thermodynamically consistent. The plots for Δy_1 and ΔP are presented in Appendix A. Table (6-8) presents the summary of the analysis obtained for the point test and direct test for this system.

Table 6-9: Results for the point and direct test performed for the data set measured for the 2-propanol (1) + 4-methyl-2-pentanone (2) at 323.15 K, 338.15 K and 353.15 K

	NRTL-HOC	NRTL-NTH	WILSON-HOC	UNIQUAC-HOC
		323.15 K		
Δ Pavg/ kPa	0.011	0.010	0.010	0.010
Δy_1	0.006	0.006	0.006	0.006
RMSD $\delta \ln(\gamma_1/\gamma_2)$	0.050	0.053	0.051	0.051
		338.15 K		
Δ Pavg/ kPa	0.024	0.025	0.023	0.023
Δy_1	0.006	0.007	0.006	0.006
RMSD $\delta \ln(\gamma_1/\gamma_2)$	0.053	0.059	0.055	0.056
		353.15 K		
Δ Pavg/ kPa	0.019	0.024	0.022	0.022
Δy_1	0.006	0.008	0.006	0.006
RMSD $\delta \ln(\gamma_1/\gamma_2)$	0.053	0.066	0.053	0.053

6.5.3 Consistency results for the 2-pentanone (1) + 2-methyl propan-1-ol (2) system.

The four thermodynamic model combinations used for the regression of the experimental VLE data set were found to fit the data well. The point and direct test employed for the consistency testing of the measured data set for the three isotherms (343.15 K, 358.15 K and 363.15 K) were passed excellently. For the point test, Δy_{1avg} values obtained for the three isotherms were the same with all the model combinations except for the NRTL-NTH at 343.15 K which was 0.004, the value provided by the other models was 0.005. The root mean square deviation obtained for the direct test was from 0.031 to 0.037 when the four model combinations were used. This value fall on index two of the Van Ness consistency table indicating high quality data sets. Both the point and direct test were passed for this system and the data sets were found to be thermodynamic consistent. The plots for the Δy_{1avg} and ΔP_{avg} are shown in Appendix A. Table (6-9) gives the general analysis of the Δy_{1avg}, ΔP_{avg} and the RMSD $\delta\ln(\gamma_1/\gamma_2)$ obtained for the data sets at the three isotherms.

Table 6-10: Results for the point and direct test performed for the data set measured for the 2-pentanone (1) + 2-methylpropan-1-ol at 343.15 K, 358.15 K and 363.15 K

	NRTL-HOC	NRTL-NTH	WILSON-HOC	UNIQUAC-HOC
		343.15 K		
Δ Pavg/ kPa	0.006	0.006	0.006	0.006
Δy_1	0.005	0.004	0.005	0.005
RMSD $\delta\ln(\gamma_1/\gamma_2)$	0.036	0.033	0.035	0.035
		358.15 K		
Δ Pavg/ kPa	0.015	0.014	0.015	0.014
Δy_1	0.005	0.005	0.005	0.005
RMSD $\delta\ln(\gamma_1/\gamma_2)$	0.031	0.032	0.033	0.033
		363.15 K		
Δ Pavg/ kPa	0.026	0.026	0.026	0.026
Δy_1	0.005	0.005	0.005	0.005
RMSD $\delta\ln(\gamma_1/\gamma_2)$	0.035	0.036	0.037	0.037

6.6 Experimental infinite dilution activity coefficient

Infinite dilution activity coefficients are used in separation technology for the production of high purity reagents. Simple extrapolation of the binary liquid phase activity coefficient curves to the end points can give inaccurate values for γ_1^{∞}, as a result of this; the IDACs for each isotherm measured in this work were calculated using two approaches; The method of Ellis and Jonah (Ellis.and Jonah, 1962) as modified by Maher and Smith (Smith, 1979) and the Wilson (1964) method, The second virial coefficients were estimated using the HOC method as this was used to account for the non-ideality in the vapour phase and the Racket equation was used to calculate the liquid molar volumes. These are reported in Table (6-10). The limiting values $(P_D/x_1x_2)^{\infty}$, were determined with the method of Maher and Smith (1979) for the newly measured systems. The evaluation of infinite dilution activity coefficient has been discussed in Chapter 3. (P_D/x_1x_2) was determined by extrapolating a plot of P_D/x_1x_2 vs. x_1 to $x_1 = 0$. If the slope of the plot is not linear, then Maher and Smith suggest that x_1x_2/P_D be plotted against x_l, then the derivative and γ^{∞} can be determined. The plots showing (x_1x_2/P_D) vs x_1 as $x_1 \rightarrow 0$ and x_1x_2/P_D vs as $x_1 \rightarrow 1$ obtained for the system 1-propanol (1) + 4-methyl-2-pentanone (2) at 338.15 K are presented in Figures (6-38) and (6-39) respectively. The plots for the other isotherms can be found in Appendix B

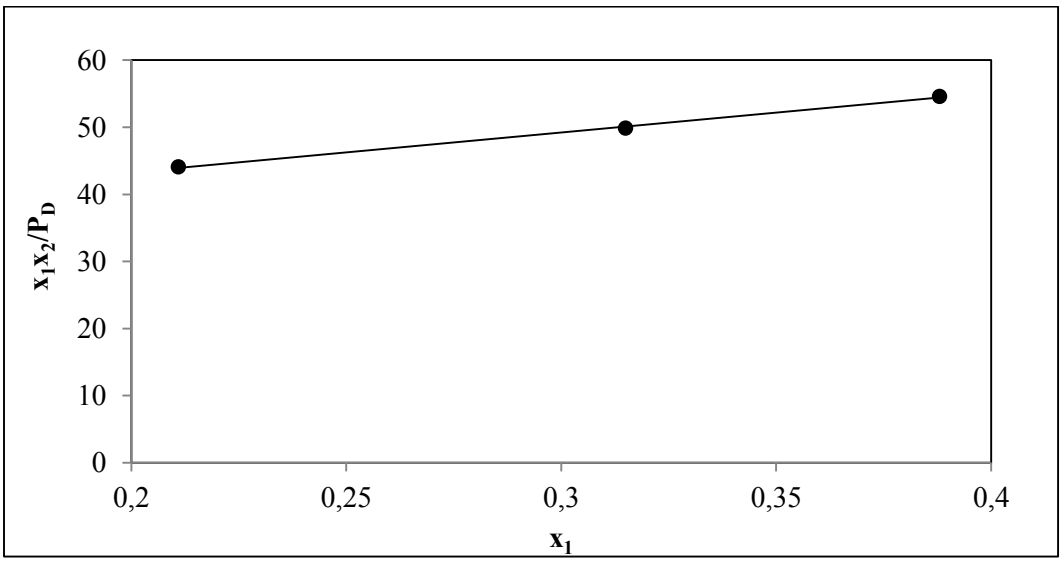

Figure 6-38: Plot of (x_1x_2/P_D) vs x_1 as $x_1 \rightarrow 1$ for 1-propanol (1) + 4-methyl-2-pentanone (2) system at 338.15 K

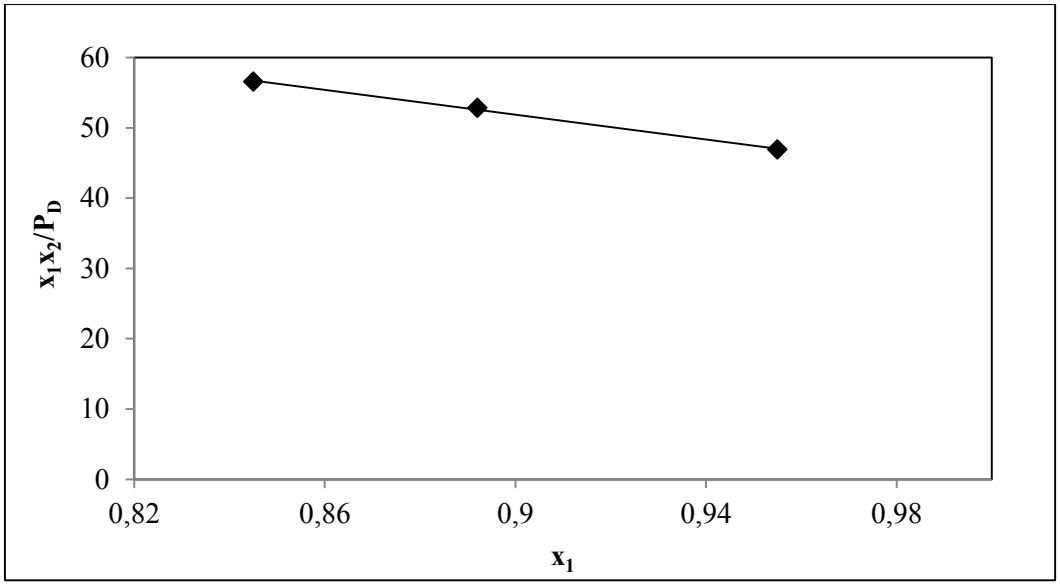

Figure 6-39: Plot of (x_1x_2/ P_D) vs x_1 as $x_1 \rightarrow 0$ for 1-propanol (1) + 4-methyl-2-pentanone (2) system at 338.15 K.

Table 6-11: Second virial coefficients and liquid molar volumes calculated for this work

Component	**Temperature (K)**	**V_i (cm^3/mol)**	**B_{ii} (cm^3/mol)**	**B_{12} (cm^3/mol)**
1-propanol (i=1)	338.15	78.06	-1398.28	-1065.39
	353.15	79.87	-1159.88	-946.78
	368.15	81.83	-980.62	-847.01
2-propanol (i=2)	323.15	77.38	-1626.07	-1147.45
	338.15	79.34	-1328.22	-1013.04
	353.15	81.47	-1108.10	-901.11
4-methyl-2-pentanone (i=2)	338.15	118.33	-2403.12	
	353.15	120.67	-2085.65	
	368.15	123.18	-1827.45	
	323.15	116.13	-2799.75	
	338.15	118.33	-2403.12	
	353.15	120.67	-2085.65	
2-pentanone (i=1)	343.15	100.63	-1782.63	-1032.37
	358.15	102.88	-1577.21	-921.90
	363.15	103.67	-1516.74	-889.05
2-methylpropan-1-ol (i=2)	343.15	98.19	-2045.94	
	358.15	100.37	-1595.18	
	363.15	101.14	-1478.85	

Table 6-12: comparison of the infinite dilution activity coefficient values obtained by extrapolation of the experimental γ_i with values calculated using the Maher and Smith (1979) method and the Wilson (1964) method for the isothermal VLE systems measured

System	T (K)	a		b		c	
		γ_1^∞	γ_2^∞	γ_1^∞	γ_2^∞	γ_1^∞	γ_2^∞
1-propanol (1) + 4-methyl-2-pentanone	338.15	2.20	1.94	1.03	1.96	2.23	1.94
	353.15	1.85	1.78	1.01	1.59	1.86	1.78
	368.15	1.66	1.61	1.02	1.50	1.66	1.61
2-propanol (1) + 4-methyl-2-pentanone	323.15	2.08	2.26	1.01	-	1.73	1.71
	338.15	1.89	2.02	1.02	1.89	1.90	2.03
	353.15	1.62	1.85	1.03	1.89	1.63	1.86
2-pentanone (1) + 2-methylpropan-1-ol	343.15	1.63	1.57	1.66	1.43	1.63	1.57
	358.15	1.35	1.46	1.02	1.33	1.35	1.46
	363.15	1.34	1.39	1.34	1.29	1.34	1.39

a: Extrapolated γ_i^∞ from experimental γ_i

b: calculated γ_i^∞ using the method of Maher and Smith (1979)

c: calculated γ_i^∞ using the Wilson's (1964) method

Table (6-11) shows the comparison of the infinite dilution activity coefficient values obtained for the newly measured isothermal VLE data sets. Taking a close look at the table it can be clearly seen that there is not much difference between $\gamma_1^\infty$and γ_2^∞ values obtained by extrapolating the experimental γ_i and the Wilson's (1964) equation. This resulted from the accuracy of the Wilson model to fit the experimental data well and thus any significant difference is not expected. However, the Wilson method cannot be relied on for some isotherms where the model over predicted the experimental gamma1 values. There are significant discrepancies between the values calculated by the Maher and Smith method and the extrapolated experimental values, this may have been due to the equation of state used bearing in mind that γ_i^∞ is dependent upon the equation of state used and the accuracy of the estimate of the partial derivative of $(\partial P/\partial x_1)$ (Maher and Smith, 1979), which is based on the linearity of the P_D/x_1x_2 plot or the inverse.

Furthermore, there was no γ_2^{∞} value calculated for the system 2-propanol (1) + 4-methyl-2-pentanone at 323.15 K with the Maher and Smith (1979) method because none of the plots of P_D/x_1x_2 vs x_1 and (x_1x_2/ P_D) vs x_1 gave a linear slope, hence the method of Maher and Smith could not be used. The values calculated by the Maher and Smith method should be more reliable because this method relies on the accuracy of the pressure deviation with respect to the liquid phase composition and not on the extrapolation of activity coefficient plot fitted to a suitable polynomial equation. These calculated values could not be compared with literature values because they are unavailable.

6.7 Excess Thermodynamic Properties

The excess Gibbs energy (G^E), excess enthalpy (H^E) and excess entropy (TS^E) for each isothermal VLE system were calculated. The NRTL with the model parameters obtained from the regression of the newly measured sets of isothermal VLE data was used to calculate G^E/RT over the entire composition range since the NRTL and Wilson's models gave the best fit to the isothermal VLE data sets. The excess enthalpies (H^E) were determined from the Gibbs-Helmholtz equation (Equation 3-85) and excess entropies (S^E) were obtained from Equation (3-86). Values obtained for the excess thermodynamic properties for the isothermal VLE systems in this work are reported in Tables (6-12) to (6-20).

Table 6-13: Excess Gibbs energy (G^E) values obtained for the system 1-propanol (1) + 4-methyl-2-pentanone (2).

molar excess Gibbs energy (J/mol)			
x_1	338.15 K	353.15 K	368.15 K
0.000	0.000	0.000	0.000
0.100	170.151	161.525	137.851
0.200	304.355	287.352	243.348
0.300	402.030	377.478	317.259
0.400	462.533	431.860	360.276
0.500	485.151	450.415	373.022
0.600	469.106	433.019	356.052
0.700	413.543	379.506	309.860
0.800	317.530	289.672	234.878
0.900	180.051	163.267	131.484
1.000	0.000	0.000	0.000

Table 6-14: Excess enthalpy values (H^E) obtained for the system 1-propanol (1) + 4-methyl-2-pentanone (2).

molar excess enthalpy (J/mol)			
x_1	338.15 K	353.15 K	368.15 K
0.000	0.000	0.000	0.000
0.100	490.689	535.188	581.617
0.200	911.167	993.797	1080.012
0.300	1246.923	1360.001	1477.986
0.400	1483.519	1618.054	1758.426
0.500	1606.507	1752.194	1904.204
0.600	1601.339	1746.558	1898.079
0.700	1453.287	1585.080	1722.591
0.800	1147.355	1251.404	1359.968
0.900	668.191	728.787	792.012
1.000	0.000	0.000	0.000

Table 6-15: Excess entropy values (TS^E) obtained for the system 1-propanol (1) + 4-methyl-2-pentanone (2).

molar excess entropy (J/mol.K)			
x_1	338.15 K	353.15 K	368.15 K
0.000	0.000	0.000	0.000
0.100	320.538	373.663	443.766
0.200	606.812	706.445	836.664
0.300	844.892	982.523	1160.727
0.400	1020.987	1186.193	1398.150
0.500	1121.356	1301.779	1531.182
0.600	1132.234	1313.539	1542.027
0.700	1039.745	1205.573	1412.732
0.800	829.825	961.732	1125.089
0.900	488.141	565.520	660.527
1.000	0.000	0.000	0.000

Table 6-16: Excess Gibbs energy (G^E) values obtained for the system 2-propanol (1) + 4-methyl-2-pentanone (2).

	molar excess Gibbs energy (J/mol)		
x_1	323.15 K	338.15 K	353.15 K
0.000	0.000	0.000	0.000
0.100	181.015	173.838	131.800
0.200	324.927	309.025	237.706
0.300	430.754	405.683	316.584
0.400	497.419	463.868	367.231
0.500	523.737	483.571	388.363
0.600	508.408	464.717	378.611
0.700	450.007	407.170	336.515
0.800	346.973	310.726	260.514
0.900	197.595	175.114	148.938
1.000	0.000	0.000	0.000

Table 6-17: Excess enthalpy (H^E) values obtained for the system 2-propanol (1) + 4-methyl-2-pentanone (2).

molar excess enthalpy (J/mol)			
x_1	323.15 K	338.15 K	353.15 K
0.000	0.000	0.000	0.000
0.100	650.729	712.542	777.159
0.200	1157.025	1266.932	1381.824
0.300	1519.489	1663.826	1814.712
0.400	1738.379	1903.509	2076.130
0.500	1813.582	1985.855	2165.944
0.600	1744.584	1910.303	2083.540
0.700	1530.431	1675.808	1827.780
0.800	1169.690	1280.800	1396.950
0.900	660.397	723.128	788.706
1.000	0.000	0.000	0.000

Table 6-18: Excess entropy (TS^E) values obtained for the system 2-propanol (1) + 4-methyl-2-pentanone (2).

molar excess entropy (J/mol.K)			
x_1	323.15 K	338.15 K	353.15 K
0.000	0.000	0.000	0.000
0.100	469.713	538.704	645.359
0.200	832.098	957.906	1144.118
0.300	1088.735	1258.143	1498.127
0.400	1240.960	1439.641	1708.899
0.500	1289.845	1502.285	1777.582
0.600	1236.176	1445.586	1704.930
0.700	1080.424	1268.638	1491.265
0.800	822.718	970.074	1136.437
0.900	462.802	548.014	639.767
1.000	0.000	0.000	0.000

Table 6-19: Excess Gibbs energy (G^E) values obtained for the system 2-pentanone (1) + 2-methylpropan-1-ol (2).

molar excess Gibbs energy (J/mol)			
x_1	343.15 K	358.15 K	363.15 K
0.000	0.000	0.000	0.000
0.100	121.219	98.290	98.066
0.200	210.363	171.435	169.927
0.300	269.627	220.809	217.464
0.400	301.033	247.702	242.415
0.500	306.450	253.326	246.388
0.600	287.608	238.819	230.869
0.700	246.110	205.253	197.237
0.800	183.439	153.636	146.771
0.900	100.975	84.920	80.658
1.000	0.000	0.000	0.000

Table 6-20: Excess enthalpy (H^E) values obtained for the system 2-pentanone (1) + 2-methylpropan-1-ol (2).

molar excess enthalpy (J/mol)			
x_1	343.15 K	358.15 K	363.15 K
0.000	0.000	0.000	0.000
0.100	519.640	566.062	581.978
0.200	900.621	981.079	1008.663
0.300	1153.059	1256.069	1291.385
0.400	1286.148	1401.047	1440.439
0.500	1308.260	1425.135	1465.204
0.600	1227.035	1336.654	1374.236
0.700	1049.459	1143.214	1175.357
0.800	781.928	851.782	875.731
0.900	430.310	468.752	481.932
1.000	0.000	0.000	0.000

Table 6-21: Excess enthalpy (TS^E) values obtained for the system 2-pentanone (1) + 2-methylpropan-1-ol (2).

molar excess entropy (J/mol.K)			
x_1	343.15 K	358.15 K	363.15 K
0.000	0.000	0.000	0.000
0.100	398.421	467.773	483.912
0.200	690.258	809.644	838.737
0.300	883.432	1035.260	1073.921
0.400	985.115	1153.345	1198.024
0.500	1001.810	1171.809	1218.816
0.600	939.427	1097.835	1143.366
0.700	803.349	937.961	978.119
0.800	598.489	698.146	728.960
0.900	329.335	383.833	401.274
1.000	0.000	0.000	0.000

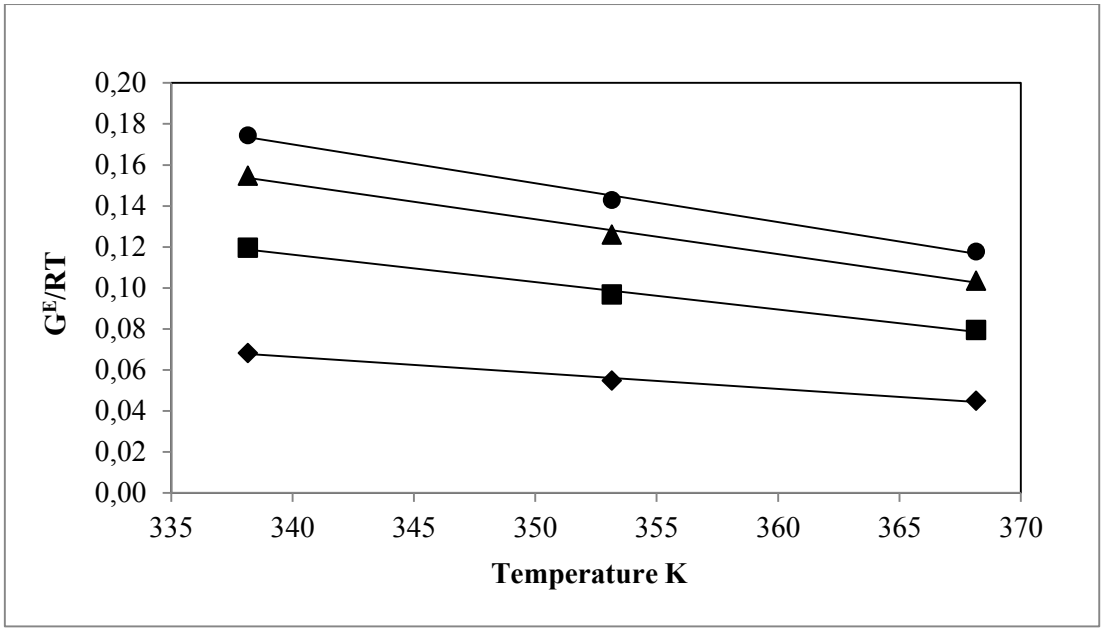

Figure 6-40: Plot used for the determination of the molar excess enthalpy values for the 1-propanol (1) + 4-methyl-2-pentanone (2) system at 338.15 K, 353.15 K and 368.15 K. (♦), 0.1, (■), 0.2, (▲), 0.3 and (●), 0.4.

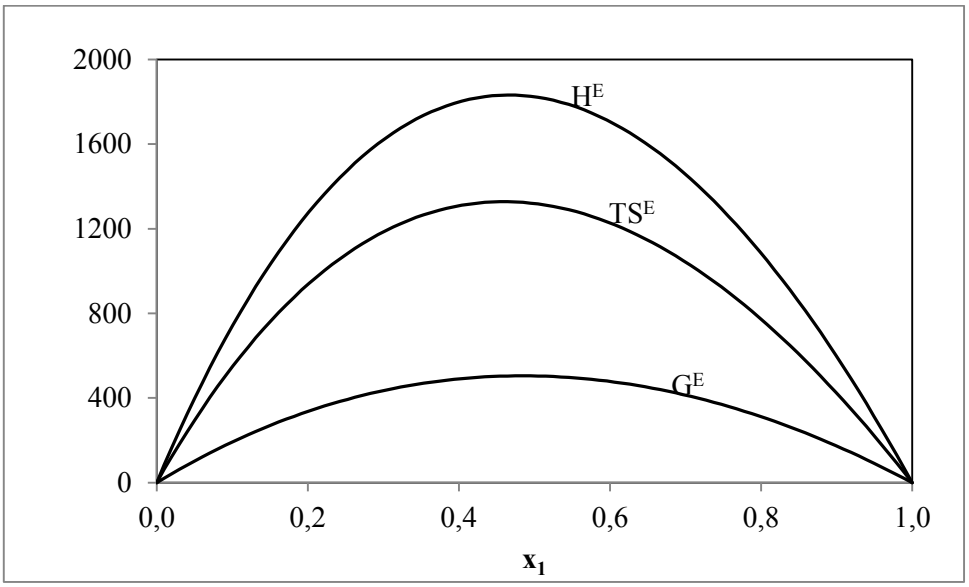

Figure 6-41: Excess thermodynamic properties (H^E, G^E and TS^E) for 1-propanol (1) + 4-methyl-2-pentanone (2) system at 338.15 K

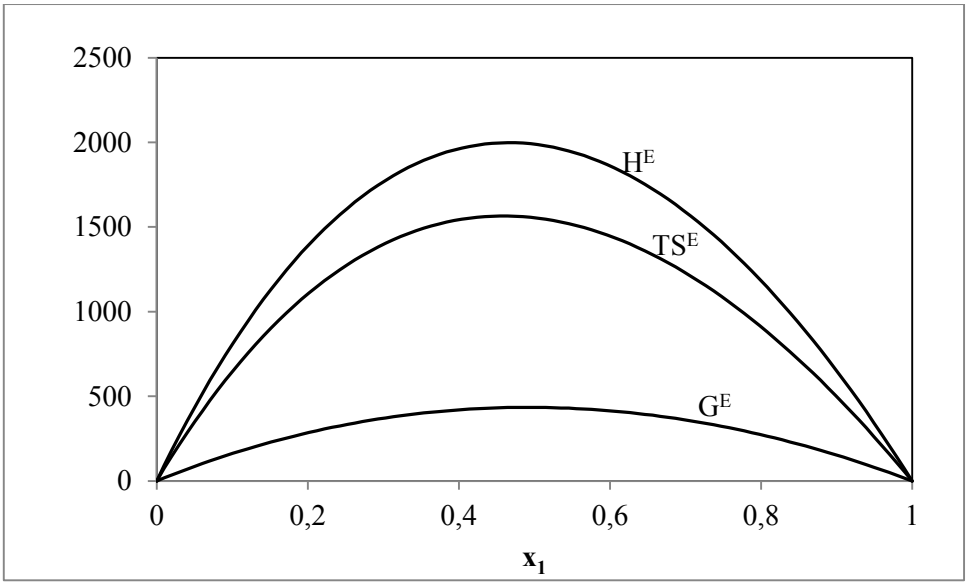

Figure 6-42: Excess thermodynamic properties (H^E, G^E and TS^E) for 1-propanol (1) + 4-methyl-2-pentanone (2) system at 353.15 K

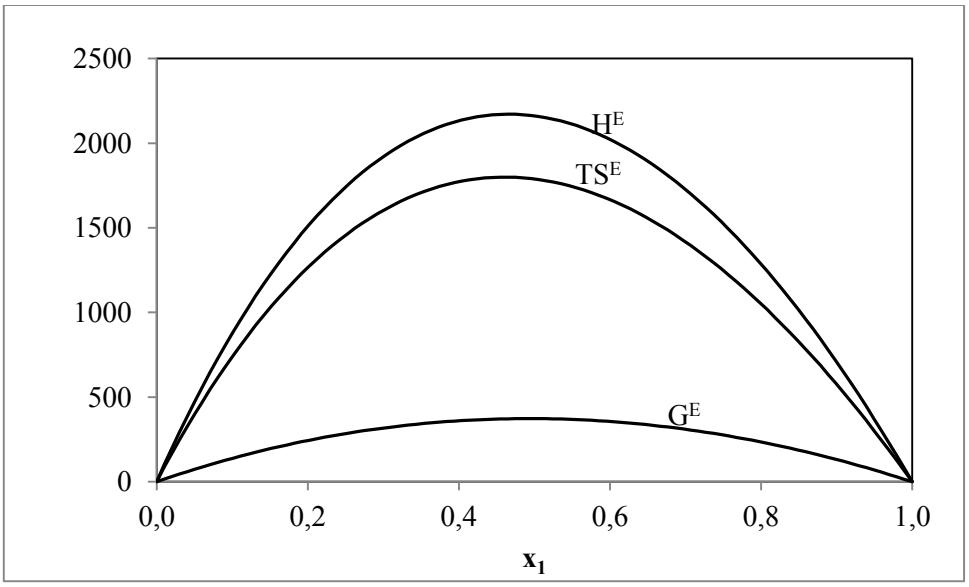

Figure 6-43: Excess thermodynamic properties (H^E, G^E and TS^E) for 1-propanol (1) + 4-methyl-2-pentanone (2) system at 368.15 K

It can be seen from the three plots that the H^E for the 1-propanol (1) + 4-methyl-2-pentanone (2) system is greater than zero and nearly symmetrical with mole fractions for the three isotherms. For two polar mixtures, (e.g. alcohol + ketone) the sign and magnitude of H^E depends upon the relative strengths of the interactions between the like molecules which are present in the pure liquids and the interactions between unlike molecules which result from the mixing process (Ott, 1996).

CHAPTER 7

CONCLUSION

Due to the lack of experimental data of some alcohols + ketones systems required for industrial use, isothermal VLE measurements that comprised some of the alcohols and ketones systems were carried out in this work. This work also included thermodynamic modelling of the measured data to obtain the model parameters for each system studied. A literature data survey on VLE systems and the conditions of their availability was done before choosing the systems measured which were: 1-propanol (1) + 4-methyl-2-pentanone (2) (at 338.15, 353.15 and 368.15 K), 2-propanol (1) + 4-methyl-2-pentanone (2) (at 323.15, 338.15 and 353.15 K) and 2-pentanone (1) + 2-methylpropan-1-ol (2) (at 343.15, 358.15 and 363.15 K). The isothermal VLE data measured for these systems constitute new experimental data currently not available in the open literature. The apparatus employed for the measurement was the VLE glass recirculating still designed by Raal and Mühlbauer (1998) and which was later modified by Bhownath (Bhownath, 2008).

A test system of cyclohexane (1) + ethanol (2) was measured at 313.15 K and at 40 kPa in order to ensure reliability of the apparatus and the operating procedures used. The data measured for the test system at the two conditions (313.15 K and 40 kPa) were found to be in fairly good agreement with the literature data (Joseph, 2001).

The new experimental data were modelled using the combined method with suitable thermodynamic models available in the ASPEN PLUS simulator tool. The γ-Φ approach was used for the regression of the measured data employing three activity coefficient models viz: WILSON (1964), NRTL (Renon and Prausnitz, 1968) and UNIQUAC (Abrams and Prausnitz, 1975) models in ASPEN PLUS to account for the liquid phase non-ideality and two correlations of the virial equation of state, namely: HOC (Hayden and O'Connell, 1974) and NTH (Nothnagel et.al., 1973) for the vapour phase non-ideality. The maximum likelihood optimization technique was used as this gave the best fit to the data sets in comparison to the ordinary least squares and the modified Baker's methods.

The combination of the three activity coefficient models with the HOC equation of state model gave satisfactory fits to the newly measured VLE data. Considering the deviation

between the experimental and regressed values obtained for the vapour phase compositions, pressure and gamma, the NRTL-HOC model combination gave the best fit to all the systems investigated.

All the systems measured were found to exhibit common VLE behavior except for the 1-propanol (1) + 4-methyl-2-pentanone (2) system, where a minimum boiling azeotrope was displayed at 353.15 K (at $x_1 = 0.11$). Therefore a normal distillation method is not suitable for the separation of these two components at isotherm 353.15 K.

The newly measured isothermal VLE data except for the 2-propanol (1) + 4-methyl-2-pentanone (2) data are concluded to be thermodynamically consistent based on the results of the point test (Van Ness, 1973) and direct test (Van Ness, 1995) that were performed for the data sets. For the point test, Δy_{1avg} values obtained for almost all the data agreed with the suggestion of 0.01 by Danner and Gess (1995). The highest Δy1avg obtained was 0.012 for the methyl isobutyl ketone (1) + 1-propanol (2) system at 368.15 K; however values for Δy_{1avg} for the other data sets were less than 0.01. For the 2-propanol (1) + 4-methyl-2-pentanone (2) data set, the values obtained for the Δy and ΔP failed in random scattering about zero which was as a result of the systematic error in the calibration of the PT100 temperature probe and the pressure transducer although the Δy values obtained were less than 0.01. Also for the direct test, the root mean square deviations obtained for all the systems fall between indexes 1 to 4 on the Van Ness consistency index table.

CHAPTER 8

RECOMMENDATION

It is recommended that the azeotropic nature of the newly measured isothermal VLE systems should be looked into for further studies. It was discovered that for the 1-propanol (1) + 4-methyl-2-pentanone (2) system, there was an occurrence of azeotrope at isotherm 353.15 K (at $x_1=y_1= 0.11$). More isothermal measurements are also recommended to be undertaken for the newly measured VLE systems.

The NRTL-HOC and WILSON-HOC model combinations were found to give the best fits for all the newly measured data sets, these two model combinations are therefore recommended for the regression of the data sets.

The HOC and NTH second virial coefficient correlations were utilized in this work to correct the vapour phase non idealities and both provided good correlations for the data sets, other equation of state models are also recommended to be applied like the Tsonopoulos (1974) and Pitzer-Curl (1957) correlations.

REFERENCES

Abbott, M., M. (1986). *"Low pressure phase equilibria: Measurement of VLE", Fluid Phase Equilibria* (Vol. 29, pp. 193–207).

Abrams, D S, and Prausnitz, J. M. (1975). "Statistical Thermodynamics of Liquid Mixtures: A New Expression for the Excess Gibbs Energy of Partly or Completely Miscible Systems." *American Institute of Chemical Engineers Journal*.

Arthur Rose, E. T. W. (1955). Vapour liquid Equilibrium Self-Lagging Stills. *Industrial & Engineering Chemistry*, *47*(8), 1528–1533.

Baker, L. E., Pierce, A. C., & Luks, K. D. (1982). No Title. *Soc. Pet. Eng. J.*, *22*, 731.

Bhownath, R., & Africa, S. (2008). The Use of n-Dodecane as a Solvent in the Extraction of Light Alcohols from Water, (June).

Carveth. (1899). No Title. *Phsical Chemistry*, *3*, 193.

Clifford, S. L. (2004). Equilibrium And Molecular Simulation Of Carboxylic.

Dortmund Data Bank. (2013). *DDBST Software and Separation Technology GmbH*. Oldenburg.

Dvoskin, N. (2004). *"Thermodynamic Equilibrium of New Organic Mixtures For Absorption Heat Pumps."*

Ellis, S. R. M., Garbett, R. D. (1960). "A new equilibrium still for the study of partially miscible systems." *Industrial Engineering Chemistry*, *52*, 385–388.

Ellis, S.R.M.a nd Jonah, D. A. (1962). Prediction of activity coefficients at infinite dilution. *Chemical Engineeting Science*, *17*(971-976).

Englezos, P, Lee, J D, Susilo, R. (2005). " Liquid Liquid Equilibrium Data of water with Neohexane , Methyl cyclohexane, tert butyl Methyl ether, n- heptane and Vapour Liquid Liquid Equilibrium with methane." *Fluid Phase Equilibrium*, *231*, 20–26.

Fredunslund, A, Gmehling, J and Rasmussen, P. (1977). *"Vapour-Liquid Equilibrium using UNIFAC." Elsevier*. Amsterdam.

Gess, M A, Danner, R P and Nagvekar, M. (1991). "Thermodynamics Analysis of Vapour-Liquid Equilibria: Recommended Models and a Standard Data Base." *American Institute of Chemical Engineers Journal*.

Gillepse, D. T. . (1946). "Vapour-Liquid Equillibrium Still for Miscible Liquids". *Industrial and Engineering Chemistry*, *18*, 575–577.

Gmehling, J and Onken, U and Arlt, W. (Wolfgang). (n.d.). *vapour-liquid equilibrium data collection;DECHEMA Chemistry Data Series*. *Vapor-Liquid Equilibrium Data Collection; Chemistry Data Series; Dechema: Frankfurt* (Vol. I, p. 312). Frankurt/Main.

Hala, E, Pick, J. Fried, V. & V. . (1958). *Vapour Liquid Equilibrium",* (1st Editio). Oxford: Pergamon Press,.

Hala, E, Pick, J. Fried, V. & V. . (1967). *"Vapour Liquid Equilibrium",* (2nd ed.). Oxford: Pergamon Press,.

Hayden, J. D. and O. (1975). "Generalized Method for Predicting Second Virial Coefficients." *Industrial and Engineering Chemistry. Process Design and Development*, *14*, 209–216.

Hayden, J. G., & Connell, J. P. O. (1973). Generalized Method for Predicting Second Virial Coefficients, *14*(192), 209–216.

Heertjes, P. (1960). "Determination of Vapour-Liquid Equilibria of Binary Systems." *Chemical and Process Engineering*, *41*, 385–386.

Iwarere, S. A. (2009). Measurement Of Phase Equilibria For Oxygenated Hydrocarbon Systems.

Joseph, M. A. (2001). *Computer-Aided Measurement of Vapour-Liquid Equilibria in a Dynamic Still at Sub-Atmospheric Pressures.* University of Kwazulu-Natal, Durban, South Africa.

Joseph, M. A., Ramjugernath, D., & Raal, J. D. (2002). Computer-aided Measurement of Vapour- Liquid Equilibria in a Dynamic Still at Sub- Atmospheric Pressures. *Dev. Chem. Eng. Mineral Process., 10*(5/6), 615–637.

Kneisl, P, Zondlo, J W and Wallace, B. W. (1989). "The Effect of Fluid Properties on Ebulliometer Operation." *Fluid Phase Equilibria*, *46*, 85–94.

M, P. J. (1968). Local Compositions in Thermodynamic Excess Functions for Liquid Mixtures. *AIChE J.*, *14*, 135.

M., W. G. (1964). Vapor–Liquid Equilibrium. XI. A New Expression for the Excess Free Energy of Mixing. *J. Am. Chem. Soc.*, *86*, 127.

Malanowski, S. (1982). 8, 197; 9, 31 1. *Fluid Phase Equilibria*, *8*(197), 9.

Malanowski, S. O. (1982). "Experimental Methods for Vapour-Liquid Equilibria. Circulation Methods. *Fluid Phase Equilibria*, *8*, pp. 197–219.

McClellan, A. L. (1963-1974). *"Tables of Experimental Dipole Moments."* W. H. Freeman, San Francisco.

Moodley, K. (2012). *Automation of a Static-Synthetic Apparatus for Vapour- Liquid Equilibrium Measurement*. University of KwaZulu-Natal.

Morachevsky, A G and Zharov, V T, Z. P. K. (1963). The Relation between the Temperature, Pressure, and Composition Change and the Co. *Zh. Fiz. Khim.*, *36*, 42.

Nala, M. E. (2012). Measurements of Phase Equilibrium for Systems Containing Oxygenated Compounds By, (July).

Narasigadu, C. (2006). Phase Equilibrium Investigation Of The Water And Acetonitrile Solvent With Heavy Hydrocarbons.

Narasigadu, C., Naidoo, P., Coquelet, C., Richon, D., & Ramjugernath, D. (2013). Fluid Phase Equilibria A novel static analytical apparatus for phase equilibrium measurements. *Fluid Phase Equilibria*, *338*, 188–196. doi:10.1016/j.fluid.2012.11.008

Ndlovu, M. (2005). Development Of A Dynamic Still For Measuring Low Pressure Vapour-Liquid-Liquid Equilibria.

NIST Technical Note 1297 1994 Edition Guidelines for Evaluating and Expressing the Uncertainty of NIST Measurement Results NIST Technical Note 1297 1994 Edition Guidelines for Evaluating and Expressing the Uncertainty of NIST Measurement Results. (1994).

Nothnagel, K.-H., Abrams, D. S., & Prausnitz, J. M. (1973). Generalized Correlation for Fugacity Coefficients in Mixtures at Moderate Pressures. Application of Chemical Theory of Vapor Imperfections. *Industrial & Engineering Chemistry Process Design and Development*, *12*(1), 25–35. doi:10.1021/i260045a006

Ott, J. B. (1996). Applications of Calorimetry to Nonelectrolyte Solutions, (1), 987–1004.

Pillay, J. C. (2009). Binary Vapour-Liquid Equilibria For Oxygen- Containing Compounds. Master of Science in Engineering (Chemical Engineering) Dissertation, University of KwaZulu-Natal, South Africa

Pitzer, K S and Curl, R. F. (1957). "Emperical Equation for the Second Virial Coefficient." *Journal of the American Chemical Society*, *79*, 2369–2370.

Pitzer, K S, Lippmann, D Z, Curl, R F, Huggins, C M and Petersen, D. E. (1955). "The Volumetric and Thermodynamic Properties of Fluids. II. Compressibility Factor, Vapour Pressure and Entropy of Vapourization." *Journal of the American Chemical Society*, *77*, 3433–3440.

Plus, A. (n.d.). Aspen Plus 7 10.

Poling, B. E., & Prausnitz, J. M. (5th Edition). *The Properties Of Gases And Liquids*.

Prausnitz J M, L. R. N. and de A. E. G. (1999). *Molecular Thermodynamics of Fluid Phase Equilibria* (3rd ed.). New York: Prentice-Hall).

Prausnitz, J M, Anderson, T F, Grens, E A, Eckert, C A, Hseih, R and O'Connell, J. P. (1980). *"Computer Calculations for Multicomponent Vapour-Liquid and Liquid-Liquid Equilibria."* Englewood Cliffs, New Jersey: Prentice-Hall.

Raal, J. D. and A. L. M. (1998). *"Phase Equillibria Measurements and Computation."* Washington DC: Taylor & Francis.

Raal, J. D., & Muhlbauer, A. L. (1994). "The Measurement of High Pressure Vapour-Liquid-Equilibria." *Dev. Chem. Eng. Mineral Process.*

Ramjugernath, D. (2000). *"High Pressure Phase Equilibrium Studies."* University of Natal.

Reddy, P. (2006). *"Development of a novel apparatus for Vapour-Liquid Equilibrium Measurements at Moderate Pressures."* University of KwaZulu-Natal.

Reid, R C, Prausnitz, J M and Polling, B. E. (1988). *"The Properties of Gases and Liquids."* New York: McGraw-Hill.

Renon, H and Prausnitz, J. M. (1968). "Local Compositions in Thermodynamic Excess Functions for Liquid Mixtures." *American Institute of Chemical Engineers Journal*, *14*, 135–144.

Seader, J.D. and Henley, E. J. (1998). *Separation Process Principles*. United States of America: John Wiley and Sons, Inc.

Sewnarain, R, Raal, J D and Ramjugernath, D. (2002). "Isobaric Vapour-Liquid Equilibria for the Systems Propionic Acid + Butyric Acid, Isobutyric Acid + Butyric Acid, Butyric Acid + Isovaleric Acid, and Butyric Acid + Hexanoic Acid at 14 kPa." *Journal of Chemical Engineering Data*, *47*, 603–607.

Smith, M. and. (1979). Data . Effect of Equation of State Used, *18*(4), 354–357.

Smith, J M, Van Ness, H C and Abbott, M. M. (2004). *"Introduction to Chemical Engineering Thermodynamics"* (7th ed.). New York.

Stockhardt, J S & Hull, C. M. (1931). Vapour Liquid Equilibria and Boiling Point Composition Relations form Systems n- Butanol - water and Isobutanol - Water". *Industrial Engineering Chemistry*, *123*, p 1438 – 1440.

Swietoslawski, W. (1945). *"Ebulliometric Measurements."* Reinhold, New York.

Technology, A. (n.d.). Aspen Physical Property System - Physical Property Methods.

Thornton, J. D. (1951). "An improved type of vapour-liquid equilibrium still." *Journal of Applied Chemistry*, *1*(6), 237–239.

Tsonopoulos, C. (1974). "An Emperical Correlation of Second Virial Coefficients." *American Institute of Chemical Engineers Journal*, *20*, 263–272.

Tsuboka, T and Katayama, T. (1975). "Modified Wilson Equation for Vapour-Liquid and Liquid-Liquid Equilibria." *Journal of Chemical Engineering of Japan*, *8*, 181–187.

Uusi-kyyny, P. (2004). *"Vapour Liquid Equilibrium Measurements Vapour Liquid Equilibrium Measurements."* Helsinki University of Technology (Espoo, Finland).

Van Ness, H. C. (1995). Thermodynamics in the treatment of vapor/liquid equilibrium (VLE) data. *Pure and Applied Chemistry*, *67*(6), 859–872. doi:10.1351/pac199567060859

Van Ness, H.C. Byer, S.M. Gibbs, R. E. (1973). "Part I. An Appraisal of Data Reduction Methods." *AIChe J.*, *19*, 238.

Walas, S. M. (1985). *"Phase Equilibrium in Chemical Engineering."* Butterworth, Boston.

Wilson, G. M. (1964). Vapor-Liquid Equilibrium. XI. A New Expression for the Excess Free Energy of Mixing. *Journal of the American Chemical Society*, *86*(2), 127–130. doi:10.1021/ja01056a002

Yerazunis, S, Plowright, J D and Smola, F. M. (1964). "Vapour-Liquid Equilibrium Determination by a New Apparatus." *American Institute of Chemical Engineers Journal*, *10*(660-665).

APPENDIX A **(REGRESSED BINARY VLE DATA)**

This appendix presents the P-x-y and x-y plots showing the comparison of the three activity coefficient models (NRTL, WILSON and UNIQUAC) combined with the HOC equation of state model that was used for the regression of the data measured in this work. The P-x-y and x-y plots showing the comparison of the HOC and NTH models had been presented in the discussion part of this work (Chapter 6).

A.1. 1-propanol (1) + 4-methyl-2-pentanone (2) system

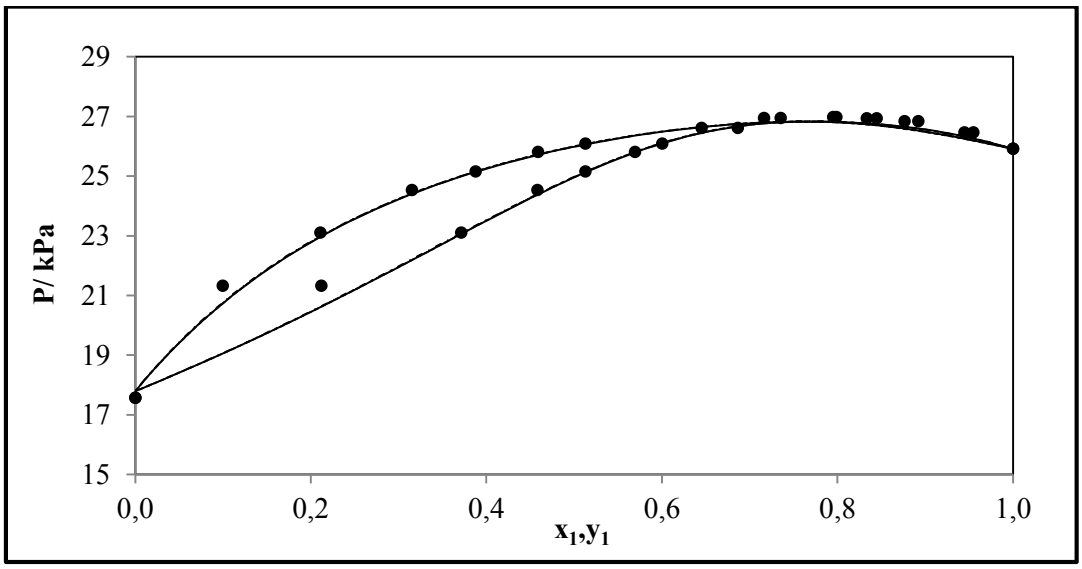

Figure A- 1: Fit of the NRTL-HOC, WILSON-HOC and UNIQUAC-HOC models to the P-x-y plot of the 1-propanol (1) + 4-methyl-2-pentanone (2) system at 338.15 K for the combined method: (•) this work, (—) NRTL-HOC, (— - - —) WILSON-HOC, (.....) UNIQUAC-HOC

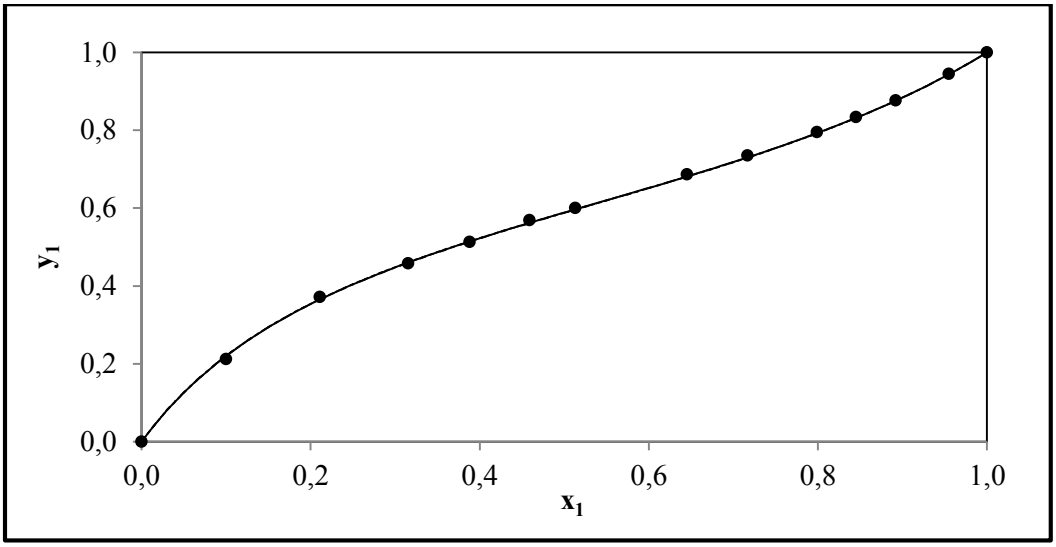

Figure A- 2: Fit of the NRTL-HOC, WILSON-HOC and UNIQUAC-HOC models to the x-y plot of the 1-propanol (1) + 4-methyl-2-pentanone (2) system at 338.15 K for the combined method: (•) this work, (—) NRTL-HOC, (— - - —) WILSON-HOC, (.....) UNIQUAC-HOC

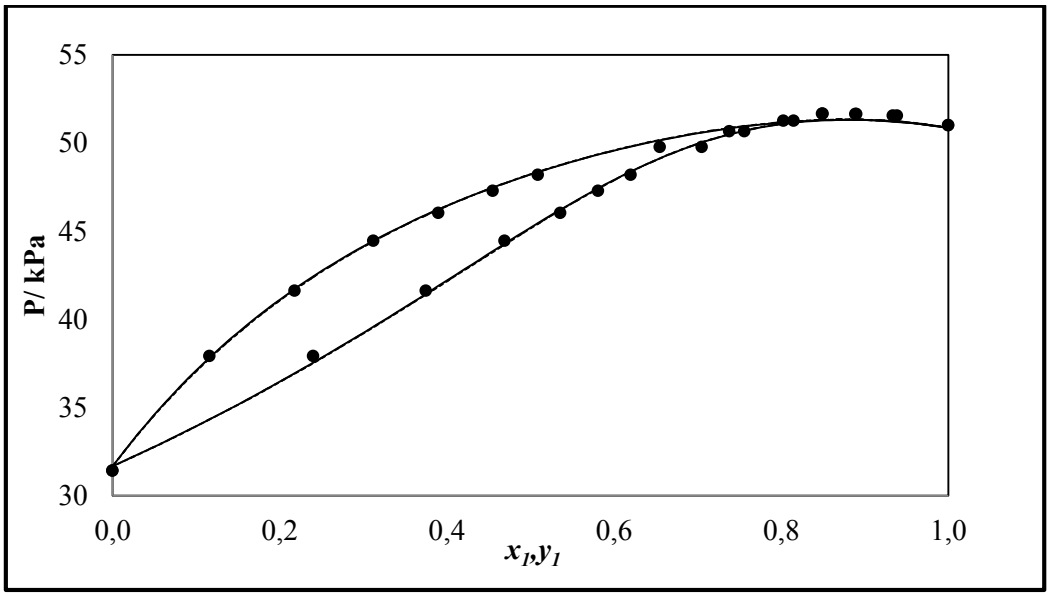

Figure A- 3: Fit of the NRTL-HOC, WILSON-HOC and UNIQUAC-HOC models to the P- x-y plot for the 1-propanol (1) + 4-methyl-2-pentanone (2) system at 353.15 K for the combined method: (•) this work, (—) NRTL-HOC, (— - - —) WILSON-HOC, (.....) UNIQUAC-HOC

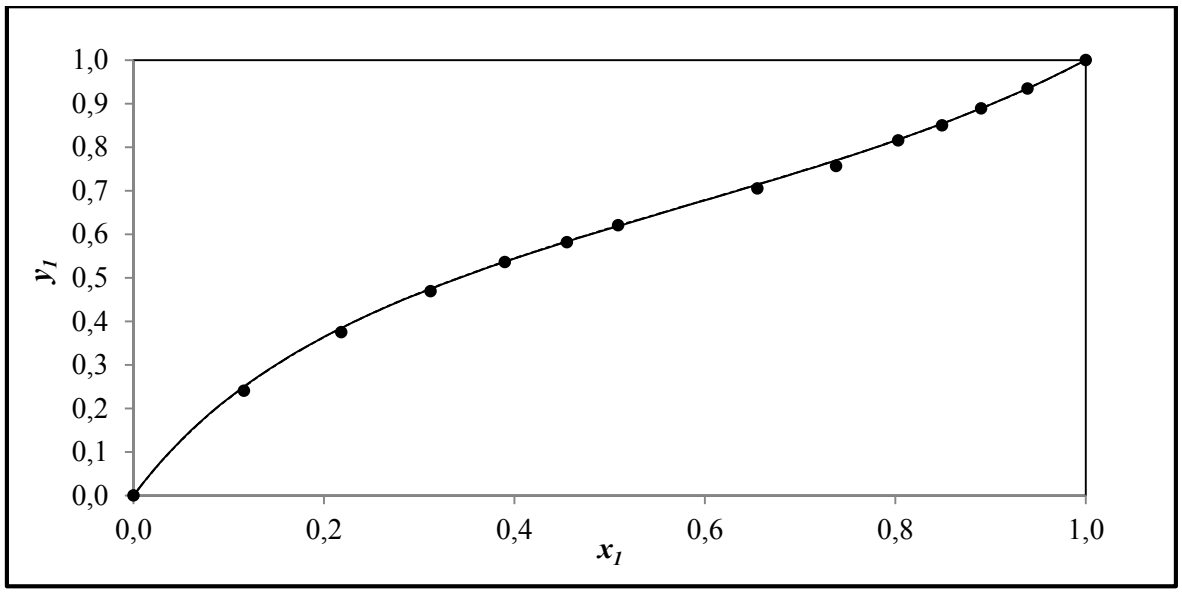

Figure A- 4: Fit of the NRTL-HOC, WILSON-HOC and UNIQUAC-HOC models to the x-y plot of the 1-propanol (1) + 4-methyl-2-pentanone (2) system at 353.15 K for the combined method: (•) this work, (—) NRTL-HOC, (— - - —) WILSON-HOC, (.....) UNIQUAC-HOC

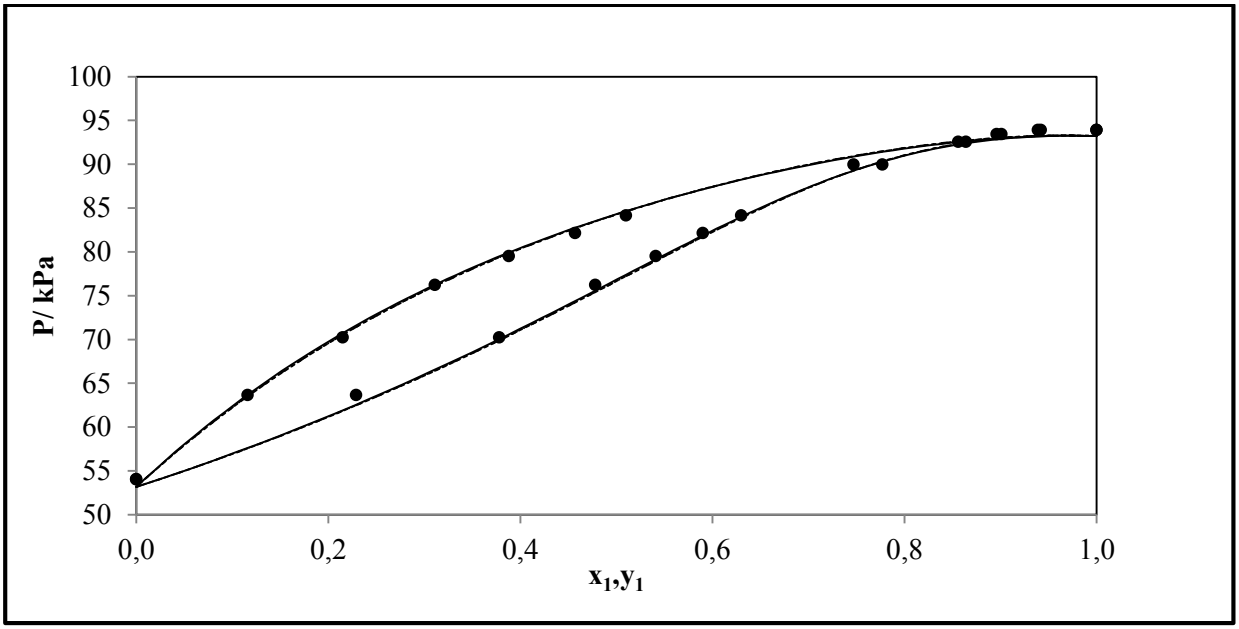

Figure A- 5: Fit of the NRTL-HOC, WILSON-HOC and UNIQUAC-HOC models to the P-x-y plot of the 1-propanol (1) + 4-methyl-2-pentanone (2) system at 368.15 K for the combined method: (•) this work, (—) NRTL-HOC, (— - - —) WILSON-HOC, (.....) UNIQUAC-HOC

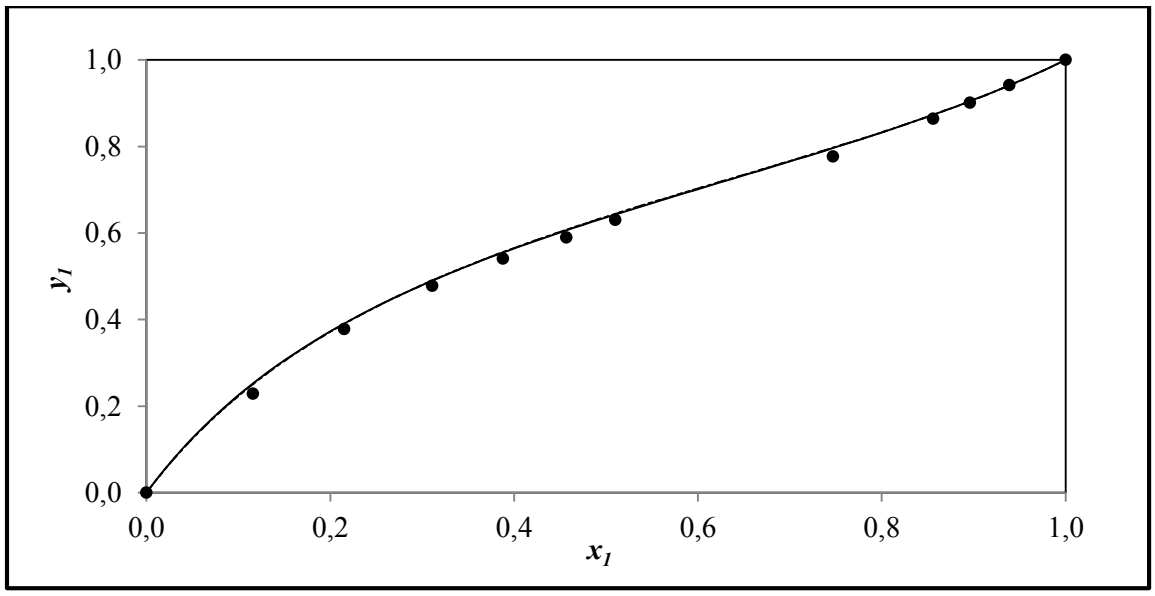

Figure A- 6: Fit of the NRTL-HOC, WILSON-HOC and UNIQUAC-HOC models to the x-y plot of the 1-propanol (1) + 4-methyl-2-pentanone (2) system at 368.15 K for the combined method: (•) this work, (—) NRTL-HOC, (— - - —) WILSON-HOC, (.....) UNIQUAC-HOC

A.2. 2-propanol (1) + 4-methyl-2-pentanone (2) system

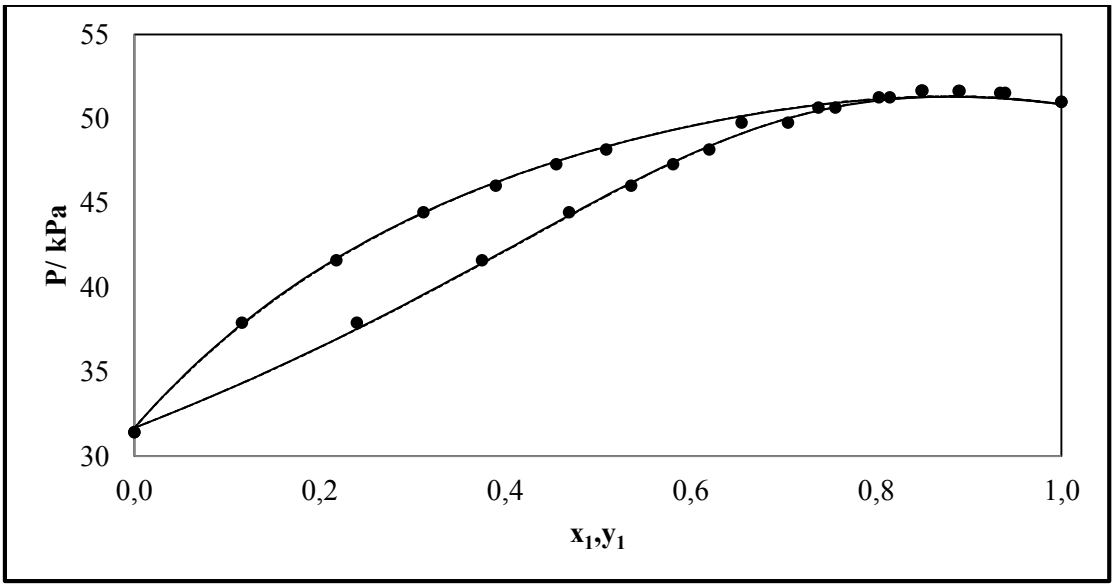

Figure A- 7: Fit of the NRTL-HOC, WILSON-HOC and UNIQUAC-HOC models to the P-x-y plot of the 2-propanol (1) + 4-methyl-2-pentanone (2) system at 323.15 K for the combined method: (•) this work, (—) NRTL-HOC, (— - - —) WILSON-HOC, (.....) UNIQUAC-HOC

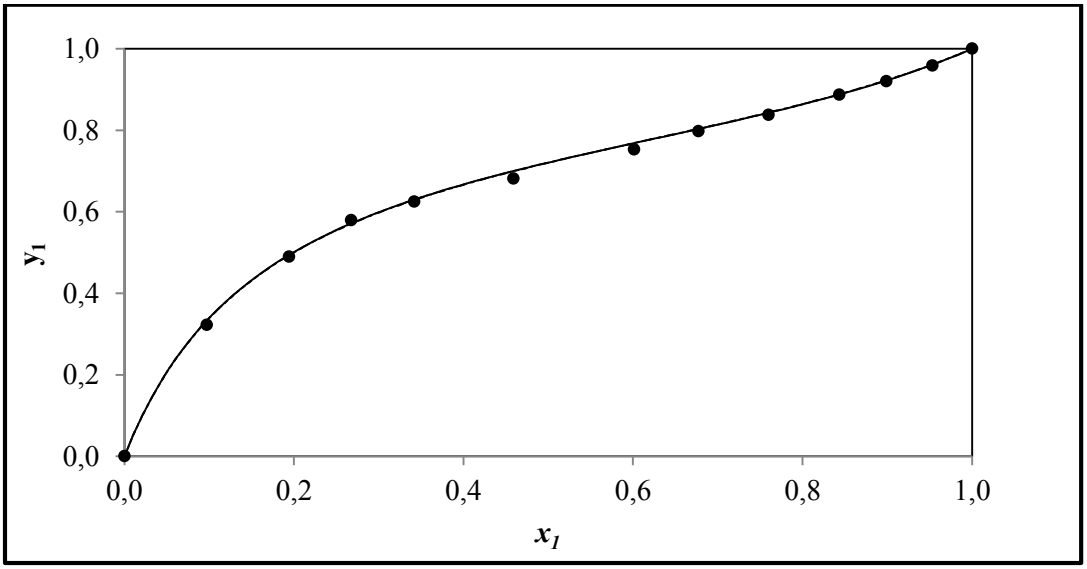

Figure A- 8: Fit of the NRTL-HOC, WILSON-HOC and UNIQUAC-HOC models to the x-y plot of the 2-propanol (1) + 4-methyl-2-pentanone (2) system at 323.15 K for the combined method: (•) this work, (—) NRTL-HOC, (— - - —) WILSON-HOC, (.....) UNIQUAC-HOC

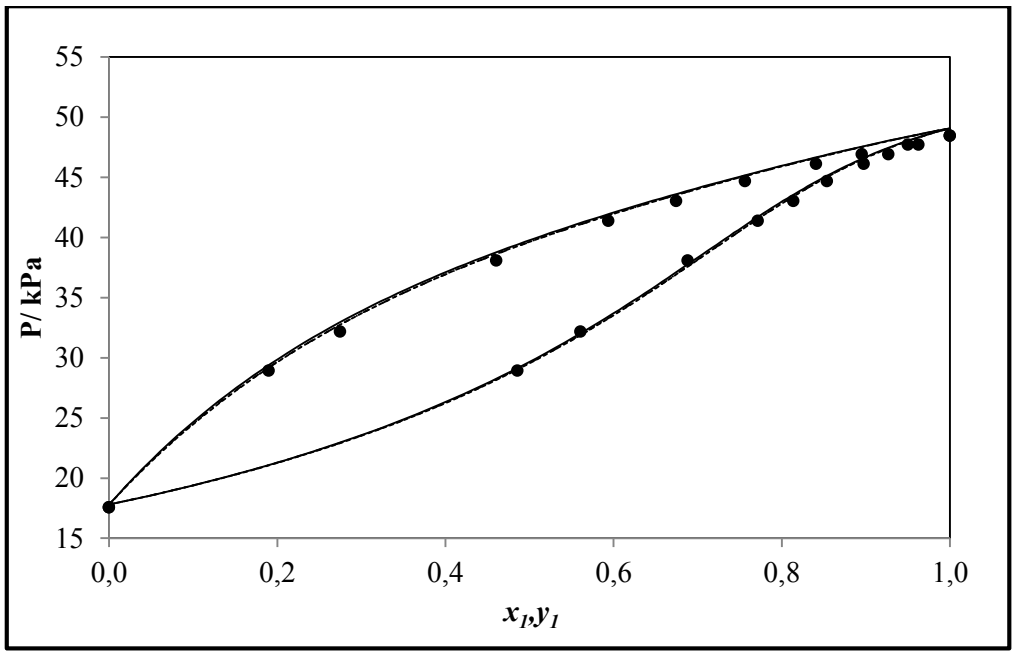

Figure A- 9: Fit of the NRTL-HOC, WILSON-HOC and UNIQUAC-HOC models to the P-x-y plot of the 2-propanol (1) + 4-methyl-2-pentanone (2) system at 338.15 K for the combined method: (•) this work, (—) NRTL-HOC, (— - - —) WILSON-HOC, (.....) UNIQUAC-HOC

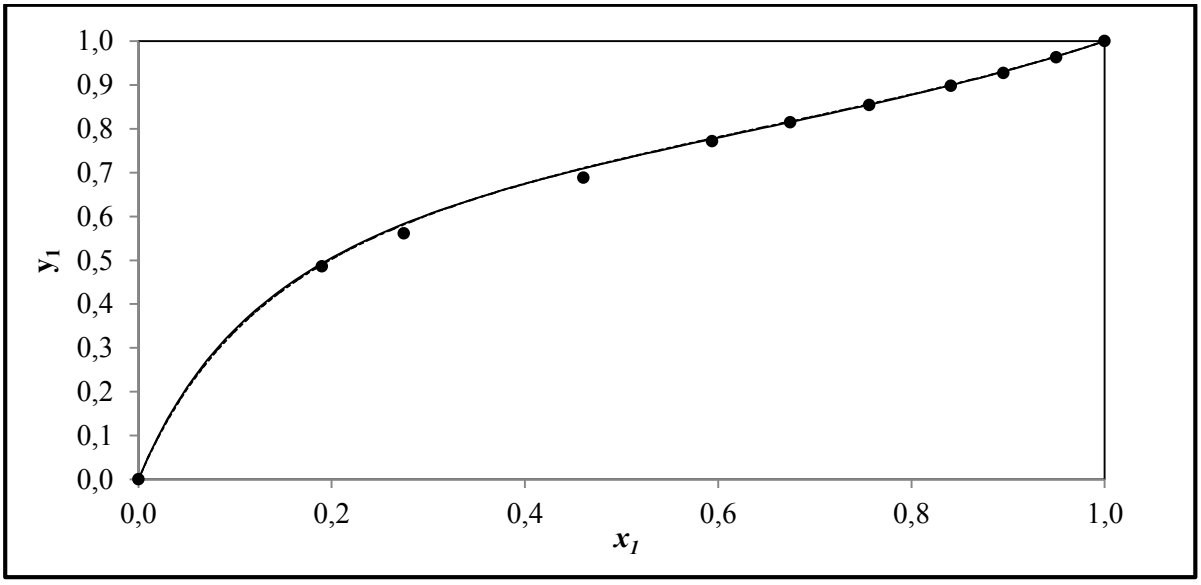

Figure A- 10: Fit of the NRTL-HOC, WILSON-HOC and UNIQUAC-HOC models to the x-y plot of the 2-propanol (1) + 4-methyl-2-pentanone (2) system at 338.15 K for the combined method: (•) this work, (—) NRTL-HOC, (— - - —) WILSON-HOC, (.....) UNIQUAC-HOC

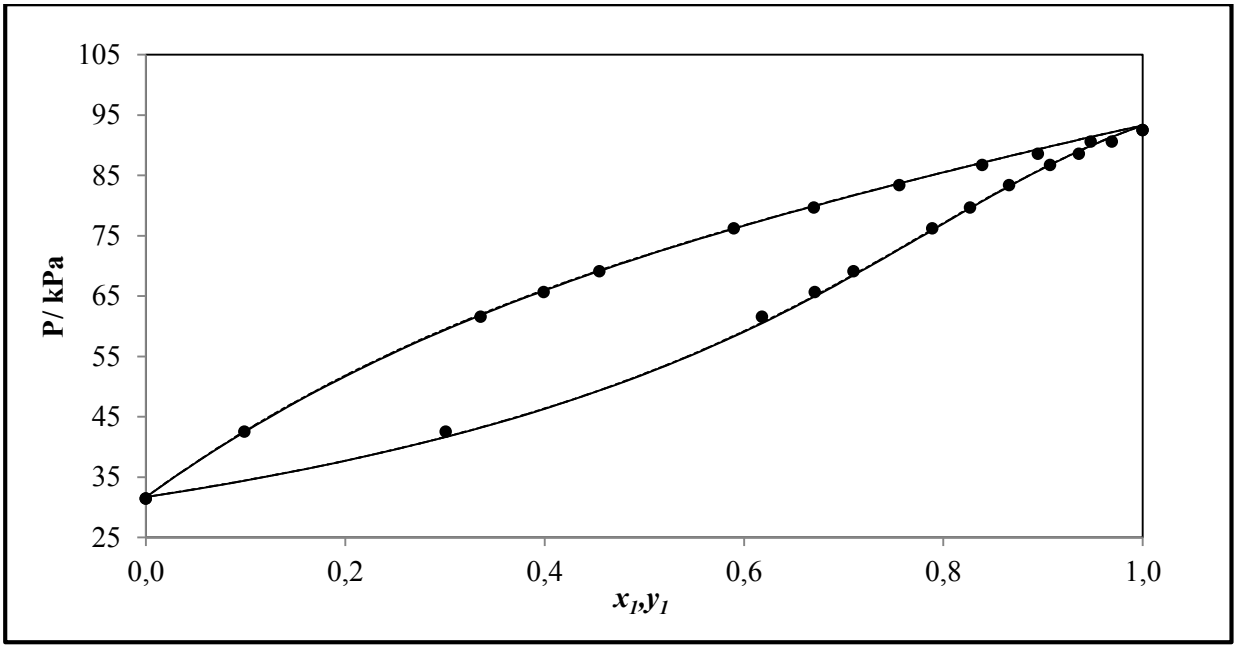

Figure A- 11: Fit of the NRTL-HOC, WILSON-HOC and UNIQUAC-HOC models to the P-x-y plot of the 2-propanol (1) + 4-methyl-2-pentanone (2) system at 353.15 K for the combined method: (•) this work, (—) NRTL-HOC, (— - - —) WILSON-HOC, (.....) UNIQUAC-HOC

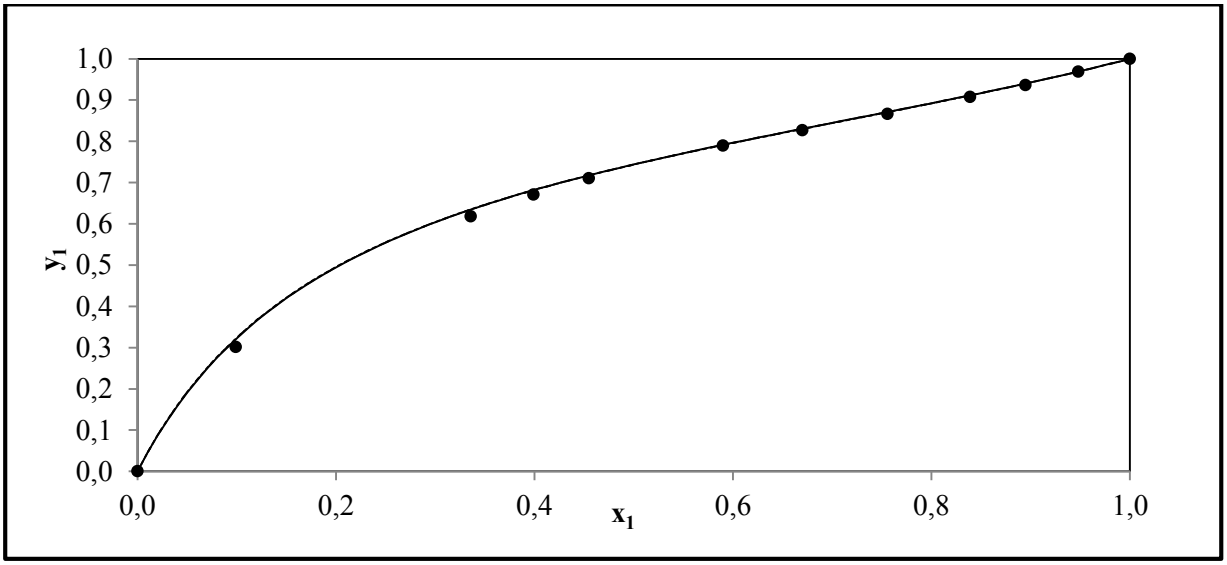

Figure A- 12: Fit of the NRTL-HOC, WILSON-HOC and UNIQUAC-HOC models to the x-y plot of the 2-propanol (1) + 4-methyl-2-pentanone (2) system at 353.15 K for the combined method: (•) this work, (—) NRTL-HOC, (— - - —) WILSON-HOC, (.....) UNIQUAC-HOC

A.3. 2-pentanone (1) + 2-methylpropan-1-ol

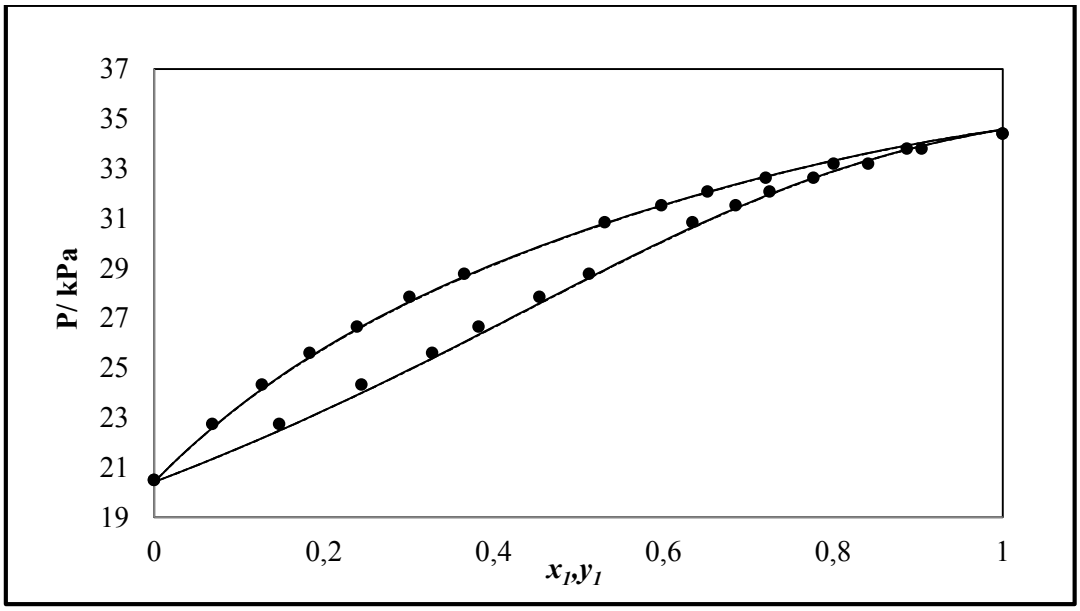

Figure A- 13: Fit of the NRTL-HOC, WILSON-HOC and UNIQUAC-HOC models to the P-x-y plot of the 2-pentanone (1) + 2-methylpropan-1-ol (2) system at 343.15 K for the combined method: (•) this work, (—) NRTL-HOC, (— - - —) WILSON-HOC, (.....) UNIQUAC-HOC

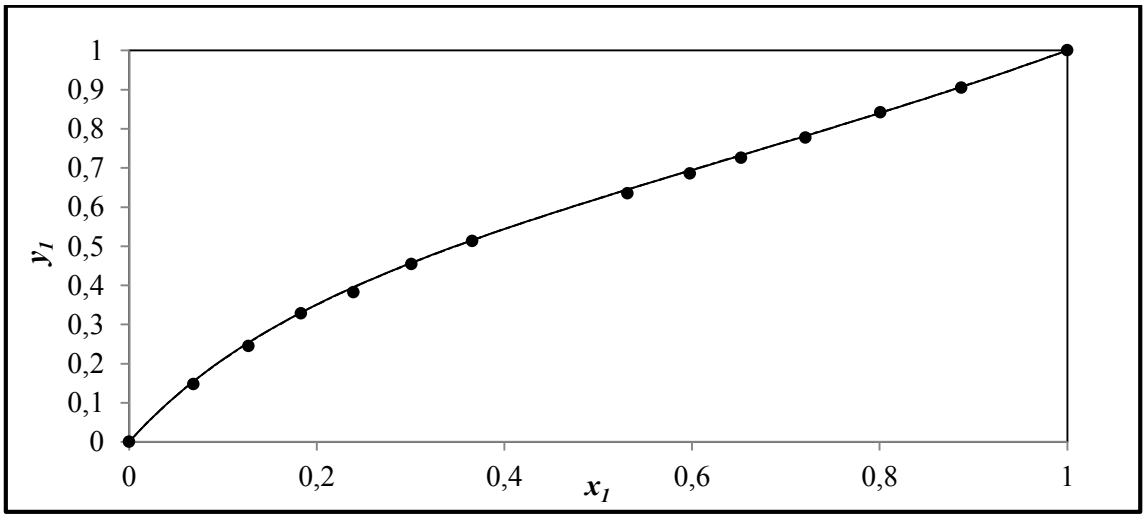

Figure A- 14: Fit of the NRTL-HOC, WILSON-HOC and UNIQUAC-HOC models to the x-y plot of the 2-pentanone (1) + 2-methylpropan-1-ol (2) system at 343.15 K for the combined method: (•) this work, (—) NRTL-HOC, (— - - —) WILSON-HOC, (.....) UNIQUAC-HOC

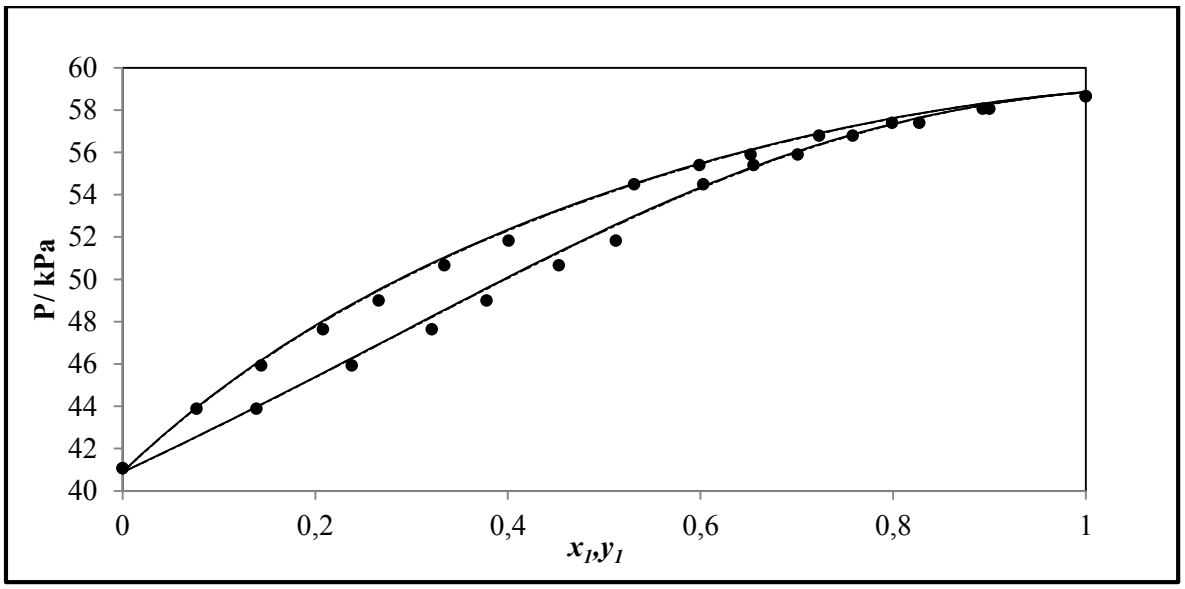

Figure A- 15: Fit of the NRTL-HOC, WILSON-HOC and UNIQUAC-HOC models to the P-x-y plot of the 2-pentanone (1) + 2-methylpropan-1-ol (2) system at 358.15 K for the combined method: (•) this work, (—) NRTL-HOC, (— - - —) WILSON-HOC, (.....) UNIQUAC-HOC

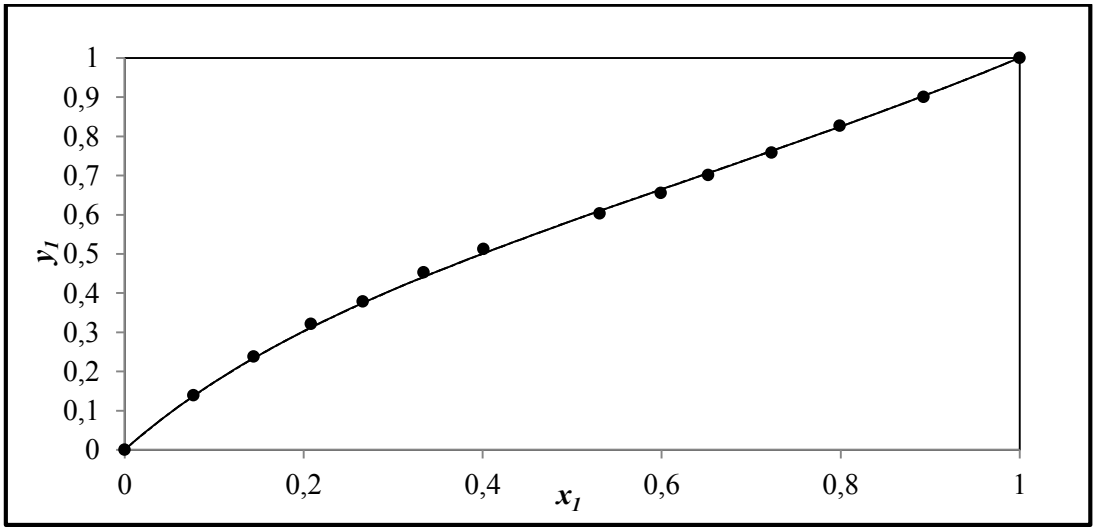

Figure A- 16: Fit of the NRTL-HOC, WILSON-HOC and UNIQUAC-HOC models to the x-y plot of the 2-pentanone (1) + 2-methylpropan-1-ol (2) system at 358.15 K for the combined method: (•) this work, (—) NRTL-HOC, (— - - —) WILSON-HOC, (.....) UNIQUAC-HOC

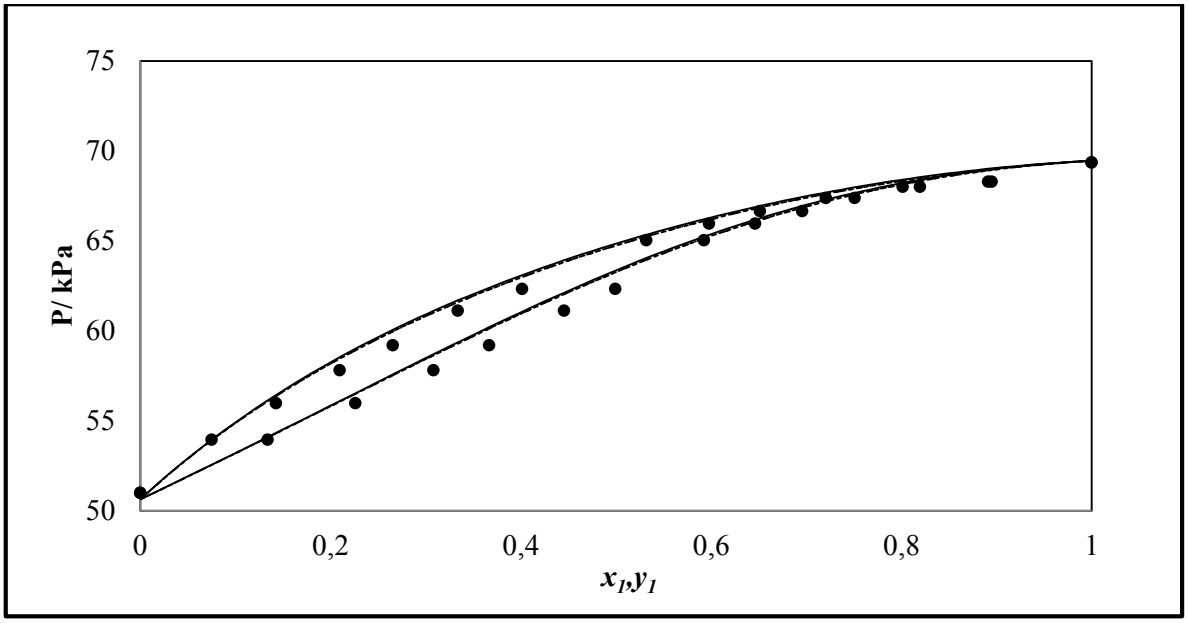

Figure A- 17: Fit of the NRTL-HOC, WILSON-HOC and UNIQUAC-HOC models to the P-x-y plot of the 2-pentanone (1) + 2-methylpropan-1-ol (2) system at 363.15 K for the combined method: (•) this work, (—) NRTL-HOC, (— - - —) WILSON-HOC, (.....) UNIQUAC-HOC

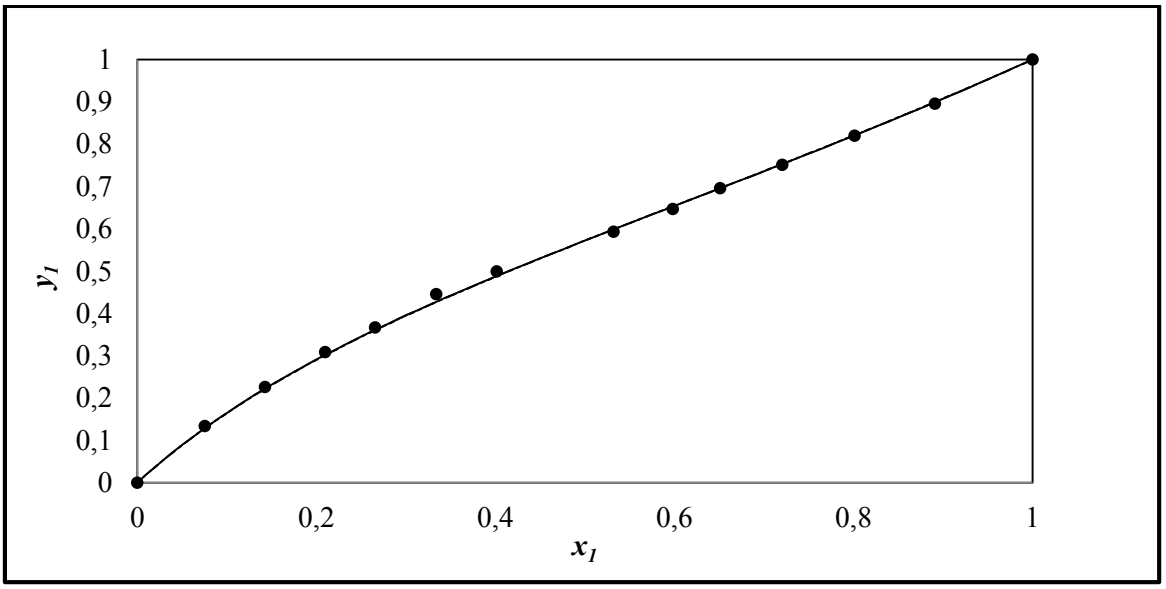

Figure A- 18: Fit of the NRTL-HOC, WILSON-HOC and UNIQUAC-HOC models to the x-y plot of the 2-pentanone (1) + 2-methylpropan-1-ol (2) system at 363.15 K for the combined method: (•) this work, (—) NRTL-HOC, (— - - —) WILSON-HOC, (.....) UNIQUAC-HOC

A.4 Thermodynamic consistency testing

A.4.1 1-propanol (1) + 4-methyl-2-pentanone (2) system

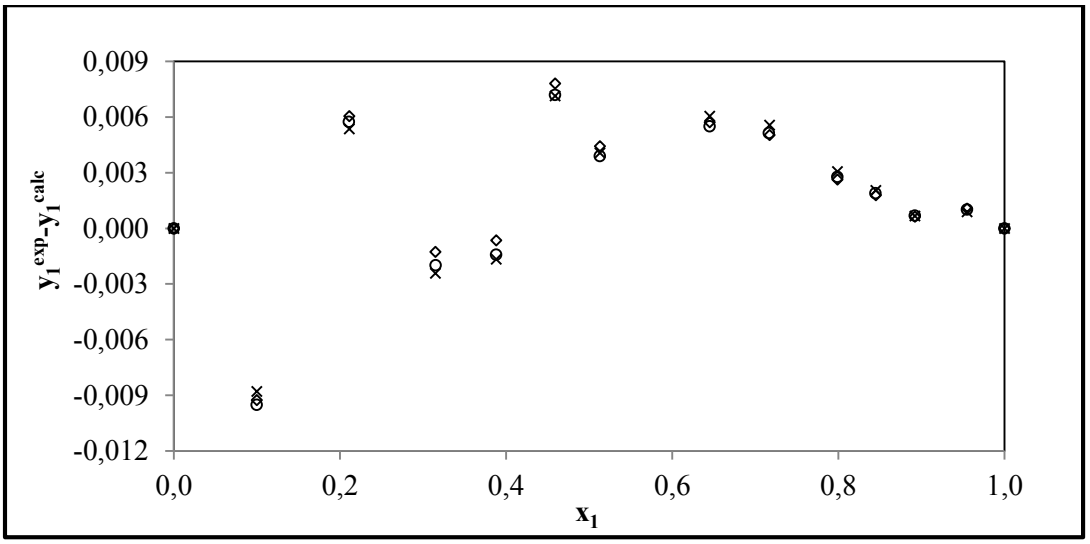

Figure A- 19: Point test (varying activity coefficient model): Δy_1 for the 1-propanol (1) + 4-methyl-2-pentanone (2) system at 338.15K: (○) NRTL-HOC, (◊) WILSON-HOC, (×) UNIQUAC -HOC

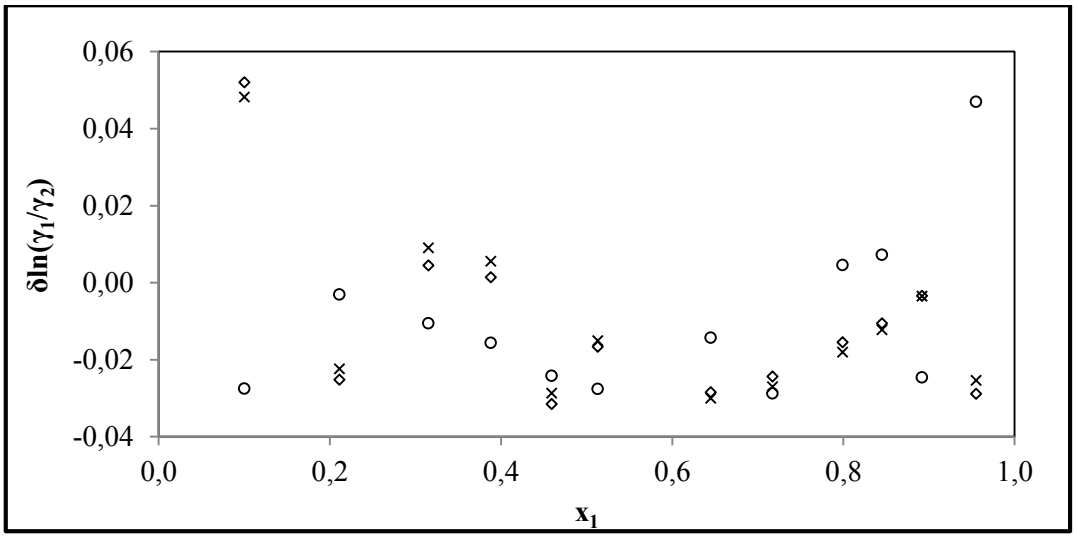

Figure A- 20: Direct test (varying activity coefficient model): $\delta\ln(\gamma_1/\gamma_2)$ for the 1-propanol (1) + 4-methyl-2-pentanone (2) system at 338.15K: (○) NRTL-HOC, (◊) WILSON-HOC, (×) UNIQUAC -HOC

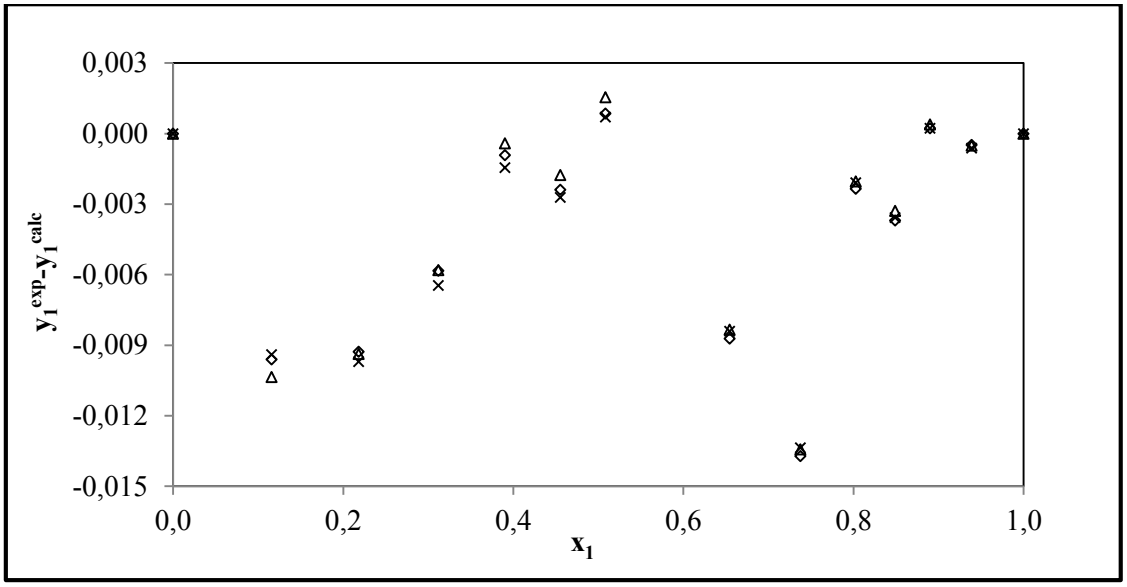

Figure A- 21: Point test (varying activity coefficient model): Δy_1 for the 1-propanol (1) + 4-methyl-2-pentanone (2) system at 353.15K: (○) NRTL-HOC, (◊) WILSON-HOC, (×) UNIQUAC -HOC

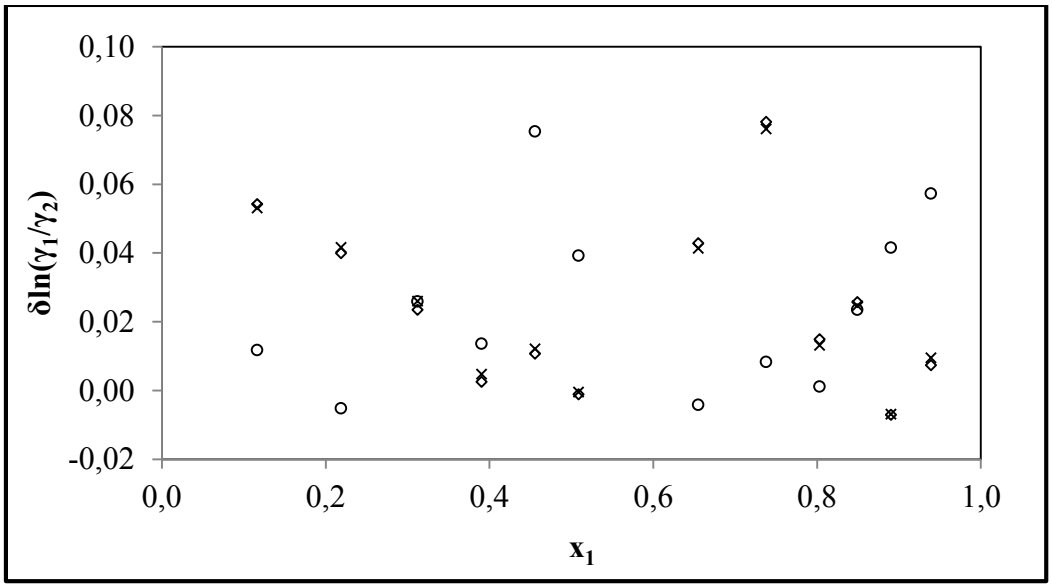

Figure A- 22: Direct test (varying activity coefficient model): $\delta\ln(\gamma_1/\gamma_2)$ for the 1-propanol (1) + 4-methyl-2-pentanone (2) system at 353.15 K : (○) NRTL-HOC, (◊) WILSON-HOC, (×) UNIQUAC -HOC

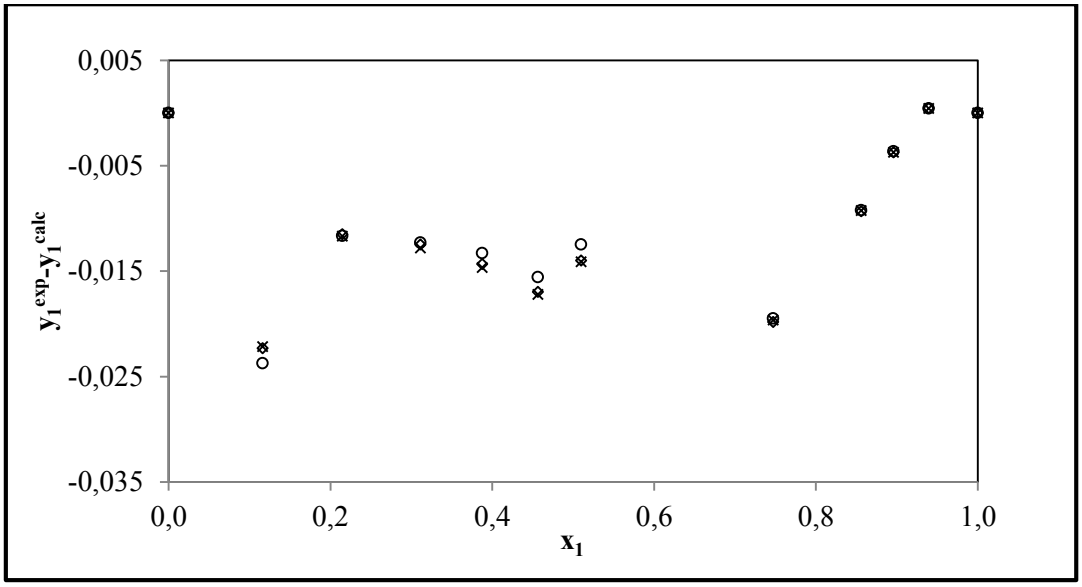

Figure A- 23: Point test (varying activity coefficient model): Δy_1 for the 1-propanol (1) + 4-methyl-2-pentanone (2) system at 368.15K: (○) NRTL-HOC, (◊) WILSON-HOC, (×) UNIQUAC -HOC

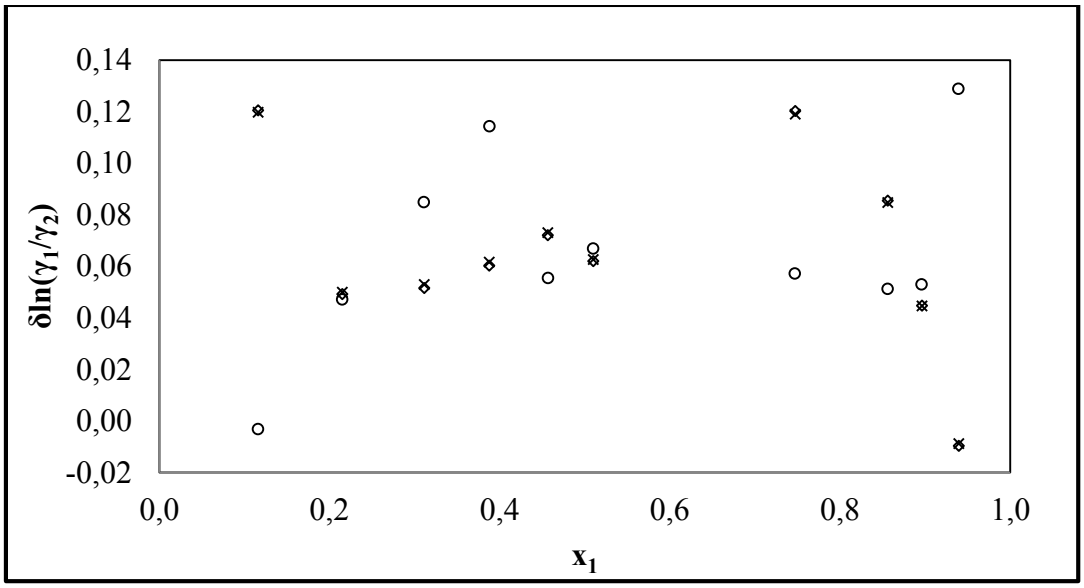

Figure A- 24: Direct test (varying activity coefficient model): $\delta\ln(\gamma_1/\gamma_2)$ for the 1-propanol (1) + 4-methyl-2-pentanone (2) system at 368.15 K : (○) NRTL-HOC, (◊) WILSON-HOC, (×) UNIQUAC -HOC

A.5 2-propanol (1) + 4-methyl-2-pentanone (2) system

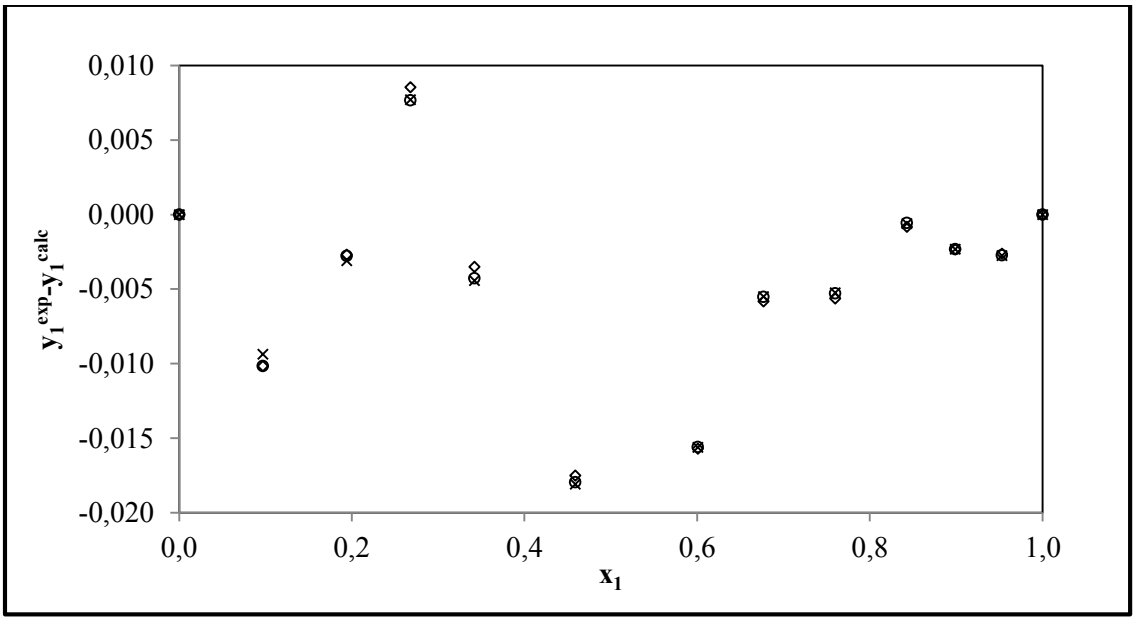

Figure A- 25: Point test (varying activity coefficient model): Δy_1 for the 2-propanol (1) + 4-methyl-2-pentanone (2) system at 323.15K: (○) NRTL-HOC, (◊) WILSON-HOC, (×) UNIQUAC -HOC

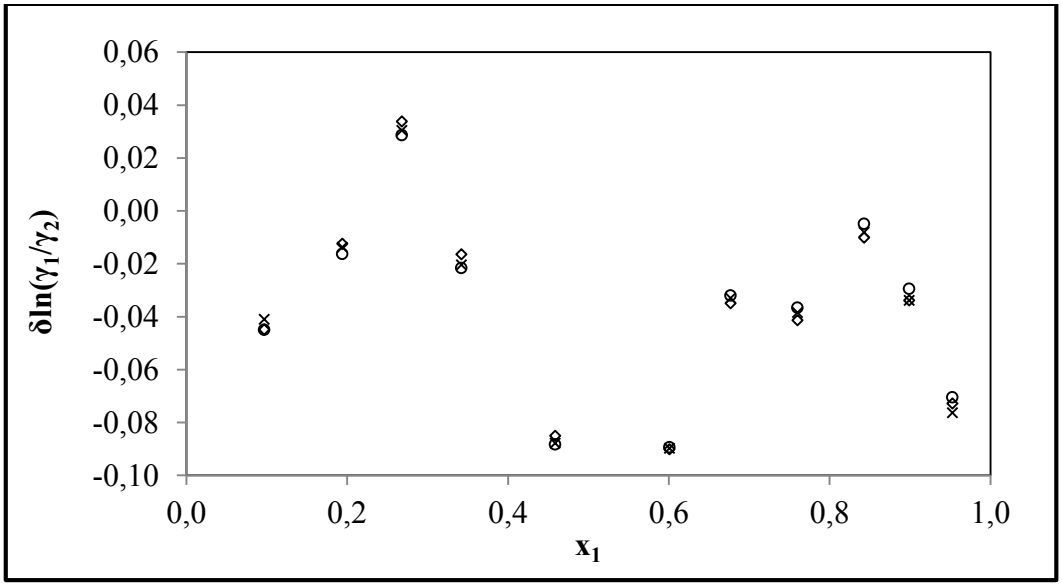

Figure A- 26: Direct test (varying activity coefficient model): $\delta\ln(\gamma_1/\gamma_2)$ for the 2-propanol (1) + 4-methyl-2-pentanone (2) system at 323.15K: (○) NRTL-HOC, (◊) WILSON-HOC, (×) UNIQUAC -HOC

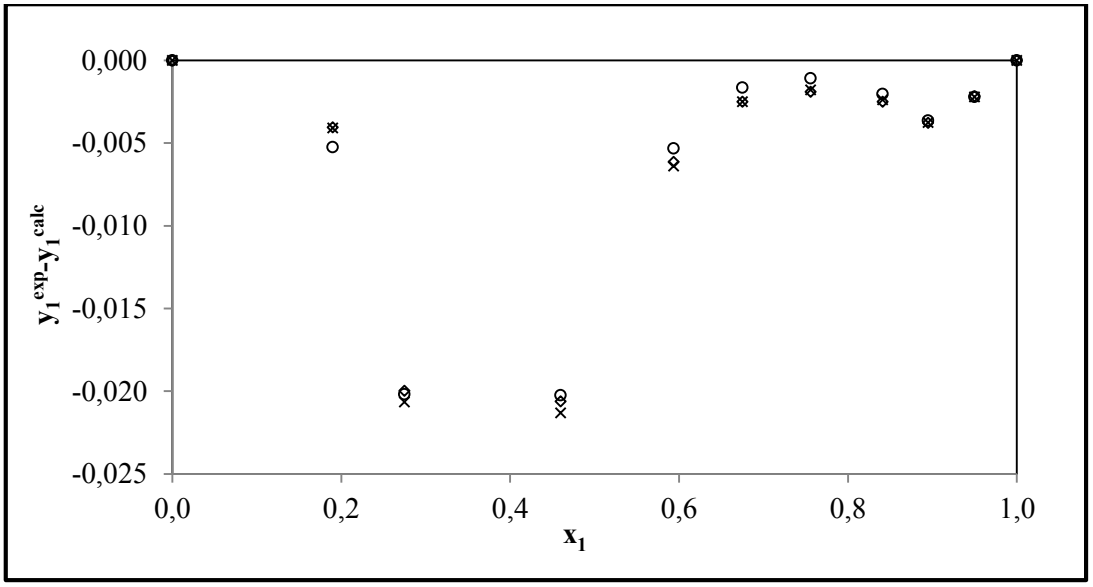

Figure A- 27: Point test (varying activity coefficient model): Δy_1 for the 2-propanol (1) + 4-methyl-2-pentanone (2) system at 338.15K: (○) NRTL-HOC, (◊) WILSON-HOC, (×) UNIQUAC -HOC

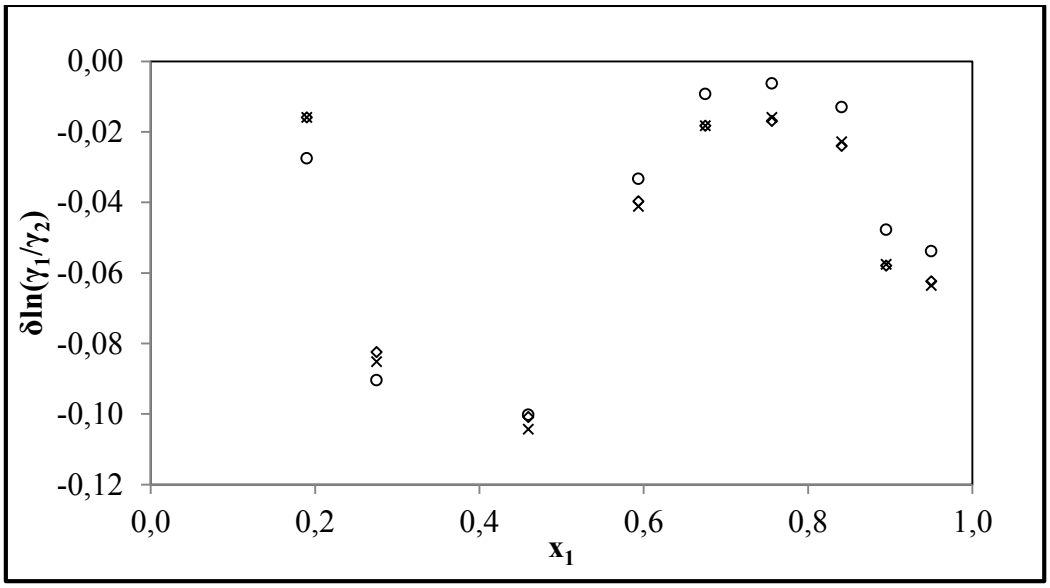

Figure A- 28: Direct test (varying activity coefficient model): $\delta\ln(\gamma_1/\gamma_2)$ for the 2-propanol (1) + 4-methyl-2-pentanone (2) system at 338.15K: (○) NRTL-HOC, (◊) WILSON-HOC, (×) UNIQUAC -HOC

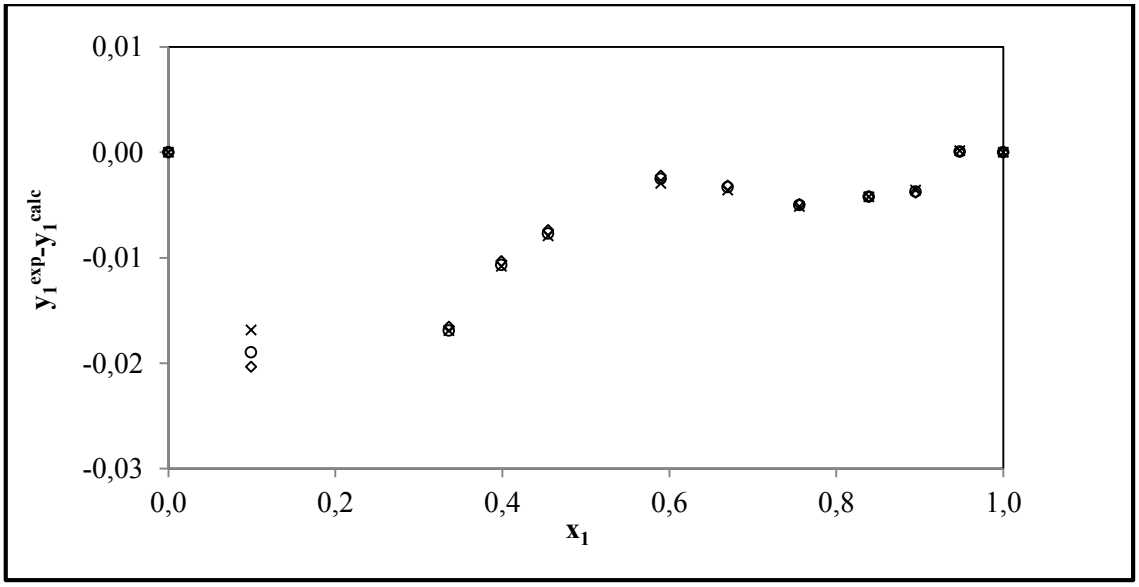

Figure A- 29: Point test (varying activity coefficient model): Δy_1 for the 2-propanol (1) + 4-methyl-2-pentanone (2) system at 353.15K: (○) NRTL-HOC, (◊) WILSON-HOC, (×) UNIQUAC -HOC

A.6 2-pentanone (1) + 2-methylpropan-1-ol (2) system

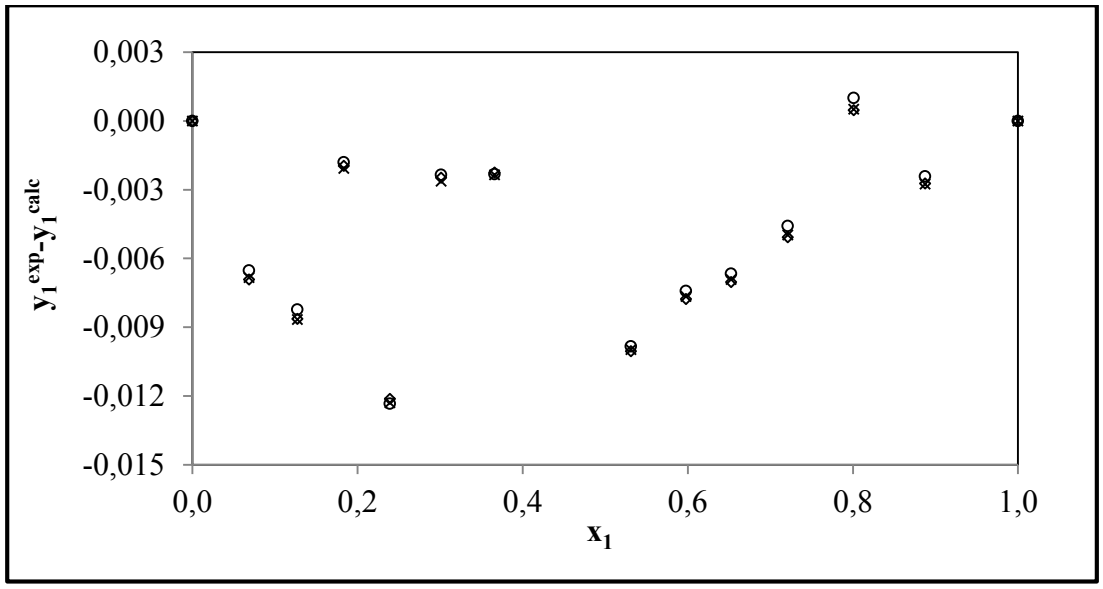

Figure A- 30: Point test (varying activity coefficient model): Δy_1 for the 2-pentanone (1) + 2-methylpropan-1-ol (2) system at 343.15K: (○) NRTL-HOC, (◊) WILSON-HOC, (×) UNIQUAC -HOC

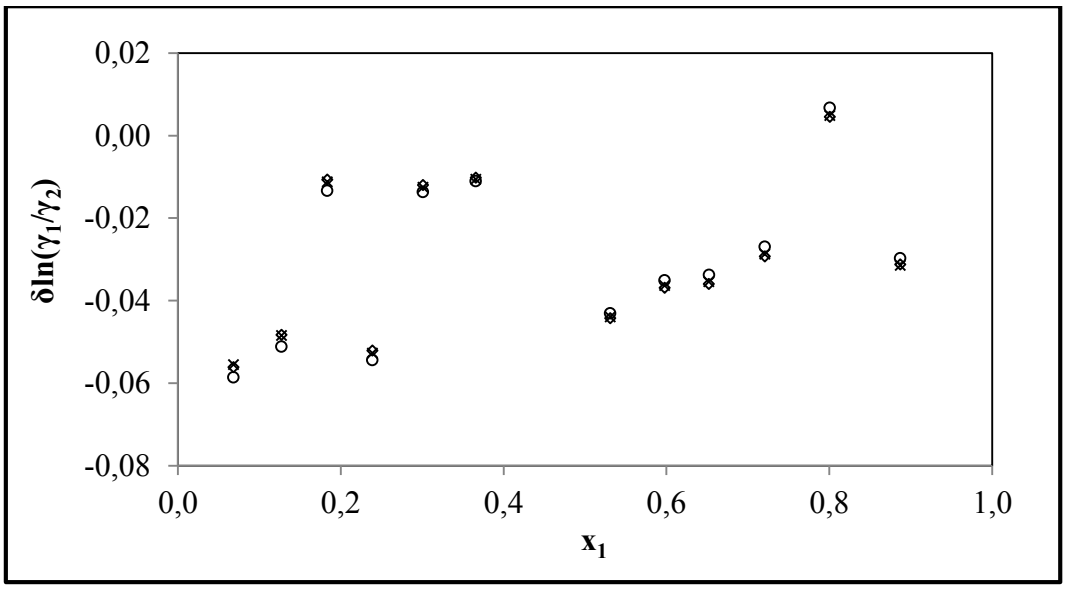

Figure A- 31: Direct test (varying activity coefficient model): $\delta\ln(\gamma_1/\gamma_2)$ for the 2-pentanone (1) + 2-methylpropan-1-ol (2) system at 343.15K: (○) NRTL-HOC, (◊) WILSON-HOC, (×) UNIQUAC –HOC

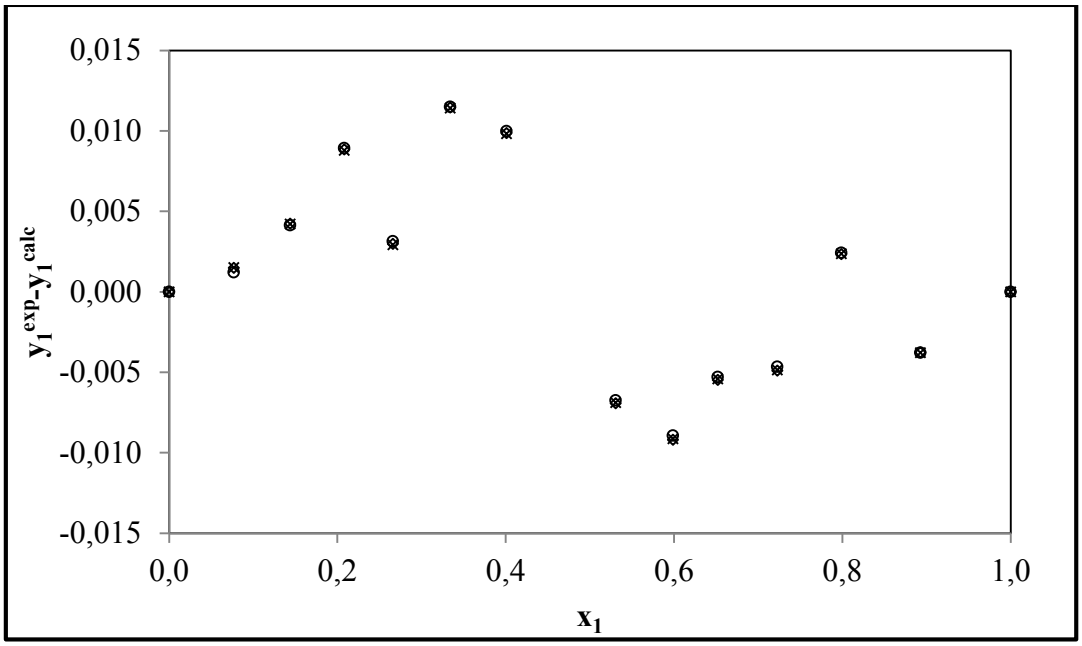

Figure A- 32: Point test (varying activity coefficient model): Δy_1 for the 2-pentanone (1) + 2-methylpropan-1-ol (2) system at 358.15K: (○) NRTL-HOC, (◊) WILSON-HOC, (×) UNIQUAC –HOC

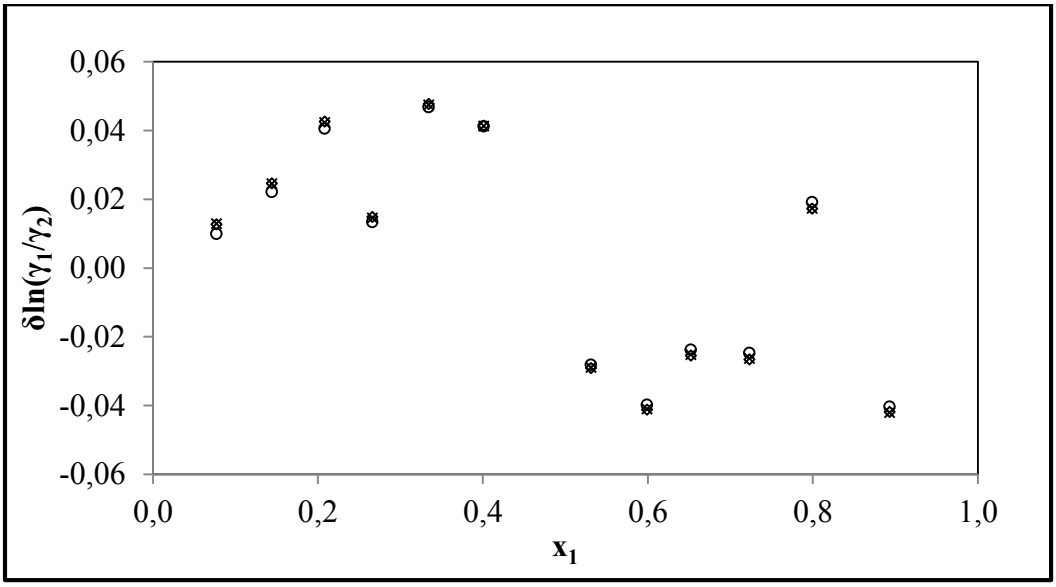

Figure A- 33: Direct test (varying activity coefficient model): $\delta\ln(\gamma_1/\gamma_2)$ for the 2-pentanone (1) + 2-methylpropan-1-ol (2) system at 358.15 K: (○) NRTL-HOC, (◊) WILSON-HOC, (×) UNIQUAC –HOC

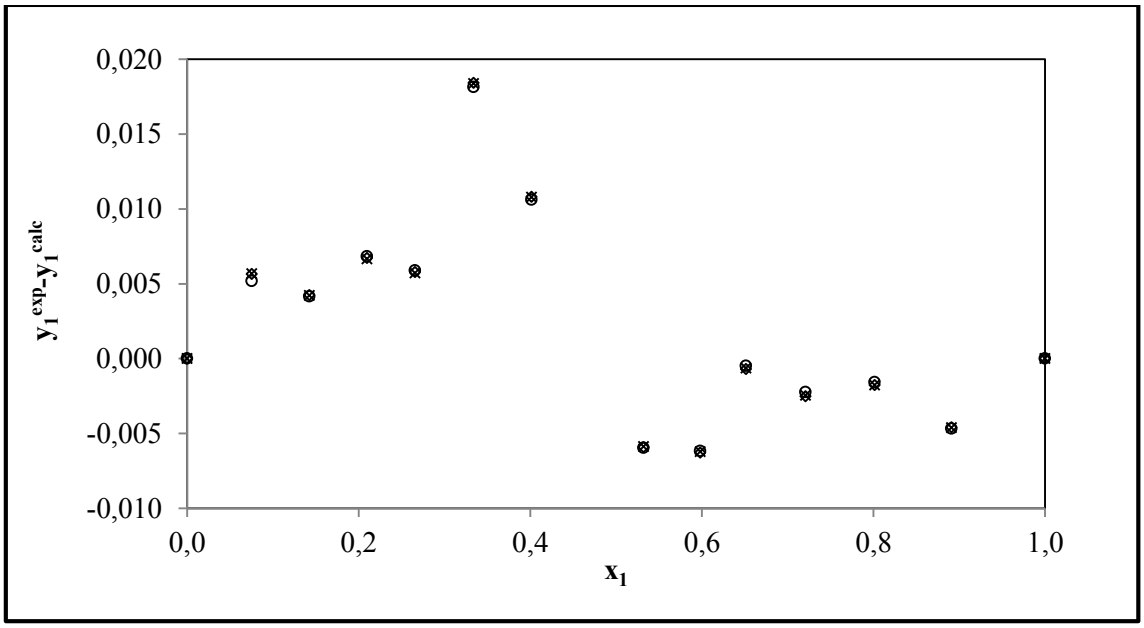

Figure A- 34: Point test (varying activity coefficient model): Δy_1 for the 2-pentanone (1) + 2-methylpropan-1-ol (2) system at 363.15K: (○) NRTL-HOC, (◊) WILSON-HOC, (×) UNIQUAC –HOC

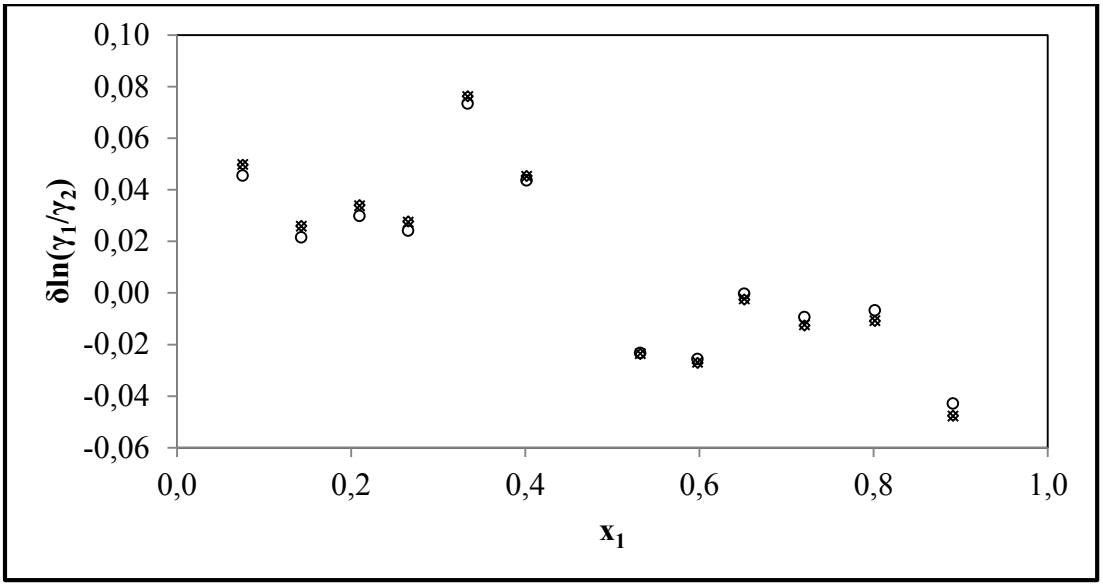

Figure A- 35: Direct test (varying activity coefficient model): $\delta\ln(\gamma_1/\gamma_2)$ for the 2-pentanone (1) + 2-methylpropan-1-ol (2) system at 363.15 K: (○) NRTL-HOC, (◊) WILSON-HOC, (×) UNIQUAC –HOC

APPENDIX B **(INFINITE DILUTION ACTIVITY COEFFICIENT)**

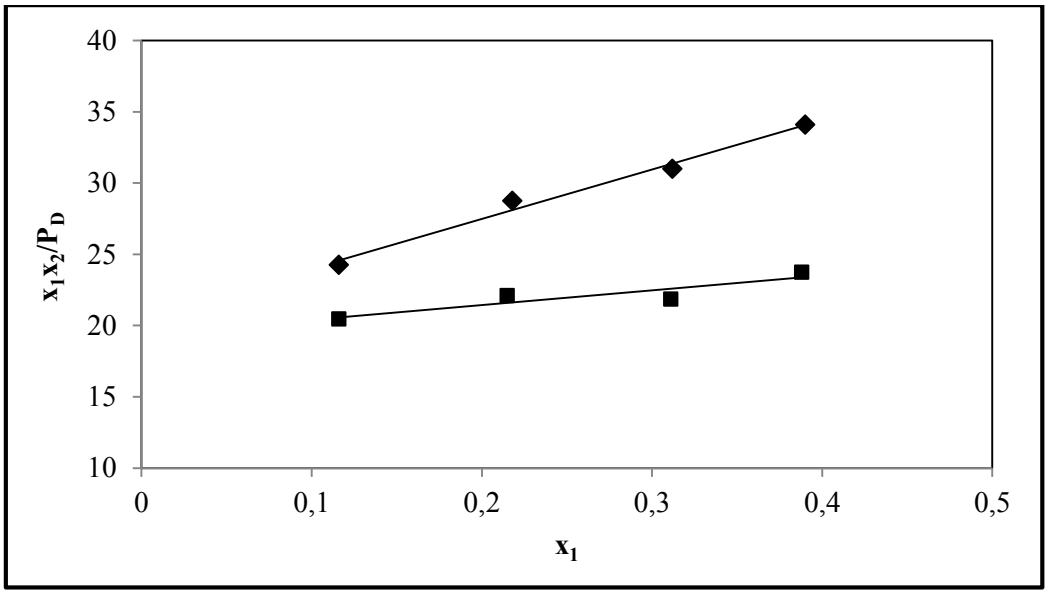

Figure B- 1: Plot of (x_1x_2/P_D) vs x_1 as $x_1 \rightarrow 0$ for 1-propanol (1) + 4-methyl-2-pentanone (2) at 353.15 K (♦) and 368.15 K (■)

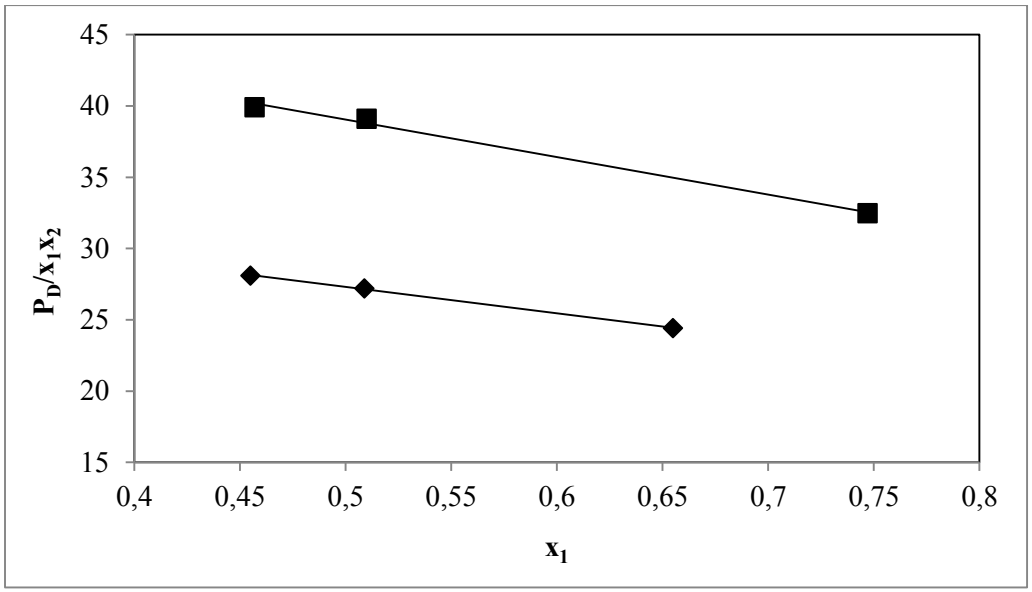

Figure B- 2: Plot of (P_D/x_1x_2) vs x_1 as $x_1 \rightarrow 1$ for 1-propanol (1) + 4-methyl-2-pentanone (2) at 353.15 K (♦) and 368.15 K (■)

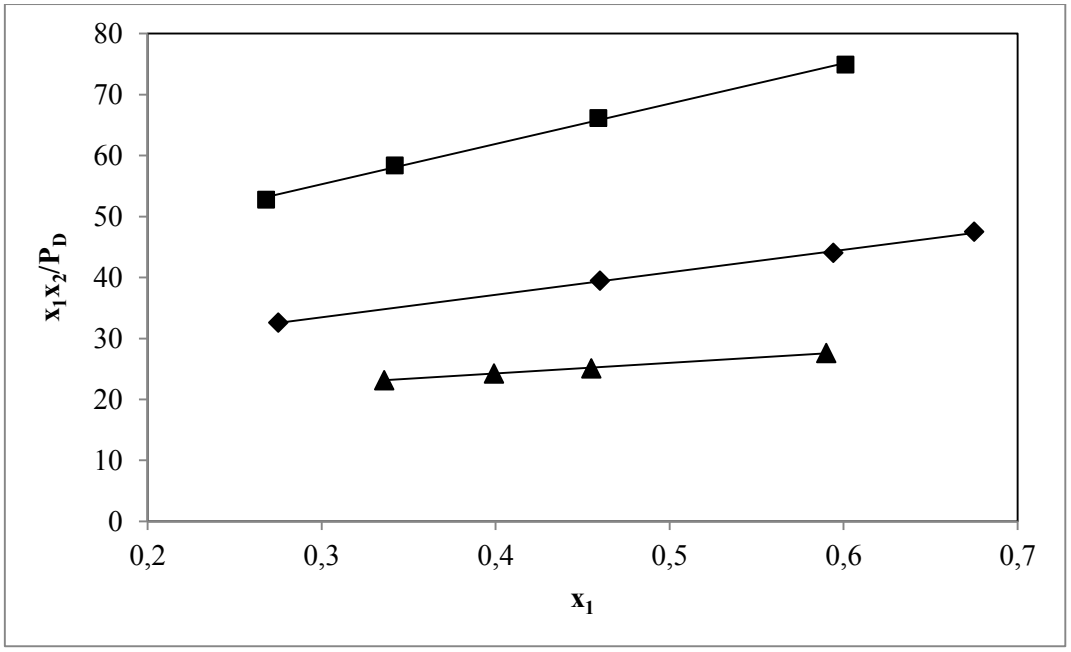

Figure B- 3: Plot of (x_1x_2/P_D) vs x_1 as $x_1 \rightarrow 0$ for 2-propanol (1) + 4-methyl-2-pentanone (2) at 323.15 K (■), 338.15.15 K (♦) and 353.15 K (▲)

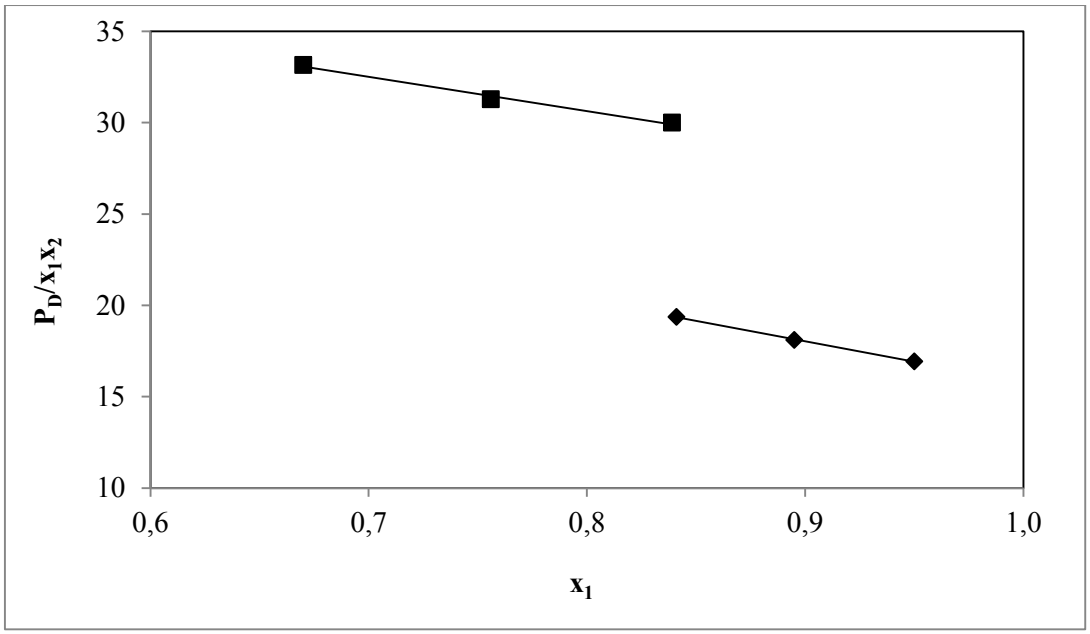

Figure B- 4: Plot of (P_D/x_1x_2) vs x_1 as $x_1 \rightarrow 1$ for 2-propanol (1) + 4-methyl-2-pentanone (2) at 338.15 K (♦) and 353.15 K (■)

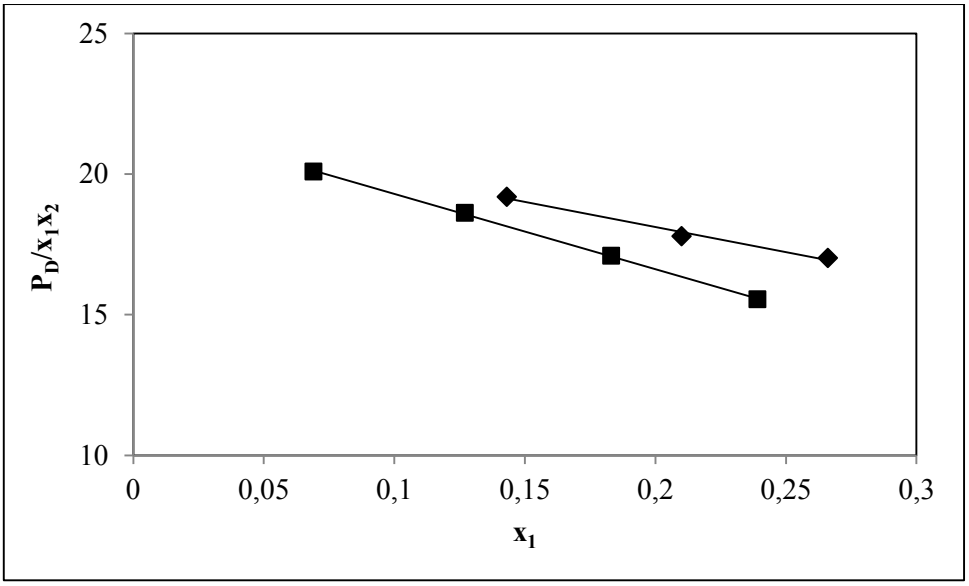

Figure B- 5: Plot of (P_D/x_1x_2) vs x_1 as $x_1 \rightarrow 0$ for 2-pentanone (1) + 2-methylpropan-1-ol (2) at 343.15 K (■) and 363.15 K (♦)

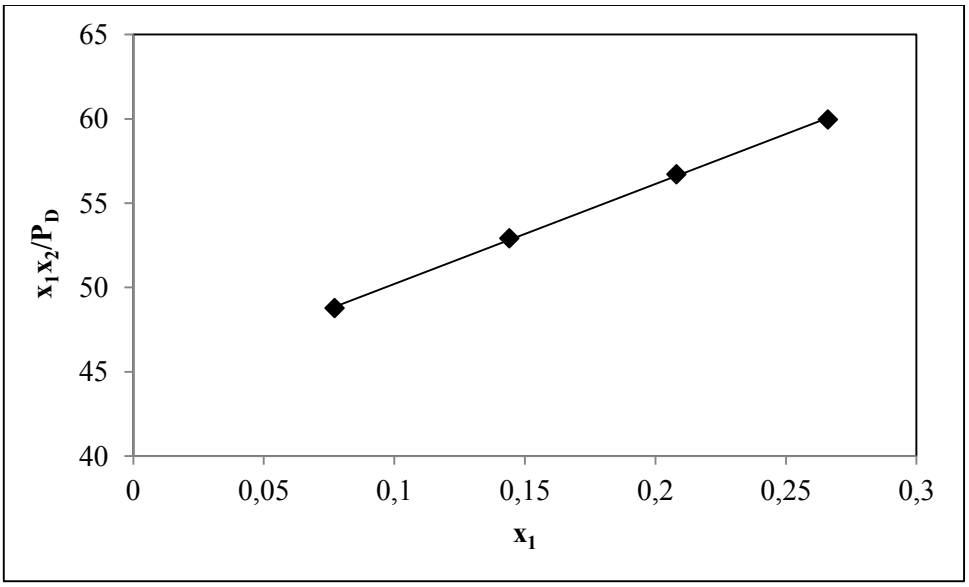

Figure B- 6: Plot of (x_1x_2/P_D) vs x_1 as $x_1 \rightarrow 0$ for 2-pentanone (1) + 2-methylpropan-1-ol (2) at 358.15 K

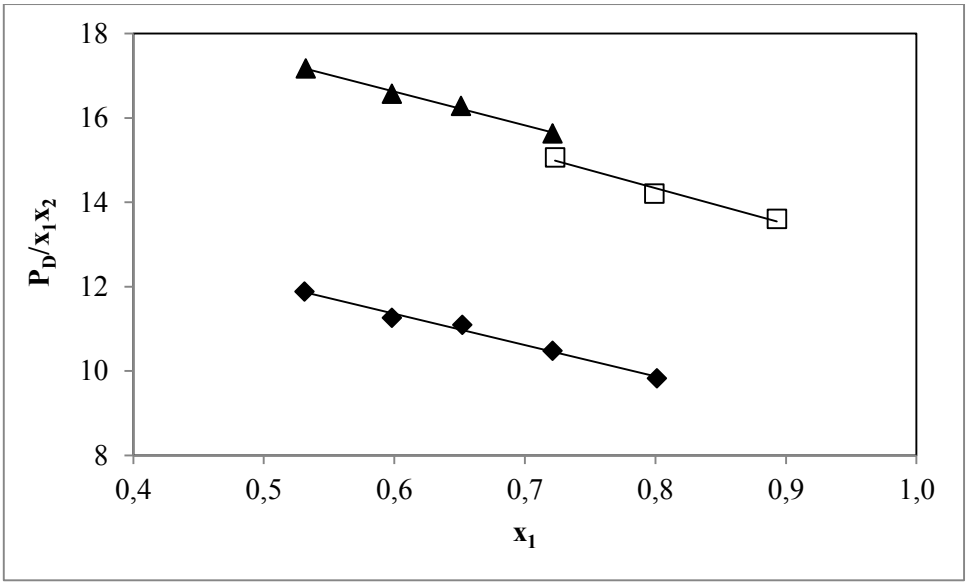

Figure B- 7: Plot of (P_D/x_1x_2) vs x_1 as $x_1 \rightarrow 1$ for 2-pentanone (1) + 2-methylpropan-1-ol (2) at 343.15 K (♦), 358.15 K (□) and 363.15 K (▲)

APPENDIX C **(EXCESS THERMODYNAMIC PROPERTIES)**

The plots of the excess thermodynamic properties (G^E, H^E and TS^E) for the newly measured systems of 2-propanol (1) + 4-methyl-2-pentanone (2) and 2-pentanone (1) + 2-methylpropan-1-ol are presented below; the plots for 1-propanol (1) + 4-methyl-2-pentanone (2) have been reported in Chapter 6.

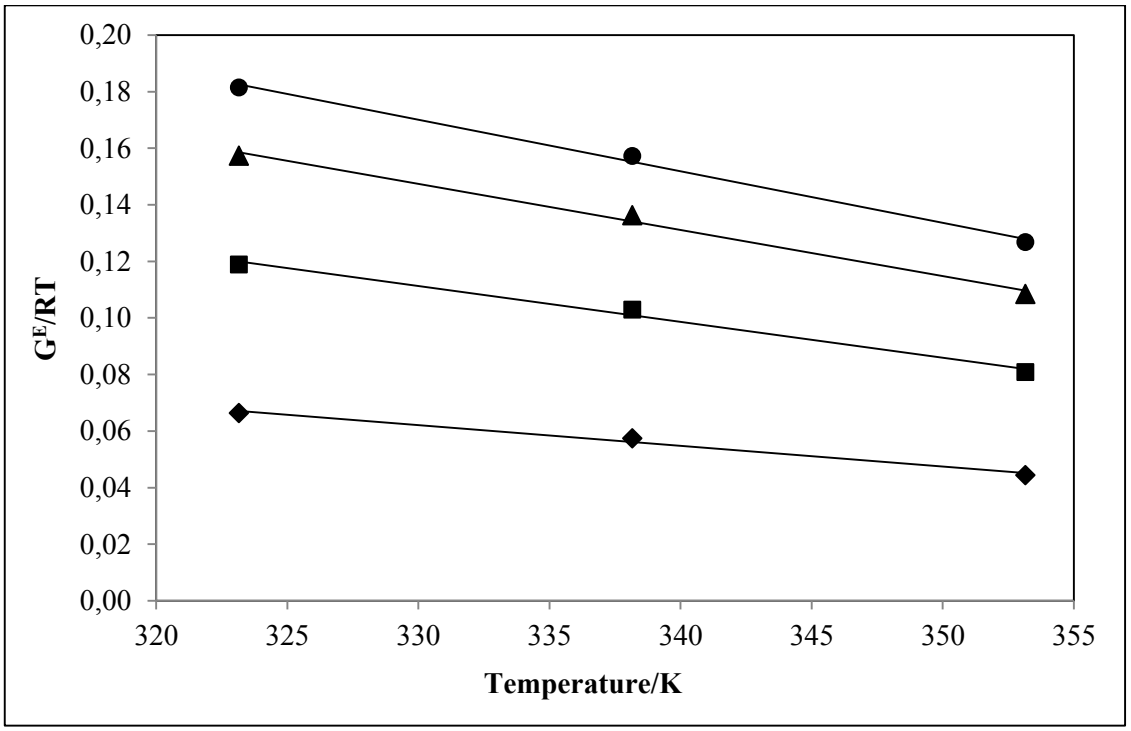

Figure C- 1: Plot used for the determination of the molar excess enthalpy values for 2-propanol (1) + 4-methyl-2-pentanone (2) system at 323.15 K, 338.15 K and 358.15 K. (♦), 0.1, (■), 0.2, (▲), 0.3 and (●), 0.4.

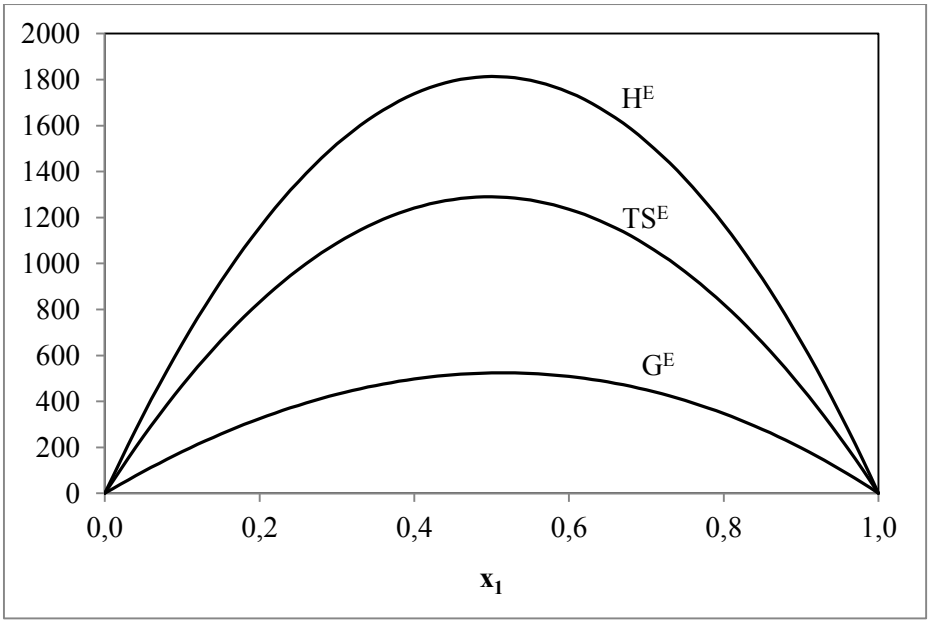

Figure C- 2: Excess thermodynamic properties (H^E, G^E and TS^E) for 2-propanol (1) + 4-methyl-2-pentanone (2) system at 323.15 K.

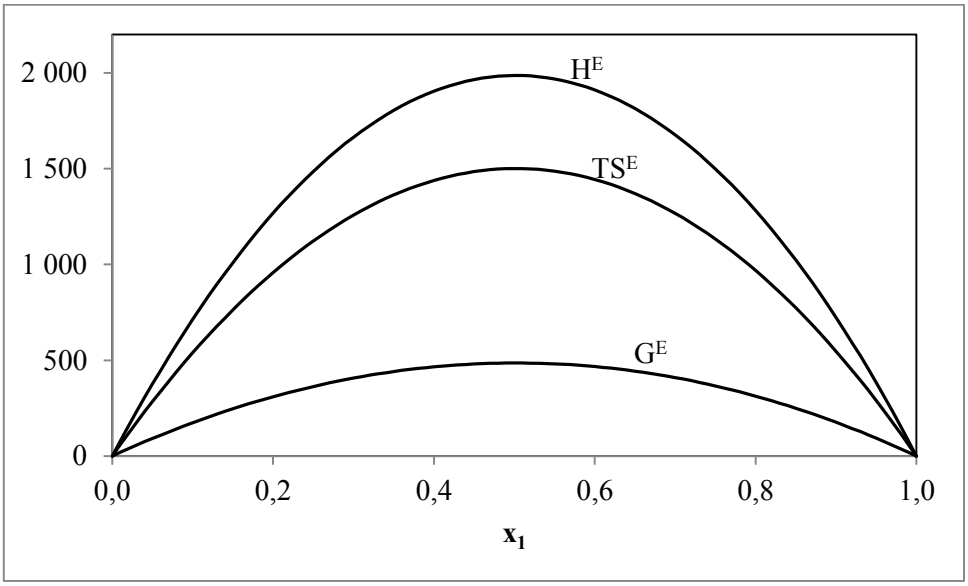

Figure C- 3 : Excess thermodynamic properties (H^E, G^E and TS^E) for 2-propanol (1) + 4-methyl-2-pentanone (2) system at 338.15 K.

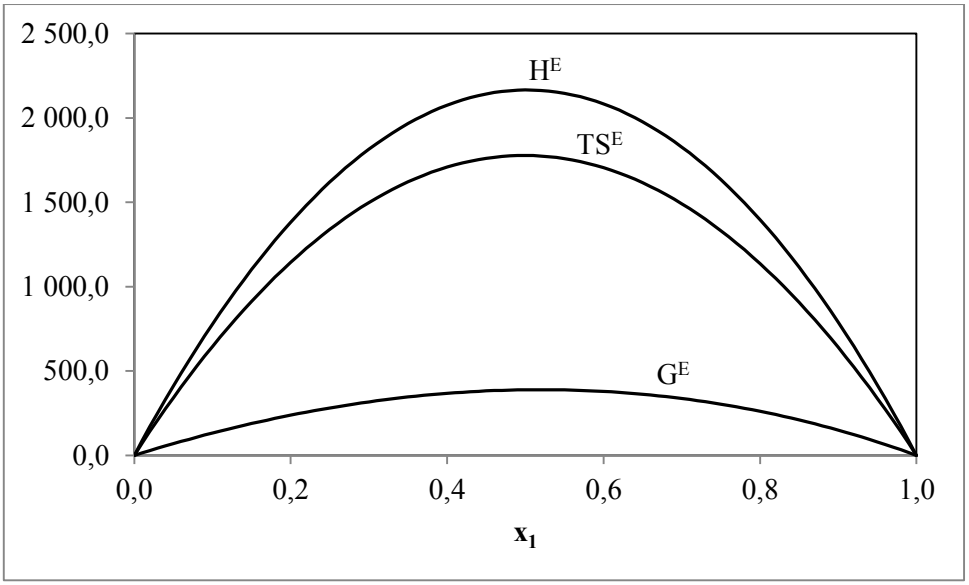

Figure C- 4: Excess thermodynamic properties (H^E, G^E and TS^E) for 2-propanol (1) + 4-methyl-2-pentanone (2) system at 353.15 K.

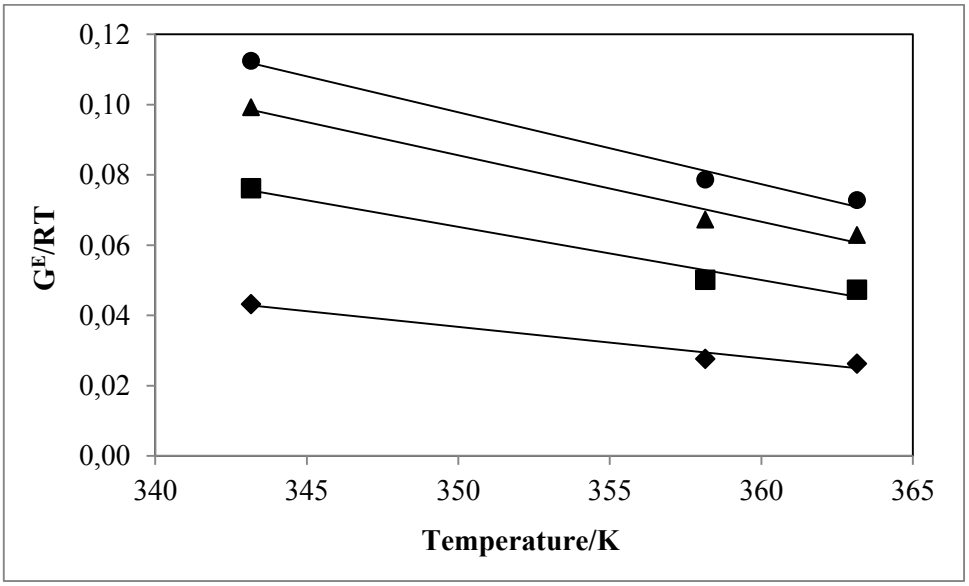

Figure C- 5: Plot used for the determination of the molar excess enthalpy values for 2-pentanone (1) + 2-methylpropan-1-ol (2) system at 343.15 K, 358.15 K and 363.15 K. (♦), 0.1, (■), 0.2, (▲), 0.3 and (●), 0.4.

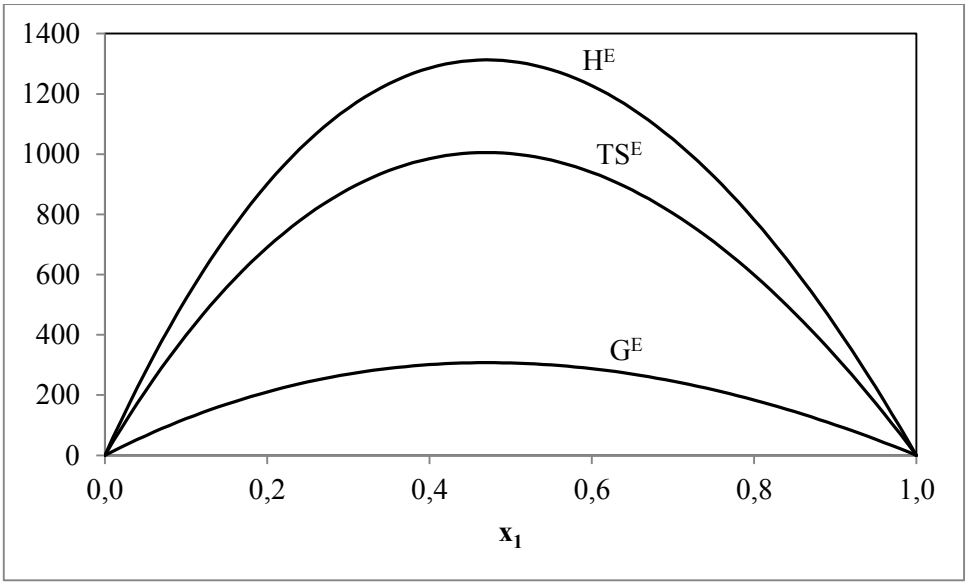

Figure C- 6: Excess thermodynamic properties (H^E, G^E and TS^E) for 2-pentanone (1) +2-methylpropan-1-ol (2) system at 343.15 K.

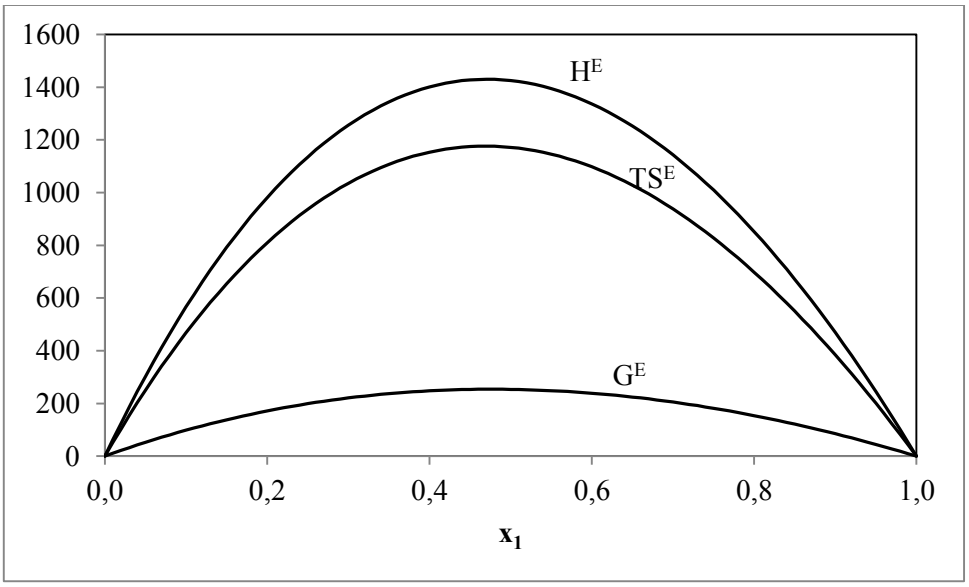

Figure C- 7: Excess thermodynamic properties (H^E, G^E and TS^E) for 2-pentanone (1) +2-methylpropan-1-ol (2) system at 358.15 K.

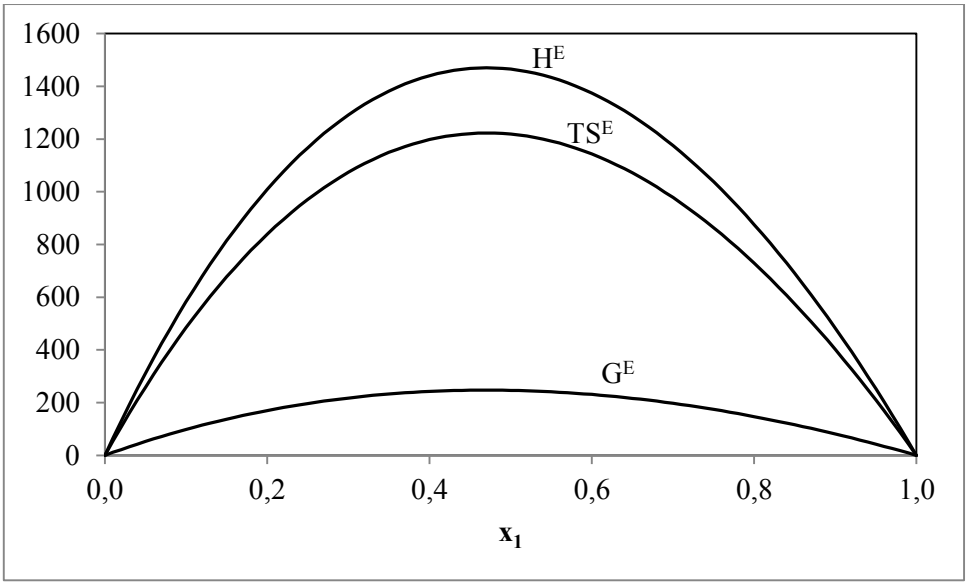

Figure C- 8: Excess thermodynamic properties (H^E, G^E and TS^E) for 2-pentanone (1) +2-methylpropan-1-ol (2) system at 363.15 K.